

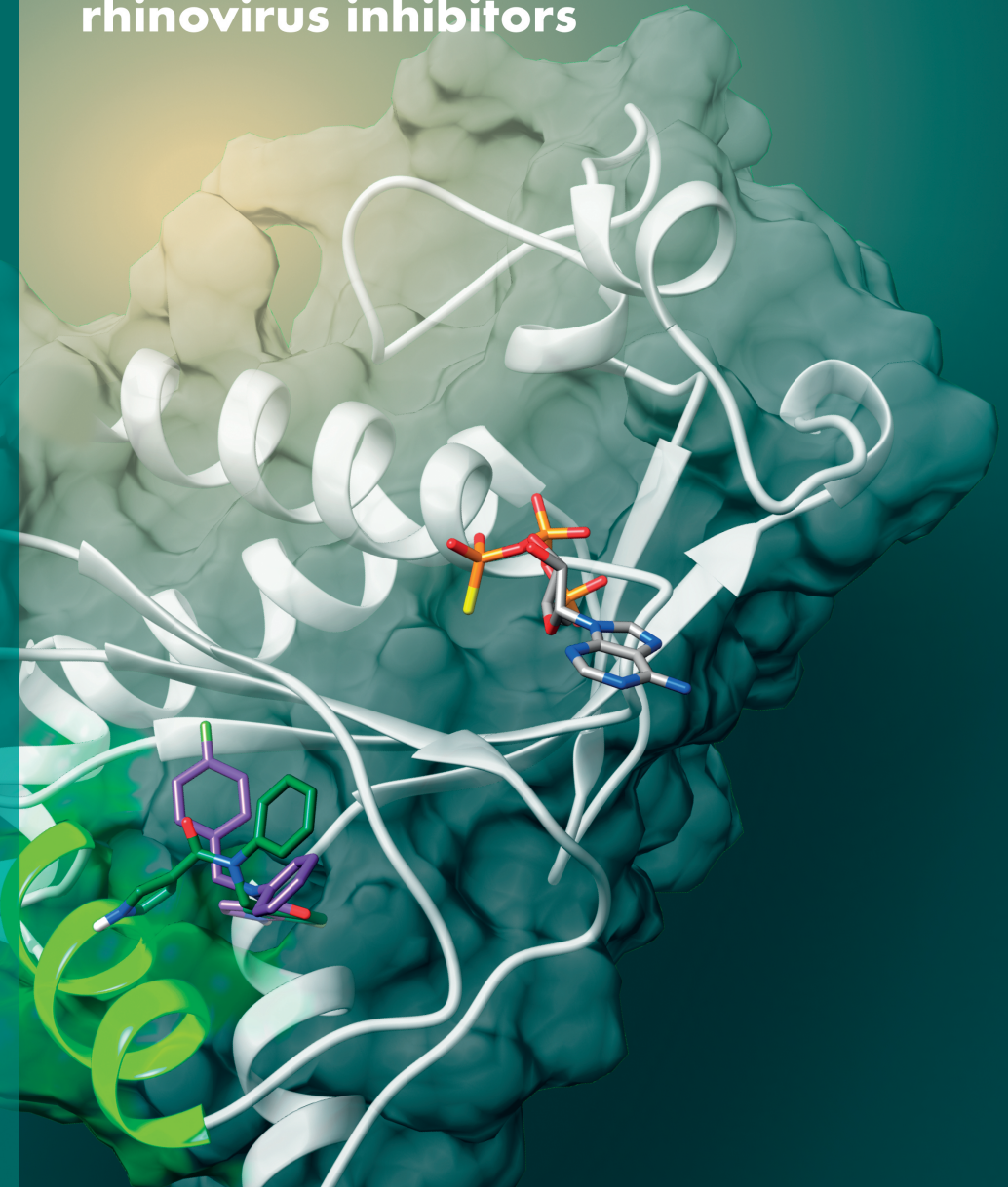
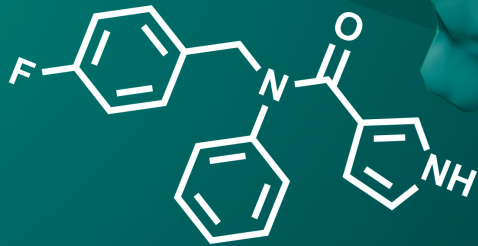
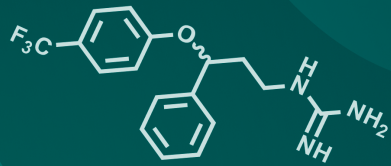
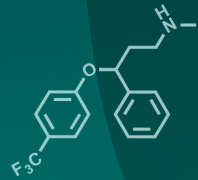
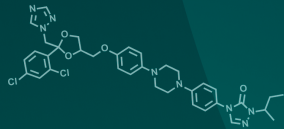
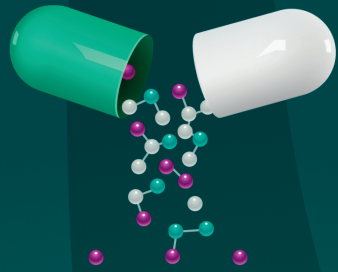
LISA BAUER

From repurposed drugs to pan-enterovirus and rhinovirus inhibitors

LISA BAUER

2021

From repurposed drugs to pan-enterovirus and rhinovirus inhibitors



From repurposed drugs to pan-enterovirus and rhinovirus inhibitors

Lisa Bauer

From repurposed drugs to pan-enterovirus and rhinovirus inhibitors

Ontwikkeling van breed-werkende remmers van enterovirussen en rhinovirussen

(met een samenvatting in het Nederlands)

Proefschrift

ter verkrijging van de graad van doctor aan de
Universiteit Utrecht
op gezag van de
rector magnificus, prof.dr. H.R.B.M. Kummeling,
ingevolge het besluit van het college voor promoties
in het openbaar te verdedigen op

dinsdag 2 februari 2021 des middags te 12.45 uur

door

Lisa Bauer

geboren op 28 december 1987
te Vienna, Oostenrijk

Colofon

From repurposed drugs to pan-enterovirus and rhinovirus inhibitors, Lisa Bauer
ISBN/EAN: 978-94-6416-256-1

Copyright © 2020 Lisa Bauer

All rights reserved. No part of this thesis may be reproduced, stored or transmitted in any way or by any means without the prior permission of the author, or when applicable, of the publishers of the scientific papers.

Cover design: Pietro Lodi, Lisa Bauer

Figure design: Denise Seitner, Pietro Lodi and Lisa Bauer

Layout and design: Stijn Eikenaar | persoonlijkproefschrift.nl

Printing: Ridderprint | www.ridderprint.nl

The research described in this thesis was financially supported by the EU Horizon 2020 Framework Program Project "ANTIVIRALS", a Marie Curie Initial Training Network (GA 642434) Printing of this thesis was partly sponsored by the graduate school "*Infection and Immunity*"

Promotor:

Prof. dr. F.J.M. van Kuppeveld

Copromotor:

Dr. J.R.P.M. Strating

Dedicated to my sister

Schlaueit ohne Mut ist Quatsch.
Mut ohne Schlaueit ist Unsinn.
Erich Kästner

Table of Content

Chapter 1	General Introduction	9
Chapter 2	Direct-acting antivirals and host-targeting strategies to combat enterovirus infection	41
Chapter 3	Structure-activity relationship study of itraconazole, a broad-range inhibitor of picornavirus replication that targets oxysterol-binding protein (OSBP)	57
Chapter 4	Fluoxetine inhibits enterovirus replication by targeting the viral 2C protein in a stereospecific manner	83
Chapter 5	Synthesis and antiviral effect of novel fluoxetine analogues as enterovirus 2C inhibitors	115
Chapter 6	Rational design of highly potent broad-spectrum enterovirus inhibitors targeting the nonstructural protein 2C	145
Chapter 7	General Discussion	207
Chapter 8	Addendum	231

Chapter

General Introduction

1

The human body is exposed to a large variety of different pathogens such as viruses, bacteria, fungi, worms and helminths. Viruses are obligate, intracellular parasites comprised of genetic material (DNA or RNA) which is surrounded by a protein coat and sometimes a membrane. They are capable of infecting all living organisms and cause a broad range of diseases. One of the biggest virus families is the *Picornaviridae* family which includes numerous important animal and human pathogens. Several prototypic picornaviruses belong to the *Enterovirus* (EV) genus which comprises the well-known human pathogen poliovirus (PV) and coxsackieviruses, numbered enteroviruses (eg. EV-A71 and EV-D68) and rhinoviruses. These viruses can cause a broad spectrum of diseases ranging from mild diseases such as hand-foot-and-mouth disease and conjunctivitis to severe diseases such as meningitis, encephalitis and acute flaccid paralysis, especially in young children and immunocompromised individuals. Overall, viral infections can be prevented by vaccines and treated with neutralizing antibodies or antiviral drugs. For EVs, vaccines are only available against PV and EV-A71 but not against the other EV serotypes. Given the high number of different EV and RV serotypes (> 250 serotypes), the development of a broad spectrum of EV and RV vaccines is unfeasible. A complementary strategy is the development of highly potent broad-spectrum antivirals. Currently, there is no antiviral therapy licensed for the treatment of any EV infection. This thesis focuses on the *Enterovirus* genus and provides valuable insights into the antiviral effects and mode-of-action of repurposed drugs and novel compounds that interfere with enterovirus replication.

1. Picornaviruses

Discovery of first picornaviruses

In 1898, Friedrich Löffler and Paul Frosch reported that the animal disease Foot-and-mouth disease is associated with a pathogen which is permitted to pass filters that normally retain bacterial life forms. It was identified that calves infected with a filtered inoculum from blisters of cows suffering from lesion in their mouth and on their feet still developed the same disease.^{1,2} Thus, they identified that the Foot-and-Mouth disease virus (FMDV), a member of the *Picornaviridae* family (*Aphthovirus* genus), is the causative agent of the highly infectious Foot-and-Mouth disease. The discovery of the first animal virus -FMDV- by Löffler and Frosch was one of the biggest milestones in the history of virology.

In 1908, Karl Landsteiner and Erwin Popper investigated the fatal case of poliomyelitis, a paralytic disease. They homogenized tissue from the central nervous system of a deceased young boy, filtered the homogenate and injected it into monkeys.³ The monkeys developed a similar disease, resulting in paralysis and subsequently death. This was the key experiment showing the viral nature of poliomyelitis and the first human virus, termed poliovirus (PV), was identified.

Classification of picornaviruses

PV also belongs to the *Picornaviridae* family but is classified within the genus *Enterovirus* (Figure 1). Since then, many more important pathogens belonging to the *Picornaviridae* virus family have been identified. The *Picornaviridae* family currently consists of 110 species grouped into 47 genera (<http://www.picornaviridae.com>, stand October 2019).⁴ It is one of the largest virus families harboring many clinically important animal and human pathogens. This thesis focuses on the *Enterovirus* genus.

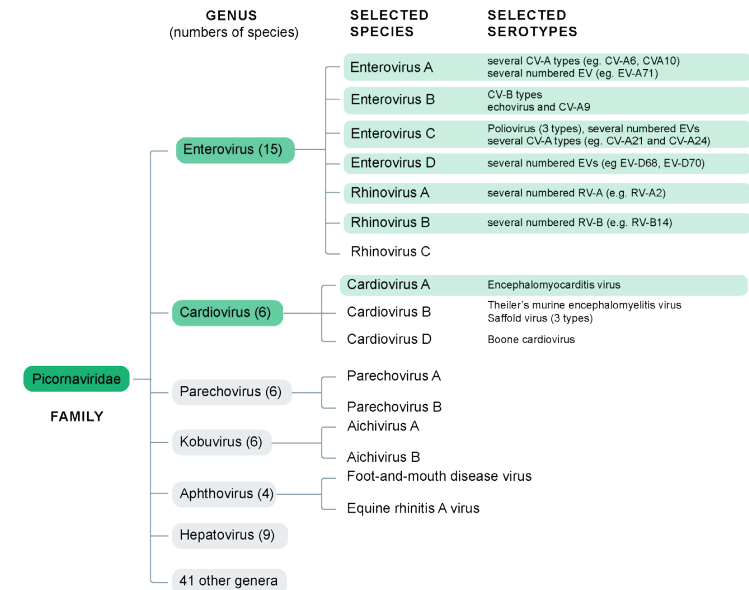


Figure 1. Classification of picornaviruses. Depicted are the different genera of the family Picornaviridae and highlighted in green are the members of relevant viruses used in this thesis.

Clinical impact of human enteroviruses

The EV genus is by far the biggest group within the *Picornaviridae* family and comprises human and animal pathogens responsible for many outbreaks and tremendous socioeconomical and medical burden. The serotypes of the genus *Enterovirus* are currently categorized into 12 EV species (species A- L) and three rhinoviruses (RV, species A-C). Four EV (EV-A, -B, -C, -D) and all three RV species comprise different serotypes that cause the most common infections known to mankind.⁴ The primary transmission is via the fecal-oral route, but rhinoviruses and several enteroviruses (e.g. EV-D68) are transmitted via the respiratory route. The two predominant replication sites are the gastro-intestinal tract and the respiratory tract from where the viruses can enter the blood stream and spread systematically. This can result in severe complications and

sometimes even fatal diseases (reviewed in ⁵). Many enteroviruses can spread to the central nervous system (CNS), however, the exact mechanism of how they enter the CNS remains to be established.⁶⁻⁸

PV is the prototypic member of the EV-C species and the causative agent of the paralytic disease poliomyelitis. Although PV infections are mostly asymptomatic, they can cause a variety of symptoms of which acute flaccid paralysis (AFP) can cause lifelong disability. PV causes the most devastating and widespread morbidity and mortality of all EV genotypes. The virus gained attention during the severe polio epidemics in the 1940s and 1950s.⁹ Photographs of young children lying in “iron lungs”, machines that induced artificial breathing because they were suffering from respiratory paralysis, spread around the world. These outbreaks initiated the development of poliovirus vaccines. The inactivated PV (IPV) vaccine and the live attenuated oral PV vaccine (OPV) were instrumental in preventing poliomyelitis. In 1988 the WHO launched the global poliovirus eradication campaign initiative with the goal to eradicate poliomyelitis. There are several obstacles to the elimination of poliomyelitis and the virus still poses a threat to some parts of the world. One reason for this is poor vaccination coverage due to technical or social problems in several regions in the world (Pakistan and Afghanistan according to polioeradication.org, stand December 2019). Additionally, the virus also re-emerges because of declining vaccination coverage as recently observed in the Philippines.¹⁰ Another threat is posed by occasional outbreaks which are caused by the OPV. The OPV is extremely safe and effective, but for immunization the virus needs to replicate in the gut. In extremely rare cases the live attenuated virus can cause paralysis. The live attenuated vaccine strain can revert back to the neurovirulent polio of poliovirus or can recombine with other closely related EV. All circulating viruses which are derived from the OPV are called vaccine derived poliovirus (VDPV).

Other important EV members are the coxsackie A and B viruses, echoviruses, numbered enteroviruses and rhinoviruses. Though often self-limiting, these infections can cause major complications resulting in life-threatening conditions especially in infants, young children and immunocompromised individuals. Infections can cause a wide range of clinical manifestations ranging from hand-foot-and-mouth disease, conjunctivitis, aseptic meningitis, myocarditis, severe neonatal sepsis-like disease, upper and lower respiratory diseases to acute flaccid paralysis and acute flaccid myelitis (reviewed in ⁵). Rhinoviruses are the causative agent of the common cold and can infect the upper and lower respiratory tract. RV infections are a serious threat to people with asthma, chronic obstructive pulmonary disease (COPD) and cystic fibrosis since these viruses can trigger exacerbations of the underlying conditions. Despite their clinical importance, neither vaccines nor antivirals are available and treatment is limited to supportive care.

In recent years, several non-polio EVs gained particular attention as being serious health threats because of their neurotropism. One of these is EV-A71, the causative agent of Hand-foot-and-mouth (HFMD) disease. Typical symptoms are fever, sore throat, mouth ulcers and maculopapular rashes on hands and feet. Outbreaks of

EV-A71 have been reported worldwide but more frequently in the Asia-Pacific region (Australian, Japan, Malaysia, Taiwan, Vietnam and China).¹¹ Neurological manifestations such as encephalomyelitis, encephalitis, AFP, aseptic meningitis and cardiopulmonary complications such as cardiorespiratory failure, pulmonary edema and myocarditis, raised particular concern in regards to EV-A71.¹²⁻¹⁴ Recently, several inactivated EV-A71 vaccines were approved in China.¹⁵

Over the last years, the serotype EV-D68 also emerged in large outbreaks worldwide. EV-D68 is an atypical enterovirus and behaves rather like a rhinovirus because it causes respiratory infections. The virus was first classified as rhinovirus 87 and reclassified to EV-D68 in 2002. In the majority of patients, EV-D68 causes mild respiratory illness. However, latest outbreaks of EV-D68 in the USA induced severe respiratory illness and at the same time an increase in neurological “polio like” complications were observed. This correlation of respiratory disease with “polio-like” symptoms suggested potential neurotropism of EV-D68.¹⁶⁻¹⁹ Recently, improved diagnostic techniques established the detection of EV-D68 and pan-serology showed EV-D68 antibodies in the cerebrospinal fluid, providing evidence for a causative role of EVD68 in AFM.^{20,21}

The main causative agent of hemorrhagic conjunctivitis, a painful and very contagious eye infection, is CVA24v. It caused several outbreaks and two pandemics.²² In addition to the hemorrhagic conjunctivitis, CV24v received attention because it also causes respiratory symptoms and neurological complications (AFP).^{23,24}

Other important picornaviruses

Apart from the already discussed EV, several other important human and animal pathogens belong to the *Picornaviridae* family. Hepatitis A is a liver disease caused by the ubiquitously encountered Hepatitis A virus belonging to the genus *Hepatovirus*. Improved sanitation and the successful vaccine development significantly reduced the incidents of Hepatitis A worldwide. The genus *Parechovirus* consists of several serotypes which are increasingly recognized as important pathogens that cause sepsis-like illness and severe neurological manifestation in young infants. Recently, it was also reported that parechoviruses causes epidemic myalgia, myocarditis and pneumonia in adults.²⁵⁻²⁷ Aichivirus is a poorly characterized virus belonging to the *Kobuvirus* genus causing severe gastroenteritis in children under the age of 5, especially in developing countries.²⁸

Besides human pathogens the *Picornaviridae* family also harbors a large amount of animal viruses. The best-known picornavirus affecting animals is the aforementioned FMDV. It affects wild and domesticated cloven-hoofed ruminants including cattle, swine, goats and sheep. The typical symptoms of infected animals are vesicular lesions in the mouth and claws. Outbreaks of FMDV affects the national and international trade of livestock and animal products and leads to enormous economic losses and social consequences. Formalin-inactivated vaccines are available to contain and control FMDV outbreaks in endemic countries but the vaccine is not widely applied due to poor immunization. The *Cardiovirus* genus contains several animal viruses and

representative members are encephalomyocarditis virus (EMCV) and Theiler's Murine encephalomyelitis virus. The latter is an enteric pathogen of mice and induces mild gastroenteritis following oronasal infection; in rare cases severe CNS complications were observed.²⁹ EMCV has been detected in a wide range of wild and domestic animals such as voles, squirrels, elephants, swine, wild boar, raccoons, antelopes, lions, birds and several non-human primate species worldwide.^{30,31} Pigs are the most affected species and the symptoms range from acute myocarditis and reproductive failures to the death of piglets.^{30,32-34} The genus of *Cardiovirus* also harbors the human Saffold virus. Infections by this virus are ubiquitous and asymptomatic in young children, but have also been associated with several clinical diseases such as gastroenteritis, respiratory diseases and neurological complications.³⁵

2. The enterovirus life cycle

As with intracellular parasites, viruses heavily depend on several functions of the host cell. They commandeer the host machinery, alter the host metabolism and remodel the whole cell atlas into a favorable landscape ideal for virus genome replication. This results in a new generation of infectious viral particles which can subsequently infect adjacent cells. In the following section, the organization of the virus genome and the different phases of the viral life cycle will be discussed with a special focus on the modulation of the host environment to promote virus replication.

Organization of the enterovirus genome

The name Picornavirus is derived from the Latin word *pico* and the word *RNA* which already suggests that this virus family consists of small viruses with an RNA genome. Picornaviruses are non-enveloped viruses which means that the virus neither has an outer lipid membrane nor surface glycoproteins. The RNA genome is of positive polarity and immediately serves as an mRNA template for protein translation (Figure 2). The viral genome is uncapped but is instead covalently linked to the VPg (viral protein genome-linked) which is the viral non-structural protein 3B. The virus genome length ranges from 7.1 to 8.9kb and contains one open reading frame encoding for one polyprotein. The genome is divided into the P1 region, which harbors the structural proteins, followed by the P2 and P3 regions that encode proteins involved in protein processing ($2A^{pro}$, $3C^{pro}$, $3CD^{pro}$) and genome replication.

The enterovirus genome contains several structural elements such as the highly structured 5' and 3' untranslated regions (UTR) and a genome-encoded poly-A tail at the 3' end. Since the viral genome is uncapped, the internal ribosomal entry site (IRES) at the 5' UTR serves as a recruiting platform for ribosomes to initiate translation. A common feature in the picornavirus genome is the cis-replication element (CRE) which varies in the genomic location in different picornaviruses. The CRE is important for the initiation of RNA replication by uridylation of VPg, the primer for RNA synthesis.

Entry and uncoating

EVs replicate their genome exclusively in the host cytoplasm (Figure 3). In order to enter the host cell, the virus first attaches to a cell receptor followed by receptor-mediated endocytosis. Receptor usage is the key determinant for virus tropism and pathogenesis. Different types of cell surface receptors serve as receptors for EV and some of the receptors are shared between EV and some are specific to only one species.³⁶ For many EVs, the receptor binds in a depression in the capsid called the canyon which surrounds the 5-fold axis of symmetry.³⁷ Following the internalization of the virus, the genome needs to be released into the cytoplasm to ensure translation and replication. Uncoating can be triggered by receptor binding and/or low pH in the endosomal compartment resulting in a destabilization of the viral particle and thus the release of viral RNA.³⁶ As part of this process, the N-terminus of the structural protein VP1 anchors the particle to the endosomal membrane, and the myristoylated VP4 forms a pore allowing the release of the viral RNA through the endosomal membrane into the cytoplasm.³⁶

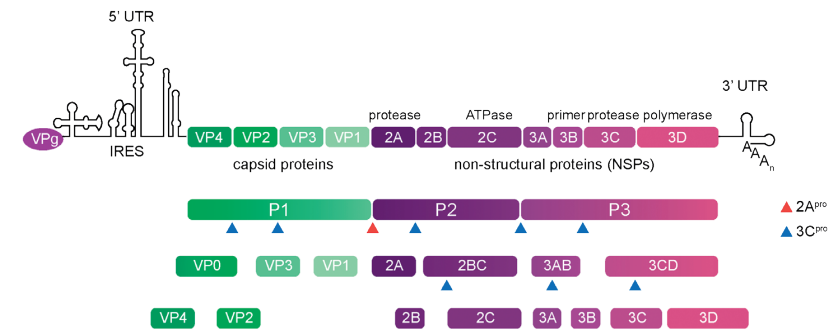


Figure 2 Schematic representation of the enterovirus genome and the encoded proteins. The genome is covalently linked to the viral protein VPg and contains one open reading frame which is divided into P1, P2 and P3 regions. The genome is flanked by the structured 5' and 3' untranslated regions (UTR), the internal ribosomal entry site (IRES) at the 5' UTR and the poly-A tail at the 3' end. The IRES mediates cap-dependent translation of one big viral polyprotein that is autocatalytically cleaved by the viral proteases $2A^{pro}$ and $3C^{pro}$ into the structural proteins (VP1, VP2, VP3, and VP4), nonstructural proteins ($2A$, $2B$, $2C$, $3A$, $3B$, $3C$, and $3D$), and several functional processing intermediates.

Genome translation

After release, the genome is immediately translated into a large polyprotein. To liberate the individual mature proteins, the polyprotein needs to be proteolytically processed (Figure 2). EVs encode the viral proteinases $2A^{pro}$, $3C^{pro}$ and $3CD^{pro}$ which are responsible for the proteolytic cleavage of the polyprotein into the individual proteins and several functional processing intermediates. Besides cleaving the polyprotein, the proteases are involved in cleaving host factors to promote viral translation, replication

and viral spreading. For example, cleavage of the host protein eIF4G and poly(A)-binding protein by viral proteases results in the host translation coming to a halt, a so called “host shut-off”.³⁸⁻⁴⁰ Furthermore, to stay undetected by the innate immune system, both viral proteases cleave several signaling proteins and thereby prevent the initiation of the antiviral response (reviewed in⁴¹)

RNA replication

Non-structural proteins are involved in the genome replication (for which the structural protein are dispensable). The viral RNA-dependent RNA polymerase 3D^{pol} is the viral protagonist in the replication machinery. 3D^{pol} uridylylates the VPg by using the secondary RNA structure CRE as a template to yield VPg-pU-PU.⁴²⁻⁴⁵ The uridylylated VPg is used as a primer by 3D^{pol} to synthesize a negative-strand RNA from the incoming RNA strand resulting in a double stranded RNA (dsRNA) intermediate. The minus-strand RNA is used as a template to produce new positive-strand RNA molecules. These are either used for another round of translation and replication or are packaged into capsid proteins to produce infectious viral progeny. A hallmark of positive RNA viruses is that the genome replication occurs in conjunctions with cellular membranes. The viruses remodel the host membrane network to generate a platform in order to sustain viral genome replication, the so-called viral replication compartments. The mechanism with which Picornaviruses usurp host membrane to create their replication organelle is discussed in detail later on.

Morphogenesis and virus release

The life cycle ends with packaging the viral RNA into icosahedral capsids to form new infectious particles. The newly synthesized positive-strand RNA can be immediately encapsidated by the viral proteins to form progeny virions. This process is linked to the replication as only newly synthesized positive-strand RNA can be incorporated into the capsid. The assembly process must be very specific for the viral RNA because of the high background of host mRNA in the cells. Two distinct mechanisms for the picornavirus morphogenesis have been proposed (reviewed in⁴⁶). One mechanism depends on a specific interaction between two viral proteins, the helicase 2C and the viral capsid protein VP3. This mechanism seems to be specific to enteroviruses.⁴⁷ The second mechanism suggests that secondary RNA structures interact with viral protein to mediate morphogenesis. This mechanism was suggested for parechoviruses, aichivirus and FMDV.⁴⁸⁻⁵⁰ For years the dogma of virus release was that virions are released through host cell lysis. However, there is increasing evidence that viruses can also be released into membrane wrapped particles independent of cell lysis.⁵¹⁻⁵³

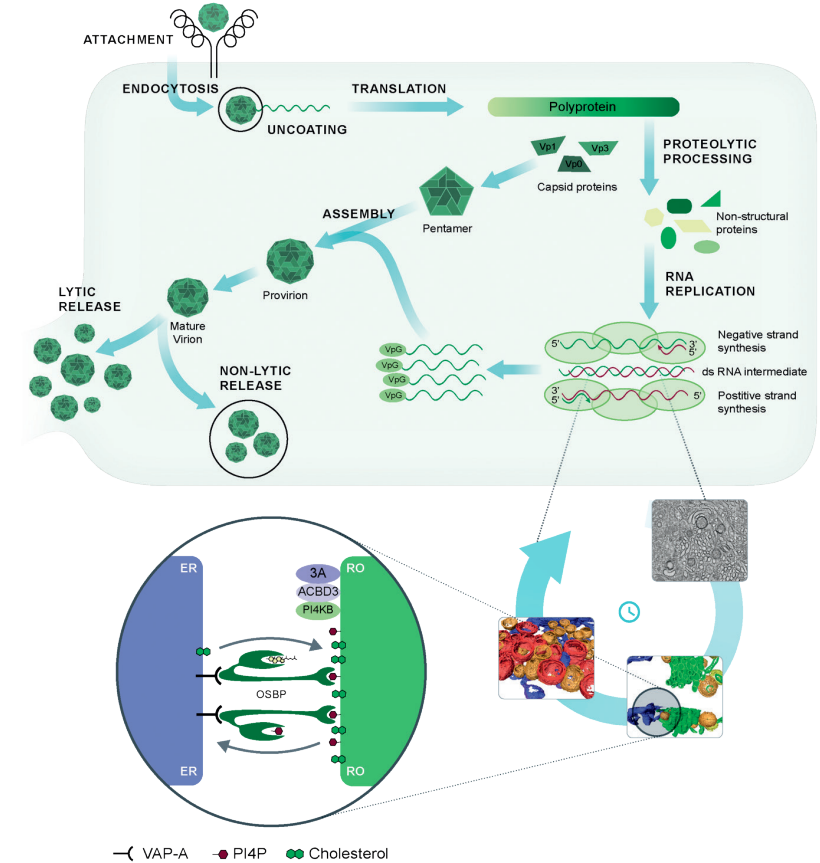


Figure 3 Enterovirus replication cycle. The EV life cycle is initiated by the attachment of the virus particle to its corresponding receptor followed by internalization into the host cell. The genome is released and translated into one polyprotein which is then processed by the viral proteases to release the individual viral proteins. The non-structural proteins rewire the cell host membrane network to generate the replication organelle (RO), where the RNA replication takes place. Genome replication starts with synthesis of complementary negative-stranded RNA, which is used as template for the synthesis of positive-strand RNA molecules. Newly synthesized positive-strand RNAs either enter a new round of genome replication or are packaged into capsid proteins to build infectious particles. Viruses are released by a non-lytic mechanism as well as upon cell lysis. Zoom in: Slice from a tomogram of a CVB3 infected cell at 5 hours post infection. Next, a model of the early-stage RO which consist of single-membrane tubular (green) and vesicular (orange, yellow) structures. A late-stage RO of CVB3 showing double-membrane vesicles (orange) and multilamellar vesicles (red). (Adapted from van der Schaar et al, Trends in Microbiology 2016, with permission). Schematically depicted is the cholesterol shuttling between the ER and the RO. The viral protein 3A recruits PI4KB via the adaptor protein ACBD3 which leads to an enrichment of PI4P lipids (purple hexagons) in the RO to recruit OSBP. OSBP binds PI4P lipids and simultaneously binds to the ER by interacting with VAP-A or -B and thereby generates a membrane contact site between the RO and ER. This allows the shuttling of cholesterol (green hexagons) by OSBP into the RO in counter-exchange for PI4P lipids.

3. Enterovirus Replication Organelles

A remarkable feature of positive-strand RNA viruses genome replication is the tight membrane association. EV reorganize the host cell's membrane network into a specialized microenvironment with unique protein and lipid composition to survive in a host cell. The formation of the replication compartments differs greatly between the virus families, but they universally depend on manipulating the host lipid synthesis and metabolism. One function of the confined replication site is to concentrate viral proteins in order to ensure efficient viral genome replication. Furthermore, it may help in evading the immune system by protecting viral dsRNA intermediate from cytosolic RNA sensors which trigger an antiviral response.

Structure of replication organelles

Like all other positive-strand RNA viruses, EVs modify the host cell membrane to create structures with novel morphology. In 1958, the first transmission electron microscopic pictures of cells infected with poliovirus showed poliovirus-induced membranous structures which were associated with genome replication only a decade later.⁵⁴ Other findings reported that the replication structure consisted of single-membrane or double-membrane vesicles (DMV) of variable size clustering in the perinuclear region.^{55,56} For a long time the discussion was whether these observed membranes structures were single- or double-membrane structures. Advancements in electron microscopy and electron tomography enabled a detailed view on the 3D structure of replication organelles and showed that the first structures detected upon infections are single-membrane tubules.⁵⁷⁻⁵⁹ As infection progresses, these tubules transform into DMVs which are enveloped by more tubules in order to generate multilamellar structures. The origin of the enterovirus replication organelle was unknown for considerable time. It was hypothesized that since the Golgi disintegrates, Golgi membranes are possibly the origin of the RO formation. Recent evidence suggests that ER membranes also play a role in early RO formation.⁶⁰

The role of viral proteins and host factors in creating replication organelles

RO formation requires a concerted action of viral proteins alone and in combination with hijacked host proteins. The viral proteins 2B, 2C and 3A as well as the precursor proteins 2BC and 3AB contain hydrophobic domains for membrane association.⁶¹⁻⁶⁵ 2B and 2C achieve membrane association with an amphipathic helix which differs between the two proteins.^{61,66} 2B targets ER and Golgi membranes act as viroporin. It has the capability to form pores resulting in membrane perturbations and altered Ca²⁺ flux.⁶⁷ The altered Ca²⁺ flux from the Golgi to the cytoplasm is thought to inhibit protein transport through the Golgi.⁶⁸ The 2BC and 2C are also involved in RO formation as overexpression of 2BC and 2C causes massive membrane rearrangement.⁶⁹⁻⁷¹

Interestingly, overexpression of 2BC in combination with 3A results in membrane reorganization comparable to infected cells.⁷² The role of 2C will be discussed later.

The small viral protein 3A is another key player in RO formation. 3A contains a C-terminal hydrophobic domain which allows for membrane association.⁶⁴ It recruits several host factors important for modifying the lipid environment. One hallmark of RO is the massive accumulation of the lipid phosphatidylinositol-4-phosphate (PI4P). PI4P is an important signaling lipid which serves as a regulator of cellular processes and is a master controller of protein and lipid fluxes via the interaction with effector proteins.⁷³ In uninfected cells, PI4P lipids are synthesized by one of the four distinct phosphatidylinositol 4-kinases (PI4K) type II and type III localized at various organelles. In uninfected cells, ACBD3 interacts with the phosphatidylinositol 4-kinase type III β (PI4KB) and recruits it to Golgi membranes and mediates its activity.⁷⁴ In EV infected cells, 3A interacts with the Golgi-resident adaptor protein acyl-CoA-binding domain-containing protein 3 (ACBD3). The interaction of 3A with ACBD3 leads to an accumulation of PI4KB at RO. PI4KB converts the phosphatidylinositol (PI) lipids into PI4P lipids thereby increasing the local concentration of PI4P lipids in the RO.⁷⁵⁻⁷⁷ Distinctly related viruses can recruit different isoforms to the replication platform in order to accumulate PI4P lipids.^{78,79}

Oxysterol-binding protein

The accumulation of PI4P at the RO is important to attract other host proteins to the RO to further modulate the lipid environment. Various cellular host proteins carry pleckstrin-homology (PH) domains which are capable of sensing PI4P lipids. These protein domains are found in several proteins such as lipid transfer protein ceramide-transfer protein (CERT) or oxysterol-binding protein (OSBP) and OSBP-related proteins (ORP).⁸⁰ These lipid transfer proteins often operate on membrane contact sites where two membranes of distinct cellular compartments are in close contact.^{81,82}

Cholesterol is an essential membrane component affecting membrane fluidity.^{83,84} It is synthesized in the ER and enriched in Golgi-membranes, late endosomes and the plasma membrane.⁸⁵ The transport into other compartments can occur via diffusions between membranes, vesicular transport and primarily through lipid transfer proteins.⁸⁶ Cholesterol transporters include OSBP and ORPs, among other lipid shuttling proteins.⁸⁷ OSBP and ORPs share an OSBP-related domain (ORD) which is responsible for accommodating lipids and shuttling them in a bidirectional manner by counter-exchange of specific lipids for PI4P.^{87,88} OSBP tethers ER-membranes and Golgi-membranes together by binding both membranes simultaneously to allow for lipid flux. OSBP connect with the ER membrane by interacting with its FFAT motif with the ER-residing protein VAP-A and VAP-B. On the other side, the PH-domain interacts with PI4P lipids which are enriched in the Golgi membrane. As a result, the membranes are tethered together and lipid flux can occur. OSBP accommodates cholesterol in the ORD domain and shuttles it from the ER into the Golgi against the concentration gradient.

This action is powered by the counterflux of PI4P lipids from the Golgi into the ER where PI4P is dephosphorylated by the Sac1 phosphatase.^{89,90}

Cholesterol is needed to grease viral ROs. EVs first exploit the enzymatic activity of PI4KB to enrich RO membranes with PI4P lipids.^{91,92} The recruitment of OSBP to the RO is ensured by the high affinity of its PH-domain to bind PI4P lipids. This enables the fueling of the RO with cholesterol by utilizing the essential host factor OSBP.^{79,91-93} Besides the ER cholesterol pool, several other possibilities for enteroviruses to grease their replication organelles with cholesterol exist. It is very likely that EVs do not rely on newly synthesized cholesterol but rather depend on existing cholesterol pools which can be stored in lipid droplets for example.⁹⁴ Additionally, EV infection results in enhanced endocytosis in order to increase cholesterol uptake.^{95,96} Mobilization of cholesterol from recycling endosome might even possibly underlie the function of OSBP since it was shown to also operate at the endosome-ER membrane contact site.⁹⁷

The accumulation of PI4P lipids at viral replication sites is not restricted to EV. It is also utilized by Cardioviruses, Kobuviruses and the distantly related flavivirus Hepatitis C virus.⁹⁸⁻¹⁰⁰ Some of these viruses (Cardioviruses and Hepatitis C virus) recruit different PI4K isoforms eg. PI4KA to increase PI4P levels at the replication compartment, but each of these viruses harnesses OSBP to accumulate cholesterol in their viral replication compartments. Thus, evolutionary distantly related viruses use a conserved pathway to hijack lipid modifying enzymes.

4. Non-structural protein 2C

The genome of EV is relatively small and encodes a small number of mature proteins to support replication. With this limited number of proteins, EV have developed strategies to coopt host protein for membrane reorganization, in order to optimize their life cycle and to counteract immune responses. EV non-structural proteins are multifunctional proteins, such as the non-structural protein 2C. 2C is involved in RNA binding, RNA replication, encapsidation, RO formation and immune evasion. It is a highly conserved protein among the *Picornaviridae* and resembles a swiss army knife as it is involved in a plethora of functions during the viral life cycle.

Role of 2C in the viral life cycle

2C is composed of around 320-330 aa and contains a motif important for nucleotide binding, a zinc finger and a protruding C-terminal domain (Figure 4). Numerous drug inhibition, genetic and biochemical studies suggest that the protein is involved in pleiotropic functions during the viral life cycle. There is genetic evidence that the 2C protein is involved in uncoating of the viral genome.¹⁰¹ Studies on the inhibitor Guanidium chloride (GuaHCl) revealed that it inhibits a function of 2C that is involved in viral genome replication.¹⁰²⁻¹⁰⁶ The 2C protein and the precursor 2BC are implicated in membrane rearrangement and assembly of membranous replication complexes.^{65,69,71,72} As previously mentioned, viral proteins can hijack host factors in order to manipulate

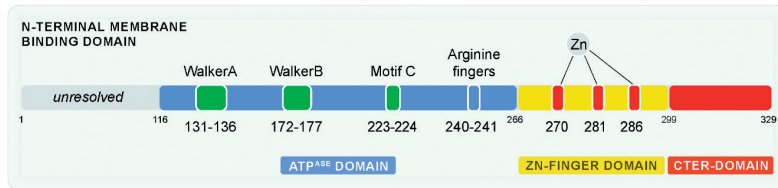
membranes, lipid homeostasis and metabolism. 2C binds the ER protein Reticulon 3 which promotes ER membrane curvature but the importance of this interaction in the RO formation is poorly understood.¹⁰⁷ Additionally, 2C interacts with several other host proteins such as COPI to facilitate RO formation.^{107,108} How the interaction of 2C with several host factors results in membrane rearrangement is largely unknown and remains to be established. During morphogenesis, 2C interacts with the capsid protein VP3 resulting in encapsidation of the RNA genome.^{47,109} Lastly, there is evidence suggesting that 2C is involved in immune evasion by blocking the function of innate immune signaling proteins which trigger immune responses.^{110,111}

2C Structure

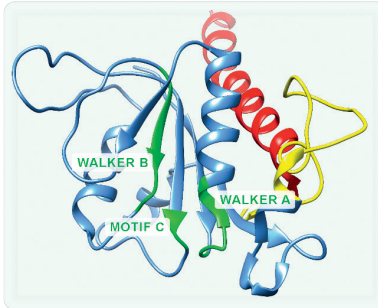
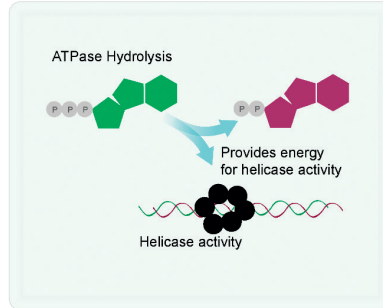
Decades ago, bioinformatic approaches predicted that the 2C is a helicase. Helicases are enzymes that bind NTP and use the energy from NTP hydrolysis to catalyze the unwinding of double-stranded nucleic acids. Biochemical research identified that the viral 2C protein functions as ATPase¹¹²⁻¹¹⁶, ATPase-dependent RNA helicase and as an ATPase-independent RNA chaperone.¹¹⁷ All of these enzymatic functions are indispensable for the viral life cycle. The ATPase domain of the protein belongs to the superfamily of SF3 helicases of the AAA+ ATPases and contains Walker A and Walker B motifs and motif C.¹¹⁸ Helicases classified into the SF3 helicases adopt a characteristic ring structure often assembled into a hexamer as described for the SV40 Large T antigen and the replication protein E1 of human papilloma virus.^{119,120} Besides the ATPase domain, 2C harbors an N-terminal membrane-associated amphipathic helix which was shown to be important for protein oligomerization and RNA binding.^{104,121} A cysteine-rich motif is a common feature of several picornaviruses except for Aphthovirus FMDV 2C. The cysteine-rich motif forms a zinc-binding site important for the ATPase activity.¹²²

Despite decades of research on 2C, the structural characterization of 2C is impeded because of insufficient solubility of the protein. First evidence that 2C oligomerizes and that an oligomeric state is needed to form an active ATPase complex was shown with poliovirus 2C fusing to an MBP tag. Negative-stain electron microscopic studies showed that higher order structures of 2C are composed out of 5-8 protomers. The oligomerization was shown to be dependent on the first 38 N-terminal amino acids.¹²³ Shortly thereafter, low resolution structures of truncated FMDV and echovirus 2C became available because full-length protein was insoluble. These first structures provided further evidence of an oligomeric state which is needed for proper functioning of an ATPase.^{122,124} Almost a decade later the first high resolution crystal structure of a soluble fragment of EV-A71 2C was published. Full length EV-A71 2C protein was insoluble. Limited trypsin proteolysis revealed a truncated protein, which lacked the first 116 amino acids (D116) that formed crystals.¹²⁵

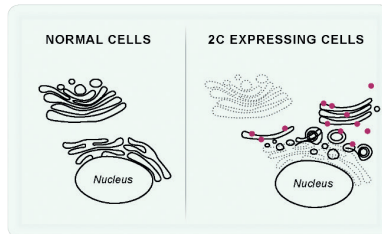
Key-features of 2C



Crystal Structure

Function 1 ATP^{ase} dependent helicase

Function 2 Membrane rearrangement



Function 3 Encapsidation

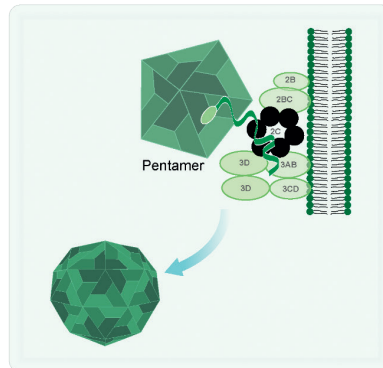


Figure 4. The non-structural protein 2C and its multiple functions. Schematic representation of the 2C protein and the functional domains. The ATPase domain is highlighted in blue with the catalytic sites in green. The zinc finger domain is highlighted in yellow and the C-terminal domain in red. The crystal structure of EV-A71 2C PDB: 5GRB, chain A was used to highlight the important functional domains within the crystal structure. Main functions of the 2C protein are shown in the boxes.

Shortly after the structure of EV-A71 2c and the crystal structure of the corresponding poliovirus 2C fragment were published.¹²⁶ As bioinformatically proposed, the crystal structures consist of three subdomains, an ATPase domain, a zinc finger domain and a long protruding C-terminal alpha helix. (figure). The crystal packing revealed a C-terminal oligomerization mechanism in which the C-terminus of a monomer dips into a pocket in the adjacent monomer in order to oligomerize. The ATP binding consists of a bipartite ATP binding site that requires elements from two adjacent 2C molecules to coordinate ATP.

This crystal structure provided valuable insight into the structure-function relationship. In this thesis, the crystal structure helped to provide initial insight into the mode-of-action of 2C inhibitors. Furthermore, it was instrumental for *de-novo* drug development of 2C inhibitors.

5. Antiviral drug development against EVs

Antiviral drug discovery is an inventive process of designing or discovering new chemical compounds, which are capable of inhibiting viruses. Despite the fact that picornaviruses have a huge clinical impact causing a wide variety of diseases, tools to combat infections are limited. Vaccines are available against PV and recently, China approved inactivated vaccines against EV-A71. There is no antiviral therapy licensed to treat EV infections and treatment is restricted to supportive care. Antiviral drug development can be split into two branches: direct-acting antivirals (DAA), which target viral proteins and host-targeting antivirals (HTA), which inhibit cellular host proteins important for the proliferation of viruses. The base of antiviral drug development is phenotypic screening of large compound libraries (Figure 5). This can be achieved in a cell-based system where virus replication leading to cell death is monitored. Alternatively, enzymatic functions of viral enzymes can be used for phenotypic screenings. Nowadays, automated high-throughput screening (HTPS) platforms can screen thousands if not millions of compounds per day. Advances in the field of structural biology fueled the development of structure-based drug discovery (SBDD) (Figure 5). This method uses the information of three-dimensional structures of a biological target for drug discovery process. An alternative is ligand-based drug discovery (LBDD) which uses the knowledge of known ligands for a certain target protein. *De-novo* drug discovery is a costly and lengthy process with very low probability of success. Compounds identified by the aforementioned approaches can be further improved by hit-to-lead optimizations by medicinal chemistry. Drug repurposing (also called drug repositioning, re-profiling or re-tasking) is an emerging strategy to identify promising candidates to open up new therapeutic avenues for counteracting viral infections. Each of the techniques are described below.

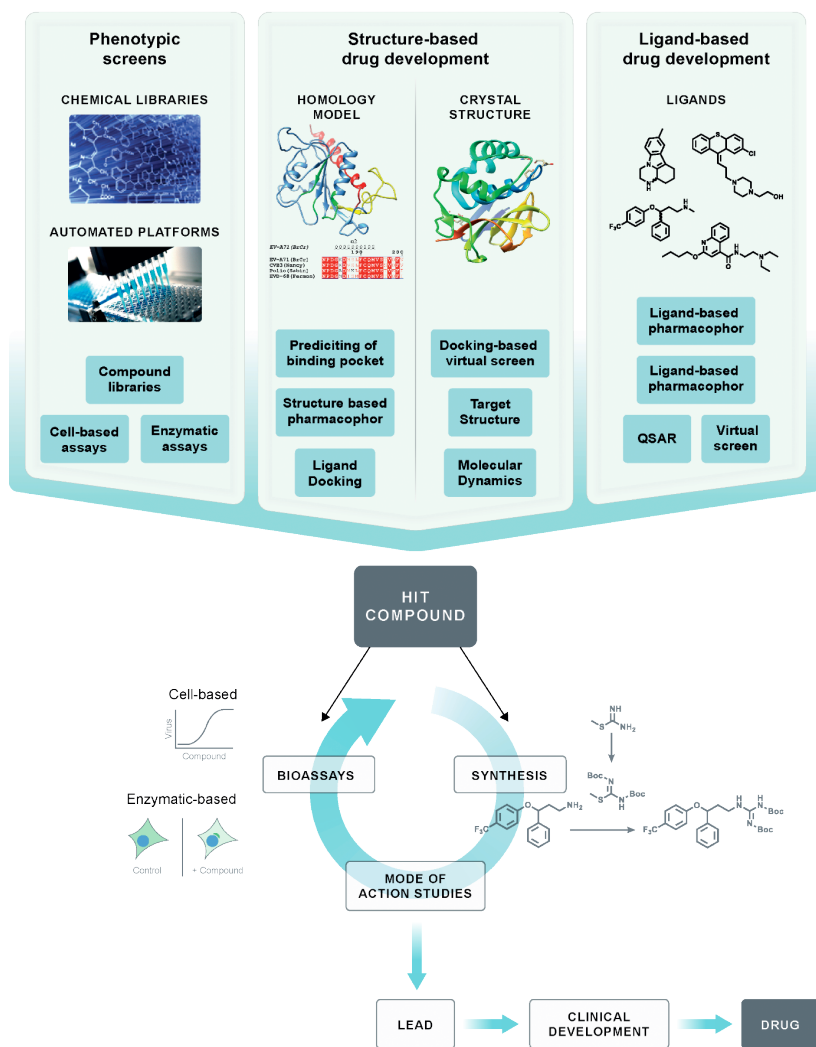


Figure 5. Drug development strategies. The goal of phenotypic screening is to identify potential hit compounds which are derived from chemical libraries. These screening platforms can be automated and are either cell-based assays or enzymatic assays. Depending on the availability of structural information, either a structure-based approach (middle panel) or a ligand-based approach (right panel) is used. These screening methods allow the identification of hit compounds. Optimization of these compounds is often followed by several cycles of lead optimization. Lead compounds are tested *in vivo* to identify drug candidates.

Phenotypic Screenings

Historically, most drugs including antivirals have been discovered by compound library screens. This method identifies small molecules, which are capable of altering a cell's phenotype. The first step relies on assay development (cell-based assays, enzymatic assays, etc.). These assays should monitor phenotypes such as cell death of host cells or enzymatic activities of recombinant viral proteins in a simple and efficient manner. Afterwards, large compound libraries can be screened and this step is often assisted by automated robotic systems (reviewed in ^{127,128}).

One of the most employed assays to identify EV inhibitors is the cytopathic effect (CPE) reduction assay. Enteroviruses cause an observable CPE, apparent as rounding, detachment and eventually the dying of cells. Compounds, which inhibit the virus at any stage during its life cycle, will prevent CPE formation. A disadvantage of a CPE reduction assay is that mode-of-actions studies are necessary to elucidate the molecular target, which can be very difficult and time consuming. Mode-of-action studies can assist in optimizing lead compounds with medicinal chemistry in order to enhance its antiviral activity. The advantage of inhibitors, which are identified by enzymatic assays, is that the target is known. However, these compounds might not be able to enter the cell or metabolize very quickly.

Structure-based drug development

SBDD development relies on the knowledge of a protein structure of a drug target. 3D structures of biological targets are not always available for SBDD. To circumvent this problem homology models (HM) can be generated *in silico*. This computer assisted method builds 3D models of a protein with a known amino acids sequence. 3D HM of the query protein are built based on available 3D structures of evolutionary closely related proteins.¹²⁹ If the sequence identity is higher than 35%, an HM can be built from the homologues structure. As with all modelling techniques it has its limitations (e.g. HM cannot predict side chain positions with high accuracy) and it can be used to assist in SBDD. In this thesis HM were generated for the lipid shuttling proteins OSBP in **chapter 3** and for the enterovirus non-structural protein 2C in **chapters 4** and **6**.

The next important step is the identification of the binding site, which can be accommodated by a ligand. In an ideal situation, a co-crystal structure with its ligand is available which defines the binding site. Alternatively, mapping of already known resistance mutations or computational methods to reveal binding sites can assist in identifying possible binding pockets. Mapping of resistance mutations can pose the problem that mutations are sometimes distantly located from the actual binding site which can be misleading in predicting the binding site. *In silico* methods comprise several algorithms to find invaginations or tunnels in the proteins to predict binding sites. Molecular dynamic (MD) simulation can also be very helpful in predicting the stability of identified binding pockets.¹³⁰ MD simulations can predict the movement of atoms of a protein with its docked or co-crystallized ligand in a molecular environment over time. After the identification of a suitable binding pocket, virtual high-throughput

screens (vHTPS) of large commercially available small molecules can be performed in order to identify potential ligands.¹³¹ These ligands can then be verified *in silico* by molecular docking and visual inspections of the docked ligands. Docking and visual inspection of the ligands of the predicted binding site does not guarantee an inhibitory effect.¹³² Molecular docking refers to several algorithms which are able to position a ligand in a defined binding pocket and calculate specific binding affinities.¹³³ Docked ligands can then be further evaluated for their stability in a certain binding pocket by MD simulation. The ligands which are selected through vHTPS and visual inspection are then investigated for their biological activity.¹³⁴ Further hit-to-lead optimization through structure-activity relationship studies (SAR) can be used to better understand the molecule. Like all drug development avenues, SBDD also has its limitations. Rarely, very potent lead compounds are identified with vHTPS in comparison to phenotypic screening. Additionally, the false/positive rate of compounds which are identified through vHTPS is very high. Using HM instead of crystal structures increases the false/positive results even further.

Structure-guided fragment-based drug discovery (FBDD) emerged over the last 20 years as an additional approach to discover new lead compounds. It is an iterative process, which involves placing fragments (organic molecules, small in size with low molecular weight) together to identify new lead compounds. Rather than screening millions of compounds, FBDD has the advantage that only a small number of fragments are used for the screening.¹³⁵ A fragment is first evaluated for binding and then it can be combined with other fragments into a drug-like inhibitor.¹³⁶ A limitation of FBDD is that biochemical assays for fragment screening are often not suitable for high throughput screens. Additionally, small fragments very often have a low affinity with their targets which makes it hard to identify potential active fragments. Ideally, the identified fragment is co-crystallized with the target protein in order to place more fragments together to reach a drug-like molecule.

Ligand-based drug development

LBDD uses information of small molecules which interact with a certain target protein.¹³⁷ It facilitates the finding of similar pharmacologically active compounds and the improvement of already pharmacological active compounds. One popular approach for LGBB are SAR studies. This method enables to investigate the different chemical moieties of a certain ligand and its biological activity. LBDD also utilizes pharmacophore modelling. A pharmacophore is a description of electronic features of a macromolecule important for the interaction with a bioactive molecule. Pharmacophore features comprise hydrogen bonds, hydrogen bond acceptors, hydrophobic interactions and positive and negatively ionized areas. Alternatively, a shared feature of the pharmacophore model can also be built from several ligands targeting the same bioactive molecule. These pharmacophore models can further be used for screening of large small compound libraries *in silico* to identify novel ligands. As with SBDD, LBDD

also often identifies many false/positive compounds. Furthermore, it has the limitation that drugs with a similar mechanism are mostly identified with lower potency.

Drug repurposing

Drug repurposing (DR) is an alternative strategy to classical drug discovery. DR consists of giving “old dogs” a new indication by exploring new pathways and targets for therapeutic intervention. Exploiting a new activity for FDA-approved drugs can be achieved with empirical, systematic screening approaches. For example, commercially available libraries of FDA-approved drugs can be used to screen *in vitro* or *in silico* for new activities (e.g. phenotypic screenings against viruses, binding towards viral proteins, molecular docking, etc.). DR has several advantages over *de-novo* drug development. The clinical development can be accelerated because profound pharmacological and toxicology drug profiles are already available. This also reduces costs, especially when the preclinical trials can be skipped and the drug enters phase II clinical trial. Another advantage is that development risks are reduced since most compounds fail in preclinical trials because of toxicity issues. One of the limitations is that molecules which are identified by DR screens, cannot be further optimized by medicinal chemistry. Any changes in the chemical backbone of the compounds results in the loss of the advantage of drug repurposing. Furthermore, the effective concentrations which are needed for the antiviral effect are often higher than plasma concentrations in humans. DR is only feasible if the effective concentration for the new usage is similar to those of the original drug. For this thesis, the two FDA-approved antifungal itraconazole and the selective serotonin reuptake inhibitor fluoxetine were of particular interest in **chapter 3** and **chapters 4** and **5**, respectively.^{91,138,139}

Itraconazole. Itraconazole (Sporanox®) (ITZ) is an FDA-approved triazole antifungal used for the treatment of systemic and superficial fungal infections. The “azoles” antifungal class inhibits the activity of the fungal enzyme CYP51 (lanosterol 14a-demethylase) which catalyzes an important step in the ergosterol biosynthesis and thus, ITZ impairs fungal cell wall integrity.¹⁴⁰ Compounds containing a triazole ring have proven to be the most potent antifungals. The human CYP51 isoform and the related drug metabolizing enzyme CYP3A4 are also inhibited by ITZ.^{141,142}

Besides the antifungal activity, ITZ has a potent anticancer activity. Deregulation of the Hedgehog (Hh) signaling pathway is associated with cancer development. ITZ directly antagonizes Hh signaling presumably by binding the protein Smoothened.¹⁴³ Cancer growth also requires angiogenesis. ITZ has potent antiangiogenic properties thanks to inhibiting key mediators of angiogenesis. ITZ impairs VEGFR2 glycosylation, trafficking and signaling through a poorly understood mechanism.^{144,145} This hinders the binding of vascular endothelial growth factor (VEGF) to its receptor VEGF receptor 2 (VEGFR2) and thus, prevents angiogenesis in cancer development. Another important signaling pathway promoting angiogenesis relies on the mechanistic target of rapamycin (mTOR) pathway. Besides disrupting VEGF-signaling, ITZ also indirectly antagonizes mTOR signaling. mTOR inhibition is mediated by the dual inhibition of cholesterol trafficking

by targeting the cholesterol binding site of Nieman-Pick disease type C1 (NPC1) and the mitochondrial protein voltage-dependent anion channel 1 (VDAC-1).¹⁴⁶⁻¹⁴⁹

In drug repurposing screens, ITZ was identified as a broad-spectrum inhibitor of numerous viruses such as EVs, Cardioviruses and the Hepatitis C virus. The aforementioned targets did not explain the antiviral activity and the lipid shuttling protein OSBP which was identified as a novel ITZ target. Mode-of-action studies revealed that ITZ directly binds OSBP and prevents OSBP-mediated lipid exchange at membrane contact sites. In **chapter 3** we set out to elucidate the pharmacophore of ITZ underlying the antiviral activity.

Fluoxetine. The blockbuster drug Fluoxetine (Prozac®) was the first major breakthrough for the treatment of depression. It was the first licensed compound of the class of selective serotonin reuptake inhibitors (SSRI). The compound was first described in 1974 and it took 16 years to complete the development of fluoxetine hydrochloride (Prozac®; Eli Lilly) which resulted in the FDA-approval on the 29th December 1987.^{150,151} In general, the class of SSRIs inhibits the serotonin transport which increases the level of synaptic serotonin (5-hydroxytryptamine) which helps in regulating mood.^{152,153} Fluoxetine is licensed for the treatment of major depression disorders, obsessive compulsive disorders, panic disorders and can also be prescribed for depressive episodes associated with bipolar disorders. The side effects of fluoxetine comprise headaches, drowsiness, diarrhea, tremors, photosensitivity, weight loss and sexual dysfunction. Furthermore, fluoxetine carries the black label for increased risks of suicide.

Besides the antipsychotic function, fluoxetine has been seen in immunomodulatory functions and anticancer activity, however the underlying mechanisms are barely understood.¹⁵⁴⁻¹⁵⁶ Another novel activity of fluoxetine is the antiviral activity. Several drug repurposing screens identified fluoxetine and the metabolic product norfluoxetine as EV inhibitors by likely targeting the non-structural protein 2C.^{138,139,157} The *in vitro* screening paved the way for the successful off-label treatment of an immunocompromised child with chronic enterovirus induced encephalitis.¹⁵⁸ This result raised more awareness for fluoxetine as a unique antiviral in clinics. Besides the potent direct-acting antiviral activity against enteroviruses, fluoxetine was shown to inhibit Dengue virus and hepatitis C virus, both members of the *Flaviviridae* family. Unlike its direct-acting antiviral activity against enteroviruses, it likely acts as a host-targeted antiviral for flaviviruses.^{159,160}

6. Aim and outline of this thesis

Continuous discovery and development of new antiviral medications and vaccines are of great importance for global health. This process is particularly important for viruses without current therapy or circulating viruses that gained resistance towards existing antivirals. EV include many important human pathogens and are the causative agent of mild and more severe disease, which can require hospitalizations especially in small children and immunocompromised individuals. Currently, there are no antivirals licensed to treat EV infections. Over the decade, several direct-acting inhibitors have been developed. An overview of these inhibitors is given in **chapter 2**. In this thesis, we focused on the identification of potential new avenues for anti-EV drug development. In **chapter 2**, an overview of direct-acting and host-targeting inhibitors, including repurposed drugs, is given. One of these repurposed drugs is ITZ, which was identified as potent inhibitor of enterovirus replication by targeting the lipid shuttling protein OSBP. In **chapter 3**, we set out to investigate the important pharmacophoric properties responsible for the antiviral activity to decouple its different pharmacological activities in order to reduce possible side-effects. **chapter 4** provides new insight into the mode-of action of another repurposed drug, the SSRI fluoxetine which targets the enterovirus 2C protein. We used a combination of virological methods, biochemistry and computational modeling to investigate the stereochemistry. These studies resulted in the identification of a potential binding pocket in 2C. In **chapter 5**, we conducted a SAR study on fluoxetine to establish the pharmacophoric features underlying its antiviral activity. In **chapter 6**, we performed a SAR study to investigate the antiviral activity of the recently identified CV-B3 inhibitor N-(4-fluorobenzyl)-N-(4-methoxyphenyl)furan-2-carboxamide, which contains a chemical backbone that resembles that of fluoxetine. Further, we provided valuable insight into a common mechanism of resistance development in 2C towards 2C inhibitors. In **chapter 7**, the results of this thesis are summarized and their implications are discussed.

References

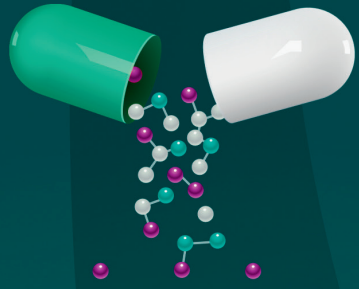
1. Loeffler, F. & Frosch, P. Summarischer Bericht über die Ergebnisse der Untersuchungen der Kommission zur Erforschung der Maul- und Klauenseuche bei dem Institut für Infektionskrankheiten in Berlin. *Centralblatt für Bakteriologie, Parasitenkunde und Infektionskrankheiten* 22, 257-259 (1897).
2. Loeffler, F. & Frosch, P. Berichte der Kommission zur Erforschung der Maul- und Klauenseuche bei dem Institut für Infektionskrankheiten in Berlin. *Centralblatt für Bakteriologie, Parasitenkunde und Infektionskrankheiten* 23, 371-391 (1898).
3. Landsteiner, K. & Popper, E. Übertragung der Poliomyelitis acuta auf Affen. *Z Immunitätsforsch* 2 377-390 (1909).
4. Zell, R. *et al.* ICTV Virus Taxonomy Profile: Picornaviridae. *J Gen Virol* 98, 2421-2422, doi:10.1099/jgv.0.000911 (2017).
5. Tapparel, C., Siegrist, F., Petty, T. J. & Kaiser, L. Picornavirus and enterovirus diversity with associated human diseases. *Infect Genet Evol* 14, 282-293, doi:10.1016/j.meegid.2012.10.016 (2013).
6. Racaniello, V. R. One hundred years of poliovirus pathogenesis. *Virology* 344, 9-16, doi:10.1016/j.virol.2005.09.015 (2006).
7. Chen, C. S. *et al.* Retrograde axonal transport: a major transmission route of enterovirus 71 in mice. *Journal of virology* 81, 8996-9003, doi:10.1128/JVI.00236-07 (2007).
8. Hixon, A. M., Clarke, P. & Tyler, K. L. Contemporary Circulating Enterovirus D68 Strains Infect and Undergo Retrograde Axonal Transport in Spinal Motor Neurons Independent of Sialic Acid. *Journal of virology* 93, doi:10.1128/JVI.00578-19 (2019).
9. Trevelyan, B., Smallman-Raynor, M. & Cliff, A. D. The Spatial Dynamics of Poliomyelitis in the United States: From Epidemic Emergence to Vaccine-Induced Retreat, 1910-1971. *Ann Assoc Am Geogr* 95, 269-293, doi:10.1111/j.1467-8306.2005.00460.x (2005).
10. Thornton, J. Polio returns to the Philippines. *Lancet* 394, 1217, doi:10.1016/S0140-6736(19)32263-9 (2019).
11. Yang, B. *et al.* Seroprevalence of Enterovirus 71 Antibody Among Children in China: A Systematic Review and Meta-analysis. *Pediatr Infect Dis J* 34, 1399-1406, doi:10.1097/INF.0000000000000900 (2015).
12. Chan, L. G. *et al.* Deaths of children during an outbreak of hand, foot, and mouth disease in sarawak, malaysia: clinical and pathological characteristics of the disease. For the Outbreak Study Group. *Clin Infect Dis* 31, 678-683, doi:10.1086/314032 (2000).
13. Ong, K. C. & Wong, K. T. Understanding Enterovirus 71 Neuropathogenesis and Its Impact on Other Neurotropic Enteroviruses. *Brain Pathol* 25, 614-624, doi:10.1111/bpa.12279 (2015).
14. Ooi, M. H., Wong, S. C., Lewthwaite, P., Cardoso, M. J. & Solomon, T. Clinical features, diagnosis, and management of enterovirus 71. *Lancet Neurol* 9, 1097-1105, doi:10.1016/S1474-4422(10)70209-X (2010).
15. Aw-Yong, K. L., NikNadia, N. M. N., Tan, C. W., Sam, I. C. & Chan, Y. F. Immune responses against enterovirus A71 infection: Implications for vaccine success. *Rev Med Virol* 29, e2073, doi:10.1002/rmv.2073 (2019).
16. Bowers, J. R. *et al.* Genomic Analyses of Acute Flaccid Myelitis Cases among a Cluster in Arizona Provide Further Evidence of Enterovirus D68 Role. *mBio* 10, doi:10.1128/mBio.02262-18 (2019).
17. Cassidy, H., Poelman, R., Knoester, M., Van Leer-Buter, C. C. & Niesters, H. G. M. Enterovirus D68 - The New Polio? *Front Microbiol* 9, 2677, doi:10.3389/fmicb.2018.02677 (2018).
18. Messacar, K. *et al.* A cluster of acute flaccid paralysis and cranial nerve dysfunction temporally associated with an outbreak of enterovirus D68 in children in Colorado, USA. *Lancet* 385, 1662-1671, doi:10.1016/S0140-6736(14)62457-0 (2015).
19. Kujawski, S. A. *et al.* Enterovirus D68-Associated Acute Respiratory Illness - New Vaccine Surveillance Network, United States, July-October, 2017 and 2018. *MMWR Morb Mortal Wkly Rep* 68, 277-280, doi:10.15585/mmwr.mm6812a1 (2019).
20. Schubert, R. D. *et al.* Pan-viral serology implicates enteroviruses in acute flaccid myelitis. *Nat Med* 25, 1748-1752, doi:10.1038/s41591-019-0613-1 (2019).
21. Mishra, N. *et al.* Antibodies to Enteroviruses in Cerebrospinal Fluid of Patients with Acute Flaccid Myelitis. *mBio* 10, doi:10.1128/mBio.01903-19 (2019).
22. Pons-Salort, M., Parker, E. P. & Grassly, N. C. The epidemiology of non-polio enteroviruses: recent advances and outstanding questions. *Curr Opin Infect Dis* 28, 479-487, doi:10.1097/QCO.000000000000187 (2015).
23. Kurokawa, M., Rai, S. K., Ono, K., Gurung, R. & Ruit, S. Viral investigation of acute hemorrhagic conjunctivitis outbreak (2003) in Nepal using molecular methods. *Southeast Asian J Trop Med Public Health* 37, 904-910 (2006).
24. Ghazali, O. *et al.* An outbreak of acute haemorrhagic conjunctivitis in Melaka, Malaysia. *Singapore Med J* 44, 511-516 (2003).
25. Kong, K. L. *et al.* Myocarditis Caused by Human Parechovirus in Adult. *Emerg Infect Dis* 23, 1571-1573, doi:10.3201/eid2309.161256 (2017).
26. Mizuta, K. *et al.* Epidemic myalgia in adults associated with human parechovirus type 3 infection, Yamagata, Japan, 2008. *Emerg Infect Dis* 18, 1787-1793, doi:10.3201/eid1811.111570 (2012).
27. Nishida, T. *et al.* Two cases of primary human parechovirus pneumonia in adults. *Respir Med Case Rep* 28, 100949, doi:10.1016/j.rmcr.2019.100949 (2019).
28. Reuter, G., Boros, A. & Pankovics, P. Kobuviruses - a comprehensive review. *Rev Med Virol* 21, 32-41, doi:10.1002/rmv.677 (2011).
29. Brahic, M., Bureau, J. F. & Michiels, T. The genetics of the persistent infection and demyelinating disease caused by Theiler's virus. *Annual review of microbiology* 59, 279-298, doi:10.1146/annurev.micro.59.030804.121242 (2005).
30. Carocci, M. & Bakkali-Kassimi, L. The encephalomyocarditis virus. *Virulence* 3, 351-367, doi:10.4161/viru.20573 (2012).
31. Helwig, F. C. & Schmidt, C. H. A Filter-Passing Agent Producing Interstitial Myocarditis in Anthropoid Apes and Small Animals. *Science* 102, 31-33, doi:10.1126/science.102.2637.31 (1945).
32. Knowles, N. J. *et al.* Molecular analysis of encephalomyocarditis viruses isolated from pigs and rodents in Italy. *Virus Res* 57, 53-62, doi:10.1016/s0168-1702(98)00081-1 (1998).
33. Love, R. J. & Grewal, A. S. Reproductive failure in pigs caused by encephalomyocarditis virus. *Aust Vet J* 63, 128-129, doi:10.1111/j.1751-0813.1986.tb07684.x (1986).
34. Koenen, F., De Clercq, K., Lefebvre, J. & Strobbe, R. Reproductive failure in sows following experimental infection with a Belgian EMCV isolate. *Vet Microbiol* 39, 111-116, doi:10.1016/0378-1135(94)90091-4 (1994).
35. Nielsen, A. C., Bottiger, B., Banner, J., Hoffmann, T. & Nielsen, L. P. Serious invasive Saffold virus infections in children, 2009. *Emerg Infect Dis* 18, 7-12, doi:10.3201/eid1801.110725 (2012).

36. Baggen, J., Thibaut, H. J., Strating, J. & van Kuppeveld, F. J. M. The life cycle of non-polio enteroviruses and how to target it. *Nat Rev Microbiol* 16, 368-381, doi:10.1038/s41579-018-0005-4 (2018).
37. Rossmann, M. G., He, Y. & Kuhn, R. J. Picornavirus-receptor interactions. *Trends in microbiology* 10, 324-331, doi:10.1016/s0966-842x(02)02383-1 (2002).
38. Krausslich, H. G., Nicklin, M. J., Toyoda, H., Etchison, D. & Wimmer, E. Poliovirus proteinase 2A induces cleavage of eucaryotic initiation factor 4F polypeptide p220. *Journal of virology* 61, 2711-2718 (1987).
39. Lloyd, R. E., Grubman, M. J. & Ehrenfeld, E. Relationship of p220 cleavage during picornavirus infection to 2A proteinase sequencing. *Journal of virology* 62, 4216-4223 (1988).
40. Joachims, M., Van Breugel, P. C. & Lloyd, R. E. Cleavage of poly(A)-binding protein by enterovirus proteases concurrent with inhibition of translation in vitro. *Journal of virology* 73, 718-727 (1999).
41. Lei, X., Xiao, X. & Wang, J. Innate Immunity Evasion by Enteroviruses: Insights into Virus-Host Interaction. *Viruses* 8, doi:10.3390/v8010022 (2016).
42. Goodfellow, I. *et al.* Identification of a cis-acting replication element within the poliovirus coding region. *Journal of virology* 74, 4590-4600, doi:10.1128/jvi.74.10.4590-4600.2000 (2000).
43. Rieder, E., Paul, A. V., Kim, D. W., van Boom, J. H. & Wimmer, E. Genetic and biochemical studies of poliovirus cis-acting replication element cre in relation to VPg uridylylation. *Journal of virology* 74, 10371-10380, doi:10.1128/jvi.74.22.10371-10380.2000 (2000).
44. Gerber, K., Wimmer, E. & Paul, A. V. Biochemical and genetic studies of the initiation of human rhinovirus 2 RNA replication: identification of a cis-replicating element in the coding sequence of 2A(pro). *Journal of virology* 75, 10979-10990, doi:10.1128/JVI.75.22.10979-10990.2001 (2001).
45. Yang, Y. *et al.* Sequence requirements for viral RNA replication and VPg uridylylation directed by the internal cis-acting replication element (cre) of human rhinovirus type 14. *Journal of virology* 76, 7485-7494, doi:10.1128/jvi.76.15.7485-7494.2002 (2002).
46. Jiang, P., Liu, Y., Ma, H. C., Paul, A. V. & Wimmer, E. Picornavirus morphogenesis. *Microbiol Mol Biol Rev* 78, 418-437, doi:10.1128/MMBR.00012-14 (2014).
47. Liu, Y. *et al.* Direct interaction between two viral proteins, the nonstructural protein 2C and the capsid protein VP3, is required for enterovirus morphogenesis. *PLoS pathogens* 6, e1001066, doi:10.1371/journal.ppat.1001066 (2010).
48. Sasaki, J. & Taniguchi, K. The 5'-end sequence of the genome of Aichi virus, a picornavirus, contains an element critical for viral RNA encapsidation. *Journal of virology* 77, 3542-3548 (2003).
49. Shakeel, S. *et al.* Genomic RNA folding mediates assembly of human parechovirus. *Nature communications* 8, 5, doi:10.1038/s41467-016-0011-z (2017).
50. Logan, G. *et al.* Deep Sequencing of Foot-and-Mouth Disease Virus Reveals RNA Sequences Involved in Genome Packaging. *Journal of virology* 92, doi:10.1128/JVI.01159-17 (2018).
51. Feng, Z. *et al.* A pathogenic picornavirus acquires an envelope by hijacking cellular membranes. *Nature* 496, 367-371, doi:10.1038/nature12029 (2013).
52. Chen, Y. H. *et al.* Phosphatidylserine vesicles enable efficient en bloc transmission of enteroviruses. *Cell* 160, 619-630, doi:10.1016/j.cell.2015.01.032 (2015).
53. Altan-Bonnet, N. & Balla, T. Phosphatidylinositol 4-kinases: hostages harnessed to build panviral replication platforms. *Trends in biochemical sciences* 37, 293-302, doi:10.1016/j.tibs.2012.03.004 (2012).
54. Kallman, F., Williams, R. C., Dulbecco, R. & Vogt, M. Fine structure of changes produced in cultured cells sampled at specified intervals during a single growth cycle of polio virus. *J Biophys Biochem Cytol* 4, 301-308, doi:10.1083/jcb.4.3.301 (1958).
55. Bienz, K., Egger, D., Rasser, Y. & Bossart, W. Kinetics and location of poliovirus macromolecular synthesis in correlation to virus-induced cytopathology. *Virology* 100, 390-399, doi:10.1016/0042-6822(80)90530-9 (1980).
56. Dales, S., Eggers, H. J., Tamm, I. & Palade, G. E. Electron Microscopic Study of the Formation of Poliovirus. *Virology* 26, 379-389, doi:10.1016/0042-6822(65)90001-2 (1965).
57. Limpens, R. W. *et al.* The transformation of enterovirus replication structures: a three-dimensional study of single- and double-membrane compartments. *mBio* 2, doi:10.1128/mBio.00166-11 (2011).
58. Belov, G. A. *et al.* Complex dynamic development of poliovirus membranous replication complexes. *Journal of virology* 86, 302-312, doi:10.1128/JVI.05937-11 (2012).
59. Belov, G. A. & Sztul, E. Rewiring of cellular membrane homeostasis by picornaviruses. *Journal of virology* 88, 9478-9489, doi:10.1128/JVI.00922-14 (2014).
60. Melia, C. E. *et al.* Origins of Enterovirus Replication Organelles Established by Whole-Cell Electron Microscopy. *mBio* 10, doi:10.1128/mBio.00951-19 (2019).
61. van Kuppeveld, F. J., Galama, J. M., Zoll, J., van den Hurk, P. J. & Melchers, W. J. Coxsackie B3 virus protein 2B contains cationic amphipathic helix that is required for viral RNA replication. *Journal of virology* 70, 3876-3886 (1996).
62. Paul, A. V., Molla, A. & Wimmer, E. Studies of a putative amphipathic helix in the N-terminus of poliovirus protein 2C. *Virology* 199, 188-199, doi:10.1006/viro.1994.1111 (1994).
63. Echeverri, A. C. & Dasgupta, A. Amino terminal regions of poliovirus 2C protein mediate membrane binding. *Virology* 208, 540-553, doi:10.1006/viro.1995.1185 (1995).
64. Towner, J. S., Ho, T. V. & Semler, B. L. Determinants of membrane association for poliovirus protein 3AB. *The Journal of biological chemistry* 271, 26810-26818, doi:10.1074/jbc.271.43.26810 (1996).
65. Teterina, N. L., Gorbalenya, A. E., Egger, D., Bienz, K. & Ehrenfeld, E. Poliovirus 2C protein determinants of membrane binding and rearrangements in mammalian cells. *Journal of virology* 71, 8962-8972 (1997).
66. Teterina, N. L. *et al.* Testing the modularity of the N-terminal amphipathic helix conserved in picornavirus 2C proteins and hepatitis C NS5A protein. *Virology* 344, 453-467, doi:10.1016/j.virol.2005.08.044 (2006).
67. Agirre, A., Barco, A., Carrasco, L. & Nieva, J. L. Viroporin-mediated membrane permeabilization. Pore formation by nonstructural poliovirus 2B protein. *The Journal of biological chemistry* 277, 40434-40441, doi:10.1074/jbc.M205393200 (2002).
68. van Kuppeveld, F. J., de Jong, A. S., Melchers, W. J. & Willems, P. H. Enterovirus protein 2B po(u)res out the calcium: a viral strategy to survive? *Trends in microbiology* 13, 41-44, doi:10.1016/j.tim.2004.12.005 (2005).
69. Aldabe, R. & Carrasco, L. Induction of membrane proliferation by poliovirus proteins 2C and 2BC. *Biochem Biophys Res Commun* 206, 64-76, doi:10.1006/bbrc.1995.1010 (1995).
70. Banerjee, R., Tsai, W., Kim, W. & Dasgupta, A. Interaction of poliovirus-encoded 2C/2BC polypeptides with the 3' terminus negative-strand cloverleaf requires an intact stem-loop b. *Virology* 280, 41-51, doi:10.1006/viro.2000.0770 (2001).

71. Cho, M. W., Teterina, N., Egger, D., Bienz, K. & Ehrenfeld, E. Membrane rearrangement and vesicle induction by recombinant poliovirus 2C and 2BC in human cells. *Virology* 202, 129-145, doi:10.1006/viro.1994.1329 (1994).
72. Suhy, D. A., Giddings, T. H., Jr. & Kirkegaard, K. Remodeling the endoplasmic reticulum by poliovirus infection and by individual viral proteins: an autophagy-like origin for virus-induced vesicles. *Journal of virology* 74, 8953-8965 (2000).
73. D'Angelo, G., Vicinanza, M., Di Campli, A. & De Matteis, M. A. The multiple roles of PtdIns(4)P -- not just the precursor of PtdIns(4,5)P2. *Journal of cell science* 121, 1955-1963, doi:10.1242/jcs.023630 (2008).
74. Klima, M. *et al.* Structural insights and in vitro reconstitution of membrane targeting and activation of human PI4KB by the ACBD3 protein. *Scientific reports* 6, 23641, doi:10.1038/srep23641 (2016).
75. Hsu, N. Y. *et al.* Viral reorganization of the secretory pathway generates distinct organelles for RNA replication. *Cell* 141, 799-811, doi:10.1016/j.cell.2010.03.050 (2010).
76. van der Schaar, H. M. *et al.* A novel, broad-spectrum inhibitor of enterovirus replication that targets host cell factor phosphatidylinositol 4-kinase IIIbeta. *Antimicrobial agents and chemotherapy* 57, 4971-4981, doi:10.1128/AAC.01175-13 (2013).
77. Lyoo, H. *et al.* ACBD3 Is an Essential Pan-enterovirus Host Factor That Mediates the Interaction between Viral 3A Protein and Cellular Protein PI4KB. *mBio* 10, doi:10.1128/mBio.02742-18 (2019).
78. van der Schaar, H. M., Dorobantu, C. M., Albulescu, L., Strating, J. R. & van Kuppeveld, F. J. Fat(al) attraction: Picornaviruses Usurp Lipid Transfer at Membrane Contact Sites to Create Replication Organelles. *Trends in microbiology* 24, 535-546, doi:10.1016/j.tim.2016.02.017 (2016).
79. Dorobantu, C. M. *et al.* Modulation of the Host Lipid Landscape to Promote RNA Virus Replication: The Picornavirus Encephalomyocarditis Virus Converges on the Pathway Used by Hepatitis C Virus. *PLoS pathogens* 11, e1005185, doi:10.1371/journal.ppat.1005185 (2015).
80. Olkkonen, V. M. & Li, S. Oxysterol-binding proteins: sterol and phosphoinositide sensors coordinating transport, signaling and metabolism. *Progress in lipid research* 52, 529-538, doi:10.1016/j.plipres.2013.06.004 (2013).
81. Raiborg, C., Wenzel, E. M. & Stenmark, H. ER-endosome contact sites: molecular compositions and functions. *EMBO J* 34, 1848-1858, doi:10.15252/embj.201591481 (2015).
82. De Matteis, M. A. & Rega, L. R. Endoplasmic reticulum-Golgi complex membrane contact sites. *Current opinion in cell biology* 35, 43-50, doi:10.1016/j.ceb.2015.04.001 (2015).
83. Bigay, J. & Antonny, B. Curvature, lipid packing, and electrostatics of membrane organelles: defining cellular territories in determining specificity. *Developmental cell* 23, 886-895, doi:10.1016/j.devcel.2012.10.009 (2012).
84. Janmey, P. A. & Kinnunen, P. K. Biophysical properties of lipids and dynamic membranes. *Trends in cell biology* 16, 538-546, doi:10.1016/j.tcb.2006.08.009 (2006).
85. Ikonen, E. Cellular cholesterol trafficking and compartmentalization. *Nature reviews. Molecular cell biology* 9, 125-138, doi:10.1038/nrm2336 (2008).
86. Holthuis, J. C. & Menon, A. K. Lipid landscapes and pipelines in membrane homeostasis. *Nature* 510, 48-57, doi:10.1038/nature13474 (2014).
87. Jansen, M. *et al.* Role of ORPs in sterol transport from plasma membrane to ER and lipid droplets in mammalian cells. *Traffic* 12, 218-231, doi:10.1111/j.1600-0854.2010.01142.x (2011).
88. Moser von Filseck, J., Mesmin, B., Bigay, J., Antonny, B. & Drin, G. Building lipid 'PI-Pipelines' throughout the cell by ORP/Osh proteins. *Biochemical Society transactions* 42, 1465-1470, doi:10.1042/BST20140143 (2014).
89. Mesmin, B. *et al.* A four-step cycle driven by PI(4)P hydrolysis directs sterol/PI(4)P exchange by the ER-Golgi tether OSBP. *Cell* 155, 830-843, doi:10.1016/j.cell.2013.09.056 (2013).
90. Antonny, B., Bigay, J. & Mesmin, B. The Oxysterol-Binding Protein Cycle: Burning Off PI(4)P to Transport Cholesterol. *Annual review of biochemistry* 87, 809-837, doi:10.1146/annurev-biochem-061516-044924 (2018).
91. Strating, J. R. *et al.* Itraconazole inhibits enterovirus replication by targeting the oxysterol-binding protein. *Cell reports* 10, 600-615, doi:10.1016/j.celrep.2014.12.054 (2015).
92. Roulin, P. S. *et al.* Rhinovirus uses a phosphatidylinositol 4-phosphate/cholesterol counter-current for the formation of replication compartments at the ER-Golgi interface. *Cell host & microbe* 16, 677-690, doi:10.1016/j.chom.2014.10.003 (2014).
93. Arita, M. *et al.* Oxysterol-binding protein family I is the target of minor enviroxime-like compounds. *Journal of virology* 87, 4252-4260, doi:10.1128/JVI.03546-12 (2013).
94. Laufman, O., Perrino, J. & Andino, R. Viral Generated Inter-Organelle Contacts Redirect Lipid Flux for Genome Replication. *Cell* 178, 275-289 e216, doi:10.1016/j.cell.2019.05.030 (2019).
95. Ilnytska, O. *et al.* Enteroviruses harness the cellular endocytic machinery to remodel the host cell cholesterol landscape for effective viral replication. *Cell host & microbe* 14, 281-293, doi:10.1016/j.chom.2013.08.002 (2013).
96. Albulescu, L., Wubbolts, R., van Kuppeveld, F. J. & Strating, J. R. Cholesterol shuttling is important for RNA replication of coxsackievirus B3 and encephalomyocarditis virus. *Cellular microbiology*, doi:10.1111/cmi.12425 (2015).
97. Lim, C. Y. *et al.* ER-lysosome contacts enable cholesterol sensing by mTORC1 and drive aberrant growth signalling in Niemann-Pick type C. *Nat Cell Biol* 21, 1206-1218, doi:10.1038/s41556-019-0391-5 (2019).
98. Reiss, S. *et al.* Recruitment and activation of a lipid kinase by hepatitis C virus NS5A is essential for integrity of the membranous replication compartment. *Cell host & microbe* 9, 32-45, doi:10.1016/j.chom.2010.12.002 (2011).
99. Berger, K. L. *et al.* Roles for endocytic trafficking and phosphatidylinositol 4-kinase III alpha in hepatitis C virus replication. *Proceedings of the National Academy of Sciences of the United States of America* 106, 7577-7582, doi:10.1073/pnas.0902693106 (2009).
100. Borawski, J. *et al.* Class III phosphatidylinositol 4-kinase alpha and beta are novel host factor regulators of hepatitis C virus replication. *Journal of virology* 83, 10058-10074, doi:10.1128/JVI.02418-08 (2009).
101. Li, J. P. & Baltimore, D. An intragenic revertant of a poliovirus 2C mutant has an uncoating defect. *Journal of virology* 64, 1102-1107 (1990).
102. Pincus, S. E. & Wimmer, E. Production of guanidine-resistant and -dependent poliovirus mutants from cloned cDNA: mutations in polypeptide 2C are directly responsible for altered guanidine sensitivity. *Journal of virology* 60, 793-796 (1986).
103. Pincus, S. E., Diamond, D. C., Emini, E. A. & Wimmer, E. Guanidine-selected mutants of poliovirus: mapping of point mutations to polypeptide 2C. *Journal of virology* 57, 638-646 (1986).
104. Li, J. P. & Baltimore, D. Isolation of poliovirus 2C mutants defective in viral RNA synthesis. *Journal of virology* 62, 4016-4021 (1988).

105. Tolskaya, E. A. *et al.* Genetic studies on the poliovirus 2C protein, an NTPase. A plausible mechanism of guanidine effect on the 2C function and evidence for the importance of 2C oligomerization. *J Mol Biol* 236, 1310-1323 (1994).
106. Barton, D. J. & Flanagan, J. B. Synchronous replication of poliovirus RNA: initiation of negative-strand RNA synthesis requires the guanidine-inhibited activity of protein 2C. *Journal of virology* 71, 8482-8489 (1997).
107. Tang, W. F. *et al.* Reticulon 3 binds the 2C protein of enterovirus 71 and is required for viral replication. *The Journal of biological chemistry* 282, 5888-5898, doi:10.1074/jbc.M611145200 (2007).
108. Wang, J., Wu, Z. & Jin, Q. COPI is required for enterovirus 71 replication. *PLoS One* 7, e38035, doi:10.1371/journal.pone.0038035 (2012).
109. Asare, E., Mugavero, J., Jiang, P., Wimmer, E. & Paul, A. V. A Single Amino Acid Substitution in Poliovirus Nonstructural Protein 2CATPase Causes Conditional Defects in Encapsidation and Uncoating. *Journal of virology* 90, 6174-6186, doi:10.1128/JVI.02877-15 (2016).
110. Zheng, Z. *et al.* Enterovirus 71 2C protein inhibits TNF-alpha-mediated activation of NF-kappaB by suppressing IkkappaB kinase beta phosphorylation. *J Immunol* 187, 2202-2212, doi:10.4049/jimmunol.1100285 (2011).
111. Du, H. *et al.* Enterovirus 71 2C Protein Inhibits NF-kappaB Activation by Binding to RelA(p65). *Scientific reports* 5, 14302, doi:10.1038/srep14302 (2015).
112. Gorbalenya, A. E., Koonin, E. V. & Wolf, Y. I. A new superfamily of putative NTP-binding domains encoded by genomes of small DNA and RNA viruses. *FEBS Lett* 262, 145-148, doi:10.1016/0014-5793(90)80175-i (1990).
113. Teterina, N. L., Kean, K. M., Gorbalenya, A. E., Agol, V. I. & Girard, M. Analysis of the functional significance of amino acid residues in the putative NTP-binding pattern of the poliovirus 2C protein. *J Gen Virol* 73 (Pt 8), 1977-1986, doi:10.1099/0022-1317-73-8-1977 (1992).
114. Rodriguez, P. L. & Carrasco, L. Poliovirus protein 2C has ATPase and GTPase activities. *The Journal of biological chemistry* 268, 8105-8110 (1993).
115. Pfister, T. & Wimmer, E. Characterization of the nucleoside triphosphatase activity of poliovirus protein 2C reveals a mechanism by which guanidine inhibits poliovirus replication. *The Journal of biological chemistry* 274, 6992-7001 (1999).
116. Klein, M., Eggers, H. J. & Nelsen-Salz, B. Echovirus 9 strain barty non-structural protein 2C has NTPase activity. *Virus Res* 65, 155-160 (1999).
117. Xia, H. *et al.* Human Enterovirus Nonstructural Protein 2CATPase Functions as Both an RNA Helicase and ATP-Independent RNA Chaperone. *PLoS pathogens* 11, e1005067, doi:10.1371/journal.ppat.1005067 (2015).
118. Singleton, M. R., Dillingham, M. S. & Wigley, D. B. Structure and mechanism of helicases and nucleic acid translocases. *Annual review of biochemistry* 76, 23-50, doi:10.1146/annurev.biochem.76.052305.115300 (2007).
119. Abbate, E. A., Berger, J. M. & Botchan, M. R. The X-ray structure of the papillomavirus helicase in complex with its molecular matchmaker E2. *Genes Dev* 18, 1981-1996, doi:10.1101/gad.1220104 (2004).
120. Li, D. *et al.* Structure of the replicative helicase of the oncoprotein SV40 large tumour antigen. *Nature* 423, 512-518, doi:10.1038/nature01691 (2003).
121. Banerjee, R., Echeverri, A. & Dasgupta, A. Poliovirus-encoded 2C polypeptide specifically binds to the 3'-terminal sequences of viral negative-strand RNA. *Journal of virology* 71, 9570-9578 (1997).
122. Sweeney, T. R. *et al.* Foot-and-mouth disease virus 2C is a hexameric AAA+ protein with a coordinated ATP hydrolysis mechanism. *The Journal of biological chemistry* 285, 24347-24359, doi:10.1074/jbc.M110.129940 (2010).
123. Adams, P., Kandiah, E., Effantin, G., Steven, A. C. & Ehrenfeld, E. Poliovirus 2C protein forms homo-oligomeric structures required for ATPase activity. *The Journal of biological chemistry* 284, 22012-22021, doi:10.1074/jbc.M109.031807 (2009).
124. Papageorgiou, N. *et al.* The 2C putative helicase of echovirus 30 adopts a hexameric ring-shaped structure. *Acta Crystallogr D Biol Crystallogr* 66, 1116-1120, doi:10.1107/S090744491002809X (2010).
125. Guan, H. *et al.* Crystal structure of 2C helicase from enterovirus 71. *Sci Adv* 3, e1602573, doi:10.1126/sciadv.1602573 (2017).
126. Guan, H., Tian, J., Zhang, C., Qin, B. & Cui, S. Crystal structure of a soluble fragment of poliovirus 2CATPase. *PLoS pathogens* 14, e1007304, doi:10.1371/journal.ppat.1007304 (2018).
127. Terstappen, G. C., Schlupen, C., Raggiaschi, R. & Gaviraghi, G. Target deconvolution strategies in drug discovery. *Nat Rev Drug Discov* 6, 891-903, doi:10.1038/nrd2410 (2007).
128. Kubota, K., Funabashi, M. & Ogura, Y. Target deconvolution from phenotype-based drug discovery by using chemical proteomics approaches. *Biochim Biophys Acta Proteom Proteom* 1867, 22-27, doi:10.1016/j.bbapap.2018.08.002 (2019).
129. Cavasotto, C. N. & Phatak, S. S. Homology modeling in drug discovery: current trends and applications. *Drug Discov Today* 14, 676-683, doi:10.1016/j.drudis.2009.04.006 (2009).
130. Aminpour, M., Montemagno, C. & Tuszynski, J. A. An Overview of Molecular Modeling for Drug Discovery with Specific Illustrative Examples of Applications. *Molecules* 24, doi:10.3390/molecules24091693 (2019).
131. Hospital, A., Goni, J. R., Orozco, M. & Gelpi, J. L. Molecular dynamics simulations: advances and applications. *Adv Appl Bioinform Chem* 8, 37-47, doi:10.2147/AABC.S70333 (2015).
132. Lounnas, V. *et al.* Current progress in Structure-Based Rational Drug Design marks a new mindset in drug discovery. *Comput Struct Biotechnol J* 5, e201302011, doi:10.5936/cs bj.201302011 (2013).
133. Sliwoski, G., Kothiwale, S., Meiler, J. & Lowe, E. W., Jr. Computational methods in drug discovery. *Pharmacol Rev* 66, 334-395, doi:10.1124/pr.112.007336 (2014).
134. Meng, X. Y., Zhang, H. X., Mezei, M. & Cui, M. Molecular docking: a powerful approach for structure-based drug discovery. *Curr Comput Aided Drug Des* 7, 146-157, doi:10.2174/157340911795677602 (2011).
135. Murray, C. W. & Rees, D. C. The rise of fragment-based drug discovery. *Nat Chem* 1, 187-192, doi:10.1038/nchem.217 (2009).
136. Wasko, M. J., Pellegrine, K. A., Madura, J. D. & Surratt, C. K. A Role for Fragment-Based Drug Design in Developing Novel Lead Compounds for Central Nervous System Targets. *Front Neural* 6, 197, doi:10.3389/fneur.2015.00197 (2015).
137. Wolber, G., Dornhofer, A. A. & Langer, T. Efficient overlay of small organic molecules using 3D pharmacophores. *J Comput Aided Mol Des* 20, 773-788, doi:10.1007/s10822-006-9078-7 (2006).
138. Ulferts, R. *et al.* Selective serotonin reuptake inhibitor fluoxetine inhibits replication of human enteroviruses B and D by targeting viral protein 2C. *Antimicrobial agents and chemotherapy* 57, 1952-1956, doi:10.1128/AAC.02084-12 (2013).
139. Zuo, J. *et al.* Fluoxetine Is a Potent Inhibitor of Coxsackievirus Replication. *Antimicrobial agents and chemotherapy* 56, 4838-4844, doi:10.1128/Aac.00983-12 (2012).

140. Lestner, J. & Hope, W. W. Itraconazole: an update on pharmacology and clinical use for treatment of invasive and allergic fungal infections. *Expert opinion on drug metabolism & toxicology* 9, 911-926, doi:10.1517/17425255.2013.794785 (2013).
141. Lamb, D. C. *et al.* Characteristics of the heterologously expressed human lanosterol 14 α -demethylase (other names: P45014DM, CYP51, P45051) and inhibition of the purified human and *Candida albicans* CYP51 with azole antifungal agents. *Yeast* 15, 755-763, doi:10.1002/(SICI)1097-0061(19990630)15:9<755::AID-YEA417>3.0.CO;2-8 (1999).
142. Trosken, E. R. *et al.* Comparison of lanosterol-14 α -demethylase (CYP51) of human and *Candida albicans* for inhibition by different antifungal azoles. *Toxicology* 228, 24-32, doi:10.1016/j.tox.2006.08.007 (2006).
143. Kim, J. *et al.* Itraconazole, a commonly used antifungal that inhibits Hedgehog pathway activity and cancer growth. *Cancer cell* 17, 388-399, doi:10.1016/j.ccr.2010.02.027 (2010).
144. Nacev, B. A., Grassi, P., Dell, A., Haslam, S. M. & Liu, J. O. The antifungal drug itraconazole inhibits vascular endothelial growth factor receptor 2 (VEGFR2) glycosylation, trafficking, and signaling in endothelial cells. *The Journal of biological chemistry* 286, 44045-44056, doi:10.1074/jbc.M111.278754 (2011).
145. Shi, W. *et al.* Itraconazole side chain analogues: structure-activity relationship studies for inhibition of endothelial cell proliferation, vascular endothelial growth factor receptor 2 (VEGFR2) glycosylation, and hedgehog signaling. *Journal of medicinal chemistry* 54, 7363-7374, doi:10.1021/jm200944b (2011).
146. Head, S. A. *et al.* Simultaneous Targeting of NPC1 and VDAC1 by Itraconazole Leads to Synergistic Inhibition of mTOR Signaling and Angiogenesis. *ACS chemical biology* 12, 174-182, doi:10.1021/acscchembio.6b00849 (2017).
147. Head, S. A. *et al.* Antifungal drug itraconazole targets VDAC1 to modulate the AMPK/mTOR signaling axis in endothelial cells. *Proceedings of the National Academy of Sciences of the United States of America* 112, E7276-7285, doi:10.1073/pnas.1512867112 (2015).
148. Trinh, M. N. *et al.* Triazoles inhibit cholesterol export from lysosomes by binding to NPC1. *Proceedings of the National Academy of Sciences of the United States of America* 114, 89-94, doi:10.1073/pnas.1619571114 (2017).
149. Xu, J., Dang, Y., Ren, Y. R. & Liu, J. O. Cholesterol trafficking is required for mTOR activation in endothelial cells. *Proceedings of the National Academy of Sciences of the United States of America* 107, 4764-4769, doi:10.1073/pnas.0910872107 (2010).
150. Fuller, R. W., Perry, K. W. & Molloy, B. B. Effect of an uptake inhibitor on serotonin metabolism in rat brain: studies with 3-(p-trifluoromethylphenoxy)-N-methyl-3-phenylpropylamine (Lilly 110140). *Life Sci* 15, 1161-1171, doi:10.1016/s0024-3205(74)80012-3 (1974).
151. Wong, D. T., Horng, J. S., Bymaster, F. P., Hauser, K. L. & Molloy, B. B. A selective inhibitor of serotonin uptake: Lilly 110140, 3-(p-trifluoromethylphenoxy)-N-methyl-3-phenylpropylamine. *Life Sci* 15, 471-479, doi:10.1016/0024-3205(74)90345-2 (1974).
152. Perez-Caballero, L., Torres-Sanchez, S., Bravo, L., Mico, J. A. & Berrococo, E. Fluoxetine: a case history of its discovery and preclinical development. *Expert Opin Drug Discov* 9, 567-578, doi:10.1517/17460441.2014.907790 (2014).
153. Wong, D. T., Perry, K. W. & Bymaster, F. P. Case history: the discovery of fluoxetine hydrochloride (Prozac). *Nat Rev Drug Discov* 4, 764-774, doi:10.1038/nrd1821 (2005).
154. Di Rosso, M. E., Palumbo, M. L. & Genaro, A. M. Immunomodulatory effects of fluoxetine: A new potential pharmacological action for a classic antidepressant drug? *Pharmacol Res* 109, 101-107, doi:10.1016/j.phrs.2015.11.021 (2016).
155. Di Rosso, M. E., Sterle, H. A., Cremaschi, G. A. & Genaro, A. M. Beneficial Effect of Fluoxetine and Sertraline on Chronic Stress-Induced Tumor Growth and Cell Dissemination in a Mouse Model of Lymphoma: Crucial Role of Antitumor Immunity. *Front Immunol* 9, 1341, doi:10.3389/fimmu.2018.01341 (2018).
156. Zhuo, C. *et al.* Surprising Anticancer Activities of Psychiatric Medications: Old Drugs Offer New Hope for Patients With Brain Cancer. *Front Pharmacol* 10, 1262, doi:10.3389/fphar.2019.01262 (2019).
157. Ulferts, R. *et al.* Screening of a library of FDA-approved drugs identifies several enterovirus replicaton inhibitors that target viral protein 2C. *Antimicrobial agents and chemotherapy*, doi:10.1128/AAC.02182-15 (2016).
158. Gofshteyn, J., Cardenas, A. M. & Bearden, D. Treatment of Chronic Enterovirus Encephalitis With Fluoxetine in a Patient With X-Linked Agammaglobulinemia. *Pediatr Neurol*, doi:10.1016/j.pediatrneurol.2016.06.014 (2016).
159. Medigeshi, G. R., Kumar, R., Dhamija, E., Agrawal, T. & Kar, M. N-Desmethylclozapine, Fluoxetine, and Salmeterol Inhibit Postentry Stages of the Dengue Virus Life Cycle. *Antimicrobial agents and chemotherapy* 60, 6709-6718, doi:10.1128/AAC.01367-16 (2016).
160. Young, K. C. *et al.* Fluoxetine a novel anti-hepatitis C virus agent via ROS-, JNK-, and PPARbeta/gamma-dependent pathways. *Antiviral research* 110, 158-167, doi:10.1016/j.antiviral.2014.08.002 (2014).



Chapter

Direct-acting antivirals and host-targeting strategies to combat enterovirus infection

2

Lisa Bauer^{1,*}, Heyrhyoung Lyoo^{1,*}, Hilde M. van der Schaar¹, Jeroen R.P.M. Strating¹, and Frank J.M. van Kuppeveld^{1,#}

¹Department of Infectious Diseases & Immunology, Virology Division, Faculty of Veterinary Medicine, Utrecht University, Utrecht, The Netherlands

*These authors contributed equally

Corresponding author

Current Opinion in Virology, 2017, 24, 1-8

Abstract

Enteroviruses (e.g. poliovirus, enterovirus-A71, coxsackievirus, enterovirus-D68, rhinovirus) are a large and important group of human pathogens that can cause a variety of mild and more severe diseases, especially in young children. Unfortunately, no (broad-range) antiviral drugs to treat enterovirus infections have been approved yet. Intensive research over the past decades has resulted in several direct-acting inhibitors, including capsid binders that interfere with virus entry and inhibitors of viral enzymes (protease, polymerase, and helicase) required for genome replication. In addition, host-targeting inhibitors with potential broad-spectrum activity have been identified. Furthermore, drug repurposing screens have recently uncovered promising new inhibitors with disparate viral and host targets. Together, these findings raise hope for the development of (broad-range) antiviral drugs against enteroviruses.

Highlights

- Capsids and viral enzymes are promising targets for direct-acting antiviral therapy
- Fundamental research has unveiled host factors for broad-spectrum drug development
- Drug repurposing screens have yielded new promising enterovirus inhibitors

Introduction

The Picornaviridae constitutes one of the largest families of positive-stranded RNA (+RNA) viruses, currently consisting of 31 genera. The genus Enterovirus, which is by far the largest genus, comprises many human pathogens, including poliovirus, coxsackievirus, echoviruses, numbered enteroviruses, and rhinovirus. Infections with non-polio enteroviruses can result in a wide variety of symptoms, including hand-foot-and-mouth disease, conjunctivitis, aseptic meningitis, severe neonatal sepsis-like disease and acute flaccid paralysis, whereas infections with rhinoviruses cause the common cold as well as exacerbations of asthma and COPD (reviewed in¹). Vaccines are available against poliovirus and enterovirus-A71. Development of vaccines against all enteroviruses seems unfeasible, given the large number of (sero)types (i.e. >100 non-polio enteroviruses, and >150 rhinoviruses). Hence, there is a great need for (broad-acting) antivirals against enteroviruses. Here, we will review the recent efforts to develop direct-acting antivirals as well as host factor-targeting inhibitors to treat enterovirus infections (Table 1).

Table 1. Overview of directing-acting or host-targeting inhibitors discussed in this review.

Type of inhibitors		Compounds
Capsid binder		Pirodavir ^[5] , Pleconaril ^[5] , Pocopavir ^[5] , Vapendavir ^[5]
3C ^{pro} inhibitor	peptidic mimetic	Rupintrivir (AG7088) ^[16] and its analogs ^[24-26]
	non-peptidic mimetic	DC07090 ^[27]
3D ^{pol} inhibitor	nucleoside analog	Gemcitabine ^[34] , NITD008 ^[33] , Ribavirin ^[31]
	non-nucleoside analog	Amiloride ^[5] , Aurintricarboxilic acid ^[5] , BPR-3P0128 ^[5] , DTrip-22 ^[5] , Gliotoxin ^[5] , GPC-N114 ^[36]
2C ^{ATPase} inhibitor		Dibucaine ^[65] , Fluoxetine ^[40] , Guanidine hydrochloride ^[5] , HBB ^[5] , MRL-1237 ^[5] , Pirlindole ^[65] , TBZE-029 ^[5] , Zuclopenthixol ^[65]
Host factor inhibitor	HSP90	Geldanamycin (analog 17-AAG) ^[50]
	PI4KB	BF738735 ^[5] , Enviroxime ^[5] , GW5074 ^[5] , PIK93 ^[5] , T-00127-HEV1 ^[5]
	OSBP	25-hydroxycholesterol ^[5] , AN-12-H5 ^[5] , Itraconazole ^[57] , OSW-1 ^[59] , T-00127-HEV2 ^[5]
	Cyclophilins	Cyclosporin A ^[62] , HL05100P2 ^[62] , NIM-811 ^[66]
	Glutathione	Buthionine Sulfoximine (BSO) ^[45] , TP219 ^[46]

Direct-acting antivirals

Entry inhibitors

Enterovirus capsids are icosahedral (pseudo $T=3$) structures composed of 60 copies of each of the four capsid proteins (VP1 to VP4). The enterovirus replication cycle (Figure 1B) is initiated by binding of virion to a receptor. Most enterovirus receptors are protein receptors that belong to the Ig superfamily or the integrin receptor family (receptor usage reviewed in²). These receptors bind in the “canyon”, a depression in the virion surface around the five-fold axes of symmetry². Receptor-binding induces virion destabilization and release of the “pocket factor”, a fatty acid located in a hydrophobic pocket beneath the canyon, to initiate virion uncoating².

The compounds that block cell entry are the most extensively studied class of anti-enteroviral compounds^{3,4}. These compounds, so-called “capsid binders”, replace the pocket factor in the canyon and thereby block virion uncoating. Capsid binders pleconaril (Viropharma, USA), vapendavir (a.k.a. BTA798, Biota Pharmaceuticals, USA), and pocapavir (a.k.a. V-073, ViroDefense Inc., USA) are currently under clinical evaluation, the status of which have been described last year⁵. Since then, another trial with pleconaril was conducted for the treatment of neonates with enterovirus sepsis which showed greater survival among pleconaril recipients⁶. A drawback of capsid binders is the rapid emergence of resistance, which may complicate their application in the clinic.

Many capsid binders are active against rhinovirus A and B species members³, but not against members of the rhinovirus C species^{7,8}. The recent elucidation of the atomic virion structure of rhinovirus-C15 by cryo-EM revealed a unique spiky structure with 60 “fingers”, and showed that the hydrophobic pocket is collapsed, thereby hindering the binding of capsid binders and explaining the resistance⁹.

The atomic structure of rhinovirus-C also revealed a likely binding site for sialic acid in a sequence-conserved surface depression adjacent to each finger⁹. Sialic acid was recently shown also to facilitate entry of EV-D68^{10,11}. Targeting sialic acid (reviewed in¹²), which has also been applied for influenza virus, could be an approach to inhibit rhinovirus-C and EV-D68 infections. One of the well-described drugs is DAS181, a bacterial sialidase that cleaves α 2,3- and α 2,6-sialic acid linkages¹³ and is tested in a phase II clinical trial for (para)influenza infection^{12,14}. DAS181 also inhibits EV-D68 replication *in vitro*¹⁵, but it remains to be tested *in vivo*.

Protease inhibitors

The 7.5 kb +RNA genome of enteroviruses encodes a single polyprotein harboring the structural P1 proteins and the non-structural P2 and P3 proteins (Fig 1A). This polyprotein is proteolytically processed into individual proteins by viral proteases 2A^{pro} and 3C(D)^{pro}.

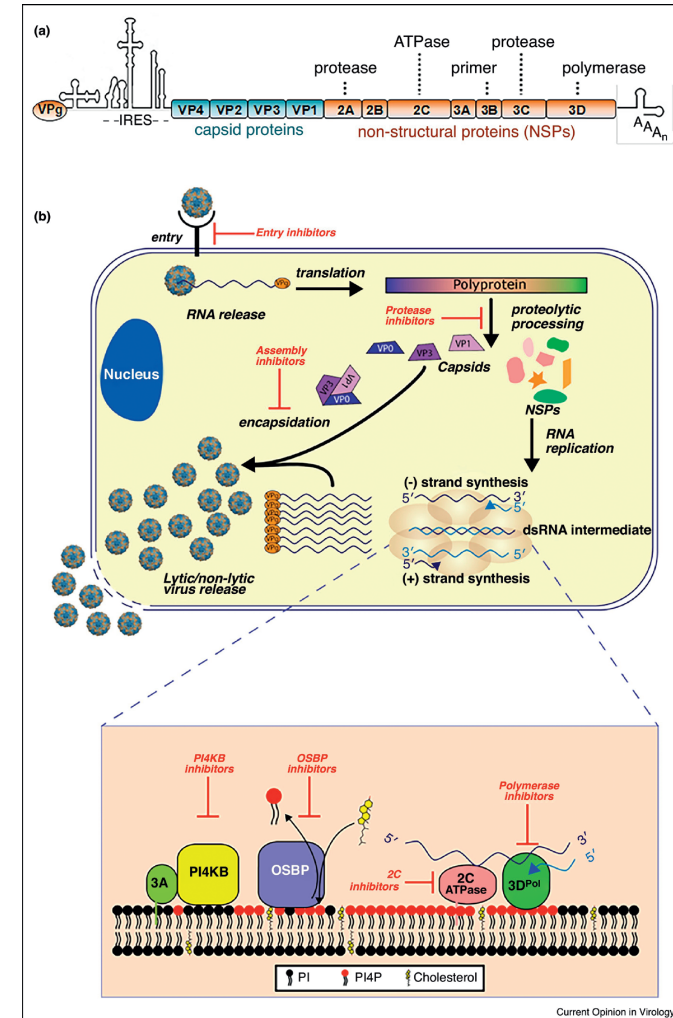


Figure 1. Enterovirus genome and replication cycle with antiviral targets. (A) Enterovirus genome encodes four structural proteins (VP1-VP4) and seven non-structural proteins (2A, 2B, 2C, 3A, 3B, 3C, and 3D). (B) The enterovirus life cycle begins with the attachment of the virus particle to a cellular receptor followed by the internalization of the particle into the host cell. The genome is released and directly translated into a polyprotein, which is processed by virally encoded proteases to release the viral proteins. Non-structural proteins rewrite host cell membranes and generate replication organelles for viral RNA replication. Genome replication starts with synthesis of complementary negative-stranded RNA, which is used as template for the synthesis of a large number of +RNA molecules. Newly synthesized +RNAs can either be used for a new round of genome replication or are packaged into capsid proteins to build infectious particles. The virus is released by a non-lytic mechanism as well as upon cell lysis. Inhibitors of the different life stages of the virus are depicted in red.

The development of protease inhibitors has been focused particularly on 3C^{pro}, since 2A^{pro} is less conserved. One of the most potent 3C^{pro} inhibitors developed over the years is rupintrivir (a.k.a. AG7088, Pfizer, USA). Rupintrivir is a peptidomimetic that irreversibly binds to the catalytic site of 3C^{pro}¹⁶. Proven very active against a broad panel of enteroviruses^{3,17-19}, this compound was selected for clinical trials, despite its poor oral bioavailability^{20,21}. Although the results of rhinovirus challenge trials were promising²², rupintrivir did not reduce disease severity in naturally infected patients²³, hence the clinical development was halted. However, many rupintrivir derivatives are currently under development²⁴⁻²⁶. Non-peptidyl small molecule inhibitors are developed to circumvent difficulties with bioavailability, but their evaluation in clinical trials has been limited thus far^{27,28}.

3D^{pol} inhibitors

The viral RNA-dependent RNA polymerase 3D^{pol} catalyzes viral RNA synthesis in replication complexes that are associated with so-called replication organelles (ROs, see below). Inhibitors of 3D^{pol} can be divided into two classes based on their mode-of-action, being nucleoside/nucleotide inhibitors (NIs) and non-nucleoside/nucleotide inhibitors (NNIs).

NIs. By mimicking nucleosides/nucleotides, NIs are incorporated into the viral genome and induce lethal mutagenesis or terminate elongation of the nascent chain^{30,31}. Until now, few NIs against enteroviruses have been developed, but compounds inhibiting other viruses offer promising results, such as ribavirin, which is clinically used for the treatment of hepatitis C virus (HCV) infections³². Another example is NITD008, which failed in preclinical studies for the treatment of dengue virus infection due to toxicity, but needs 10-fold lower concentration towards EV-71 and protected mice from lethal EV-71 challenge without showing toxicity³³. Drug repurposing – i.e. the concept of using compounds developed for a certain disease to treat a different condition – offers an attractive alternative to *de novo* drug development, as profound pharmacological and toxicological profiles are already available allowing a bypass of expensive (pre-)clinical studies. For example, the NI gemcitabine, an anticancer drug, was recently found to exert broad-spectrum anti-enterovirus activity^{34,35}. Besides incorporation into nascent viral RNA, gemcitabine has been suggested to block access of nucleotides into the active side of the polymerase and decrease the amount of triphosphates ribonucleotides by inhibiting ribonucleotide reductase, the enzyme that catalyzes the formation of deoxyribonucleotides from ribonucleotides³⁴. The dose of gemcitabine needed for antiviral activity is significantly lower than for the anticancer activity, raising hope for an application without the toxic effects that are inherent to many anticancer drugs.

NNIs. Several NNIs have been identified (e.g. gliotoxin, DTrip-22, aurincarboxylic acid, BPR-3P0128, and GPC-N114) but their mechanism of action is poorly understood, except for amiloride, which decreases the polymerase fidelity (reviewed in⁵). GPC-N114 was identified as a novel broad-range enterovirus inhibitor that targets the RNA template-primer site in the core of 3D^{pol}, making it the first anti-picornavirus compound with this

mechanism of action³⁶. Unfortunately, efficacy of GPC-N114 in animal models remains to be tested due to problems with formulating the compound for *in vivo* use. Alternative strategies for 3D^{pol} inhibition, although thus far unexplored, may be to interfere with posttranslational modifications of 3D^{pol} like sumoylation and ubiquitination, both of which are important for its activity³⁷.

2CATP^{ase} inhibitors

The highly conserved viral protein 2C, an ATPase, is an attractive target for broad-spectrum antiviral drug development. 2C^{ATPase} has several functions in genome replication (more extensively reviewed in⁵). Several structurally disparate 2C^{ATPase} inhibitors have been identified, such as guanidine hydrochloride, HBB, MRL-1237 and TBZE-029³. In addition, drug repurposing screens have recently uncovered a number of FDA-approved drugs (fluoxetine, pirlindole, dibucaine, zuclopenthixol) that inhibit replication of enterovirus species B and D members³⁸⁻⁴⁰. Since mutations in 2C^{ATPase} provide resistance to these compounds, they are considered to target 2C. Indeed, fluoxetine (i.e. Prozac) was shown to interfere with the ATPase activity of 2C^{ATPase}, but the mechanism of inhibition of the other drugs has to be unraveled³⁹. Importantly, fluoxetine was effective in an immunocompromised child with chronic enterovirus encephalitis⁴¹, underscoring the clinical potential of 2C^{ATPase} inhibitors. Recent *in vitro* experiments have confirmed the long-presumed ATP-dependent RNA helicase activity and ATPase-independent RNA chaperone functions of 2C^{ATPase}⁴², paving the way for studies to elucidate the mechanism of action of 2C^{ATPase} inhibitors in more detail.

Assembly inhibitors

Virion morphogenesis is a poorly understood, step-wise process⁴³. The first step is the liberation of P1 from the polyprotein. Assisted by the chaperone Hsp90^{43,44}, P1 is processed into VP0 (i.e. the precursor of VP4 and VP2), VP1, and VP3, which spontaneously form a protomer. Five protomers subsequently assemble into a pentamer, twelve of which in turn form an empty capsid (a.k.a. procapsid). Assembly of pentamers and procapsids is supported by glutathione (GSH) by an as yet unidentified mechanism^{45,46}. Governed by interactions between VP1/VP3 and 2C^{ATPase}^{43,47-49}, actively replicating viral RNA is included in the procapsid to form a provirion. The final step in virion morphogenesis is the cleavage of VP0 into VP4 and VP2 to form a stable icosahedral particle.

Only a few assembly inhibitors have been identified so far. Geldanamycin and its analog 17-AAG target Hsp90 to inhibit the processing of P1⁵⁰. Buthionine sulfoximine, an inhibitor of GSH synthesis, and TP219, a small molecule that covalently binds to GSH, both impede the role of GSH in morphogenesis^{45,46}. Yet, not all enteroviruses rely on GSH⁴⁶, thereby precluding GSH as an important target for broad-spectrum inhibitors.

Inhibitors of host factors

Viruses critically depend on specific host factors. In recent years new host factors have been discovered, spurring host-directed drug development. Since most enteroviruses rely on the same host factors, host-directed antivirals are likely to have broad-spectrum activity.

PI4KB

Enteroviruses, like all +RNA viruses, induce specific alterations in intracellular membranes and lipid homeostasis to form ROs. The formation of enterovirus ROs is mediated by the concerted actions of viral proteins 2B, 2C, and 3A, and a selected set of hijacked host factors (recently reviewed in²⁹). One of these pivotal host factors is phosphatidylinositol 4-kinase type III β (PI4KB)^{29,51,52}. It is recruited to membranes by the viral protein 3A and enriches ROs in phosphatidylinositol 4-phosphate (PI4P) lipids, which is essential genomic RNA replication⁵¹. As PI4KB is important for all enteroviruses, inhibitors of this enzyme (e.g. PIK93, GW5074, T-00127-HEV1 and BF738735 (reviewed in⁵) have broad-spectrum activity⁵¹⁻⁵⁴. However, some PI4KB inhibitors showed lethality in mice and affected lymphocyte function *in vitro*, which has stalled the development of PI4KB inhibitors⁵⁵.

OSBP

Itraconazole, a clinically used antifungal drug that also has anti-cancer properties, was identified in drug repurposing screens as a broad-spectrum enterovirus inhibitor^{35,56,57}. We identified the oxysterol-binding protein (OSBP) as a novel target of itraconazole responsible for the antiviral effects⁵⁶. OSBP is a PI4P-binding protein that shuttles cholesterol and PI4P at ER-Golgi membrane contact sites⁵⁸. OSBP is recruited to ROs through the PI4KB-mediated increase in PI4P and its lipid shuttling activity is essential for viral genome replication. Other OSBP inhibitors (e.g. 25-hydroxycholesterol, AN-12-H5, T-00127-HEV2 and the natural compound OSW-1) also impaired enterovirus replication^{54,59,60}. In a rhinovirus mouse model, prophylactic intranasal treatment with itraconazole reduced viral titers and pathology, raising expectations for topically applied itraconazole to prevent or treat common colds⁶¹.

Cyclophilins

Cyclophilin A plays a role during the uncoating process of EV-A71⁶². In line with this, cyclophilin A inhibitors HL05100P2 and cyclosporine A block EV-A71 replication⁶². Cyclophilins facilitate protein folding by catalyzing peptide bond isomerization and also play a role in the replication of other +RNA viruses, including HCV and coronaviruses (reviewed in⁶³). Because cyclophilin inhibitors like cyclosporine A have an immunosuppressive effect, non-immunosuppressive inhibitors (e.g. NIM-811) were developed and are currently in clinical trials for antiviral activity (e.g. alispovir, a.k.a. Debio025, for HCV treatment). It remains to be established whether uncoating of

other enteroviruses also relies on cyclophilins, thereby exploring the spectrum of anti-enteroviral activity of these inhibitors.

Outlook

Currently, there are no antiviral drugs available for the treatment of enterovirus infections, while several potent antivirals are available against HCV, a +RNA virus with a similar replication strategy. Possibly, the small market for anti-enteroviral drugs impedes extensive (industrial) efforts to develop enterovirus inhibitors. Yet, antivirals are urgently needed as enterovirus infections can be life-threatening especially in young children. Furthermore, they are expected to play a crucial role in poliovirus eradication and the post-eradication era.

The most promising targets for direct-acting antiviral drugs are 2C^{ATPase} and 3D^{pol}. Capsid binders are currently most advanced in clinical trials, but the inherent problem of rapid resistance development raises concerns. Host factors are good candidates for broad-spectrum antiviral drugs, as many host factors are shared by enteroviruses, but a potential downside is the chance of adverse effects and toxicity, as for PI4KB inhibitors. A possible new strategy is to interfere with essential protein-protein interactions, e.g. between viral proteins and host factors. Alphabodies, small cell-permeating, synthetic scaffolds that can efficiently perturb protein-protein interactions, may be a promising new technology to perturb interactions between viral proteins and host proteins, without causing the overt toxicity issues that are associated with overall inhibition of that particular host protein⁶⁴. Hence, fundamental research on the role of viral enzymes as well as essential host factors for enterovirus replication is needed for the development of broad-range antiviral drugs against these important pathogens.

Acknowledgement

This work was supported by research grants from the Netherlands Organisation for Scientific Research (NWO-VENI-863.12.005 to HMvdS, NWO-VENI-722.012.066 to JRPMS, NWO-VICI-91812628 to FJMvK); and the European Union (Horizon 2020 Marie Skłodowska-Curie ETN 'ANTIVIRALS', grant agreement number 642434) to FJMvK.

References

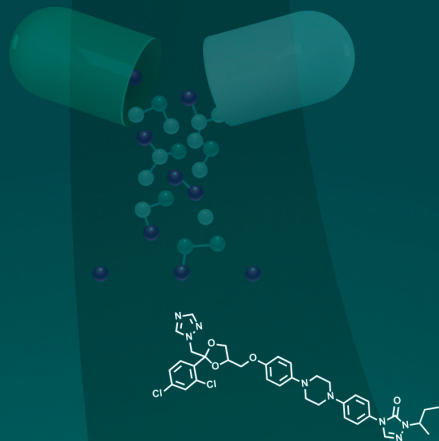
* of interest

** of outstanding interest

1. Tapparel C, Siegrist F, Petty TJ, Kaiser L: Picornavirus and enterovirus diversity with associated human diseases. *Infection, Genetics and Evolution* 2013, 14:282-293.
2. Bergelson JM, Coyne CB: Picornavirus entry. *Adv Exp Med Biol* 2013, 790:24-41.
3. De Palma AM, Vliegen I, De Clercq E, Neyts J: Selective inhibitors of picornavirus replication. *Med Res Rev* 2008, 28:823-884.
4. Thibaut HJ, De Palma AM, Neyts J: Combating enterovirus replication: state-of-the-art on antiviral research. *Biochem Pharmacol* 2012, 83:185-192.
5. van der Linden L, Wolthers KC, van Kuppeveld FJ: Replication and Inhibitors of Enteroviruses and Parechoviruses. *Viruses* 2015, 7:4529-4562.
6. Abzug MJ, Michaels MG, Wald E, Jacobs RF, Romero JR, Sanchez PJ, Wilson G, Krogstad P, Storch GA, Lawrence R, et al.: A Randomized, Double-Blind, Placebo-Controlled Trial of Pleconaril for the Treatment of Neonates With Enterovirus Sepsis. *J Pediatric Infect Dis Soc* 2016, 5:53-62.
7. Basta HA, Ashraf S, Sgro JY, Bochkov YA, Gern JE, Palmenberg AC: Modeling of the human rhinovirus C capsid suggests possible causes for antiviral drug resistance. *Virology* 2014, 448:82-90.
8. Hao W, Bernard K, Patel N, Ulbrandt N, Feng H, Svabek C, Wilson S, Stracener C, Wang K, Suzich J, et al.: Infection and propagation of human rhinovirus C in human airway epithelial cells. *J Virol* 2012, 86:13524-13532.
9. Liu Y, Hill MG, Klose T, Chen Z, Watters K, Bochkov YA, Jiang W, Palmenberg AC, Rossmann MG: Atomic structure of a rhinovirus C, a virus species linked to severe childhood asthma. *Proc Natl Acad Sci U S A* 2016, 113:8997-9002.
- ** Describes the crystal structure of rhinovirus 3 virion and reveals the mechanism of resistance to capsid binders.
10. Baggen J, Thibaut HJ, Staring J, Jae LT, Liu Y, Guo H, Slager JJ, de Bruin JW, van Vliet AL, Blomen VA, et al.: Enterovirus D68 receptor requirements unveiled by haploid genetics. *Proc Natl Acad Sci U S A* 2016, 113:1399-1404.
11. Liu Y, Sheng J, Baggen J, Meng G, Xiao C, Thibaut HJ, van Kuppeveld FJ, Rossmann MG: Sialic acid-dependent cell entry of human enterovirus D68. *Nat Commun* 2015, 6:8865.
12. Nicholls JM, Moss RB, Haslam SM: The use of sialidase therapy for respiratory viral infections. *Antiviral Res* 2013, 98:401-409.
13. Malakhov MP, Aschenbrenner LM, Smeets DF, Wandersee MK, Sidwell RW, Gubareva LV, Mishin VP, Hayden FG, Kim DH, Ing A, et al.: Sialidase fusion protein as a novel broad-spectrum inhibitor of influenza virus infection. *Antimicrob Agents Chemother* 2006, 50:1470-1479.
14. Moss RB, Hansen C, Sanders RL, Hawley S, Li T, Steigbigel RT: A phase II study of DAS181, a novel host directed antiviral for the treatment of influenza infection. *J Infect Dis* 2012, 206:1844-1851.
15. Rhoden E, Zhang M, Nix WA, Oberste MS: In Vitro Efficacy of Antiviral Compounds against Enterovirus D68. *Antimicrob Agents Chemother* 2015, 59:7779-7781.
16. Matthews DA, Dragovich PS, Webber SE, Fuhrman SA, Patick AK, Zalman LS, Hendrickson TF, Love RA, Prins TJ, Marakovits JT, et al.: Structure-assisted design of mechanism-based irreversible inhibitors of human rhinovirus 3C protease with potent antiviral activity against multiple rhinovirus serotypes. *Proc Natl Acad Sci U S A* 1999, 96:11000-11007.
17. Binford SL, Maldonado F, Brothers MA, Weady PT, Zalman LS, Meador JW, 3rd, Matthews DA, Patick AK: Conservation of amino acids in human rhinovirus 3C protease correlates with broad-spectrum antiviral activity of rupintrivir, a novel human rhinovirus 3C protease inhibitor. *Antimicrob Agents Chemother* 2005, 49:619-626.
18. Kaiser L, Crump CE, Hayden FG: In vitro activity of pleconaril and AG7088 against selected serotypes and clinical isolates of human rhinoviruses. *Antiviral Res* 2000, 47:215-220.
19. Patick AK, Binford SL, Brothers MA, Jackson RL, Ford CE, Diem MD, Maldonado F, Dragovich PS, Zhou R, Prins TJ, et al.: In vitro antiviral activity of AG7088, a potent inhibitor of human rhinovirus 3C protease. *Antimicrob Agents Chemother* 1999, 43:2444-2450.
20. Hsyu PH, Pithavala YK, Gersten M, Penning CA, Kerr BM: Pharmacokinetics and safety of an antirhinoviral agent, rupintrivir, in healthy volunteers. *Antimicrob Agents Chemother* 2002, 46:392-397.
21. Zhang KE, Hee B, Lee CA, Liang B, Potts BC: Liquid chromatography-mass spectrometry and liquid chromatography-NMR characterization of in vitro metabolites of a potent and irreversible peptidomimetic inhibitor of rhinovirus 3C protease. *Drug Metab Dispos* 2001, 29:729-734.
22. Hayden FG, Turner RB, Gwaltney JM, Chi-Burris K, Gersten M, Hsyu P, Patick AK, Smith GJ, 3rd, Zalman LS: Phase II, randomized, double-blind, placebo-controlled studies of rupintrivir nasal spray 2-percent suspension for prevention and treatment of experimentally induced rhinovirus colds in healthy volunteers. *Antimicrob Agents Chemother* 2003, 47:3907-3916.
23. Patick AK, Brothers MA, Maldonado F, Binford S, Maldonado O, Fuhrman S, Petersen A, Smith GJ, 3rd, Zalman LS, Burns-Naas LA, et al.: In vitro antiviral activity and single-dose pharmacokinetics in humans of a novel, orally bioavailable inhibitor of human rhinovirus 3C protease. *Antimicrob Agents Chemother* 2005, 49:2267-2275.
24. Tan J, George S, Kusov Y, Perbandt M, Anemuller S, Mesters JR, Norder H, Coutard B, Lacroix C, Leysen P, et al.: 3C protease of enterovirus 68: structure-based design of Michael acceptor inhibitors and their broad-spectrum antiviral effects against picornaviruses. *J Virol* 2013, 87:4339-4351.
25. Tan YW, Ang MJ, Lau QY, Poulsen A, Ng FM, Then SW, Peng J, Hill J, Hong WJ, Chia CS, et al.: Antiviral activities of peptide-based covalent inhibitors of the Enterovirus 71 3C protease. *Sci Rep* 2016, 6:33663.
26. Wu C, Zhang L, Li P, Cai Q, Peng X, Yin K, Chen X, Ren H, Zhong S, Weng Y, et al.: Fragment-wise design of inhibitors to 3C proteinase from enterovirus 71. *Biochim Biophys Acta* 2016, 1860:1299-1307.
27. Ma GH, Ye Y, Zhang D, Xu X, Si P, Peng JL, Xiao YL, Cao RY, Yin YL, Chen J, et al.: Identification and biochemical characterization of DC07090 as a novel potent small molecule inhibitor against human enterovirus 71 3C protease by structure-based virtual screening. *Eur J Med Chem* 2016, 124:981-991.
28. Patick AK: Rhinovirus chemotherapy. *Antiviral Res* 2006, 71:391-396.
29. van der Schaar HM, Dorobantu CM, Albulescu L, Strating JR, van Kuppeveld FJ: Fat(al) attraction: Picornaviruses Usurp Lipid Transfer at Membrane Contact Sites to Create Replication Organelles. *Trends Microbiol* 2016, 24:535-546.

30. Crotty S, Cameron CE, Andino R: RNA virus error catastrophe: Direct molecular test by using ribavirin. *Proceedings of the National Academy of Sciences of the United States of America* 2001, 98:6895-6900.
31. Crotty S, Maag D, Arnold JJ, Zhong WD, Lau JYN, Hong Z, Andino R, Cameron C: The broad-spectrum antiviral ribonucleoside ribavirin is an RNA virus mutagen (vol 6, pg 1375, 2000). *Nature Medicine* 2001, 7:255-255.
32. Pfeiffer JK, Kirkegaard K: A single mutation in poliovirus RNA-dependent RNA polymerase confers resistance to mutagenic nucleotide analogs via increased fidelity. *Proceedings of the National Academy of Sciences of the United States of America* 2003, 100:7289-7294.
33. Deng CL, Yeo H, Ye HQ, Liu SQ, Shang BD, Gong P, Alonso S, Shi PY, Zhang B: Inhibition of enterovirus 71 by adenosine analog NITD008. *J Virol* 2014, 88:11915-11923.
34. Kang H, Kim C, Kim DE, Song JH, Choi M, Choi K, Kang M, Lee K, Kim HS, Shin JS, et al.: Synergistic antiviral activity of gemcitabine and ribavirin against enteroviruses. *Antiviral Res* 2015, 124:1-10.
35. Zhang Z, Yang E, Hu C, Cheng H, Chen CY, Huang D, Wang R, Zhao Y, Rong L, Vignuzzi M, et al.: Cell-based high-throughput screening assay identifies 2', 2'-difluoro-2'-deoxycytidine Gemcitabine as potential anti-poliovirus agent. *ACS Infect Dis* 2016.
36. van der Linden L, Vives-Adrian L, Selisko B, Ferrer-Orta C, Liu X, Lanke K, Ulferts R, De Palma AM, Tanchis F, Goris N, et al.: The RNA template channel of the RNA-dependent RNA polymerase as a target for development of antiviral therapy of multiple genera within a virus family. *PLoS Pathog* 2015, 11:e1004733.
- ** This paper identifies the novel non nucleoside analog GPC-N114 and identifies the RNA template channel of 3D^{pol} as novel target for broad-spectrum antiviral therapy.
37. Liu Y, Zheng Z, Shu B, Meng J, Zhang Y, Zheng C, Ke X, Gong P, Hu Q, Wang H: SUMO Modification Stabilizes Enterovirus 71 Polymerase 3D to Facilitate Viral Replication. *J Virol* 2016.
38. Ulferts R, de Boer SM, van der Linden L, Bauer L, Lyoo HR, Mate MJ, Lichiere J, Canard B, Lelieveld D, Omta W, et al.: Screening of a Library of FDA-Approved Drugs Identifies Several Enterovirus Replication Inhibitors That Target Viral Protein 2C. *Antimicrob Agents Chemother* 2016, 60:2627-2638.
39. Ulferts R, van der Linden L, Thibaut HJ, Lanke KH, Leyssen P, Coutard B, De Palma AM, Canard B, Neyts J, van Kuppeveld FJ: Selective serotonin reuptake inhibitor fluoxetine inhibits replication of human enteroviruses B and D by targeting viral protein 2C. *Antimicrob Agents Chemother* 2013, 57:1952-1956.
40. Zuo J, Quinn KK, Kye S, Cooper P, Damoiseaux R, Krogstad P: Fluoxetine is a potent inhibitor of coxsackievirus replication. *Antimicrob Agents Chemother* 2012, 56:4838-4844.
41. Gofshetyn J, Cardenas AM, Bearden D: Treatment of Chronic Enterovirus Encephalitis With Fluoxetine in a Patient With X-Linked Agammaglobulinemia. *Pediatr Neurol* 2016.
- * This is the first report showing that the repurposed drugs fluoxetine could be used as potential therapy in the clinic for chronic enterovirus infection.
42. Xia H, Wang P, Wang GC, Yang J, Sun X, Wu W, Qiu Y, Shu T, Zhao X, Yin L, et al.: Human Enterovirus Nonstructural Protein 2CATPase Functions as Both an RNA Helicase and ATP-Independent RNA Chaperone. *PLoS Pathog* 2015, 11:e1005067.
- ** Paper showing that 2C^{ATPase} possesses the long-sought ATP-dependent RNA helicase activity, allowing studies to elucidate the mode of action of 2C inhibitors with a yet unknown mechanism.
43. Jiang P, Liu Y, Ma HC, Paul AV, Wimmer E: Picornavirus morphogenesis. *Microbiol Mol Biol Rev* 2014, 78:418-437.
44. Geller R, Vignuzzi M, Andino R, Frydman J: Evolutionary constraints on chaperone-mediated folding provide an antiviral approach refractory to development of drug resistance. *Genes Dev* 2007, 21:195-205.
45. Ma HC, Liu Y, Wang C, Strauss M, Rehage N, Chen YH, Altan-Bonnet N, Hogle J, Wimmer E, Mueller S, et al.: An interaction between glutathione and the capsid is required for the morphogenesis of C-cluster enteroviruses. *PLoS Pathog* 2014, 10:e1004052.
- * First description of the importance of glutathione in enterovirus morphogenesis.
46. Thibaut HJ, van der Linden L, Jiang P, Thys B, MD, Aguado L, Rombaut B, Wimmer E, Paul A, Perez-Perez MJ, et al.: Binding of glutathione to enterovirus capsids is essential for virion morphogenesis. *PLoS Pathog* 2014, 10:e1004039.
- * First description of the importance of glutathione in enterovirus morphogenesis.
47. Asare E, Mugavero J, Jiang P, Wimmer E, Paul AV: A Single Amino Acid Substitution in Poliovirus Nonstructural Protein 2CATPase Causes Conditional Defects in Encapsulation and Uncoating. *J Virol* 2016, 90:6174-6186.
48. Liu Y, Wang C, Mueller S, Paul AV, Wimmer E, Jiang P: Direct interaction between two viral proteins, the nonstructural protein 2C and the capsid protein VP3, is required for enterovirus morphogenesis. *PLoS Pathog* 2010, 6:e1001066.
49. Wang C, Jiang P, Sand C, Paul AV, Wimmer E: Alanine scanning of poliovirus 2CATPase reveals new genetic evidence that capsid protein/2CATPase interactions are essential for morphogenesis. *J Virol* 2012, 86:9964-9975.
50. Tsou YL, Lin YW, Chang HW, Lin HY, Shao HY, Yu SL, Liu CC, Chitra E, Sia C, Chow YH: Heat shock protein 90: role in enterovirus 71 entry and assembly and potential target for therapy. *PLoS One* 2013, 8:e77133.
51. Hsu NY, Illytska O, Belov G, Santiana M, Chen YH, Takvorian PM, Pau C, van der Schaar H, Kaushik-Basu N, Balla T, et al.: Viral reorganization of the secretory pathway generates distinct organelles for RNA replication. *Cell* 2010, 141:799-811.
- ** Identification of PI4KB as an important host factor for enterovirus replication. This information spurred the development of PI4KB inhibitors as broad-range enterovirus replication inhibitors.
52. van der Schaar HM, Leyssen P, Thibaut HJ, de Palma A, van der Linden L, Lanke KH, Lacroix C, Verbeke E, Conrath K, Macleod AM, et al.: A novel, broad-spectrum inhibitor of enterovirus replication that targets host cell factor phosphatidylinositol 4-kinase IIIbeta. *Antimicrob Agents Chemother* 2013, 57:4971-4981.
53. Arita M, Kojima H, Nagano T, Okabe T, Wakita T, Shimizu H: Phosphatidylinositol 4-kinase III beta is a target of enviroxime-like compounds for antipoliovirus activity. *J Virol* 2011, 85:2364-2372.
54. Roulin PS, Lotzerich M, Torta F, Tanner LB, van Kuppeveld FJ, Wenk MR, Greber UF: Rhinovirus uses a phosphatidylinositol 4-phosphate/cholesterol counter-current for the formation of replication compartments at the ER-Golgi interface. *Cell Host Microbe* 2014, 16:677-690.
55. Lamarche MJ, Borawski J, Bose A, Capacci-Daniel C, Colvin R, Dennehy M, Ding J, Dobler M, Drumm J, Gaither LA, et al.: Anti-hepatitis C virus activity and toxicity of type III phosphatidylinositol-4-kinase beta inhibitors. *Antimicrob Agents Chemother* 2012, 56:5149-5156.

56. Strating JR, van der Linden L, Albuлесcu L, Bigay J, Arita M, Delang L, Leyssen P, van der Schaar HM, Lanke KH, Thibaut HJ, et al.: Itraconazole inhibits enterovirus replication by targeting the oxysterol-binding protein. *Cell Rep* 2015, 10:600-615.
- ** Itraconazole, an FDA-approved drug to target fungal infections, is identified as a broad-spectrum enterovirus inhibitor and shown to target the lipid shuttling activity of oxysterol-binding protein that is essential for viral replication organelle formation and/or function.
57. Gao Q, Yuan S, Zhang C, Wang Y, Wang Y, He G, Zhang S, Altmeyer R, Zou G: Discovery of itraconazole with broad-spectrum in vitro anti-enterovirus activity that targets nonstructural protein 3A. *Antimicrob Agents Chemother* 2015, 59:2654-2665.
58. Mesmin B, Bigay J, Moser von Filseck J, Lacas-Gervais S, Drin G, Antonny B: A four-step cycle driven by PI(4)P hydrolysis directs sterol/PI(4)P exchange by the ER-Golgi tether OSBP. *Cell* 2013, 155:830-843.
59. Albuлесcu L, Strating JR, Thibaut HJ, van der Linden L, Shair MD, Neyts J, van Kuppeveld FJ: Broad-range inhibition of enterovirus replication by OSW-1, a natural compound targeting OSBP. *Antiviral Res* 2015, 117:110-114.
60. Arita M, Kojima H, Nagano T, Okabe T, Wakita T, Shimizu H: Oxysterol-binding protein family I is the target of minor enviroxime-like compounds. *J Virol* 2013, 87:4252-4260.
61. Shim A, Song JH, Kwon BE, Lee JJ, Ahn JH, Kim YJ, Rhee KJ, Chang SY, Cha Y, Lee YS, et al.: Therapeutic and prophylactic activity of itraconazole against human rhinovirus infection in a murine model. *Sci Rep* 2016, 6:23110.
62. Qing J, Wang Y, Sun Y, Huang J, Yan W, Wang J, Su D, Ni C, Li J, Rao Z, et al.: Cyclophilin A associates with enterovirus-71 virus capsid and plays an essential role in viral infection as an uncoating regulator. *PLoS Pathog* 2014, 10:e1004422.
- * First description of the role of cyclophilin in the uncoating process of an enterovirus and the potential of cyclophilin inhibitors to interfere with enterovirus infection.
63. Frausto SD, Lee E, Tang H: Cyclophilins as modulators of viral replication. *Viruses* 2013, 5:1684-1701.
64. Desmet J, Verstraete K, Bloch Y, Lorent E, Wen Y, Devreese B, Vandenbroucke K, Loverix S, Hettmann T, Deroo S, et al.: Structural basis of IL-23 antagonism by an Alphabody protein scaffold. *Nat Commun* 2014, 5:5237.
65. Ulferts R, de Boer M, van der Linden L, Bauer L, Lyoo HR, Mate MJ, Lichiere J, Canard B, Lelieveld D, Omta W, et al.: Screening of a library of FDA-approved drugs identifies several enterovirus replicaton inhibitors that target viral protein 2C. *Antimicrob Agents Chemother* 2016.
66. Seizer P, Klingel K, Sauter M, Westermann D, Ochmann C, Schonberger T, Schleicher R, Stellos K, Schmidt EM, Borst O, et al.: Cyclophilin A affects inflammation, virus elimination and myocardial fibrosis in coxsackievirus B3-induced myocarditis. *J Mol Cell Cardiol* 2012, 53:6-14.



Chapter

3

Structure-activity relationship study of itraconazole, a broad-range inhibitor of picornavirus replication that targets oxysterol-binding protein (OSBP)

Lisa Bauer¹, Salvatore Ferla², Sarah A. Head^{3,4}, Shridhar Bhat³, Kalyan K. Pasunooti^{3,5}, Wei Q. Shi^{3,6}, Lucian Albulescu¹, Jun O. Liu³, Andrea Brancale², Frank J.M. van Kuppeveld¹, Jeroen R.P.M. Strating^{1#}

¹ Virology Division, Department of Infectious Diseases and Immunology, Faculty of Veterinary Medicine, Utrecht University, The Netherlands

² Medicinal Chemistry, School of Pharmacy & Pharmaceutical Sciences, Cardiff University, United Kingdom

³ Department of Pharmacology, Johns Hopkins School of Medicine, Baltimore, USA

⁴ Present address: EMBL/CRG Systems Biology Research Unit, Centre for Genomic Regulation (CRG), Barcelona Institute of Science and Technology, Spain.

⁵ Present address: Division of Structural Biology & Biochemistry, School of Biological Sciences, Nanyang Technological University, Singapore

⁶ Present address: Department of Chemistry and Biochemistry, University of Arkansas, USA

Corresponding author

Antiviral Research, 2018, 156, 55-63

Abstract

Itraconazole (ITZ) is a well-known, FDA-approved antifungal drug that is also in clinical trials for its anticancer activity. ITZ exerts its anticancer activity through several disparate targets and pathways. ITZ inhibits angiogenesis by hampering the functioning of the vascular endothelial growth receptor 2 (VEGFR2) and by indirectly inhibiting mTOR signaling. Furthermore, ITZ directly inhibits the growth of several types of tumor cells by antagonizing Hedgehog signaling. Recently, we reported that ITZ also has broad-spectrum antiviral activity against enteroviruses, cardioviruses and hepatitis C virus by inhibiting oxysterol-binding protein (OSBP), a cellular lipid shuttling protein. In this study, we analyzed which structural features of ITZ are important for inhibiting the function of OSBP and virus replication. The backbone structure, consisting of five rings, and the *sec*-butyl chain are important for OSBP inhibition and antiviral activity. In contrast, the triazole moiety, which is critical for antifungal activity, is not required for antiviral activity and OSBP inhibition. The features required for activity of ITZ towards OSBP and virus replication overlap mostly with published features required for inhibition of VEGFR2 trafficking, but not Hh signaling. Furthermore, we use *in silico* studies to explore how ITZ could bind to OSBP. Our data show that several pharmacological activities of ITZ can be uncoupled, which is a critical step in the development of ITZ-based antiviral compounds with greater specificity and reduced off-target effects.

Keywords: Itraconazole, Picornavirus, Oxysterol-binding protein (OSBP), Antiviral activity, Molecular modeling

Introduction

Enteroviruses form a large group of viruses within the *Picornaviridae* family of positive-sense single stranded RNA (+RNA) viruses. The enteroviruses include many important human pathogens, including poliovirus (causative agent of poliomyelitis), coxsackieviruses and echoviruses (causative agents of encephalitis, meningitis, and hand, foot, and mouth disease) and rhinoviruses (causative agents of common cold, but also have a role in exacerbations of asthma and chronic obstructive pulmonary disease)¹. Vaccines are available against poliovirus, and an enterovirus-A71 vaccine has recently been approved in China. However, vaccination is not a feasible general strategy to prevent infections with the large amount (>250) of enterovirus (sero)types. No antiviral therapies are approved at the moment, restricting treatment of infections to supportive care. Therefore, antiviral drugs that target a broad spectrum of enteroviruses are urgently needed. Such drugs could either directly target viral proteins or act through essential host factors. Repurposing of approved drugs or compounds that have passed clinical trials, for which detailed information on safety and pharmacology is available, is an emerging alternative to the time consuming and costly *de novo* development of antiviral drugs. Recently, ITZ was identified in several drug-repurposing screens as a novel broad-spectrum anti-enteroviral agent that affects genome replication²⁻⁴. Besides enteroviruses, ITZ also inhibits picornaviruses of *Cardiovirus* genus and hepatitis C virus, a +RNA virus belonging to the *Flaviviridae* family.

ITZ (Sporanox[®]) is an FDA-approved drug that is clinically used for the treatment of fungal infections. ITZ acts by inhibiting the activity of the fungal enzyme CYP51 (lanosterol 14 α -demethylase), which catalyzes an essential step in the biosynthesis of cell membrane sterols, thus impairing fungal cell membrane integrity⁵. ITZ also inhibits the human CYP51 isoform, although ~10-fold less potently than fungal CYP51, and the related drug metabolizing enzyme CYP3A4^{6,7}. In drug-repurposing screens, ITZ was found to exert antitumor activity via a number of targets. ITZ directly inhibits cancer cells that depend on the Hedgehog (Hh) pathway by antagonizing Hh signaling⁸. Besides, ITZ possesses potent antiangiogenic activity by indirectly inhibiting mTOR and vascular endothelial growth factor receptor 2 (VEGFR2) functioning. ITZ inhibits mTOR by targeting the mitochondrial voltage-dependent anion channel 1 (VDAC1) and the lysosomal cholesterol-binding protein Niemann-Pick disease type C1 (NPC1)⁹⁻¹². ITZ interferes with the signaling activity of VEGFR2 by altering its trafficking and glycosylation^{13,14}, but the molecular target mediating this activity remains to be identified. So far, ITZ has displayed efficacy in several phase II clinical trials with patients with a number of different cancer types¹⁵⁻¹⁷.

We identified oxysterol-binding protein (OSBP) as a novel target of ITZ through which the antiviral activity is exerted⁴. OSBP shuttles lipids at membrane contact sites (MCSs), i.e. sites where two organelles come in very close proximity, between the endoplasmic reticulum (ER) and the *trans*-Golgi apparatus¹⁸. OSBP bridges the ER-Golgi MCS by simultaneously binding these two organelles. OSBP connects to the ER

via an interaction of its FFAT-motif with the ER integral membrane proteins VAP-A or VAP-B. At the other side of the MCS, the PH-domain of OSBP binds the small GTPase Arf1 and phosphatidylinositol 4-phosphate [PI(4)P] lipids to connect OSBP to the *trans*-Golgi. The C-terminal OSBP-related domain (ORD) of OSBP can accommodate the lipids cholesterol and PI(4)P in its lipophilic pocket. The ORD mediates shuttling of cholesterol from the ER to the Golgi, which occurs against the concentration gradient. A concurrent shuttling of PI(4)P from the *trans*-Golgi to the ER, where PI(4)P is hydrolyzed by the phosphatase Sac1, provides the driving force for cholesterol transport. Because PI(4)P also acts as a membrane anchor for OSBP at the *trans*-Golgi, PI(4)P shuttling allows a negative feedback of OSBP localization and, as a result, activity¹⁸. ITZ inhibits both the cholesterol and PI(4)P shuttling activity of OSBP. As a result of the latter, ITZ prevents PI(4)P removal from the Golgi, leading to an accumulation of both PI(4)P and OSBP at ER-Golgi MCSs⁴.

Like all +RNA viruses, picornaviruses rewire the cellular membrane system to generate membranous replication platforms, so-called replication organelles (ROs) (for recent reviews, see^{19,20}). Each group of viruses recruits a specific set of host proteins to the ROs through viral non-structural proteins. For example, all enteroviruses recruit the Golgi-derived enzyme phosphatidylinositol 4-kinase type III β (PI4KB), which converts PI lipids into PI(4)P, leading to an enrichment of PI(4)P at ROs^{21,22}. The cardiovirus encephalomyocarditis virus (EMCV) instead relies on a different isoform, namely phosphatidylinositol 4-kinase type III α (PI4KA), to generate PI(4)P-rich ROs²³. The PI(4)P lipids allowing the recruitment of OSBP and drive the shuttling of cholesterol to ROs^{4,23-25}. By inhibiting the lipid shuttling activity of OSBP, ITZ hampers cholesterol transport to ROs and hence interferes with RO biogenesis and viral genome replication⁴.

Here, we report a structure-activity relationship study of ITZ in which we investigated which structural features of ITZ are important for the inhibition of the lipid shuttling activity of OSBP and inhibition of virus replication. To study the antiviral effect of ITZ analogs, we used the cardiovirus EMCV as a model virus that is highly sensitive to ITZ⁴. As a read-out for inhibition of OSBP lipid shuttling activity, we used the accumulation of OSBP at the Golgi, which is induced by the inhibition of OSBP-mediated PI(4)P shuttling from the Golgi⁴. Furthermore, we performed molecular modeling studies to investigate how ITZ may bind to OSBP. We observed that the activity of the analogs towards OSBP and virus replication correlate well. Interestingly, there is a fairly good overlap of antiviral activity of most analogs with previously reported activity towards VEGFR2, but not Hh. Finally, our molecular modeling studies indicate that ITZ occupies the hydrophobic tunnel in the ORD which normally accommodates cholesterol and PI(4)P, thus offering a potential explanation of its mode of inhibition. Together, this study provides insight into the structural features of ITZ that are necessary for its OSBP-mediated antiviral activity, paving the way for further development of ITZ-based compounds as antiviral agents with greater specificity towards OSBP and fewer side activities (i.e. not targeting other ITZ targets such as CYP51 and Hh).

Results

Antiviral activity of ITZ and inhibition of OSBP

ITZ (Figure 1) consists of a core of five linearly linked rings (dioxolanyl-methoxyphenyl-piperazinyl-phenyl-triazolone) with substituents on either side of the core. The dioxolane ring carries a dichlorophenyl ring and a triazole moiety, the latter of which is essential for the CYP51-mediated antifungal activity.

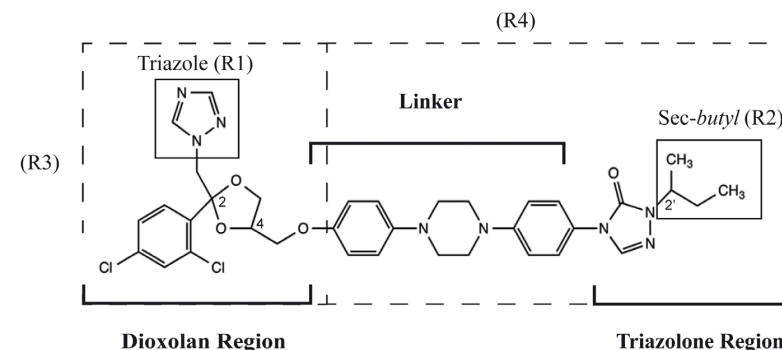


Figure 1. Structure of ITZ. ITZ has three stereogenic centers (2, 4 and 2'), giving rise to eight different stereoisomers. The boxes indicate the side-chains that are changed in the tested analogs.

The triazolone ring on the other end of the core bears a *sec*-butyl chain that is important for the activity of ITZ towards VEGFR2 and Hh²⁶. ITZ has three stereogenic centers (2, 4 and 2') and thus a total of eight possible stereoisomers. To investigate the importance of different parts of ITZ for the antiviral activity, we used a small library of ITZ stereoisomers and analogs that either lacked major parts of the molecule or that had alterations in the triazole or *sec*-butyl moieties^{10,26-28}. The antiviral activity of ITZ analogs was investigated using encephalomyocarditis virus (EMCV), a member of the *Cardiovirus* genus that, like enteroviruses, requires OSBP and is highly sensitive to ITZ^{4,23}. HeLa cells were infected with a recombinant virus encoding a *Renilla* luciferase reporter gene (RLuc-EMCV)²⁹, treated with serial dilutions of ITZ analogs, and luciferase activity was determined as a quantitative and sensitive readout for virus replication (Figure 2A). In parallel, an MTS assay was performed to test for cytotoxicity of the compounds (Figure 2B). As a readout for inhibition of the lipid shuttling activity of OSBP, cells transiently expressing EGFP-tagged OSBP were treated with 10 μ M of compound, fixed and imaged by fluorescence microscopy to assess the accumulation of OSBP at the Golgi (Figure 2C).

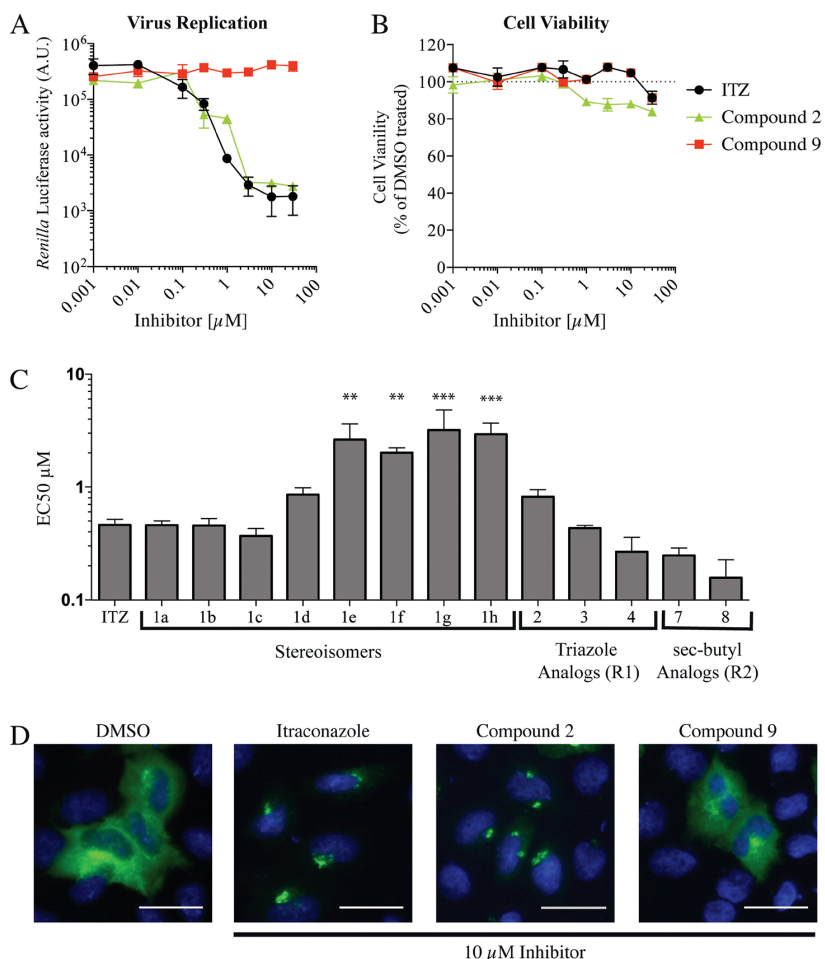


Figure 2. The effects of ITZ analogs on virus replication and OSBP redistribution. (A) HeLa R19 cells were infected with a Renilla luciferase (RLuc)-EMCV reporter virus, treated with compounds, and luciferase activity was determined as a quantitative measure of replication. Shown are ITZ as a positive control, and one representative example each of an active (compound 2) and an inactive (compound 9) analog. (B) In parallel, uninfected cells were treated with compound and cell viability was determined using an MTS assay. (C) HeLa R19 cells were transfected with a plasmid encoding EGFP-OSBP and treated for 1h with 10 μM compound. Cells were fixed, counterstained with DAPI to visualize the nuclei (blue) and imaged for OSBP localization using fluorescence microscopy. Only compounds that inhibit virus replication induce OSBP accumulation (see also Tables 1-4). Representative examples of independent technical replicates are shown. Experiments in (A) and (B) were performed as biological triplicates and mean values ± SEM are shown. Scale bars correspond to 50 μm.

Clinically administered ITZ to treat fungal infections consists of an equimolar mixture of the four *cis*-stereoisomers (2S4R2'S; 2S4R2'R; 2R4S2'S; 2R4S2'R). All eight stereoisomers (compounds **1a-h**) inhibited virus replication without notable acute cytotoxicity and induced a perinuclear OSBP accumulation indicative of an inhibition of the lipid shuttling activity of OSBP. Nevertheless, the clinically administered stereoisomers (**1a-d**) were somewhat more potent (up to ~7.5 fold) than the other stereoisomers (**1e-h**) (Table 1). The stereoisomers in clinically used ITZ were previously reported to also be most active towards VEGFR2 glycosylation (Table 1)²⁶.

Table 1. The activity of ITZ stereoisomers towards inhibition of EMCV replication, OSBP redistribution and VEGFR2 glycosylation

Compounds	Inhibition of virus replication EC50 (μM)	OSBP redistribution (10 μM)	VEGFR2 glycosylation (2 μM) ²⁶	Hh inhibition ^{b,26}
ITZ	0,46 ±(0,14)	+	++	++
1a (2S4R2'S) ^a	0,46 ±(0,08)	+	++	n.d.
1b (2S4R2'R) ^a	0,46 ±(0,12)	+	++	n.d.
1c (2R4S2'S) ^a	0,37 ±(0,06)	+	++	n.d.
1d (2R4S2'R) ^a	0,86 ±(0,22)	+	++	n.d.
1e (2S4S2'S)	2,63 ±(0,99)	+	+	n.d.
1f (2S4S2'R)	2,01 ±(0,38)	+	-	n.d.
1g (2R4R2'S)	3,21 ±(1,61)	+	+	n.d.
1h (2R4R2'R)	2,95 ±(1,26)	+	-	n.d.

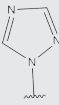
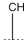
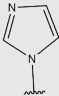
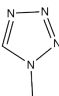
Shown are the means and the standard deviations of data from at least two independent experiments.

^a Stereoisomers are included in clinically administered ITZ.

^b Inhibition of Hh signaling, determined using a reporter for the Hh-regulated transcription factor *Gli1*²⁶. n.d.; not determined.

The triazole ring is a key feature for the antifungal effect of ITZ³⁰. To test the importance of the triazole ring for antiviral activity, we analyzed analogs that lack the triazole ring (compound **2**) or that have it substituted for an imidazole (compound **3**) or a tetrazole (compound **4**) moiety (Table 2). All compounds retained antiviral activity and induced accumulation of OSBP at the Golgi compartment, without displaying toxicity. These data indicate that the triazole moiety is not important for the antiviral activity of ITZ and that it can be removed to reduce side effects caused by inhibition of the human CYP51 or CYP3A4 enzymes.

Table 2. The effect of ITZ triazole-moiety analogs towards inhibition of EMCV replication, OSBP redistribution and VEGFR2 glycosylation

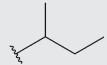
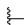
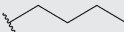
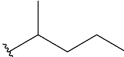
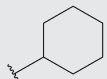
Compounds	R1	Inhibition of virus replication EC50 (μM)	OSBP redistribution (10 μM)	VEGFR2 glycosylation (2 μM) ²⁶	Hh inhibition ^{a,26}
ITZ		0,46 \pm (0,14)	+	++	++
2		0,82 \pm (0,22)	+	n.d.	n.d.
3		0,43 \pm (0,04)	+	n.d.	n.d.
4		0,26 \pm (0,16)	+	n.d.	n.d.

Shown are the means and the standard deviations of data from four independent experiments.

^a Inhibition of Hh signaling, determined using a reporter for the Hh-regulated transcription factor *Gli1*²⁶. n.d.; not determined.

Next, we analyzed a group of analogs with variations in the *sec*-butyl side chain, none of which displayed toxicity in the MTS assay (Table 3). Compound **5**, which altogether lacks the *sec*-butyl chain, did not inhibit virus replication and did not redistribute OSBP to the Golgi. Likewise, compound **6**, which has the *sec*-butyl chain substituted with a linear side chain, was inactive towards both virus replication and OSBP redistribution. In contrast, replacing the *sec*-butyl chain with a branched (compound **7**) or a cyclohexane (compound **8**) side chain did not affect the activity towards virus replication or OSBP accumulation. Together, these data indicate that a bulky, branched side chain is important for the OSBP-mediated antiviral activity of ITZ.

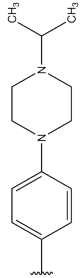
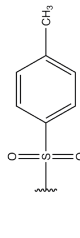
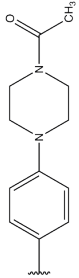

Table 3. The activity of ITZ *sec*-butyl chain analogs towards inhibition of EMCV replication, OSBP redistribution and VEGFR2 glycosylation

Compounds	R2	Inhibition of virus replication EC50 (μM)	OSBP redistribution (10 μM)	VEGFR2 glycosylation (2 μM) ²⁶	Hh inhibition ^{a,26}
ITZ		0,46 \pm (0,14)	+	++	++
5		> 10	-	-	++
6		> 10	-	-	-
7		0,25 \pm (0,07)	+	++	++
8		0,16 \pm (0,12)	+	++	-

Shown are the means and the standard deviations of data from four independent experiments^a Inhibition of Hh signaling, determined using a reporter for the Hh-regulated transcription factor *Gli1*²⁶.

Finally, we analyzed a set of analogs that lack major parts of the dioxolane or triazolone regions (Table 4). Analogs lacking the triazolone region with its *sec*-butyl side chain (terconazole, compound **9**, compound **10**) did not redistribute OSBP or inhibit virus replication. In line with this, we previously reported that ketoconazole, a clinically used antifungal drug that is virtually identical to compound **10** except that it has an imidazole ring instead of a triazole ring, lacks antiviral activity and does not affect OSBP⁴. However, since these analogs also lack the essential *sec*-butyl chain, we cannot discern whether this causes the lack of activity or whether the phenyl and triazolone rings in the core structure are also important. Compound **11**, which encompasses the linker and the triazolone region including the *sec*-butyl chain but lacks the dioxolane region, was also not able to redistribute OSBP and showed no antiviral effect. We previously reported that posaconazole, which is structurally highly similar to ITZ (it comprises a difluorobenzyl ring instead of a dichlorobenzyl ring, the dioxolane ring is substituted to an oxolane, and an elongated branched side chain), is also capable of inhibiting virus replication⁴. Although we cannot exclude a role for the dichlorobenzyl or the dioxolane ring moiety, our data indicate that the extensive core structure of ITZ consisting of the four linked rings is key to inhibition of OSBP and thereby the antiviral activity of ITZ.

Table 4. The activity of ITZ analogs with changes in the core structure towards inhibition of EMCV replication, OSBP redistribution and VEGFR2 glycosylation

Compounds	R3 / R4 ^a	Inhibition of virus replication EC50 (μM)	OSBP redistribution (10 μM)	VEGFR2 glycosylation (2 μM) ²⁶	Hh inhibition ^{a,26}
ITZ		0.46 ±(0,14)	+	+	++
Terconazole ^a		> 10	-	- ¹⁴	n.d.
9^b		> 10	-	n.d.	n.d.
10^b		> 10	-	n.d.	n.d.
11^b		> 10	-	n.d.	n.d.

Shown are the means and the standard deviations of data from four independent experiments^a compounds with change in R3; ^b compounds with change in R4

^c Inhibition of Hh signaling, determined using a reporter for the Hh-regulated transcription factor *Gliz*²⁶.
n.d.; not determined.

Molecular modeling studies

We previously showed that ITZ binds OSBP directly and inhibits its lipid shuttling function, most likely by targeting the ORD⁴. In order to investigate the presumed binding of ITZ to the ORD of OSBP, a series of molecular modeling studies were conducted. Currently, no structural data are available for the ORD of human OSBP or OSBP-related proteins (ORPs). Therefore, we decided to build a homology model for the OSBP ORD based on the crystal structure of the yeast ORP Osh4/Kes1p (32% identity), which essentially consists of an ORD only³¹. We also considered the structure of the yeast ORP Osh3, but this protein only binds PI(4)P and the binding site is too narrow to accommodate sterols. Like OSBP, Osh4 mediates an exchange of sterols for PI(4)P³². The structure of Osh4 has been resolved in complex with different sterols, with PI(4)P and in the apo form^{31,32}. The Osh4 ORD contains a hydrophobic tunnel that can accommodate sterols or one of the two fatty acyl chains of PI(4)P. Sterol binding in this tunnel induces a conformational changes that shifts an amino terminal helical lid in front of the tunnel entrance (Supplement Figure 1A). The “closed” conformation is stabilized by interactions between the lid and the sterol³¹. We assumed that ITZ binds in the hydrophobic tunnel of OSBP, similar to how sterols bind to ORPs. In support of our assumption that ITZ can bind in a sterol-binding pocket, ITZ also binds NPC1 in the sterol-binding pocket¹¹. Based on the Osh4p structures, we reasoned that ITZ should bind the apo form of OSBP, since ITZ would have a steric clash with the lid in the closed, sterol-binding conformation (Supplement Figure 2A). Hence, the apo form of Osh4 was selected as a template to build a homology model of OSBP as detailed in the methods section (Supplement Figure 1C).

We then performed molecular docking studies of ITZ into the sterol-binding pocket of OSBP. According to our models, the *sec*-butyl chain of ITZ most likely inserts deep into the hydrophobic part of the sterol-binding tunnel leaving the dioxolane ring with the triazole and dichlorobenzyl moieties outside the pocket in a more solvent exposed area. Two possible orientations were found for this part of ITZ, in one of which this part of ITZ binds in proximity to the strictly conserved OSBP “fingerprint motif” EQVSHHPP, to which the head group of PI(4)P normally binds³³ (Figure 3A). Importantly, as the hydrophobic pocket is too narrow to accommodate both ITZ and lipids (sterols or one of the legs of PI(4)P), this implies that ITZ likely competitively inhibits the lipid shuttling activity of OSBP.

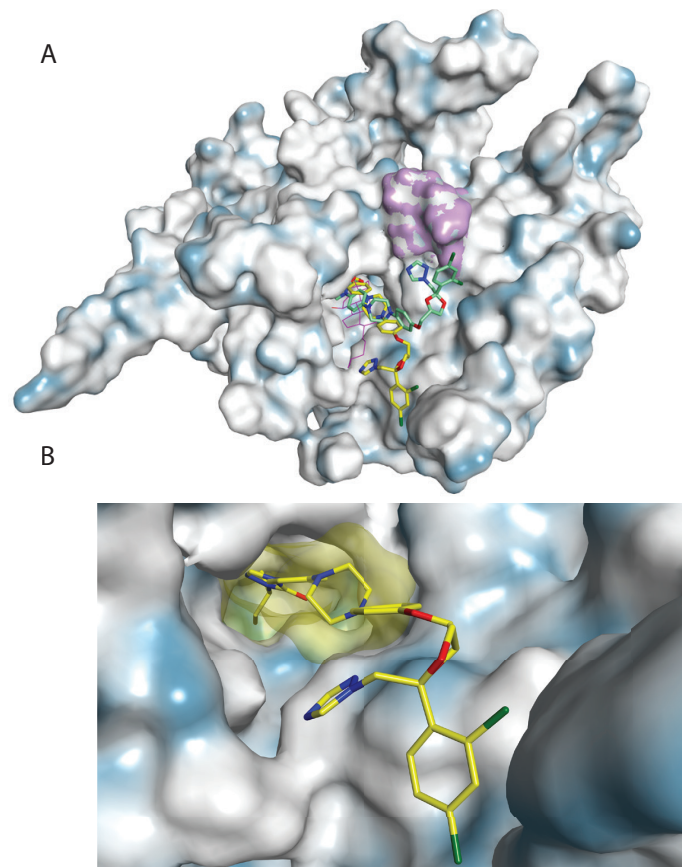


Figure 3. Modeling of the OSBP ORD structure on the crystal structure of Osh4p. (A) Homology model of the OSBP ORD in the open conformation. The *sec*-butyl chain of ITZ inserts deep in the hydrophobic tunnel, leaving the triazole-dichlorophenyl-dioxolane region outside in a more solvent exposed area. Our models calculated two possible orientations for this part (the two different models for ITZ are shown as yellow and light green carbon atoms respectively), one of which is in proximity of the strictly conserved "OSBP fingerprint motif" EQVSHHPP (lilac surface). The position of 7-hydroxycholesterol is shown in purple. (B) Zoom into the binding pocket of ITZ, only one calculated orientation of ITZ is shown.

Importantly, the model is in line with the biological data obtained with the ITZ analogs. The triazole ring, positioned outside the tunnel in a solvent-exposed area, does not make specific interaction with the ORD, which is in accordance with the experimental data that the triazole ring is not important to drive accumulation of OSBP at the Golgi. We observed that the *sec*-butyl chain is fundamental for OSBP inhibition and only substitutions by bulky, non-linear side chains are tolerated. Based on our model, we conclude that a bulkier side chain better fills the narrow binding pocket at

the bottom of the hydrophobic tunnel, whereas a linear alkyl chain has more flexibility in the tunnel and likely binds less strongly (Figure 3B). Finally, analogs that lacked part of the core structure of ITZ were inactive towards OSBP. In our model, the full length of the ITZ core is needed to bridge the distance between the pocket at the bottom of the hydrophobic tunnel in which the *sec*-butyl chain docks and the outside of the tunnel where there is sufficient space to accommodate the bulky triazole-dichlorophenyl-dioxolane region. Shorter compounds would only fill part of the tunnel and would have significantly fewer hydrophobic interactions to stabilize them in the tunnel.

Discussion

In this study, we explore the structural features of the OSBP-mediated antiviral activity of ITZ through a structure-activity relationship study and a computational model of OSBP with ITZ. All eight ITZ stereoisomers target OSBP and inhibit virus replication. This is in line with the molecular models, which predict a fairly loose fit of ITZ in the sterol-binding pocket that provides sufficient space for any of the stereoisomers. Such a loose fit is also in accordance with the strength of the interaction that we previously measured ($K_d = \sim 400$ nM)⁴, which implies a relatively weak interaction. Nevertheless, we did observe somewhat different inhibitory activities of the various stereoisomers. The clinically used stereoisomers were somewhat more potent than the non-clinically used isomers. Of the four clinically used stereoisomers, the two 2S4R stereoisomers (compounds **1a** and **1b**) were slightly more potent than the 2R4S stereoisomers (compounds **1c** and **1d**). This may indicate some (weak) interaction of the dichlorophenyl substituent, of which the positioning depends on the stereochemistry of carbons 2 and 4, with OSBP. The 2S4R isomers were also slightly more active in inhibiting angiogenesis via VEGFR2 and mTOR functioning^{3,26,34}.

We observed that the triazole moiety is not important for the OSBP-mediated antiviral activity. Since the triazole moiety is essential for the antifungal activity of ITZ³⁰, derivatives without the triazole moiety may have potential for antiviral therapy without CYP51- or CYP3A4-mediated adverse effects or the risk of inducing resistance against triazole-class antifungals in case a patient would have a fungal co-infection. Our data clearly show the importance of the *sec*-butyl chain for OSBP-mediated antiviral activity. Still, some divergence towards the structure is tolerated, provided that the side chain is branched and relatively large. Finally, the full-length core structure of ITZ appears important for the antiviral effect of ITZ to allow sufficient interactions with the hydrophobic tunnel.

Besides a broad antiviral activity, ITZ possesses a potent anticancer activity against a number of different cancer types^{13,15,17,35}. So far, only the molecular targets through which ITZ inhibits the mTOR (VDAC1, NPC-1) signaling pathway have been identified^{9,10-12,35,36}. The target through which ITZ affects the trafficking, glycosylation and functioning of VEGFR2 has remained unknown. A number of ITZ analogs that we tested here, i.e. the stereoisomers and *sec*-butyl chain analogs, have previously been investigated for their

effect on VEGFR2 glycosylation (which results from an inhibition of VEGFR2 trafficking and which correlates with impaired VEGFR2 functioning) and Hh signaling (as assayed using a reporter under control of the Hh-regulated transcription factor Gli1)²⁶. Only the *sec*-butyl chain analogs have been tested for Hh inhibition, which did not correlate with altered VEGFR2 glycosylation²⁶ and also does not correlate with antiviral activity and OSBP redistribution (Table 3). In general, we find a good, although not complete, correlation between activity of ITZ analogs towards virus replication and OSBP redistribution on the one hand and VEGFR2 glycosylation on the other hand (Tables 1-4). The clinically used stereoisomers had a somewhat higher antiviral activity and affected VEGFR2 glycosylation more severely than the non-clinically used stereoisomers (Table 1)²⁶. Only for the stereoisomers 2S4S2'R (compound **1f**) and 2R4R2'R (compound **1h**) the OSBP-mediated antiviral activity does not correlate with the previously reported effect on VEGFR2 glycosylation. At present, it is not clear whether this is truly due to different activities of those stereoisomers towards OSBP and VEGFR2 glycosylation, or whether the apparent discrepancy is caused by experimental differences (e.g. inhibitor concentrations, treatment times, cell lines, qualitative read-outs).

If indeed ITZ affects VEGFR2 via OSBP, the trafficking, glycosylation and functioning defects of VEGFR2 may well result from disturbances of cholesterol homeostasis caused by OSBP inhibition. Such a dependence of VEGFR2 on OSBP could be directly related to the sterol shuttling activity of OSBP, but may also be an indirect effect through proteins that depend on OSBP-mediated lipid homeostasis. Namely, by modulating PI(4)P levels at the Golgi, OSBP is an important regulator of the ER-Golgi MCS¹⁸ and as such of other lipid transfer proteins that operate at the ER-Golgi MCS. For example, the activity of the ceramide transfer protein CERT, which shuttles ceramide to the Golgi to allow the biosynthesis of sphingomyelin, is sensitive to OSBP inhibitors³⁷. Presumably, by perturbing the lipid composition of the Golgi apparatus, ITZ affects the overall functioning of the Golgi, which could explain the ITZ-induced changes in VEGFR2 trafficking, glycosylation and functioning.

Together, our work contributes to the development of ITZ-derived antiviral compounds with an increased specificity towards OSBP and fewer side effects. Although it may not be possible to fully uncouple all activities of ITZ, it appears that at least OSBP-mediated antiviral activity can be uncoupled from antifungal activity and Hh inhibition.

Experimental Section

Chemistry

ITZ has three chiral centers (designated 2, 4, 2') (Figure 1). The synthesis of all eight ITZ stereoisomers and of *sec*-butyl chain analogs (compounds **5-8**) has been previously described²⁶. The synthesis of the triazole deleted analog (compound **2**) was previously described in^{10,26-28}. Compound **9** was synthesized as described in²⁷, and compound **11**

was previously described in²⁸. The experimental procedure and characterization of compounds **3**, **4** and **10** are described in detail in the Supplemental methods.

Cell Culture

HeLa R19 cells were grown at 37°C, 5 % CO₂ in Dulbecco's modified Eagle's medium (DMEM, Lonza) supplemented with 10 % fetal bovine serum.

Infection Assays

RLuc-EMCV, a recombinant virus encoding a *Renilla* luciferase gene upstream of the capsid-coding region, was described before^{4,29}. Virus infections were performed by incubating subconfluent HeLa R19 cells with virus at MOI 0.1 at 37°C for 30 min. Next, the medium was removed and fresh compound-containing medium was added to the cells. After 7h the medium was discarded and cells were lysed to determine the *Renilla* luciferase activity using the *Renilla* luciferase Assay System (Promega) according to the manufacturer's protocol. Cell viability was determined in parallel using the AQueous One Solution Cell Proliferation Assay (Promega) according to the manufacturer's protocol. The optical density at 490 nm was determined using a microplate reader.

Fluorescence Microscopy

Subconfluent HeLa R19 cells grown on coverslips in 24-well plates were transfected with 200ng per well of the pEGFP-hOSBP plasmid⁴ using Fugene 6 (Promega) according to the manufacturer's instruction. After overnight expression, the medium was discarded and fresh medium containing 10µM compound was added. After 1h the cells were fixed with 4 % PFA, permeabilized with 0.1 % Triton-X100, and the nucleus was stained with DAPI as previously described⁴. Cells were embedded in FluorSave (Merck Millipore) and imaged using an Olympus BX60 fluorescence microscope.

Molecular Modeling

All molecular modeling studies were performed on a Viglen Genie Intel®Core™ i7-3770 vPro CPU@ 3.40 GHz x 8 running Ubuntu 14.04. Molecular Operating Environment (MOE) 2015.10 and Maestro (Schrödinger Release 2016-1) were used as molecular modeling software.

The homology model of the OSBP ORD was prepared with the MOE2015.10 homology tool using a single template approach following a procedure previously reported³⁸. The crystal structure of the ORD of Osh4p from *Saccharomyces cerevisiae* (PDB ID: 1Z17) in the *apo* form was used as template having a sequence similarity of 32% with the human isoform³¹. The amino acid sequence of human OSBP was loaded in MOE together with the 3D structure of the yeast isoform and manually aligned following the reported structure-based alignment of ORDs³³, and the final 3D model was obtained as Cartesian average of 10 generated intermediate models³¹. The new model was energy minimized using the Amber99 force field and then validated in terms of the stereochemical quality of the backbone, side chain and amino acid environment

using the online UCLA-DOE LAB web server. The structure of 7-hydroxycholesterol as it was co-crystallized with the ORD of Osh4 (PDB ID: 1ZHG) was inserted in the sterol-binding site of the OSBP ORD model after the superposition of the model and the crystal structure.

The new model of the ORD of human OSBP was preprocessed using the Schrödinger Protein Preparation Wizard by assigning bond orders, adding hydrogen atoms and performing a restrained energy minimization of the added hydrogen atoms using the OPLS_2005 force field. A ligands database in sdf format was prepared using MOE2015.10 and then processed using the Maestro LigPrep tool by energy minimizing the structures (OPLS_2005 force field), generating possible ionization states at pH 7±2, generating tautomers and low-energy ring conformers. A 20 Å docking grid was prepared using as centroid the area occupied by 7-hydroxycholesterol. Molecular docking of the prepared ligands was performed using Glide standard precision (SP) keeping the default parameters and setting 5 as number of output poses per input ligand to include in the solution. The docking solutions were visual inspected in MOE2015.10 to identify the potential interaction between ligand and protein.

Acknowledgments

This work was supported by research grants from the Netherlands Organisation for Scientific Research (NWO-VENI-722.012.066 to JRPMS, NWO-VICI-91812628 to FJMvK), the European Union (Horizon 2020 Marie Skłodowska-Curie ETN 'ANTIVIRALS', grant agreement number 642434 to AB and FJMvK), the PhRMA foundation (to SAH), the US National Cancer Institute (R01CA184103 to JOL), the Flight Attendant Medical Research Institute, Prostate Cancer Foundation (to JOL), and the Johns Hopkins Institute for Clinical and Translational Research (ICTR), which is funded in part by Grant Number UL1 TR 001079. SF and AB acknowledge support from the Life Science Research Network Wales grant no. NRNPGSep14008, an initiative funded through the Welsh Government's Ser Cymru program.

References

1. Tapparel, C., Siegrist, F., Petty, T. J. & Kaiser, L. Picornavirus and enterovirus diversity with associated human diseases. *Infect Genet Evol* 14, 282-293, doi:10.1016/j.meegid.2012.10.016 (2013).
2. Gao, Q. *et al.* Discovery of itraconazole with broad-spectrum in vitro antienterovirus activity that targets nonstructural protein 3A. *Antimicrobial agents and chemotherapy* 59, 2654-2665, doi:10.1128/AAC.05108-14 (2015).
3. Shim, A. *et al.* Therapeutic and prophylactic activity of itraconazole against human rhinovirus infection in a murine model. *Scientific reports* 6, 23110, doi:10.1038/srep23110 (2016).
4. Strating, J. R. *et al.* Itraconazole inhibits enterovirus replication by targeting the oxysterol-binding protein. *Cell reports* 10, 600-615, doi:10.1016/j.celrep.2014.12.054 (2015).
5. Lestner, J. & Hope, W. W. Itraconazole: an update on pharmacology and clinical use for treatment of invasive and allergic fungal infections. *Expert opinion on drug metabolism & toxicology* 9, 911-926, doi:10.1517/17425255.2013.794785 (2013).
6. Lamb, D. C. *et al.* Characteristics of the heterologously expressed human lanosterol 14alpha-demethylase (other names: P45014DM, CYP51, P45051) and inhibition of the purified human and *Candida albicans* CYP51 with azole antifungal agents. *Yeast* 15, 755-763, doi:10.1002/(SICI)1097-0061(19990630)15:9<755::AID-YEA417>3.0.CO;2-8 (1999).
7. Trosken, E. R. *et al.* Comparison of lanosterol-14 alpha-demethylase (CYP51) of human and *Candida albicans* for inhibition by different antifungal azoles. *Toxicology* 228, 24-32, doi:10.1016/j.tox.2006.08.007 (2006).
8. Kim, J. *et al.* Itraconazole, a commonly used antifungal that inhibits Hedgehog pathway activity and cancer growth. *Cancer cell* 17, 388-399, doi:10.1016/j.ccr.2010.02.027 (2010).
9. Xu, J., Dang, Y., Ren, Y. R. & Liu, J. O. Cholesterol trafficking is required for mTOR activation in endothelial cells. *Proceedings of the National Academy of Sciences of the United States of America* 107, 4764-4769, doi:10.1073/pnas.0910872107 (2010).
10. Head, S. A. *et al.* Antifungal drug itraconazole targets VDAC1 to modulate the AMPK/mTOR signaling axis in endothelial cells. *Proceedings of the National Academy of Sciences of the United States of America* 112, E7276-7285, doi:10.1073/pnas.1512867112 (2015).
11. Head, S. A. *et al.* Simultaneous Targeting of NPC1 and VDAC1 by Itraconazole Leads to Synergistic Inhibition of mTOR Signaling and Angiogenesis. *ACS chemical biology* 12, 174-182, doi:10.1021/acscchembio.6b00849 (2017).
12. Trinh, M. N. *et al.* Triazoles inhibit cholesterol export from lysosomes by binding to NPC1. *Proceedings of the National Academy of Sciences of the United States of America* 114, 89-94, doi:10.1073/pnas.1619571114 (2017).
13. Aftab, B. T., Dobromilskaya, I., Liu, J. O. & Rudin, C. M. Itraconazole inhibits angiogenesis and tumor growth in non-small cell lung cancer. *Cancer Res* 71, 6764-6772, doi:10.1158/0008-5472.CAN-11-0691 (2011).
14. Nacev, B. A., Grassi, P., Dell, A., Haslam, S. M. & Liu, J. O. The antifungal drug itraconazole inhibits vascular endothelial growth factor receptor 2 (VEGFR2) glycosylation, trafficking, and signaling in endothelial cells. *The Journal of biological chemistry* 286, 44045-44056, doi:10.1074/jbc.M111.278754 (2011).

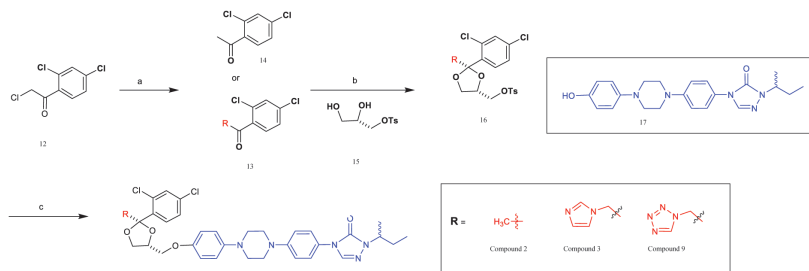
15. Antonarakis, E. S. *et al.* Repurposing itraconazole as a treatment for advanced prostate cancer: a noncomparative randomized phase II trial in men with metastatic castration-resistant prostate cancer. *The oncologist* 18, 163-173, doi:10.1634/theoncologist.2012-314 (2013).
16. Kim, D. J. *et al.* Open-label, exploratory phase II trial of oral itraconazole for the treatment of basal cell carcinoma. *Journal of clinical oncology : official journal of the American Society of Clinical Oncology* 32, 745-751, doi:10.1200/JCO.2013.49.9525 (2014).
17. Rudin, C. M. *et al.* Phase 2 study of pemetrexed and itraconazole as second-line therapy for metastatic nonsquamous non-small-cell lung cancer. *Journal of thoracic oncology : official publication of the International Association for the Study of Lung Cancer* 8, 619-623, doi:10.1097/JTO.0b013e31828c3950 (2013).
18. Mesmin, B. *et al.* A four-step cycle driven by PI(4)P hydrolysis directs sterol/PI(4)P exchange by the ER-Golgi tether OSBP. *Cell* 155, 830-843, doi:10.1016/j.cell.2013.09.056 (2013).
19. van der Schaar, H. M., Dorobantu, C. M., Albulescu, L., Strating, J. R. & van Kuppeveld, F. J. Fat(al) attraction: Picornaviruses Usurp Lipid Transfer at Membrane Contact Sites to Create Replication Organelles. *Trends in microbiology* 24, 535-546, doi:10.1016/j.tim.2016.02.017 (2016).
20. Strating, J. R. & van Kuppeveld, F. J. Viral rewiring of cellular lipid metabolism to create membranous replication compartments. *Current opinion in cell biology* 47, 24-33, doi:10.1016/j.ceb.2017.02.005 (2017).
21. Hsu, N. Y. *et al.* Viral reorganization of the secretory pathway generates distinct organelles for RNA replication. *Cell* 141, 799-811, doi:10.1016/j.cell.2010.03.050 (2010).
22. van der Schaar, H. M. *et al.* A novel, broad-spectrum inhibitor of enterovirus replication that targets host cell factor phosphatidylinositol 4-kinase IIIbeta. *Antimicrobial agents and chemotherapy* 57, 4971-4981, doi:10.1128/AAC.01175-13 (2013).
23. Dorobantu, C. M. *et al.* Modulation of the Host Lipid Landscape to Promote RNA Virus Replication: The Picornavirus Encephalomyocarditis Virus Converges on the Pathway Used by Hepatitis C Virus. *PLoS pathogens* 11, e1005185, doi:10.1371/journal.ppat.1005185 (2015).
24. Roulin, P. S. *et al.* Rhinovirus uses a phosphatidylinositol 4-phosphate/cholesterol counter-current for the formation of replication compartments at the ER-Golgi interface. *Cell host & microbe* 16, 677-690, doi:10.1016/j.chom.2014.10.003 (2014).
25. Arita, M. *et al.* Oxysterol-binding protein family I is the target of minor enviroxime-like compounds. *Journal of virology* 87, 4252-4260, doi:10.1128/JVI.03546-12 (2013).
26. Shi, W. *et al.* Itraconazole side chain analogues: structure-activity relationship studies for inhibition of endothelial cell proliferation, vascular endothelial growth factor receptor 2 (VEGFR2) glycosylation, and hedgehog signaling. *Journal of medicinal chemistry* 54, 7363-7374, doi:10.1021/jm200944b (2011).
27. Shi, W., Nacev, B. A., Bhat, S. & Liu, J. O. Impact of Absolute Stereochemistry on the Antiangiogenic and Antifungal Activities of Itraconazole. *ACS Med Chem Lett* 1, 155-159, doi:10.1021/ml1000068 (2010).
28. Chong, C. R. *et al.* Inhibition of angiogenesis by the antifungal drug itraconazole. *ACS chemical biology* 2, 263-270, doi:10.1021/cb600362d (2007).
29. Albulescu, L. *et al.* Broad-range inhibition of enterovirus replication by OSW-1, a natural compound targeting OSBP. *Antiviral research* 117, 110-114, doi:10.1016/j.antiviral.2015.02.013 (2015).
30. Odds, F. C., Brown, A. J. & Gow, N. A. Antifungal agents: mechanisms of action. *Trends in microbiology* 11, 272-279 (2003).
31. Im, Y. J., Raychaudhuri, S., Prinz, W. A. & Hurley, J. H. Structural mechanism for sterol sensing and transport by OSBP-related proteins. *Nature* 437, 154-158, doi:10.1038/nature03923 (2005).
32. de Saint-Jean, M. *et al.* Osh4p exchanges sterols for phosphatidylinositol 4-phosphate between lipid bilayers. *The Journal of cell biology* 195, 965-978, doi:10.1083/jcb.201104062 (2011).
33. Tong, J., Yang, H., Yang, H., Eom, S. H. & Im, Y. J. Structure of Osh3 reveals a conserved mode of phosphoinositide binding in oxysterol-binding proteins. *Structure* 21, 1203-1213, doi:10.1016/j.str.2013.05.007 (2013).
34. Shim, J. S. *et al.* Divergence of Antiangiogenic Activity and Hepatotoxicity of Different Stereoisomers of Itraconazole. *Clin Cancer Res* 22, 2709-2720, doi:10.1158/1078-0432.CCR-15-1888 (2016).
35. Tsubamoto, H. *et al.* Itraconazole Inhibits AKT/mTOR Signaling and Proliferation in Endometrial Cancer Cells. *Anticancer Res* 37, 515-519, doi:10.21873/anticancer.11343 (2017).
36. Liang, G. *et al.* Itraconazole exerts its anti-melanoma effect by suppressing Hedgehog, Wnt, and PI3K/mTOR signaling pathways. *Oncotarget*, doi:10.18632/oncotarget.15324 (2017).
37. Perry, R. J. & Ridgway, N. D. Oxysterol-binding protein and vesicle-associated membrane protein-associated protein are required for sterol-dependent activation of the ceramide transport protein. *Molecular biology of the cell* 17, 2604-2616, doi:10.1091/mbc.E06-01-0060 (2006).
38. Bassetto, M. *et al.* Design and synthesis of novel bicalutamide and enzalutamide derivatives as antiproliferative agents for the treatment of prostate cancer. *Eur J Med Chem* 118, 230-243, doi:10.1016/j.ejmech.2016.04.052 (2016).

Supporting Information

Supplementary Methods

Chemistry

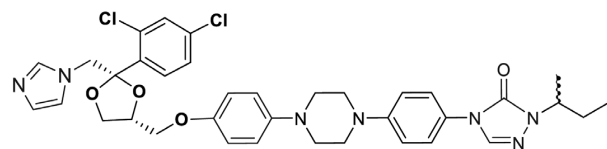
General scheme for Compounds 2, 3, and 4:



Reagents and conditions: (a) Imidazole or tetrazole, DCM, reflux, 12 h; (b) **3**, TfOH, toluene, rt, 60 h; (c) **5**, NaH, DMF, 80 °C, 12 h. The experimental procedures and the characterization for compounds **12** and **16** have been described previously (Chong et al., 2007) (Shi et al., 2010) (Shi et al., 2011) (Head et al., 2015).

To a solution of tosylate (**16**) (1 eq) in dry DMF was added sodium hydride (NaH, 60% dispersion in mineral oil, (1.5 eq)) under argon atmosphere. After the reaction mixture was stirred at 50°C for 1 hour. A solution of **17** (1.2 eq) in DMF was added slowly at the same temperature. After the addition the temperature was increased to 90°C and stirred for another 3 hours. The reaction mixture was quenched by the saturated sodium chloride, and the resulting mixture was extracted twice with dichloromethane. The organic fractions were dried over Na₂SO₄, filtered and concentrated under vacuum to yield the crude product that was purified by column chromatography to afford the desired products.

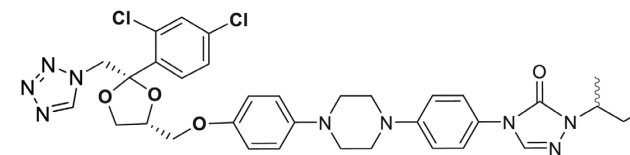
4-(4-(4-(4-(((2S,4R)-2-((1H-imidazol-1-yl)methyl)-2-(2,4-dichlorophenyl)-1,3-dioxolan-4-yl)methoxy)phenyl)piperazin-1-yl)phenyl)-1-sec-butyl-1H-1,2,4-triazol-5(4H)-one (Compound 3)



¹H NMR (500 MHz, CDCl₃, δ_H): 7.61 (s, 1H), 7.58 (d, *J* = 8.0 Hz, 1H), 7.53 (bs, 1H), 7.46 (d, *J* = 2.5 Hz, 1H), 7.42 (d, *J* = 9.5 Hz, 2H), 7.26 (dd, *J* = 8.2, 2.2 Hz, 2H), 7.03 (d, *J* = 9 Hz, 2H), 7.00-6.98 (m, 1H), 6.93 (d, *J* = 9.0 Hz, 2H), 6.78 (d, *J* = 9.5 Hz, 2H), 4.51 (d, *J* = 15.0 Hz, 1H), 4.41 (d, *J* = 15.0 Hz, 1H), 4.41 (d, *J* = 15.0 Hz, 1H), 4.34 – 4.28 (m, 2H), 3.87 (dd, *J* = 8.5, 6.5 Hz, 1H), 3.74 – 3.72 (m, 2H), 3.36 (t, *J* = 5.0 Hz, 4H), 3.32 – 3.31 (m, 1H), 3.23 (t, *J* = 5.0 Hz, 4H), 1.89 – 1.83 (m, 1H), 1.74 – 1.71 (m, 1H), 1.39 (d, *J* = 7.0 Hz, 3H), 0.90 (t, *J* = 7.0 Hz, 3H).

¹³C NMR (125 MHz, CDCl₃, δ_C): 152.7, 152.1, 150.6, 146.0, 136.0, 134.6, 134.0, 133.0, 131.4, 129.5, 127.3, 125.9, 123.6, 118.5, 116.7, 115.3, 108.0, 74.8, 67.7, 67.6, 52.7, 50.6, 49.3, 28.5, 19.3, 10.8.

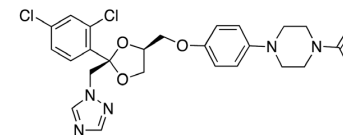
4-(4-(4-(4-(((2S,4R)-2-((1H-tetrazol-1-yl)methyl)-2-(2,4-dichlorophenyl)-1,3-dioxolan-4-yl)methoxy)phenyl)piperazin-1-yl)phenyl)-1-sec-butyl-1H-1,2,4-triazol-5(4H)-one (Compound 4)



¹H NMR (500 MHz, CDCl₃, δ_H): 8.46 (s, 1H), 7.61 (s, 1H), 7.55 (d, *J* = 8.5 Hz, 1H), 7.48 (d, *J* = 2.0 Hz, 1H), 7.43 (d, *J* = 9 Hz, 2H), 7.24 (dd, *J* = 8.5, 2.0 Hz, 1H), 7.03 (d, *J* = 9.0 Hz, 2H), 6.81 (d, *J* = 9.0 Hz, 2H), 5.36 (d, *J* = 14.0 Hz, 1H), 5.27 (d, *J* = 14.0 Hz, 1H), 4.38 (t, *J* = 5.0 Hz, 1H), 4.31-4.27 (m, 1H), 3.95 (dd, *J* = 8.5, 6.5 Hz, 1H), 3.88 – 3.83 (m, 2H), 3.53 (dd, *J* = 9.5, 6.5 Hz, 1H), 3.38 (bs, 4H), 3.26 (bs, 4H), 1.89 – 1.83 (m, 1H), 1.74 – 1.69 (m, 1H), 1.39 (d, *J* = 7.0 Hz, 3H), 0.90 (t, *J* = 7.5 Hz, 3H).

¹³C NMR (125 MHz, CDCl₃, δ_C): 162.5, 152.8, 152.7, 152.0, 136.3, 133.9, 133.3, 131.5, 130.1, 129.6, 127.2, 123.6, 116.8, 115.4, 107.4, 74.8, 67.9, 67.6, 56.6, 52.7, 36.5, 31.0, 28.5, 19.2, 10.8.

1-[4-(4-(((2R,4S)-2-(2-(2,4-dichlorophenyl)-2-((1H-1,2,4-triazol-1-yl)methyl)-1,3-dioxolan-4-yl)methoxy)phenyl)piperazin-1-yl)ethan-1-one (CAS # 67915-35-9) (Compound 10)

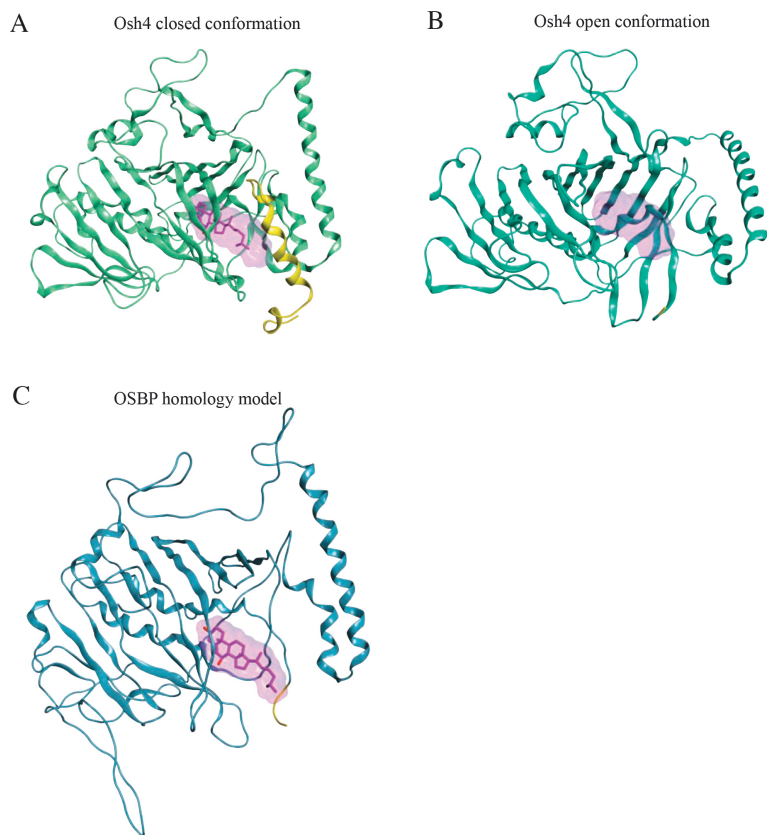


This compound was synthesized according to the procedure delineated previously (Tanoury et al., 2003), and the characterization described below is in agreement with the data given in that article.

¹H NMR (400 MHz, CDCl₃): δ 8.21 (s, 1H), 7.92 (s, 1H), 7.57 (d, *J* = 8.4 Hz, 1H), 7.46 (d, *J* = 1.9 Hz, 1H), 7.24 (dd, *J* = 8.8, 1.9 Hz, 1H), 6.89 (d, *J* = 8.9 Hz, 2 H), 6.79 (d, *J* = 8.9 Hz, 2H), 4.82 (q_{AB}, *J* = 14.5 Hz, 2H), 4.35 (m, 1H), 3.93 (t, *J* = 6.6 Hz, 1H), 3.78 (m, 3H), 3.61 (m, 2H), 3.46 (dd, *J* = 9.7 Hz, 1H), 3.05 (m, 3H), 2.18 (s, 2H), 1.58 (s, 3H).

MALDI-MS (matrix: DHB): *m/z* = 532 (MH⁺, base peak), 554 (M+Na⁺).

Supplementary Figures



Supplementary Figure 1. Structure of Osh4 and OSBP homology model. (A) Crystal structure of the “closed” conformation of the Osh4p ORD co-crystallized with 7-hydroxycholesterol (PDB ID: 1ZHT) (carbon atoms of 7-hydroxycholesterol are displayed in purple). The flexible amino terminal helix lid (yellow ribbon) is blocking the tunnel entrance. (B) The crystal structure shows the open conformation of Osh4 (PDB ID: 1ZI7). (C) Homology model of the OSBP ORD in the open conformation. Part of the disordered flexible lid is shown as a yellow line, which in this conformation shifts away from the sterol-binding tunnel, allowing access of ligands and inhibitors. 7-hydroxycholesterol was inserted in the sterol-binding tunnel of the model based upon superposition of the OSBP model with the Osh4p “closed” crystal structure.

Supplementary Table

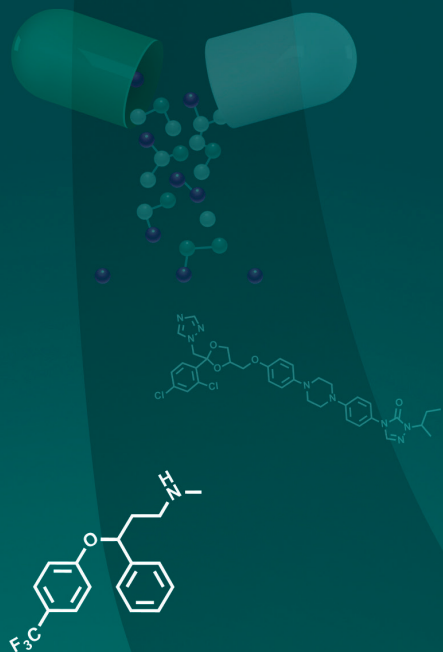
In this table all four different experiments with EC50, the mean values and the standard deviation (SD) are displayed. All values are in μM.

Compound Nr	Inhibition of virus replication EC50 (μM)				Mean μM	SD (μM)			
ITZ	0,33	0,33	0,42	0,74	0,54	0,36	0,52	0,46	0,14
1a			0,52	0,53		0,45	0,34	0,46	0,08
1b			0,32	0,61		0,36	0,54	0,46	0,12
1c			0,43	0,31		*	*	0,37	0,06
1d			0,85	0,51		1,09	0,99	0,86	0,22
1e			1,64	3,62		*	*	2,63	0,99
1f			1,42	2,41		2,29	1,93	2,01	0,38
1g			1,60	4,82		*	*	3,21	1,61
1h			1,47	3,11		4,89	2,31	2,95	1,26
2		0,69		0,62		0,77	1,19	0,82	0,22
3		0,50		0,38		0,44	0,41	0,43	0,04
4		0,01		0,26		0,38	0,42	0,26	0,16
5		>10		>10		>10	>10		
6		>10		>10		>10	>10		
7		0,35		0,23		0,26	0,15	0,25	0,07
8		0,01		0,11		0,34	0,17	0,16	0,12
Terconazole		>10		>10		>10			
9		>10		>10		>10			
10		>10		>10		>10			
11		>10		>10		>10			

* indicates that these compounds were scarce and could not be tested in this experiment.

Supplementary References

1. Chong, C.R., Xu, J., Lu, J., Bhat, S., Sullivan, D.J., Jr., Liu, J.O., 2007. Inhibition of angiogenesis by the antifungal drug itraconazole. *ACS chemical biology* 2, 263-270.
2. Head, S.A., Shi, W., Zhao, L., Gorshkov, K., Pasunooti, K., Chen, Y., Deng, Z., Li, R.J., Shim, J.S., Tan, W., Hartung, T., Zhang, J., Zhao, Y., Colombini, M., Liu, J.O., 2015. Antifungal drug itraconazole targets VDAC1 to modulate the AMPK/mTOR signaling axis in endothelial cells. *Proceedings of the National Academy of Sciences of the United States of America* 112, E7276-7285.
3. Shi, W., Nacev, B.A., Aftab, B.T., Head, S., Rudin, C.M., Liu, J.O., 2011. Itraconazole side chain analogues: structure-activity relationship studies for inhibition of endothelial cell proliferation, vascular endothelial growth factor receptor 2 (VEGFR2) glycosylation, and hedgehog signaling. *Journal of medicinal chemistry* 54, 7363-7374.
4. Shi, W., Nacev, B.A., Bhat, S., Liu, J.O., 2010. Impact of Absolute Stereochemistry on the Antiangiogenic and Antifungal Activities of Itraconazole. *ACS Med Chem Lett* 1, 155-159.
5. Tanoury, G.J., Hett, R., Wilkinson, H.S., Wald, S.A., Senanayake, C.H., 2003. Total synthesis of (2R,4S,2' S,3' R)-hydroxyitraconazole: implementations of a recycle protocol and a mild and safe phase-transfer reagent for preparation of the key chiral units. *Tetrahedron-Asymmetr* 14, 3487-3493.



Chapter

4

Fluoxetine inhibits enterovirus replication by targeting the viral 2C protein in a stereospecific manner

Lisa Bauer^{1,*}, Roberto Manganaro^{2,*}, Birgit Zonsics^{2,*},
Jeroen R.P.M. Strating^{1,†}, Priscila El Kazzi³, Moira Lorenzo
Lopez², Rachel Ulferts^{1,‡}, Clara van Hoey⁴, Maria J. Maté³,
Thierry Langer⁴, Bruno Coutard^{3,5}, Andrea Brancale²,
Frank J.M. van Kuppeveld^{1,#}

¹ Virology Division, Department of Infectious Diseases
and Immunology, Faculty of Veterinary Medicine,
Utrecht University, The Netherlands

² School of Pharmacy and Pharmaceutical Sciences,
Cardiff University, United Kingdom

³ Architecture et Fonction des Macromolécules
Biologiques, Aix-Marseille Université, France

⁴ Department of Pharmaceutical Chemistry, Faculty of
Life Sciences, University of Vienna, Austria

⁵ Unité des Virus Emergents, Marseille, France

[†] Present address: Viroclinics, Rotterdam, The
Netherlands

[‡] present address: The Francis Crick Institute, London,
United Kingdom

* These authors contributed equally

Corresponding author

ACS Infectious Diseases 2019, 5, 1609-1623

Abstract

Enteroviruses (family *Picornaviridae*) comprise a large group of human pathogens against which no licensed antiviral therapy exists. Drug-repurposing screens uncovered the FDA-approved drug fluoxetine as replication inhibitor of enterovirus B and D species. Fluoxetine likely targets the non-structural viral protein 2C, but detailed mode-of-actions studies are missing because structural information of 2C of fluoxetine-sensitive enteroviruses is lacking. We here show that broad-spectrum anti-enteroviral activity of fluoxetine is stereospecific concomitant with binding to recombinant 2C. (*S*)-fluoxetine inhibits with 5-fold lower EC_{50} than racemic fluoxetine. Using a homology model of 2C of the fluoxetine-sensitive enterovirus coxsackievirus B3 (CVB3) based upon a recently elucidated structure of a fluoxetine-insensitive enterovirus, we predicted stable binding of (*S*)-fluoxetine. Structure-guided mutations disrupted binding and rendered CVB3 resistant to fluoxetine. The study provides new insights into the anti-enteroviral mode-of-action of fluoxetine. Importantly, using only (*S*)-fluoxetine would allow for lower dosing in patients, thereby likely reducing side effects.

Keywords:

antiviral, enteroviruses, drug-repurposing, virus replication, molecular modelling,

Introduction

The genus *Enterovirus* within the *Picornaviridae* family includes many medically and socioeconomically important pathogens, which are among the most common infections in mankind. Four enterovirus (EV) species (EV-A, -B, -C and -D) and three rhinovirus (RV) species (RV-A, -B and -C) include serotypes that are known to cause human infections, like poliovirus, coxsackie A and B viruses, echoviruses, numbered enteroviruses (e.g. EV-A71 and EV-D68) and rhinovirus. Infections with enteroviruses can cause a broad spectrum of diseases ranging from hand-foot-and-mouth disease, conjunctivitis, aseptic meningitis, severe neonatal sepsis-like disease, to acute flaccid paralysis, whereas infection with rhinoviruses cause the common cold, as well as exacerbations of asthma and chronic obstructive pulmonary disease (COPD) ¹. These viral infections are often self-limiting but can also result in severe complications especially in young children. To date, no antiviral therapy to treat enterovirus infections has been approved and treatment remains limited to supportive care. Worldwide vaccination campaigns have almost eradicated poliomyelitis. However, the vaccines against poliovirus and a recently in China approved EV-A71 vaccine, are currently the only ones developed against enteroviruses. Vaccination is likely not a feasible general strategy to prevent enterovirus infections given the enormous amount (>250) of enterovirus (sero)types. Hence, the development of broad-spectrum anti-enteroviral drugs could be a promising alternative.

Enteroviruses are small, non-enveloped, positive-sense, single-stranded RNA viruses with an icosahedral capsid. The genome of ~ 7.5 kb encodes a single polyprotein that is auto-processed into structural proteins (VP1, VP2, VP3, VP4), non-structural proteins (2A, 2B, 2C, 3A, 3B, 3C, 3D) and several functional processing intermediates. The viral non-structural proteins, particularly the protease 3C^{pro} and the RNA-dependent RNA polymerase 3D^{pol}, are attractive targets for antiviral drug development ².

The viral protein 2C is the most conserved non-structural protein among picornaviruses, which makes it particularly interesting for broad-spectrum anti-enteroviral drug design. The viral 2C protein functions as ATPase ³⁻⁵, ATPase-dependent RNA helicase and as an ATPase-independent RNA chaperone ⁶, all of these enzymatic functions are indispensable for the viral life cycle. The ATPase domain of the protein belongs to the superfamily of SF3 helicases of the AAA+ ATPases and contains Walker A and Walker B motifs and motif C ⁷. Besides the ATPase domain, 2C harbors an N-terminal membrane-associated helical domain, a cysteine-rich motif and putative RNA binding motifs. 2C has been implicated in pleiotropic functions such as uncoating ⁸, cellular membrane rearrangement ⁹⁻¹², RNA binding ¹³⁻¹⁵, RNA replication ¹⁶⁻²¹, immune evasion ²² and encapsidation ²³⁻²⁶. Although 2C has a central role in the viral life cycle, the exact details of its involvement remain poorly understood.

Over the past decades, structurally disparate 2C inhibitors such as guanidine hydrochloride (GuaHCl), 2-(*a*-hydroxybenzyl)-benzimidazole HBB, MRL-1237 and TBZE-029 have been identified ^{2, 27-30}. An emerging concept to discover new antivirals is drug

repurposing. This strategy offers an attractive alternative to *de novo* drug development, as profound pharmacological and toxicological profiles of the compounds are already available. Furthermore, when the repurposed drug can be used at a similar dosage as for the original indication it may directly enter phase 2 clinical trials³¹⁻³², thereby reducing development cost and time. Several drug-repurposing screens have uncovered FDA-approved drugs as inhibitors of enterovirus replication². Some of these compounds are thought to inhibit the non-structural protein 2C because non-synonymous resistance mutations occur in 2C. Fluoxetine (Prozac®), a selective serotonin reuptake inhibitor (SSRI) that is FDA-approved for the treatment of major depression and anxiety disorders, was identified as a potent inhibitor of EV-B and -D species but EV-A, EV-C or rhinovirus species remained unaffected³³⁻³⁵. Besides its anti-enteroviral activity, fluoxetine was also shown to inhibit dengue virus and hepatitis C virus, two members of the *Flaviviridae* family, where it likely acts as a host-targeting rather than a direct-acting antiviral as it is the case for enteroviruses³⁶⁻³⁷. Fluoxetine has already been successfully used to treat an immunocompromised child with life-threatening chronic enterovirus encephalitis³⁸, underscoring the potential of fluoxetine for the application as an anti-enteroviral compound. Although various 2C inhibitors have been discovered over the years, their mode-of-action is still poorly understood.

Here, we set out to investigate how fluoxetine targets 2C of coxsackievirus B3 (CVB3), a virus model commonly used as a prototype for enterovirus B species. Fluoxetine has one chiral center, resulting into 2 enantiomers and we experimentally showed that only the *S*-enantiomer inhibits enterovirus replication by directly binding to the viral protein 2C. Based on the recently published crystal structure of the catalytic domain of EV-A71 2C protein³⁹, a homology model for the corresponding part of CVB3 2C was generated. Two pockets flanking a stretch of amino acids that often mutate to convey resistance against 2C inhibitors (224AGSINA229) were identified. Molecular dynamics simulations predicted a stable interaction for the (*S*)-fluoxetine in only one of these pockets. Mutations of residues deep in the predicted binding pocket confer resistance to fluoxetine and contribute to the understanding of the antiviral mode-of-action. Thus, we identified for the first time a putative binding pocket for antiviral compounds in the non-structural enterovirus protein 2C.

Results

(*S*)-fluoxetine inhibits CVB3 replication by binding to the non-structural protein 2C

Fluoxetine is clinically used as racemic mixture (1:1 enantiomeric ratio) and both enantiomers are of equal pharmacological activity towards the serotonin transporter SERT⁴⁰. The racemic compound was identified in drug-repurposing screens as an inhibitor of replication of EV-B and EV-D species³³⁻³⁴. Since fluoxetine has one chiral center, we investigated the antiviral properties of both enantiomers (Figure 1A). Coxsackievirus B3 (CVB3), a member of the EV-B genus, causes a readily observable

cytopathic effect (CPE), apparent as rounding, detachment and eventually dying of the cell. The racemic mixture and both enantiomers purchased from two different vendors (Sigma Aldrich and Carbosynth), were tested in a multicycle CPE-reduction assay to elucidate whether the compounds inhibit virus replication and thereby prevent the development of CPE. In parallel, cytotoxicity of the compounds was determined using an MTS assay.

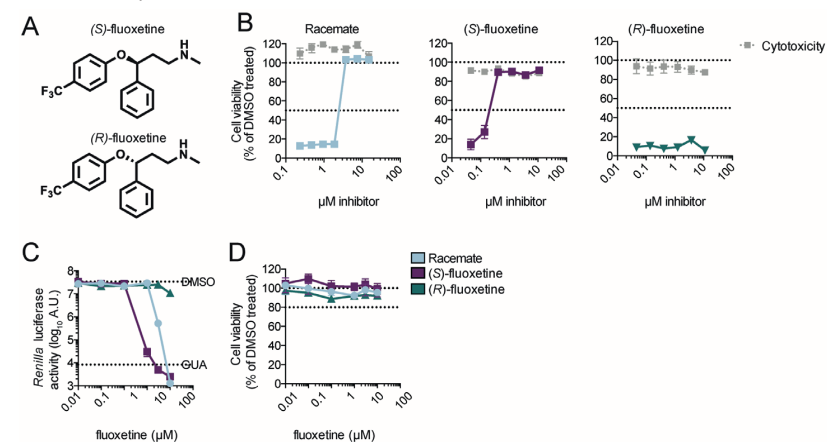


Figure 1. Fluoxetine inhibits CVB3 replication in a stereospecific manner (A) The two enantiomers of fluoxetine. (B) Multicycle CPE reduction assay to determine the antiviral activity of fluoxetine enantiomers. HeLa R19 cells were treated with serial dilutions of racemic, (*S*)-, or (*R*)-fluoxetine and infected with coxsackievirus B3 (CVB3) at MOI 0.001. In parallel, cells were treated with compound only to assess cytotoxicity. After three days, cell viability was determined using an MTS assay. Data are from one experiment representative of at least three independent experiments. (C) In a single cycle assay, HeLa R19 cells were infected with Renilla luciferase (RLuc)-CVB3 reporter virus, treated with serial dilutions of racemic, (*S*)-, or (*R*)-fluoxetine, and luciferase activity was determined at seven hours post infection as a quantitative measure of replication. (D) In parallel, uninfected cells were treated with compound and cell viability was determined using an MTS assay. Data are from one experiment representative of two independent experiments.

HeLa R19 cells were infected with CVB3 at MOI 0.001, which yields complete cell death within three days of incubation. The racemic mixture inhibited CVB3 with 50% effective concentration (EC_{50}) of $3.2 \pm 0.95 \mu\text{M}$, while the *S*-enantiomer inhibited with an EC_{50} of $0.4 \pm 0.15 \mu\text{M}$ (Figure 1B). In contrast, the *R*-enantiomer did not show any protection against CVB3 (Figure 1B). To validate these findings in a single cycle assay, HeLa R19 cells were infected with RLuc-CVB3 and the cells were treated with serial dilutions of the corresponding compounds. Cells were lysed 7 hours post infection and luciferase activity was measured as a quantitative and sensitive readout for viral replication. At the same time, cytotoxicity of the compounds was determined with an MTS assay and the CC_{50} of the compounds in HeLa R19 cells ranges from $23 \mu\text{M}$ to $28 \mu\text{M}$ (Table 1). The racemic mixture and the *S*-enantiomer exerted antiviral activity with a ~5-fold higher potency for the *S*-enantiomer (EC_{50} $0.42 \pm 0.17 \mu\text{M}$) compared to

the racemic mixture (EC_{50} $2.02 \pm 0.94 \mu\text{M}$) (Figure 1C). Again, the *R*-enantiomer did not show an antiviral effect (Figure 1C, D).

Table 1. Antiviral activity of stereoisomers of fluoxetine

Virus	Species	Strain	Racemic	(S)-fluoxetine	(R)-fluoxetine	SI _{Racemic}	SI _{(S)-fluoxetine}
EV-A71	EV-A	BrCr	NA	NA	NA	NA	NA
CVB3	EV-B	Nancy	2.02 ± 0.52	0.42 ± 0.17	NA	14.51	71.56
PV-1	EV-C	Sabin1	NA	NA	NA	NA	NA
EV-D68	EV-D	Fermon	1.85 ± 0.10	0.67 ± 0.22	NA	21.72	42.73
HRV-A2	RV-A		NA	7.95 ± 0.39	NA	NA	3.60
HRV-B14	RV-B		NA	6.34 ± 1.02	NA	NA	4.52
CC_{50}			29.32 ± 0.35	28.63 ± 1.02	23.63 ± 1.40		

Shown are EC_{50} and CC_{50} values in μM . Data represents mean values \pm SD calculated from at least three different experiments. NA = not active. SI= Selectivity index (CC_{50}/EC_{50})

Antiviral effect of (S)-fluoxetine against other enteroviruses

Previously, it was shown that the racemic mixture of fluoxetine inhibits enterovirus B and D replication prototyped by CVB3 (strain Nancy) and EV-D68 (strain Fermon)³³⁻³⁴. As the *S*-enantiomer is more active towards CVB3 than the racemic mixture, we reassessed the antiviral activity of (S)-fluoxetine against a panel of enteroviruses. As expected, the racemic mixture is only active against enterovirus B and D, *eg* CVB3 and EV-D68 (strain Fermon) species (Table 1)^{34, 41}. (S)-fluoxetine is not only more potent than the racemic mixture towards CVB3 but also towards EV-D68. Strikingly, while the racemic mixture does not confer any antiviral effect against rhinoviruses, the *S*-enantiomer inhibits rhinovirus 2 (HRV-2) or HRV-14 replication, with EC_{50} of $7.95 \pm 0.39 \mu\text{M}$ and $6.34 \pm 1.02 \mu\text{M}$ respectively (Table 1). The *S*-enantiomer was not active against EV-A71 (strain BrCr) and poliovirus (strain Sabin) at concentration up to $30 \mu\text{M}$. Higher concentrations could not be reached due to cytotoxicity of (S)-fluoxetine. We cannot exclude that (S)-fluoxetine would also inhibit other enteroviruses at higher concentrations in other systems in which the CC_{50} is much higher.

Fluoxetine directly binds to recombinant 2C protein in vitro

To gain further insights into the fluoxetine mode-of-action we next investigated whether it directly binds to 2C protein. Production and purification of full-length 2C protein usually leads to a polydisperse preparation, which is problematic for binding assays. By removing the first 36 amino acids of the N-terminus, a homogenous preparation of monomeric protein can be obtained and used for binding assays, namely thermal shift assay (TSA) and isothermal titration calorimetry (ITC)³⁵. First, TSA was used to detect a direct binding of the racemic mixture and the enantiomers of fluoxetine to CVB3 2C. In this assay, the increase of the melting temperature (T_m) of

the protein reflects the binding of a ligand. The racemic mixture was able to induce a dose-dependent increase of the T_m of 2C protein in a range of $10 \mu\text{M}$ to $250 \mu\text{M}$ (Figure 2A) while at higher concentrations the T_m decreased. By contrast, the *S*-enantiomer of fluoxetine was able to thermally stabilize the 2C protein in a concentration-dependent manner (Figure 2A) with no destabilization at high concentrations of compound, suggestive of a direct binding of (S)-fluoxetine to the protein. As positive control we used dibucaine, an established 2C inhibitor³⁵.

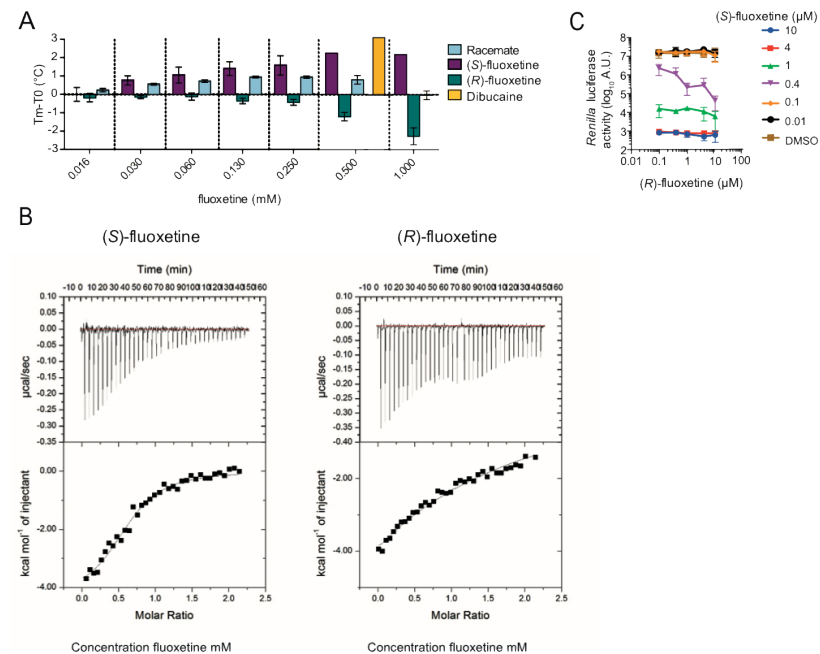


Figure 2. (S)-fluoxetine binds to the non-structural protein 2C in vitro. (A) The binding of racemic, (S)-, and (R)-fluoxetine to recombinant CVB3 2C was determined by thermal shift assay. The thermal stabilization of 2C by racemic and (S)-fluoxetine, represented by an increase in melting temperature, indicates binding of the compounds to 2C. (B) The binding of (S)- and (R)-fluoxetine to 2C were determined by isothermal calorimetry. As positive control the know 2C inhibitor dibucaine was used³⁵. Raw data are depicted at the top, and the integrated data are depicted at the bottom. Data are shown fitted to a one-site binding model. (C) HeLa R19 cells were infected with RLuc-CVB3 and the cells were treated with a fixed concentration of (S)-fluoxetine combined with serial dilutions of (R)-fluoxetine. Error bars depict standard error of the mean calculated from biological triplicates. Data representative of two independent experiments.

Interestingly, the *R*-enantiomer appeared to have a destabilizing effect on the protein at high concentrations (Figure 2A). The unexpected pattern of the racemic mixture may be explained by the collective effects of (S)-fluoxetine (stabilization) and (R)-fluoxetine (destabilization). To confirm these results, we next quantified the binding of (S)- and (R)-fluoxetine to 2C protein by ITC. The *S*-enantiomer bound to 2C with a

dissociation equilibrium constant (K_d) of $\sim 9.5 \mu\text{M}$ (Figure 2B). 2C partly aggregated during the titration of (*R*)-fluoxetine, in agreement with the results obtained by TSA. It was therefore not possible to retrieve a precise K_d , but when fitting the experimental data to a one-site binding model the observed K_d was higher than $200 \mu\text{M}$ (Figure 2B).

Thus, together with the data obtained in the antiviral assay, binding of (*S*)-fluoxetine is likely responsible for the 2C-mediated antiviral effect. However, given the difference of binding of (*S*)-fluoxetine to the recombinant protein ($10 \mu\text{M}$) and the EC_{50} in cell-based assays ($<1 \mu\text{M}$), off-target effects cannot be formally ruled out. Still, (*R*)-fluoxetine did affect the 2C protein in the TSA and ITC at high concentrations. Therefore, we investigated whether (*R*)-fluoxetine can exert any additional effect on virus replication in combination with (*S*)-fluoxetine. To this end, the effect of different concentrations of (*S*)-fluoxetine combined with increasing concentrations of the *R*-enantiomer on CVB3 replication was determined. At high concentrations of (*S*)-fluoxetine ($4 \mu\text{M}$ and $10 \mu\text{M}$), replication of CVB3 was completely inhibited and as expected no additional effect of (*R*)-fluoxetine could be observed (Figure 2C). At low concentrations of (*S*)-fluoxetine CVB3 replication was not impaired, nor could an additional effect of the *R*-enantiomer be observed (Figure 2C), in line with the absence of antiviral activity of (*R*)-fluoxetine alone (Figure 1B, 1C). Strikingly, when cells were treated with the approximate EC_{50} concentration of (*S*)-fluoxetine ($0.4 \mu\text{M}$), (*R*)-fluoxetine exerted a clear dose-dependent inhibition of virus replication (Figure 2C). Hence, (*R*)-fluoxetine can apparently exert weak antiviral activity that could come from the destabilization of the 2C protein or from the broad-spectrum antiviral effect induced by the targeting of a cellular partner³⁶⁻³⁷.

Fragment screening identifies key parts of fluoxetine involved in targeting 2C

To gain more information about which chemical moieties of fluoxetine are involved in exerting the antiviral activity, we tested six different fragments of fluoxetine (Figure 3A) in a CPE reduction assay using CVB3. Fragments **1**, **2** and **4** were synthesized, whereas fragments **3**, **5** and **6** were purchased and tested as received without further purification. Only fragment **1** showed a weak antiviral activity in the multicycle assay at concentrations close to cytotoxic concentrations (Figure 3B). To exclude that inhibition of the virus is caused by an unspecific cytotoxic effect, the fragments were also tested in a single cycle assay using a RLuc-CVB3. HeLa R19 cells were infected with RLuc-CVB3, treated with $100 \mu\text{M}$ or $10 \mu\text{M}$ of each fragment respectively, and luciferase activity at 7 hours post infection was determined as a quantitative and sensitive readout for virus replication. In this single cycle assay, fragment **1** showed an antiviral effect at $100 \mu\text{M}$ (Supplementary Figure 1A). In parallel, acute cytotoxicity of the fragments was excluded using an MTS assay (Supplementary Figure 1B). To further affirm that the observed weak antiviral activity of fragment **1** is specific and not due to cytotoxicity, we tested whether two other fluoxetine-insensitive viruses were affected by fragment **1**. Cells were infected with EV-A71 or *Renilla* luciferase-expressing encephalomyocarditis

virus (RLuc-EMCV)⁴²⁻⁴³ and as positive controls guanidium chloride (Gua) a replication inhibitor for EV-A71 and CVB3 and dipyrindamole (DIP) a replication inhibitor for EMCV were used. The virus titers and replication were determined by endpoint titration and a luciferase assay, respectively. Both viruses were not inhibited by fragment **1** at $100 \mu\text{M}$ (Figure 3C), indicating that the inhibitory effect of fragment **1** on CVB3 replication is specific.

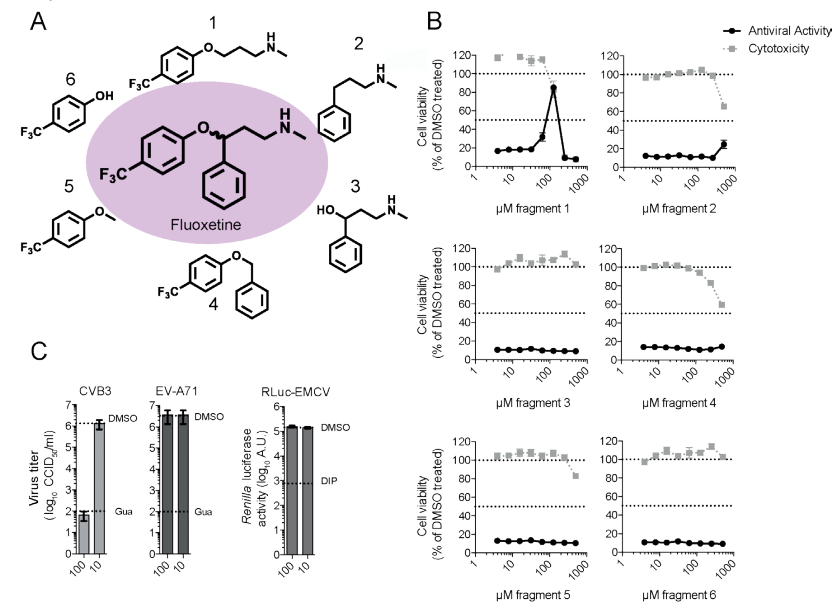


Figure 3. Fragment screening identifies key parts of fluoxetine involved in targeting 2C (A) Molecular structures of fluoxetine and the different fragments that were used. (B) CPE-reduction assay as performed in Figure 1B. (C) HeLa R19 cells were infected with either CVB3, EV-A71 and RLuc-EMCV in order to exclude an unspecific antiviral effect of fragment **1**. The replication inhibitor guanidium chloride (GuaHCl, 2 mM) was used in the case of CVB3 and EV-A71 as positive control. Dipyrindamole (DIP, 100 μM) was used as positive control replication inhibitor during RLuc-EMCV infection.

Finally, we investigated binding of the fluoxetine fragments to recombinant 2C using a thermal shift assay (TSA). The binding of low molecular weight molecules usually has a moderate effect on protein stability ($<1^\circ\text{C}$ in protein stabilization) and concentrations should be $>100 \mu\text{M}$ to observe protein stabilization⁴⁴. Therefore, we tested the fragments in the TSA at a concentration range from $100 \mu\text{M}$ to $400 \mu\text{M}$. Neither fragment **1** nor any other fragment was able to stabilize the 2C protein at the indicated concentrations (Supplementary Figure 1C). At present we can only speculate why fragment **1** exerts weak antiviral activity but does not stabilize 2C in the TSA. Possibly, the amount of recombinant 2C protein in the *in vitro* assay is higher than in an infection setting, which would require a higher concentration of the compound to

induce a shift in the melting temperature of 2C. It can however be noticed that the effect of fragments on T_m is usually very modest because the energy of binding is weak⁴⁴. Taken together, fragment **1** was able to inhibit CVB3 replication, but a direct binding could not be observed in the TSA.

Identification of a potential binding pocket for fluoxetine on 2C

After having investigated chemical properties of fluoxetine that are important for its antiviral activity, we next wanted to further characterize the possible intermolecular interactions between (S)-fluoxetine and 2C. Because structures of 2C of fluoxetine-sensitive viruses were not available we resorted to an *in silico* modelling approach. We first generated a homology model of CVB3 2C (Figure 4A) based on the crystal structure of a part of 2C of the fluoxetine-insensitive virus EV-A71³⁹. The crystalized part of EV-A71 2C covers amino acids 116-329. In this region, the sequence identity and similarity between EV-A71 and CVB3 2C is 62% and 80%, respectively.

Enterovirus 2C belongs to a family of AAA+ ATPases, which oligomerize in hexameric ring structures in which the ATP is coordinated by two monomers³⁹. Such ring structures were observed in low resolution electron microscopy structures of 2C proteins from poliovirus and food-and-mouth disease virus, a picornavirus from the aphthovirus genus⁴⁵⁻⁴⁶. The published EV-A71 2C structure (PDB: 5GRB) shows a C-terminal interaction between two adjacent 2C molecules to form a bipartite binding site for the ATP. In total there are six protein chains in the crystal structure of which only chain A and B are fully resolved, whereas all the others have at least one gap³⁹. The co-crystallized ATP molecules adopt different conformations for each chain and only chains A and F crystallize in a conformation resembling a bipartite binding site with both monomers forming hydrogen bonds with the ATP. Therefore, chain A was used as a template to generate the homology model of CVB3 2C (Figure 4A). Superimposition onto the EV-A71 2C structure resulted in a CVB3 2C model with a reasonably good fit and an overall RMSD of 0.30 Å from the template with the highest deviation for residues N257 (1.65 Å) and D274 (2.08 Å).

The CVB3 2C homology model was used to search for pockets in which fluoxetine may bind. Because mutations in the flexible 224AGSINA229 loop confer resistance to fluoxetine³⁴, we focused on pockets near this loop. Two potential binding pockets flanking the 224AGSINA229 loop were identified, termed site A and site B (Figure 4B). Site A faces away from the ATP binding site, is confined by the 224AGSINA229 loop on one side and hydrophilic residues (D245, R295 and R296) on the other side. Site A is a deep, lipophilic pocket, whereas site B is a rather shallow pocket and lies between the 224AGSINA229 loop and the 175-183 loop, which is downstream of the Walker B motif. In the crystal structure of EV-A71 and in the CVB3 homology model both sites might considerably change their shapes due to loop movements. However, site A is not affected to the point of blocking the binding of fluoxetine, while site B is. Both enantiomers of fluoxetine were docked into each of the two pockets for further computational investigations (Figure 4B). In site A both enantiomers docked in proximity

of the residues A229 and I227 of the 224AGSINA229 loop. The 4-(trifluoromethyl) benzene moiety occupied the hydrophobic bottom of the pocket consisting of the residues L178, C179, V187 and F190. Instead, in site B both enantiomers were mostly exposed to the solvent.

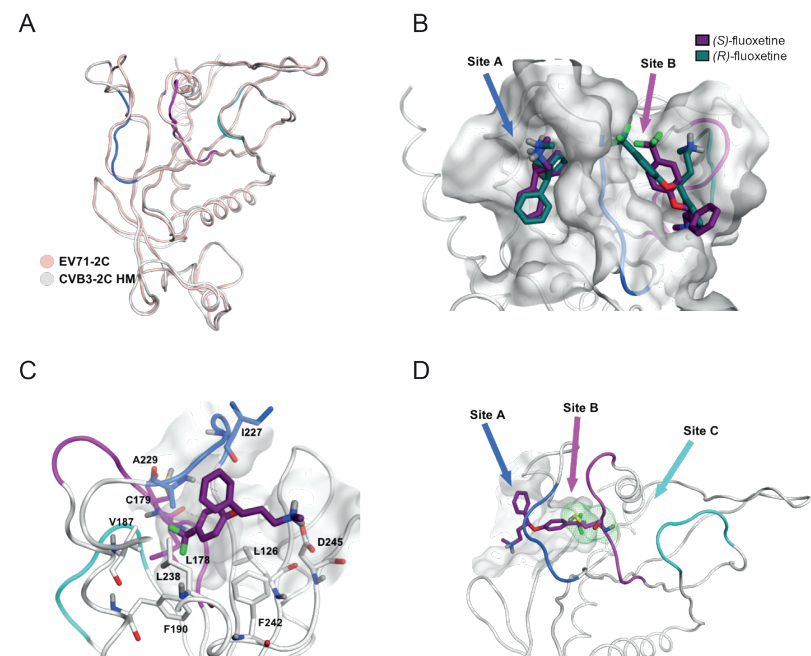


Figure 4. Predicted fluoxetine binding sites on CVB3 2C protein (A) Homology model of the 2C protein of CVB3 built on the crystal structure of EV-A71. Ribbon and carbon atoms of 224AGSINA229 loop are in blue, the 175-183 loop in violet and the 158-164 loop in cyan (B) S- and R-enantiomers of fluoxetine docked into sites A and B of the homology model. (C) View of (S)-fluoxetine in site A as identified in the molecular dynamics simulations, comprising the residues L126, L178, C179, V187, F190, I227, A229, L238, F242, D245. The trifluoromethyl moiety of fluoxetine is buried deep inside the hydrophobic pocket. (D) Three possible entrances of (S)-fluoxetine to reach C179 (green line surface).

Molecular dynamics simulations reveal stable positioning of (S)-fluoxetine in pocket A

After the selection of the possible pockets near the AGSINA motif, the binding sites containing both enantiomers were subjected to molecular dynamics simulations. The 224AGSINA229 loop is thought to be flexible thereby alternating the shape of the two identified pockets, resulting in different predicted binding modes compared to the docking. To evaluate how stable the fluoxetine enantiomers docked into the pockets and to address why mutations in this loop can cause resistance towards fluoxetine, the

docking models of (*S*)-fluoxetine and (*R*)-fluoxetine in site A and site B were subjected to molecular dynamics simulations. For each enantiomer docked into either site, three independent molecular dynamic simulations of 100 ns were performed. The calculated binding energies of (*S*)- or (*R*)-fluoxetine into site A and site B from the molecular dynamics simulations are listed in Table 2. The simulations showed that (*S*)-fluoxetine bound stronger to 2C than (*R*)-fluoxetine in both site A and site B. We observed that (*R*)-fluoxetine dissociated from pocket A as well as pocket B in one of the three independent simulations, suggesting that (*R*)-fluoxetine cannot engage in stable interaction with 2C. In site B, movement of the 224AGSINA229 loop was observed, making the hydrophobic pocket accessible for the 4-(trifluoromethyl)benzene moiety of fluoxetine. However, visual inspection and the binding energies of the molecular dynamics suggested that site A provides a more stable binding pocket for (*S*)-fluoxetine, defined by the residues L126, L178, V187, F190, L238, I227, A229, F242 (Figure 4C).

Table 2. Binding energies of the protein ligand complexes during MD simulations

	Compound	MD1	MD2	MD3
Site A	(<i>R</i>)-fluoxetine	-29.71*	-42.70	-19.85*
	(<i>S</i>)-fluoxetine	-41.63	-42.28	-41.54
Site B	(<i>R</i>)-fluoxetine	-29.59*	-42.95	-27.38
	(<i>S</i>)-fluoxetine	-34.79	-29.88	-30.83*

Values indicated are calculated $\Delta G_{\text{binding}}$ average values over the 100 ns of each of the three independent molecular dynamics simulations (MD) for the indicated ligands in site A or B (kJ/mol). The most favorable complex according to the simulations is (*S*)-fluoxetine in site A. For all the other complexes in at least one simulation the ligand dissociated from the protein (indicated by *).

In each independent repetition of the molecular dynamics simulation on (*S*)-fluoxetine in site A, the compound was oriented such that the 4-(trifluoromethyl)benzene moiety occupied the hydrophobic pocket (Figure 4C). During the molecular dynamics simulations, a hydrogen bond repeatedly formed between the amino acid D245 and the positively charged amino group of (*S*)-fluoxetine (Figure 4C). We conclude, in line with the antiviral data and binding assays from the *in silico* approach that (*S*)-fluoxetine binds stronger to 2C than the *R*-enantiomer. Furthermore, on the basis of our *in silico* analyses we conclude that (*S*)-fluoxetine most likely binds 2C to site A.

Mutations in the identified binding pocket confer resistance to (*S*)-fluoxetine

The triple amino acid substitution A224V-I227V-A229V (AVIVAV) in CVB3 2C, clustered in the 224AGSINA229 region, was previously shown to confer resistance to the racemic fluoxetine mixture³⁴ and to several other 2C inhibitors²⁹. Likewise, the triple mutant provided resistance to (*S*)-fluoxetine (Figure 5A). This resistance is specific, as AVIVAV mutations did not confer resistance to BF738735, a compound that inhibits

enterovirus replication via a different mechanism, namely by targeting the cellular protein PI4KIII β , which is essential for enterovirus replication⁴⁷.

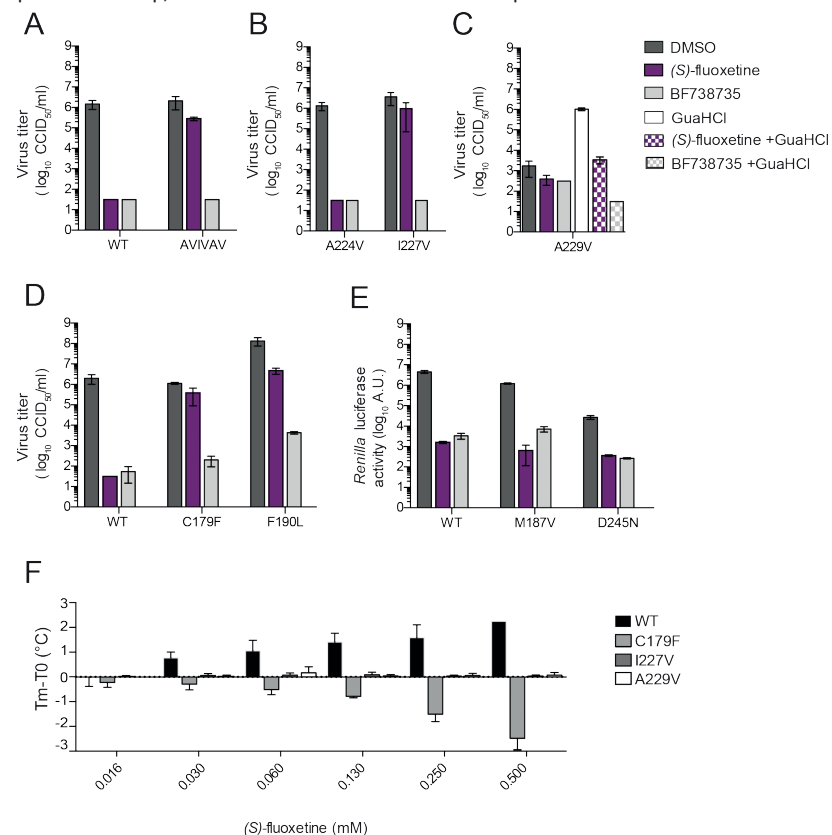


Figure 5. Mutations in the identified binding pocket confer resistance towards (*S*)-fluoxetine. (A) HeLa R19 cells were infected with WT CVB3 or the AVIVAV mutant (A224V-I227V-A229V triple mutant) at a MOI 0.1 and treated with 1 μM (*S*)-fluoxetine or 1 μM BF738735 as a control replication inhibitor that acts via the host protein PI4KIII β ⁴⁸. Eight hours post infection, cells were freeze-thawed and virus titers were determined by endpoint titration. Means and standard deviations were calculated from biological triplicate. (B) The individual A224V and I227V mutations were tested for resistance towards (*S*)-fluoxetine as in (A). (C) The guanine chloride-dependent virus A229V was tested for dependency on (*S*)-fluoxetine. Experiments were performed similar as in (A). Because the A229V virus is dependent on GuaHCl, sensitivity to the inhibitors was also tested in the presence of 1 mM GuaHCl (blocked bars). (D) Residues in the hydrophobic binding pocket were mutated (C179F and F190L) and tested for resistance towards (*S*)-fluoxetine as in (A). (E) Residues at the surface of the hydrophobic binding pocket (V187M and D245N) were substituted in the Renilla luciferase virus and sensitivity to (*S*)-fluoxetine was determined as in Figure 1C. (F) The binding of (*S*)-fluoxetine to recombinant WT CVB3 2C or 2C harboring the resistance mutations C179F, I227V and A229V was tested using thermal shift assay as in Figure 2A. In all panels data are shown from one experiment representative of at least two independent experiments. Error bars depict standard error of the mean calculated from biological triplicates

To dissect the contribution of the individual mutations to the resistance, several CVB3 mutant viruses containing either the single mutations A224V, I227V and A229V were made. The A224V mutation alone did not confer resistance to the compounds (Figure 5B). The single mutation I227V provided a high level of resistance towards (*S*)-fluoxetine, but not the control compound BF738735 (Figure 5B). This is in concordance with a recently published report, which raised resistant mutants towards racemic fluoxetine and identified the mutations I227V and N228S⁴¹. The A229V single mutant virus was previously described to be dependent on all structurally divergent 2C inhibitors tested (GuaHCl, HBB, TBZE-029 and MRL-1237)²⁹, meaning that these mutant viruses are not inhibited by the compounds but instead strictly require them for efficient replication. Strikingly, the A229V virus was not dependent on (*S*)-fluoxetine at the concentration tested (Figure 5C). To test whether the A229V virus is resistant to (*S*)-fluoxetine we assessed replication in the presence of both GuaHCl (to allow replication) and (*S*)-fluoxetine. However, the A229V mutation does not confer resistance to (*S*)-fluoxetine.

To find experimental support for the predicted binding pocket, we next investigated the importance of key residues in site A pocket by mutational analysis. We first mutated two amino acids that are located deep within site A and tested whether they could confer resistance to (*S*)-fluoxetine. These mutations are C179F, which – like C179Y – provides resistance towards several structurally different 2C inhibitors⁴¹, and F190L, which raises resistance to a novel 2C inhibitor⁴⁹. In line with our model, viruses containing the C179F or the F190L mutation in 2C were highly resistant to (*S*)-fluoxetine (Figure 5D). We next investigated two amino acids that are located near the edge of site A. V187 was substituted by a M, because the corresponding amino acid 187 in the fluoxetine-insensitive virus EV-A71 is a methionine and we hypothesized that this methionine may contribute to the insensitivity of EV-A71 to fluoxetine. The amino acid D245 displayed repeated interactions with the positively charged amino group of (*S*)-fluoxetine in the molecular dynamics simulations (Figure 4C). We therefore decided to remove the charge of this residue by replacing it with asparagine. However, neither the V187M nor the D245N mutations provided resistance to (*S*)-fluoxetine (Figure 5E), which seems to contradict our computation-based hypothesis that (*S*)-fluoxetine binds to site A interacting with C187 and D245. Fluoxetine may bind in a slightly different conformation within the pocket that does not involve interactions with these two residues, thus mutations would not confer resistance. That would still explain why the C179F and F190L mutations confer resistance. Alternatively, fluoxetine may access residues C179 and F190 from a third entrance site (Site C), schematically depicted in Figure 4D (cyan arrow), and therefore being unaffected by the mutations in site A and the 224AGSINA229 loop. However, neither in the homology model nor in the EV-A71 crystal structure the supposed site C presents an obvious cavity for potential ligand entrance towards the residues C179 and F190. Because of flexibilities in the loops ranging from amino acid residue 158 to 163, 175 to 183 and 224 to 229 other conformations likely exist so that site C may become accessible. In that case the

occurrence of mutations in the 224AGSINA229 loop and how they can confer resistance is more difficult to explain. We propose the hypothesis that conformational changes over a longer range could affect the shape of the pocket and therefore slight changes in the distant 224AGSINA229 loop might be sufficient to convey resistance. Clearly, actual crystallographic data of (*S*)-fluoxetine bound to 2C is needed to definitively resolve this point.

Finally, we wanted to address whether resistance mutations in 2C affect binding of (*S*)-fluoxetine to 2C. Recombinant 2C proteins harboring the resistance mutations I227V or C179F or the A229V mutation were produced and binding was tested by TSA (Figure 5F). (*S*)-fluoxetine was not able to stabilize any of the mutated 2C proteins from thermal denaturation, implying that the substitutions abrogated fluoxetine binding to 2C. Unexpectedly, the C179F substitution made 2C more sensitive to thermal denaturation in the presence of (*S*)-fluoxetine when compared to the C179F mutant without compound (ΔT_m -2.5°C). The A229V substitution nullified thermal stabilization of 2C by (*S*)-fluoxetine, suggesting that this mutation abrogated binding of (*S*)-fluoxetine. However, the GuaHCl-dependency of the A229V virus required combining GuaHCl and (*S*)-fluoxetine in the TSA experiment, which may add confounding effects (Figure 5C).

Summarized, mutations at position I227 in the 224AGSINA229 loop, as well as the C179F and F190L mutations at the bottom of the binding site A confer resistance to (*S*)-fluoxetine, while the V187M and D245N mutations, which are more at the edge of the pocket, do not.

Discussion

Enteroviruses are a major global health burden, but currently no antiviral therapy is available. The high degree of conservation makes the enterovirus 2C protein an attractive target for the development of broad-spectrum enterovirus inhibitors (Supplementary Figure 3). Several compounds, including a number of repurposed drugs, have been identified as inhibitors of enterovirus replication by targeting 2C (reviewed in²), but to date the molecular mechanisms underlying the antiviral effects are lacking. Fluoxetine, one of the identified compounds, is an FDA-approved drug that is used as a highly selective inhibitor of SERT for the treatment of major depression and anxiety disorders. In this study, we provide new insights into how the repurposed drug fluoxetine acts as antiviral compound against CVB3.

Fluoxetine has one chiral center and only the *S*-enantiomer of fluoxetine has anti-enteroviral activity and binds to 2C *in vitro*. In previous studies the racemic mixture of fluoxetine inhibited EV-B and EV-D species, but not EV-A, EV-C and rhinoviruses³³⁻³⁴. Here we show that the *S*-enantiomer, but not the *R*-enantiomer, has a clearly increased antiviral potency compared to the racemic mixture against CVB3 and also EV-D68, while the cytotoxicity in cell culture is comparable (Table 1). Unexpectedly, we observed that the *S*-enantiomer also exerts antiviral activity against rhinoviruses. Presumably, the antiviral activity of the racemic mixture against rhinoviruses is so weak that it cannot be

separated from cytotoxicity effects. We cannot exclude that (*S*)-fluoxetine would also inhibit EV-A or EV-C species at even higher concentrations, but this cannot be tested in the current model systems due to cytotoxicity. Another explanation for why EV-A and EV-C species are not sensitive to fluoxetine is that there could be strain-specific differences in the sensitivity towards inhibitors. For example, we show that also (*S*)-fluoxetine does not inhibit EV-A71 (strain BrCr). It is unknown why EV-A71 is resistant to (*S*)-fluoxetine, further in-depth investigations are needed to gain a better understanding of the underlying mechanism of resistance of EV-A71. However, a different EV-A71 strain was shown to be sensitive to racemic fluoxetine⁴¹. Thus, it is possible that different EV-A and EV-C strains are sensitive towards (*S*)-fluoxetine.

The *in vivo* efficacy of fluoxetine towards enterovirus infections has until now been relatively poorly studied. Recent outbreaks of acute flaccid myelitis (AFM) in the US are – at least in part – associated with EV-D68⁵⁰. In a mouse model for EV-D68 associated paralysis, fluoxetine did not have an effect on motor impairment of mice or viral load in muscle and spinal cord, but instead seemed to slightly aggravate disease⁵¹. Because in human AFM cases treatment options other than supportive care are lacking, several clinicians have tried off-label use of fluoxetine to treat pediatric patients. A retrospective study of safety and efficacy of fluoxetine to treat AFM revealed no beneficial effect of fluoxetine⁵². Instead, fluoxetine-treated patients had somewhat more severe symptoms, suggesting a negative effect of fluoxetine on AFM, in line with the mouse model⁵¹. However, this retrospective study had some limitations that make it difficult to draw definitive conclusions. For example, patients had been treated with different dosing regimens. Furthermore, fluoxetine treatment was started only after onset of AFM symptoms when irreversible neuronal damage may already have been inflicted. Moreover, viral loads were not tested, leaving the question unanswered whether the virus was still actively replicating at the time of treatment and – if so – whether fluoxetine had any effect on viral loads. In contrast, in a pancreatitis mouse model the racemic fluoxetine mixture reduced the levels of CVB4 infectious particles in heart and pancreas and reduced pancreatitis severity when it was given one day prior to CVB4 infection and subsequently every day post infection⁵³. Finally, in a case study of an immunocompromised child with chronic EV-B induced encephalitis, off-label use of fluoxetine eliminated the virus and led to recovery of the patient³⁸. These seemingly opposing results stress the importance of further *in vivo* studies of fluoxetine to combat different enterovirus and treat different types of enterovirus-associated diseases. The plasma concentration of fluoxetine ranges from 91 to 300 ng/ml after 30 days of dosing 40 mg/day⁵⁴. The metabolite norfluoxetine, which also shows antiviral activity³³, reaches a plasma concentration from 72 to 258 ng/ml. The slow elimination of fluoxetine together with the metabolite norfluoxetine should reach a sufficient plasma concentration that correspond with the EC₅₀ in cell culture (~1 μM, which corresponds to ~150 ng/ml).

In contrast to the SSRI activity, leading to the antidepressant effect of fluoxetine, the 2C-mediated antiviral activity of fluoxetine is stereoselective, lending further support to

the idea that the antiviral activity is unrelated to the known SSRI activity of fluoxetine. This implies that, when fluoxetine is used as an antiviral treatment, any potential SSRI-related side effects can be reduced by providing only (*S*)-fluoxetine, which is then at lower overall concentration. However, when only (*S*)-fluoxetine is used, the advantages of drug repurposing of fluoxetine, which is licensed as a racemic mixture, are nullified and new safety studies are needed. Fragment 1, which contains the 4-(trifluoromethyl) benzene moiety and the amino group, gave the first indication for the importance of these chemical features for the antiviral effect. From there on, structure activity relationship studies could help to design new molecules with even a stronger antiviral effect, but reduced or suppressed SERT inhibition.

To investigate the mode-of-action of how fluoxetine binds to enterovirus 2C, we built a homology model of CVB3 based on the crystal structure of the fluoxetine-insensitive EV-A71 2C. In the predicted binding model, the 4-(trifluoromethyl)benzene group of fluoxetine occupies the deep hydrophobic pocket close to residues L126, L178, V187, F190, L238, I227, A229, F242. Mutational studies to test the binding hypothesis were designed and mutations at the bottom of the predicted pocket reduced (*S*)-fluoxetine binding by providing resistance. The mutations on the borders of the pocket did not confer resistance to (*S*)-fluoxetine therefore we cannot exclude alternative entrance sites to the hydrophobic cavity. Crystallographic data is needed to yield ultimate clarity about the binding mode.

2C is a member of the SF3 helicases of the AAA+ ATPase superfamily and contains Walker A and B motifs, which are important for recognizing the triphosphate of ATP, and a short motif C that is located on top of Walker B⁷. The residues L178 and C179 in the predicted binding pocket are located within the Walker B motif or immediately thereafter. Furthermore, the 224AGSINA229 loop, which harbors resistance mutations and lines the edge of the predicted pocket, is directly C-terminal to the motif C. Residues L238, F242 and D245 are in proximity to the arginine fingers (R240 and R241), which play an important role in the ATPase domain and are required for ATP hydrolysis. Hence, it is conceivable that fluoxetine inhibits ATPase activity allosterically through relatively short-range effects although alternative modes, e.g. through long-range effects, cannot be excluded. Still, the exact molecular details of how fluoxetine inhibits the ATPase activity of 2C remain to be determined.

The 224AGSINA229 loop forms a hot-spot for resistance mutations against fluoxetine and many other 2C inhibitors, while fewer mutations have been found in the predicted fluoxetine binding pocket. The residues in the pocket are evolutionarily highly conserved, implying that there is little room for variation that could induce resistance in the pocket residues without affecting virus fitness. In contrast, the 224-229 loop diverges more between enterovirus species, suggesting that the loop allows for more sequence diversity that could yield resistance (Supplementary Figure 3). The 224AGSINA229 loop is conserved between the fluoxetine sensitive viruses CVB3 and EV-D68, but the motif differs in the fluoxetine resistant viruses EV-A71 and poliovirus (Supplementary Figure 3). The corresponding 224AGSINA229 loops might be more

rigid in these latter viruses, thereby interfering with fluoxetine binding. Mutations in the 224AGSINA229 loop confer resistance not only against fluoxetine, but also against several other compounds, including TBZE-029, HBB and MRL-1237 and GuaHCl²⁹. Resistance mutations may favor a conformation of the 224AGSINA229 loop in which the binding pocket is not accessible for fluoxetine anymore. Furthermore, the mutations may change the flexibility of the loop in such a way that the inhibitory effect of fluoxetine is circumvented. Further biophysical studies are needed to decipher how the resistance mutations affect the overall stability of the protein or the accessibility of the binding pocket. However, addressing the possible role of *S*-fluoxetine in the hexamerisation of 2C is presently not possible because the production of homogenous 2C protein in its biologically relevant oligomerization state has not yet been achieved.

In conclusion, this study sheds new light onto how the 2C inhibitor fluoxetine may target the enterovirus 2C protein. In particular, the discovery of the stereoselective activity will fuel further mode-of-action studies and support the rational design of novel, fluoxetine-derived broad-spectrum enterovirus inhibitors.

Methods

Cells and Reagents

Buffalo Green Monkey cells (BGM) and HeLa R19 cells were cultured in Dulbecco's modified Eagle's medium (DMEM, Lonza) supplemented with 10 % fetal bovine serum (FBS, Lonza). Huh7-Lunet 7/T7, a stable cell pool expressing T7 RNA polymerase and blasticidin *S*-deaminase⁵⁵, were cultured in DMEM supplemented with 10% FBS and 10 µg/ml blasticidin (Sigma-Aldrich). All cell lines were grown at 37°C in 5 % CO₂. Guanidine hydrochloride (GuaHCl) was purchased from Sigma-Aldrich. Racemic mixture of fluoxetine was purchased from Sigma-Aldrich. The *S*- and *R*-enantiomers were purchased either from Sigma-Aldrich or Carbosynth. BF738735 was provided by Galapagos NV⁴⁸. Dibucaine was purchased from Sigma-Aldrich. GuaHCl was dissolved in water at 2M stock concentration and all other compounds were dissolved in DMSO at 10 mM stock concentration.

Viruses

EV-A71 (strain BrCr), PV1 (strain Sabin, ATCC) and EV-D68 (strain Fermon) were obtained from the National Institute for Public Health and Environment (RIVM) in the Netherlands. HRV-2 and HRV-14 were obtained from Joachim Seipelt from the Medical University of Vienna in Austria. RLuc-CVB3, which contains a *Renilla* luciferase gene upstream of the capsid coding region, was obtained by transfecting Huh7-Lunet/T7 cells with MluI-linearized pRLuc-53CB3/T7 plasmid as described⁵⁶. RLuc-encephalomyocarditis virus (EMCV, strain mengovirus), encoding a *Renilla* luciferase gene upstream of the capsid-coding region, was described before⁴²⁻⁴³. CVB3 (strain Nancy) and CVB3 2C mutant viruses were obtained by transfecting BGM cells with RNA transcripts derived from the full-length infectious clones p53CB3/T7 as described in⁵⁷.

The mutations 2C[A224V], 2C[I227V], 2C[A229V], 2C[A224V/I227V], 2C[A224V/A229V], 2C[I227V/A229V], 2C[A224V/I227V/A229V], 2C[C179F] and 2C[F190L] were introduced into the p53CB3/T7 infectious clone and 2C[V187M] and 2C[D245N] were introduced into the pRLuc-53CB3/T7 using site directed mutagenesis. *In vitro* transcribed RNA transcripts were transfected into HeLa R19 cells to obtain virus. To ensure that the introduced mutations are retained in the generated virus, viral RNA was isolated with NucleoSpin[®] RNA Virus kit (Macherey-Nagel) according to the manufacturer's protocol and the presence of the desired mutations was confirmed by Sanger sequencing. Virus titers were determined by endpoint dilution titration and calculated according to the method of Reed and Muench⁵⁸ and expressed as 50% cell culture infective dose (CCID₅₀).

Single-cycle virus infection

Virus infections were performed by incubating subconfluent HeLa R19 cells with virus at a multiplicity of infection (MOI 0.1) at 37°C for 30 min. Next, the medium was removed and fresh (compound-containing) medium was added to the cells. At the indicated time points, the medium was discarded and cells were lysed. For measurements of infectious particles, virus was released from the cells by three freeze-thawing cycles. Virus titers were determined by end-point dilution assay and calculated by the method of Reed and Muench⁵⁸. In the case of infection with RLuc-CVB3 and RLuc-EMCV, cells were lysed 6-7 hrs post infection and the *Renilla* luciferase Assay System (Promega) was used to determine the luciferase activity. Where indicated, cell viability was determined in parallel using the Aqueous One Solution Cell Proliferation Assay (Promega) according to the manufacturer's protocol. Optical density at 490 nm was determined using a microplate reader.

Multicycle virus infection

Subconfluent layers of HeLa R19 cells were seeded in 96-wells and treated with serial dilutions of the corresponding compounds. Cells were infected with CVB3 at the lowest possible MOI (MOI 0.001) resulting in full CPE within 3 days. Subsequently the cells were incubated at 37°C for 3 days until full CPE was observed in the virus infected untreated cell controls. Cell viability was determined in parallel using the Aqueous One Solution Cell Proliferation Assay (Promega) according to the manufacturer's protocol. The optical density at 490 nm was determined using a microplate reader. Raw OD values were converted to percentage of untreated and uninfected cell control after subtraction of the background.

Binding of fluoxetine to recombinant WT and mutant 2C proteins

The DNA fragment coding for CVB3 2C (amino acids 37 to 329) was cloned downstream of a cleavable thioredoxin-hexahistidine tag. Mutations were introduced into the 2C coding sequence by PCR-based site-directed mutagenesis. The recombinant WT and mutant proteins were produced in *Escherichia coli* T7 Express

(New England BioLabs) at 17°C. Protein purification and tag removal were performed under nondenaturing conditions as previously described³⁵. The final size-exclusion chromatography step was performed with a buffer containing 10 mM HEPES and 300 mM NaCl (pH 7.5). The binding of fluoxetine or corresponding fragments on WT and mutant 2C proteins was monitored by fluorescence-based thermal shift assay (TSA) using a Bio-Rad CFX Connect. TSA plates were prepared by dispensing into each well the 2C protein (final concentration of 15 µM in 50 mM Tris, 300 mM NaCl, pH 8) which was mixed with 1 µL of fragment or fluoxetine (from 20 mM stock in 100% DMSO, 1 mM final concentration in 4% DMSO) and a SYPRO orange solution in concentrations recommended by the manufacturer in a final volume of 25 µL. The experiments were performed under a temperature gradient ranging from 20 to 95°C (incremental steps of 0.2°C/12 seconds). The denaturation of the proteins was monitored by following the increase of the fluorescence emitted by SYPRO orange that binds exposed hydrophobic regions of the denatured protein. The melting temperature (T_m) was calculated as the mid-log of the transition phase from the native to the denatured protein using a Boltzmann model (Origin software). The reference unfolding temperature of proteins in 4% DMSO (T_o) was subtracted from the values in the presence of fragment (T_m) to obtain thermal shifts, $\Delta T_m = T_m - T_o$.

The binding of (*S*)- and (*R*)-fluoxetine to WT CVB3 2C was further characterized by isothermal titration calorimetry (ITC) using a MicroCal iTC200 instrument (Malvern). Experiments were carried out at 20°C in a solution containing 10 mM HEPES, 300 mM NaCl, and 0.8% DMSO (pH 7.5). The 2C protein concentration in the cell was 80 µM whereas the fluoxetine concentration in the syringe was 400 µM. For (*R*)-fluoxetine, two injections were necessary. Heats of dilution were measured by injecting the ligand into the protein solution. Titration curves were fitted by using MicroCal Origin software, assuming one set of sites, and enthalpy changes (ΔH), dissociation equilibrium constants (K_d), and stoichiometry were extracted.

Molecular modelling

The computational studies were carried out on 1.80 GHz Intel Xeon (8 cores) processor-based system, running Ubuntu 14.04 LTS, using Molecular Operating Environment (MOE) 2015.10 (Chemical Computing Group Inc. 2016) and Maestro v11.4 (Schrödinger LLC, New York, NY, 2017). The homology model was generated with MOE using integrated sequence alignment and structure preparation tools for the template. Preparation of the structure for docking and molecular dynamic simulations and subsequent data analysis was carried out with Maestro. Docking experiments were performed using the GlideSP module in Maestro, running the default settings. The molecular dynamics simulations were performed using Desmond package (Desmond Molecular Dynamics System, D. E. Shaw Research, New York, NY, 2018. Maestro-Desmond Interoperability Tools, Schrödinger, New York, NY, 2018). Pictures of molecular modelling were prepared using MOE.

Homology modelling

The protein sequence of CVB3 (strain Nancy) 2C protein was downloaded from Uniprot (ID: P03313 amino acids 1101-1429). The structures reported in³⁹, especially 5GRB, was used as a starting point in this study and was retrieved from the Protein Data Bank. 5GRB contains ATPγS and was the structure used for the computational studies. The sequence of CVB3 was aligned to the sequence of the crystalized EV-A71 using MOE. 5GRB chain A was used as a structural template for the homology model. The homology model was built with the Amber12:EHT force field⁵⁹⁻⁶⁰. Automatic detection of disulfide bridges was disabled. Ten intermediate models were generated and refined using a medium refinement by molecular mechanics (highly tethered minimization to relieve steric strains). The final model was calculated using Coulomb and Generalized Born / Volume Integral (GB/VI) interaction energies⁶¹ and was not further refined.

After the generation of the homology model the structure was revised using the Structure Preparation function in MOE. In order to further evaluate the quality of the homology model for future studies the phi/psi angles were analyzed in the Ramachandran plot using the Protein Geometry tool of MOE. Identified outliers were investigated and, if relevant, corrected manually. Then the validation of the model was carried out using RAMPAGE Ramachandran plot analysis (accessed at mordred.bio.cam.ac.uk/~rapper/rampage.php). Amino acid environment analysis was carried out using the SAVES server v3.0 (<http://servicesn.mbi.ucla.edu/SAVES/>) comprising Verify 3D⁶²⁻⁶⁵.

Site Finder

The site identification tool Site Finder, which is comprised in the software suite MOE, was run on the prepared CVB3 homology model to identify possible active sites for the known 2C targeting compounds. Two binding pockets (termed site A and site B) were selected on the basis of their vicinity to known mutations in the 224AGSINA229 loop that convey resistance against several known 2C inhibitors including fluoxetine^{29, 34-35}. For both pockets, a set of dummy atoms was created in the positions of the alpha spheres that are used to determine pockets in Site Finder.

Docking

After the identification of site A and site B, both the compounds and the protein were prepared for the docking with Glide. The homology model of CVB3 was prepared with the Protein Preparation Wizard embedded in Maestro. For each binding site a grid box for the positioning of the molecules during the docking was generated setting the centers of the boxes to the coordinates of representative dummy atoms generated by Site Finder. The stereochemistry on the chiral center of fluoxetine was defined using the molecule builder in MOE and the two enantiomers were saved in separate .sdf files. Both of them were subjected to the ligand preparation protocol (ligprep) in Maestro creating up to 32 conformations each. Then, all conformations obtained for (*R*)- and (*S*)-fluoxetine, were docked with Maestro Glide in standard precision (SP) mode into

each binding site. The poses were inspected for their fit within the pockets and their interactions with the protein. The best protein-ligand complexes for each site and each enantiomer were saved and prepared for molecular dynamics (MD) simulations.

Molecular dynamics simulations

All MD simulations were performed using Desmond, part of the Maestro v11.4 simulation package (Schrödinger LLC, New York, NY, 2017). OPLS3 was used as the force field. The complexes of (*R*)-fluoxetine and (*S*)-fluoxetine docked to 2C of CVB3 were placed in a cubic box (buffer 10 Å) using the TIP3P water model. The negative charges on the protein were neutralized adding Na⁺ atoms to the system. Magnesium chloride (10 mM) was added to the box to simulate physiological conditions. Before the MD simulation the system was first equilibrated for 112 ps at 10 K in an NVT ensemble and then simulated for 48 ps at constant pressure of 1 atm using the NPT ensemble. All MD simulations were performed for 100 ns at constant temperature (300 K) and pressure recording snapshots every 160 ps.

The estimated $\Delta G_{\text{binding}}$ was calculated using the Desmond command-line script thermal_mmgbsa.py. After splitting the trajectory file of the MD simulation into snapshots the script is calculating the average computed binding energy of the ligand (Table 2 and Supplementary Figure 2).

Chemistry

All solvents and reagents used were obtained from commercial sources unless otherwise indicated. All reactions were performed under a nitrogen atmosphere. ¹H and ¹³C NMR spectra were recorded with a Bruker Avance DPX500 spectrometer operating at 500 MHz for ¹H and 125 MHz for ¹³C, with Me₄Si as internal standard. Deuterated dimethyl sulfoxide (DMSO) was used as the solvent for NMR experiments. ¹H chemical shifts values (δ) are referenced to the residual non-deuterated components of the NMR solvents (δ = 2.50 ppm for DMSO). The ¹³C chemical shifts (δ) are referenced to DMSO (central peak, δ = 39.5 ppm). Thin layer chromatography (TLC) was performed on Silica gel plates (Merck Kieselgel 60 F254), which were developed by the ascending method. Column chromatography was performed on an Isolera Biotage system. Purity of synthesized compounds was determined by UPLC-UV-MS analysis (Waters UPLC system with both Diode Array detection and Electrospray (+ve and -ve ion) MS detection). The purity of all compounds was determined to be >95% by UPLC using the eluents H₂O containing 0.1% Trifluoroacetic acid (eluent A) and Acetonitrile containing 0.1% Trifluoroacetic acid (eluent B) at the following conditions: Waters Acquity UPLC BEH C18 1.7 μ m 2.1x50 mm column, 0.5 mL/min, column temperature 40°C. Sample diluent: Acetonitrile. Sample concentration 10 μ g/mL. Injection volume 2 μ L, gradient 90% eluent A (0.1 min), 90%-0% eluent A (1.5 min), 0% eluent A (1.4 min), 90% eluent A (0.1 min) (method 1).

Synthesis of 1-(3-bromopropoxy)-4-(trifluoromethyl)benzene (intermediate)

To a solution of 1,3-dibromopropane (6.17 mmol) and potassium carbonate (4.63 mmol) in DMF (3 mL), 4-(trifluoromethyl)phenol (3.08 mmol) in DMF (1.2 mL) was added dropwise, the reaction mixture was stirred at room temperature for two hours and then heated to 70°C for two hours. The mixture was filtrated, diluted with ethyl acetate (10 mL) and washed with water (3x10 mL). The organic layer was dried over sodium sulphate and evaporated under reduced pressure. The residue was purified by flash column chromatography eluting with n-hexane/EtOAc 100:0 v/v increasing to n-hexane/EtOAc 70:30 v/v. 207 mg of 1-(3-bromopropoxy)-4-(trifluoromethyl)benzene were obtained in 47% yield as a yellow oil. ¹H NMR (DMSO) δ 7.65 (d, *J* = 8.7 Hz, 2H), 7.14 (d, *J* = 8.7 Hz, 2H), 4.17 (t, *J* = 6.0 Hz, 2H), 3.68 (t, *J* = 6.6 Hz, 2H), 2.28 (p, *J* = 6.3 Hz, 2H). ¹⁹F NMR (DMSO) δ -59.83 (s, 3F). ¹³C NMR (DMSO) δ 161.67, 127.44 (m), 125.02 (q, *J* = 271.0 Hz), 121.73 (q, *J* = 32.1 Hz), 115.44, 32.08, 31.50.

Synthesis of fragment 1: *N*-methyl-3-(4-(trifluoromethyl)phenoxy)propan-1-amine

To a round bottom flask containing methylamine in absolute ethanol (2 mL) cooled to 0°C a solution of 1-(3-bromopropoxy)-4-(trifluoromethyl)benzene (0.80 mmol) in EtOH absolute (0.8 mL) was added dropwise. The reaction mixture was stirred at room temperature overnight. The mixture was filtrated. The obtained residue was dissolved in DCM (10 mL). The organic layer was washed with saturated aqueous NaHCO₃ and brine, dried over Na₂SO₄ and concentrated *in vacuo*. The residue was treated with HCl in diethyl ether. The resulting solid was then filtered and washed with diethyl ether to give 131 mg of *N*-methyl-3-(4-(trifluoromethyl)phenoxy)propan-1-amine hydrochloride salt as a white powder in a yield of 69%. ¹H NMR (DMSO) δ 8.65 (s, 2H), 7.68 (d, *J* = 8.6 Hz, 2H), 7.13 (d, *J* = 8.6 Hz, 2H), 4.16 (t, *J* = 6.1 Hz, 2H), 3.06 (d, *J* = 7.4 Hz, 2H), 2.58 (s, 3H), 2.13 – 2.04 (m, 2H). ¹⁹F NMR (DMSO) δ -59.78. ¹³C NMR (DMSO) δ 161.58, 127.43 (q, *J* = 3.7 Hz), 125.02 (q, *J* = 271.1 Hz), 121.76 (q, *J* = 32.2 Hz), 115.48, 65.58, 46.14, 33.07, 25.71. UPLC: retention time = 1.521 min., MS [ESI, m/z]: 234.1 [M+Na]⁺.

Synthesis of fragment 2: *N*-methyl-3-phenylpropan-1-amine

To a round bottom flask containing methylamine in absolute ethanol (2.18 mL), a solution of (3-bromopropyl)benzene (1.25 mmol) in EtOH absolute (0.87 mL) was added dropwise at 0°C. The reaction mixture was stirred at room temperature overnight. The solid residue was filtered and washed with EtOH absolute to give 195 mg of *N*-methyl-3-phenylpropan-1-amine in a yield of 75% as a white powder. ¹H NMR (DMSO) δ 8.48 (s, 2H), 7.35 – 7.27 (m, 2H), 7.26 – 7.17 (m, 3H), 2.91 – 2.85 (m, 1H), 2.65 (t, *J* = 7.7 Hz, 2H), 2.55 (s, 3H), 1.94 – 1.85 (m, 2H). ¹³C NMR (DMSO) δ 141.13, 128.92, 128.73, 126.57, 48.30, 32.88, 32.32, 27.57.

Synthesis of fragment 4: 1-(benzyloxy)-4-(trifluoromethyl)benzene

To a solution of 4-(trifluoromethyl)phenol (1.233 mmol), in DMF (3 mL), 1.553 mmol of (bromomethyl)benzene (1.553 mmol) and potassium carbonate (4.932 mmol) were added. The obtained mixture was stirred at 105°C for four hours. After the reaction completion, the mixture was filtrated, diluted with ethyl acetate (10 mL) and washed with water (3x10 mL). The organic layer was dried over sodium sulfate and evaporated under reduced pressure. The residue was purified by flash column chromatography eluting with *n*-Hexane/DCM 100:0 v/v increasing to 0:100 v/v, obtaining 212 mg of 1-(benzyloxy)-4-(trifluoromethyl)benzene in a yield of 75% as a white powder. ¹H NMR (DMSO) δ 7.66 (d, *J* = 8.5 Hz, 2H), 7.49 – 7.44 (m, 2H), 7.44 – 7.38 (m, 2H), 7.38 – 7.32 (m, 1H), 7.20 (d, *J* = 8.5 Hz, 2H), 5.20 (s, 2H). ¹⁹F NMR (DMSO) δ -59.81. ¹³C NMR (DMSO) δ 161.64, 136.88, 128.98, 128.50, 128.25, 127.42 (q, *J* = 3.7 Hz), 125.02 (q, *J* = 271.1 Hz), 121.74 (q, *J* = 32.1 Hz), 115.77, 70.00.

Purchased fragments

Fragments **3** (3-(methylamino)-1-phenylpropan-1-ol), and fragment **6** (4-(trifluoromethyl)phenol) were purchased from Sigma Aldrich, possess a purity grade of >97% and were used as received. Fragment **3** was obtained as racemic mixture. Fragment **5** (4-(trifluoromethyl)anisole) was ordered from Alfa Aesar >98% pure. The fragments were dissolved in DMSO at a stock concentration of 100 mM.

Calculations

The concentration of compound that inhibits virus-induced cell death by 50% (50% effective concentration [EC₅₀]) was calculated by nonlinear regression analysis. Cytotoxicity of the compounds was assessed in a similar set-up, and 50% cytotoxic concentration (CC₅₀) values were derived from cell viability values determined with an MTS assay. Each experiment was performed at least in triplicate. The nonlinear regression and the graphs were made with GraphPad Prism Version 6.

Acknowledgments

This work was supported by research grants from the Netherlands Organisation for Scientific Research (NWO-ECHO-711.017.002 to FJMvK and JRPMS; NWO-VICI-91812628 to FJMvK), the European Union (Horizon 2020 Marie Skłodowska-Curie ETN 'ANTIVIRALS', grant agreement number 642434 to TL, BC, AB and FJMvK).

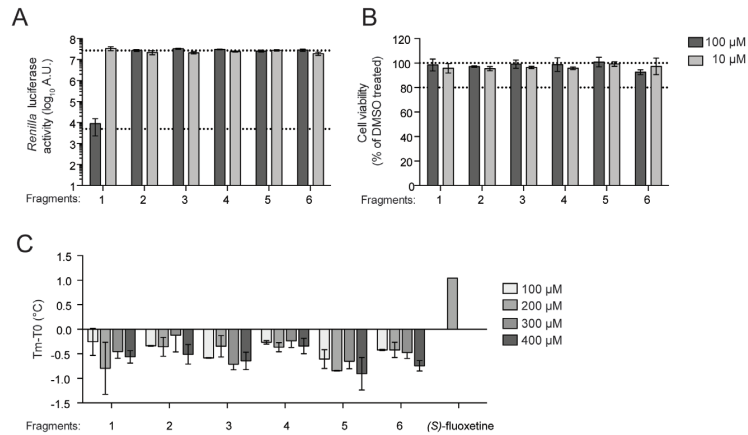
References

1. Tapparel, C.; Siegrist, F.; Petty, T. J.; Kaiser, L., Picornavirus and enterovirus diversity with associated human diseases. *Infect Genet Evol* 2013, *14*, 282-93.
2. Bauer, L.; Lyoo, H.; van der Schaar, H. M.; Strating, J. R.; van Kuppeveld, F. J., Direct-acting antivirals and host-targeting strategies to combat enterovirus infections. *Current opinion in virology* 2017, *24*, 1-8.
3. Rodriguez, P. L.; Carrasco, L., Poliovirus protein 2C has ATPase and GTPase activities. *The Journal of biological chemistry* 1993, *268* (11), 8105-10.
4. Pfister, T.; Wimmer, E., Characterization of the nucleoside triphosphatase activity of poliovirus protein 2C reveals a mechanism by which guanidine inhibits poliovirus replication. *The Journal of biological chemistry* 1999, *274* (11), 6992-7001.
5. Klein, M.; Eggers, H. J.; Nelsen-Salz, B., Echovirus 9 strain barty non-structural protein 2C has NTPase activity. *Virus Res* 1999, *65* (2), 155-60.
6. Xia, H.; Wang, P.; Wang, G. C.; Yang, J.; Sun, X.; Wu, W.; Qiu, Y.; Shu, T.; Zhao, X.; Yin, L.; Qin, C. F.; Hu, Y.; Zhou, X., Human Enterovirus Nonstructural Protein 2CATPase Functions as Both an RNA Helicase and ATP-Independent RNA Chaperone. *PLoS pathogens* 2015, *11* (7), e1005067.
7. Singleton, M. R.; Dillingham, M. S.; Wigley, D. B., Structure and mechanism of helicases and nucleic acid translocases. *Annual review of biochemistry* 2007, *76*, 23-50.
8. Li, J. P.; Baltimore, D., An intragenic revertant of a poliovirus 2C mutant has an uncoating defect. *Journal of virology* 1990, *64* (3), 1102-7.
9. Cho, M. W.; Teterina, N.; Egger, D.; Bienz, K.; Ehrenfeld, E., Membrane rearrangement and vesicle induction by recombinant poliovirus 2C and 2BC in human cells. *Virology* 1994, *202* (1), 129-45.
10. Aldabe, R.; Carrasco, L., Induction of membrane proliferation by poliovirus proteins 2C and 2BC. *Biochem Biophys Res Commun* 1995, *206* (1), 64-76.
11. Teterina, N. L.; Gorbalenya, A. E.; Egger, D.; Bienz, K.; Ehrenfeld, E., Poliovirus 2C protein determinants of membrane binding and rearrangements in mammalian cells. *Journal of virology* 1997, *71* (12), 8962-72.
12. Suhy, D. A.; Giddings, T. H., Jr.; Kirkegaard, K., Remodeling the endoplasmic reticulum by poliovirus infection and by individual viral proteins: an autophagy-like origin for virus-induced vesicles. *Journal of virology* 2000, *74* (19), 8953-65.
13. Banerjee, R.; Echeverri, A.; Dasgupta, A., Poliovirus-encoded 2C polypeptide specifically binds to the 3'-terminal sequences of viral negative-strand RNA. *Journal of virology* 1997, *71* (12), 9570-8.
14. Banerjee, R.; Dasgupta, A., Interaction of picornavirus 2C polypeptide with the viral negative-strand RNA. *J Gen Virol* 2001, *82* (Pt 11), 2621-7.
15. Banerjee, R.; Tsai, W.; Kim, W.; Dasgupta, A., Interaction of poliovirus-encoded 2C/2BC polypeptides with the 3' terminus negative-strand cloverleaf requires an intact stem-loop b. *Virology* 2001, *280* (1), 41-51.
16. Li, J. P.; Baltimore, D., Isolation of poliovirus 2C mutants defective in viral RNA synthesis. *Journal of virology* 1988, *62* (11), 4016-21.
17. Teterina, N. L.; Kean, K. M.; Gorbalenya, A. E.; Agol, V. I.; Girard, M., Analysis of the functional significance of amino acid residues in the putative NTP-binding pattern of the poliovirus 2C protein. *J Gen Virol* 1992, *73* (Pt 8), 1977-86.

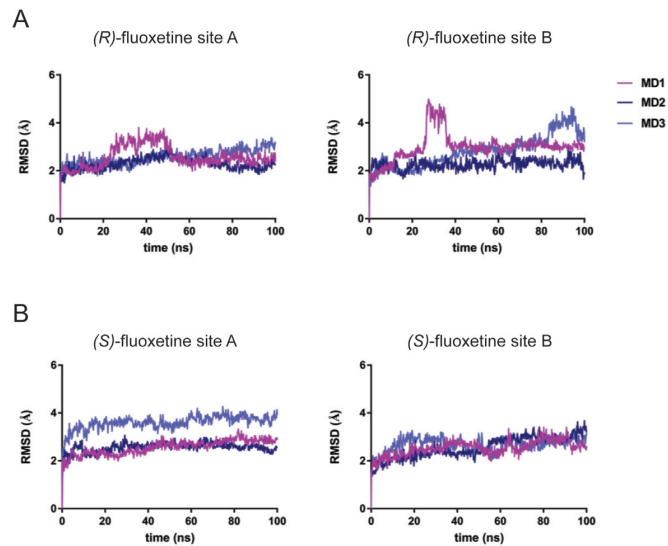
18. Tolskaya, E. A.; Romanova, L. I.; Kolesnikova, M. S.; Gmyl, A. P.; Gorbalenya, A. E.; Agol, V. I., Genetic studies on the poliovirus 2C protein, an NTPase. A plausible mechanism of guanidine effect on the 2C function and evidence for the importance of 2C oligomerization. *J Mol Biol* 1994, *236* (5), 1310-23.
19. Barton, D. J.; Flanagan, J. B., Synchronous replication of poliovirus RNA: initiation of negative-strand RNA synthesis requires the guanidine-inhibited activity of protein 2C. *Journal of virology* 1997, *71* (11), 8482-9.
20. Teterina, N. L.; Levenson, E.; Rinaudo, M. S.; Egger, D.; Bienz, K.; Gorbalenya, A. E.; Ehrenfeld, E., Evidence for functional protein interactions required for poliovirus RNA replication. *Journal of virology* 2006, *80* (11), 5327-37.
21. Tang, W. F.; Yang, S. Y.; Wu, B. W.; Jheng, J. R.; Chen, Y. L.; Shih, C. H.; Lin, K. H.; Lai, H. C.; Tang, P.; Horng, J. T., Reticulon 3 binds the 2C protein of enterovirus 71 and is required for viral replication. *The Journal of biological chemistry* 2007, *282* (8), 5888-98.
22. Zheng, Z.; Li, H.; Zhang, Z.; Meng, J.; Mao, D.; Bai, B.; Lu, B.; Mao, P.; Hu, Q.; Wang, H., Enterovirus 71 2C protein inhibits TNF-alpha-mediated activation of NF-kappaB by suppressing IkkappaB kinase beta phosphorylation. *J Immunol* 2011, *187* (5), 2202-12.
23. Vance, L. M.; Moscufo, N.; Chow, M.; Heinz, B. A., Poliovirus 2C region functions during encapsidation of viral RNA. *Journal of virology* 1997, *71* (11), 8759-65.
24. Verlinden, Y.; Cuconati, A.; Wimmer, E.; Rombaut, B., The antiviral compound 5-(3,4-dichlorophenyl) methylhydantoin inhibits the post-synthetic cleavages and the assembly of poliovirus in a cell-free system. *Antiviral research* 2000, *48* (1), 61-9.
25. Liu, Y.; Wang, C.; Mueller, S.; Paul, A. V.; Wimmer, E.; Jiang, P., Direct interaction between two viral proteins, the nonstructural protein 2C and the capsid protein VP3, is required for enterovirus morphogenesis. *PLoS pathogens* 2010, *6* (8), e1001066.
26. Wang, C.; Ma, H. C.; Wimmer, E.; Jiang, P.; Paul, A. V., A C-terminal, cysteine-rich site in poliovirus 2C(ATPase) is required for morphogenesis. *J Gen Virol* 2014, *95* (Pt 6), 1255-65.
27. van der Linden, L.; Wolthers, K. C.; van Kuppeveld, F. J., Replication and Inhibitors of Enteroviruses and Parechoviruses. *Viruses* 2015, *7* (8), 4529-62.
28. Hadaschik, D.; Klein, M.; Zimmermann, H.; Eggers, H. J.; Nelsen-Salz, B., Dependence of echovirus 9 on the enterovirus RNA replication inhibitor 2-(alpha-Hydroxybenzyl)-benzimidazole maps to nonstructural protein 2C. *Journal of virology* 1999, *73* (12), 10536-9.
29. De Palma, A. M.; Heggermont, W.; Lanke, K.; Coutard, B.; Bergmann, M.; Monforte, A. M.; Canard, B.; De Clercq, E.; Chimirri, A.; Purstinger, G.; Rohayem, J.; van Kuppeveld, F.; Neyts, J., The thiazolobenzimidazole TBZE-029 inhibits enterovirus replication by targeting a short region immediately downstream from motif C in the nonstructural protein 2C. *Journal of virology* 2008, *82* (10), 4720-30.
30. Shimizu, H.; Agoh, M.; Agoh, Y.; Yoshida, H.; Yoshii, K.; Yoneyama, T.; Hagiwara, A.; Miyamura, T., Mutations in the 2C region of poliovirus responsible for altered sensitivity to benzimidazole derivatives. *Journal of virology* 2000, *74* (9), 4146-54.
31. Ashburn, T. T.; Thor, K. B., Drug repositioning: identifying and developing new uses for existing drugs. *Nat Rev Drug Discov* 2004, *3* (8), 673-83.
32. Mercorelli, B.; Palu, G.; Loregian, A., Drug Repurposing for Viral Infectious Diseases: How Far Are We? *Trends in microbiology* 2018, *26* (10), 865-876.
33. Zuo, J.; Quinn, K. K.; Kye, S.; Cooper, P.; Damoiseaux, R.; Krogstad, P., Fluoxetine Is a Potent Inhibitor of Coxsackievirus Replication. *Antimicrobial agents and chemotherapy* 2012, *56* (9), 4838-4844.
34. Ulferts, R.; van der Linden, L.; Thibaut, H. J.; Lanke, K. H.; Leyssen, P.; Coutard, B.; De Palma, A. M.; Canard, B.; Neyts, J.; van Kuppeveld, F. J., Selective serotonin reuptake inhibitor fluoxetine inhibits replication of human enteroviruses B and D by targeting viral protein 2C. *Antimicrobial agents and chemotherapy* 2013, *57* (4), 1952-6.
35. Ulferts, R.; de Boer, M.; van der Linden, L.; Bauer, L.; Lyoo, H. R.; Mate, M. J.; Lichiere, J.; Canard, B.; Lelieveld, D.; Omata, W.; Egan, D.; Coutard, B.; van Kuppeveld, F. J., Screening of a library of FDA-approved drugs identifies several enterovirus replicaton inhibitors that target viral protein 2C. *Antimicrobial agents and chemotherapy* 2016.
36. Young, K. C.; Bai, C. H.; Su, H. C.; Tsai, P. J.; Pu, C. Y.; Liao, C. S.; Lin, Y. M.; Lai, H. W.; Chong, L. W.; Tsai, Y. S.; Tsao, C. W., Fluoxetine a novel anti-hepatitis C virus agent via ROS-, JNK-, and PPARbeta/gamma-dependent pathways. *Antiviral research* 2014, *110*, 158-67.
37. Medigesini, G. R.; Kumar, R.; Dhamija, E.; Agrawal, T.; Kar, M., N-Desmethyloclozapine, Fluoxetine, and Salmeterol Inhibit Postentry Stages of the Dengue Virus Life Cycle. *Antimicrobial agents and chemotherapy* 2016, *60* (11), 6709-6718.
38. Gofshteyn, J.; Cardenas, A. M.; Bearden, D., Treatment of Chronic Enterovirus Encephalitis With Fluoxetine in a Patient With X-Linked Agammaglobulinemia. *Pediatr Neurol* 2016.
39. Guan, H.; Tian, J.; Qin, B.; Wojdyla, J. A.; Wang, B.; Zhao, Z.; Wang, M.; Cui, S., Crystal structure of 2C helicase from enterovirus 71. *Sci Adv* 2017, *3* (4), e1602573.
40. Robertson, D. W.; Jones, N. D.; Swartzendruber, J. K.; Yang, K. S.; Wong, D. T., Molecular structure of fluoxetine hydrochloride, a highly selective serotonin-uptake inhibitor. *Journal of medicinal chemistry* 1988, *31* (1), 185-9.
41. Zuo, J.; Kye, S.; Quinn, K. K.; Cooper, P.; Damoiseaux, R.; Krogstad, P., Discovery of Structurally Diverse Small-Molecule Compounds with Broad Antiviral Activity against Enteroviruses. *Antimicrobial agents and chemotherapy* 2015, *60* (3), 1615-26.
42. Albuлесcu, L.; Wubbolts, R.; van Kuppeveld, F. J.; Strating, J. R., Cholesterol shuttling is important for RNA replication of coxsackievirus B3 and encephalomyocarditis virus. *Cellular microbiology* 2015.
43. Strating, J. R.; van der Linden, L.; Albuлесcu, L.; Bigay, J.; Arita, M.; Delang, L.; Leyssen, P.; van der Schaar, H. M.; Lanke, K. H.; Thibaut, H. J.; Ulferts, R.; Drin, G.; Schlinck, N.; Wubbolts, R. W.; Sever, N.; Head, S. A.; Liu, J. O.; Beachy, P. A.; De Matteis, M. A.; Shair, M. D.; Olkkonen, V. M.; Neyts, J.; van Kuppeveld, F. J., Itraconazole inhibits enterovirus replication by targeting the oxysterol-binding protein. *Cell reports* 2015, *10* (4), 600-15.
44. Coutard, B.; Decroly, E.; Li, C.; Sharff, A.; Lescar, J.; Bricogne, G.; Barral, K., Assessment of Dengue virus helicase and methyltransferase as targets for fragment-based drug discovery. *Antiviral research* 2014, *106*, 61-70.
45. Adams, P.; Kandiah, E.; Effantin, G.; Steven, A. C.; Ehrenfeld, E., Poliovirus 2C protein forms homo-oligomeric structures required for ATPase activity. *The Journal of biological chemistry* 2009, *284* (33), 22012-21.
46. Sweeney, T. R.; Cisnetto, V.; Bose, D.; Bailey, M.; Wilson, J. R.; Zhang, X.; Belsham, G. J.; Curry, S., Foot-and-mouth disease virus 2C is a hexameric AAA+ protein with a coordinated ATP hydrolysis mechanism. *The Journal of biological chemistry* 2010, *285* (32), 24347-59.
47. van der Schaar, H. M.; Leyssen, P.; Thibaut, H. J.; de Palma, A.; van der Linden, L.; Lanke, K. H.; Lacroix, C.; Verbeken, E.; Conrath, K.; Macleod, A. M.; Mitchell, D. R.; Palmer, N. J.; van de Poel, H.; Andrews, M.; Neyts, J.; van Kuppeveld, F. J., A novel, broad-spectrum inhibitor of enterovirus replication that targets host cell factor phosphatidylinositol 4-kinase IIIbeta. *Antimicrobial agents and chemotherapy* 2013, *57* (10), 4971-81.

48. MacLeod, A. M.; Mitchell, D. R.; Palmer, N. J.; Van de Poel, H.; Conrath, K.; Andrews, M.; Leyssen, P.; Neyts, J., Identification of a series of compounds with potent antiviral activity for the treatment of enterovirus infections. *ACS Med Chem Lett* 2013, 4 (7), 585-9.
49. Thibaut HJ, L. C., Coutard, Van der Linden L, Canard B, De Palma AM, Van Kuppeveld F, Jung YS and Neyts J A novel class of highly potent small molecule inhibitors of entero/rhinovirus replication that target the non structural protein 2C. https://rega.kuleuven.be/cmt/jn/poster/2013/2013_ht/Poster%20ICAR%202013%20MOA%20KRICT.pdf (accessed 22.02).
50. Holm-Hansen, C. C.; Midgley, S. E.; Fischer, T. K., Global emergence of enterovirus D68: a systematic review. *Lancet Infect Dis* 2016, 16 (5), e64-e75.
51. Hixon, A. M.; Clarke, P.; Tyler, K. L., Evaluating Treatment Efficacy in a Mouse Model of Enterovirus D68-Associated Paralytic Myelitis. *J Infect Dis* 2017, 216 (10), 1245-1253.
52. Messacar, K.; Sillau, S.; Hopkins, S. E.; Otten, C.; Wilson-Murphy, M.; Wong, B.; Santoro, J. D.; Treister, A.; Bains, H. K.; Torres, A.; Zabrocki, L.; Glanternik, J. R.; Hurst, A. L.; Martin, J. A.; Schreiner, T.; Makhani, N.; DeBiasi, R. L.; Kruer, M. C.; Tremoulet, A. H.; Van Haren, K.; Desai, J.; Benson, L. A.; Gorman, M. P.; Abzug, M. J.; Tyler, K. L.; Dominguez, S. R., Safety, tolerability, and efficacy of fluoxetine as an antiviral for acute flaccid myelitis. *Neurology* 2018.
53. Benkahla, M. A.; Alidjinou, E. K.; Sane, F.; Desailoud, R.; Hober, D., Fluoxetine can inhibit coxsackievirus-B4 E2 in vitro and in vivo. *Antiviral research* 2018, 159, 130-133.
54. Amsterdam, J. D.; Fawcett, J.; Quitkin, F. M.; Reimherr, F. W.; Rosenbaum, J. F.; Michelson, D.; Hornig-Rohan, M.; Beasley, C. M., Fluoxetine and norfluoxetine plasma concentrations in major depression: a multicenter study. *Am J Psychiatry* 1997, 154 (7), 963-9.
55. Backes, P.; Quinkert, D.; Reiss, S.; Binder, M.; Zayas, M.; Rescher, U.; Gerke, V.; Bartenschlager, R.; Lohmann, V., Role of annexin A2 in the production of infectious hepatitis C virus particles. *Journal of virology* 2010, 84 (11), 5775-89.
56. Lanke, K. H.; van der Schaar, H. M.; Belov, G. A.; Feng, Q.; Duijsings, D.; Jackson, C. L.; Ehrenfeld, E.; van Kuppeveld, F. J., GBF1, a guanine nucleotide exchange factor for Arf, is crucial for coxsackievirus B3 RNA replication. *Journal of virology* 2009, 83 (22), 11940-9.
57. Wessels, E.; Duijsings, D.; Lanke, K. H.; van Dooren, S. H.; Jackson, C. L.; Melchers, W. J.; van Kuppeveld, F. J., Effects of picornavirus 3A Proteins on Protein Transport and GBF1-dependent COP-I recruitment. *Journal of virology* 2006, 80 (23), 11852-60.
58. Reed, L. J.; Muench, H., A simple method of estimating fifty percent endpoints *American Journal of Epidemiology* 1938, 27 (3), 493-497.
59. D.A. Case, T. A. D., T.E. Cheatham, III, C.L. Simmerling, J. Wang, R.E. Duke, R. Luo, R.C. Walker, W. Zhang, K.M. Merz, B. Roberts, S. Hayik, A. Roitberg, G. Seabra, J. Swails, A.W. Götz, I. Kolossváry, K.F. Wong, F. Paesani, J. Vanicek, R.M. Wolf, J. Liu, X. Wu, S.R. Brozell, T. Steinbrecher, H. Gohlke, Q. Cai, X. Ye, J. Wang, M.-J. Hsieh, G. Cui, D.R. Roe, D.H. Mathews, M.G. Seetin, R. Salomon-Ferrer, C. Sagui, V. Babin, T. Luchko, S. Gusarov, A. Kovalenko, and P.A. Kollman AMBER 12. <http://ambermd.org/doc12/Amber12.pdf> (accessed 11.03.2019).
60. Gerber, P. R.; Muller, K., MAB, a generally applicable molecular force field for structure modelling in medicinal chemistry. *J Comput Aided Mol Des* 1995, 9 (3), 251-68.
61. Labute, P., The generalized Born/volume integral implicit solvent model: estimation of the free energy of hydration using London dispersion instead of atomic surface area. *J Comput Chem* 2008, 29 (10), 1693-8.
62. Bowie, J. U.; Luthy, R.; Eisenberg, D., A method to identify protein sequences that fold into a known three-dimensional structure. *Science* 1991, 253 (5016), 164-70.
63. Luthy, R.; Bowie, J. U.; Eisenberg, D., Assessment of protein models with three-dimensional profiles. *Nature* 1992, 356 (6364), 83-5.
64. Colovos, C.; Yeates, T. O., Verification of protein structures: patterns of nonbonded atomic interactions. *Protein Sci* 1993, 2 (9), 1511-9.
65. Pontius, J.; Richelle, J.; Wodak, S. J., Deviations from standard atomic volumes as a quality measure for protein crystal structures. *J Mol Biol* 1996, 264 (1), 121-36.

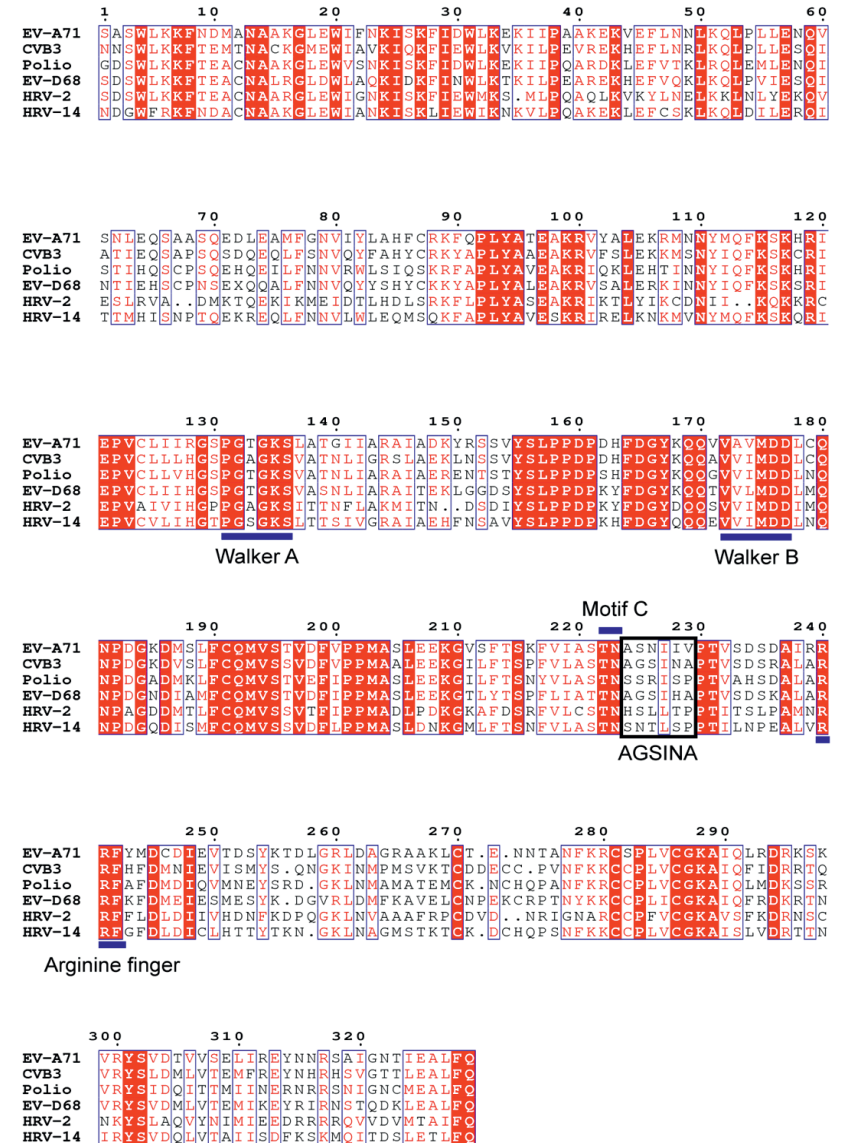
Supplementary Information



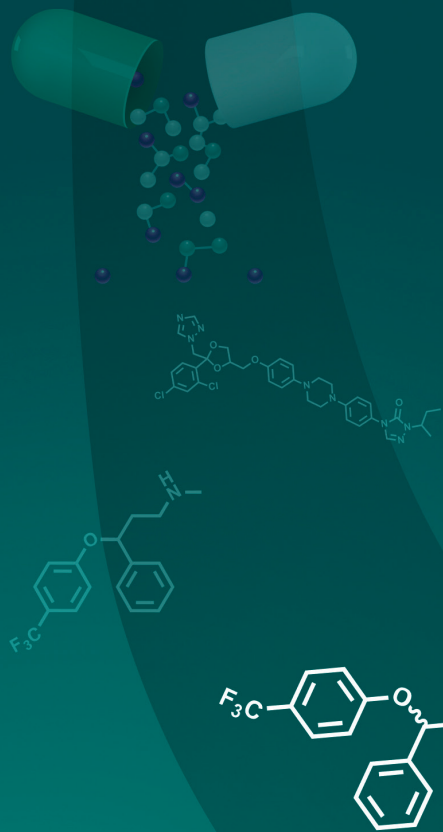
Supplementary Figure 1. Antiviral activity and binding of fragments to 2C. (A) In a single cycle assay, HeLa R19 cells were infected with *Renilla* luciferase (RLuc)-CVB3 reporter virus (MOI 0.1), treated with 100 or 10 µM of fragment, and luciferase activity was determined as a quantitative measure of replication. (B) In parallel, cell viability was determined with an MTS assay. (C) The interaction of the fragments to the 2C protein of CVB3 was determined by thermal shift assays similar as in Figure 1E.



Supplementary Figure 2. Root mean square deviation (RMSD) of the protein ligand complexes during MD simulations. Indicator for stability or conformational changes during the simulations. (A) The movement of (*R*)-fluoxetine in site A and site B is shown over 100 ns time during the molecular dynamics. (B) The movement of (*S*)-fluoxetine in site A and site B is shown over 100 ns time during the molecular dynamics.



Supplementary Figure 3. Multiple sequence alignment of 2C proteins from different enteroviruses. The multiple sequence alignment of EV-A71, CVB3, Polio-1, EV-D68, HRV-2 and HRV-14 was done with Clustal Omega. Residues in the catalytic center important for ATPase activity are highlighted in blue. The 224AGSINA229 region is highlighted in a black box. Conserved residues are highlighted with red background and similar residues are in red letters.



Chapter

5

Synthesis and antiviral effect of novel fluoxetine analogues as enterovirus 2C inhibitors

Roberto Manganaro^{1*}, Birgit Zonsics^{1*}, Lisa Bauer^{2*},
Maira Lorenzo Lopez¹, Tim Donselaar², Marleen
Zwaagstra², Fabiana Saporito¹, Salvatore Ferla¹, Jeroen
R.P.M. Strating², Bruno Coutard³, Daniel L. Hurdiss²,
Frank J.M. van Kuppeveld², Andrea Brancale^{1,#}

¹ School of Pharmacy & Pharmaceutical Sciences, Cardiff
University, United Kingdom

² Virology Division, Department of Infectious Diseases
and Immunology, Faculty of Veterinary Medicine,
Utrecht University, The Netherlands;

³ Unité des Virus Emergents, Aix-Marseille Université,
France

* These authors contributed equally

Corresponding author

Antiviral Research 2020, 178, 104781

Abstract

Enteroviruses (EV) are a group of positive-strand RNA (+RNA) viruses that include many important human pathogens (e.g. poliovirus, coxsackievirus, echovirus, numbered enteroviruses and rhinoviruses). Fluoxetine was identified in drug repurposing screens as potent inhibitor of enterovirus B and enterovirus D replication. In this paper we are reporting the synthesis and the antiviral effect of a series of fluoxetine analogues. The results obtained offer a preliminary insight into the structure-activity relationship of its chemical scaffold and confirm the importance of the chiral configuration. We identified a racemic fluoxetine analogue, **2b**, which showed a similar antiviral activity compared to (*S*)-fluoxetine. Investigating the stereochemistry of **2b** revealed that the *S*-enantiomer exerts potent antiviral activity and increased the antiviral spectrum compared to the racemic mixture of **2b**. In line with the observed antiviral effect, the *S*-enantiomer displayed a dose-dependent shift in the melting temperature in thermal shift assay, indicative for direct binding to the recombinant 2C protein.

Keywords:

Enterovirus; 2C Inhibitors; Fluoxetine; Thermal shift assay.

Enteroviruses (EV) form the largest genus in the *Picornaviridae* family of positive-strand RNA (+RNA) viruses and include many important human pathogens (e.g. poliovirus, coxsackievirus, echovirus, numbered enteroviruses and rhinoviruses). Infections with EV cause a wide variety of clinical manifestations ranging from mild diseases like hand-foot-and-mouth disease, conjunctivitis to severe conditions like aseptic meningitis, severe neonatal sepsis like diseases and acute flaccid paralysis and myelitis. Rhinoviruses (RV) cause the common cold and can trigger exacerbation of asthma and chronic obstructive pulmonary disease (COPD).¹ These diseases are mostly self-limiting but can give rise to life-threatening respiratory and/or neurological complications especially in infants, young children and immunocompromised individuals. The increasing outbreaks of EV-D68 and several other emerging enteroviruses (e.g. EV-A71 and CV-A16) with severe neurological complications worldwide exemplify the public health threat emerging from EVs²⁻⁴ Despite their huge socioeconomical and medical burden, vaccines only exist against poliovirus and EV-A71, for which vaccines were recently approved in China.⁵ Currently, no antiviral therapy to combat EV infections is approved and treatment is limited to supportive care.

Fluoxetine (Prozac[®]), a selective serotonin reuptake inhibitor (SSRI) licensed for the treatment of major depression and anxiety disorders, was identified in drug repurposing screens as potent inhibitor of enterovirus B and enterovirus D replication.^{6,7} Mode-of-action studies revealed that only the *S*-enantiomer of fluoxetine inhibits viral replication by directly binding to the non-structural protein 2C.⁸ The ATP^{ase} dependent RNA helicase 2C is a highly conserved non-structural protein among EVs and involved in pleiotropic functions during the viral life cycle (uncoating, RNA replication, encapsidation, membrane rearrangement).⁹⁻¹⁷ Fluoxetine was shown to inhibit EV-B replication in mice and additionally has already been successfully used to treat an immunocompromised child with life-threatening chronic enterovirus encephalitis.^{18,19} Together this indicates that fluoxetine offers a potential option as antiviral therapy for clinical use. Here, we report an initial investigation of a series of fluoxetine analogues, in which we introduce some basic changes in the original scaffold, to gain an early insight into the structure-activity relationships of fluoxetine.

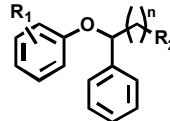
We previously reported a profiling of several fluoxetine fragments and described that the fragment *N*-Methyl-3-(4-(trifluoromethyl)phenoxy)propan-1-amine showed modest antiviral activity against coxsackievirus B3 (CVB3).²⁰ This result indicated that the structural features of the trifluoro-phenoxy moiety and the amino moiety are essential for the antiviral activity whereas the 3-phenyl moiety seems dispensable. The *para*-trifluoro-phenoxy moiety is crucial for the SSRI activity because changes of the substituent lower the affinity towards the serotonin transporter (SERT)²¹. Hence, fluoxetine analogues with modifications on the CF₃-substituent positions on the phenoxy ring were synthesized. Rather than in *para* position, the CF₃ group was placed in *ortho* or in *meta* position on compounds **1a** and **1b**, respectively. In compounds **1c** and **1d**, an additional substituent in *ortho* position was introduced to the parent compound²².

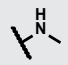
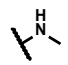
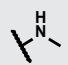
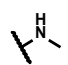
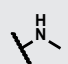
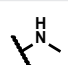
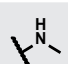
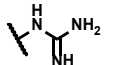
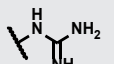
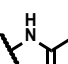
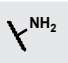
The second moiety of interest was the methylamine group. The well-characterised pan-enterovirus inhibitor guanidine hydrochloride (GuaHCl) has been shown to target 2C²³. We designed fluoxetine analogues substituting the methylamine group with GuaHCl. Compounds **5a** and **5b** differ in the length of the linker chain accounting for the additional atom in GuaHCl compared to the methylamine. Further, in compound **3** the *N*-methyl group was replaced by an acetyl group, to explore the need of a basic nitrogen in that position.

CVB3 causes an observable cytopathic effect (CPE) apparent as rounding, detachment and eventually dying of cells. The newly synthesized compounds were tested in a multicycle CPE-reduction assay to elucidate whether they were capable of inhibiting virus replication and thereby preventing the formation of CPE similar to fluoxetine. Therefore, subconfluent HeLaR19 cells were treated with a concentration range of compounds and the cells were immediately infected with CVB3 at MOI 0.001 resulting in full CPE in the infected control without compound treatment within 3 days. In parallel, cytotoxicity was determined using a colorimetric method using the (3-(4,5-dimethylthiazol-2-yl)-5-(3-carboxymethoxyphenyl)-2-(4-sulfophenyl)-2H-tetrazolium) salt (MTS). It should be noted at this point that all compounds were synthesized as racemic mixture and therefore both the racemic mixture as well as the enantiomers of fluoxetine were used as positive controls. Changing the CF₃ substituent from *para* to *ortho* or *meta* position or introducing a second substituent on the ring abolished the antiviral activity of compounds **1a-1d** (Table 1). On the contrary, compounds **2a**, **2b** and **4a**, which contained changes on the amino moiety, retained antiviral activity. Changing the *N*-methyl group to the acetamide group resulted in the inactive compound **3** (Table1).

Like fluoxetine, compound **2b** was synthesized and tested as a racemic mixture. It proves to be as potent in inhibiting CVB3 replication as (*S*)-fluoxetine and 10-fold more potent than racemic fluoxetine. To exclude a cell-type specific effect of the antiviral efficacy and to evaluate the cytotoxicity of compounds **2a** and **2b**, multicycle assays using different cell lines was performed. Subconfluent HEK239T cells and HAP1 cells were treated with serial dilution of the compounds **2a** and **2b** and cytotoxicity as well as antiviral activity against CVB3 were evaluated in parallel. Compound **2a** and compound **2b** show the same range of antiviral activity against CVB3 in all cell lines. Importantly, both compounds are 2- to 3-fold less cytotoxic than racemic or (*S*)-fluoxetine in all three cell lines tested (Table 2). For unknown reasons, compounds **2a** and **2b** did not show antiviral activity in the monkey cell lines BGM and Vero (data not shown). Taken together, changes in the trifluoro phenoxy part of the molecule resulted in loss of antiviral activity. Modifications on the amine part were tolerated and increased the antiviral activity and the selectivity index (SI) of the compounds slightly.

Table 1. Sensitivity of CVB3 to Fluoxetine Analogues



Compound	n	R ₁	R ₂	EC ₅₀ (μM)	CC ₅₀ (μM)	SI
(<i>RS</i>)-fluoxetine	2	4-CF ₃		3.03 ± 0.56	18.81 ± 1.36	6.21
(<i>S</i>)-fluoxetine	2	4-CF ₃		0.50 ± 0.14	21.63 ± 1.40	43.26
(<i>R</i>)-fluoxetine	2	4-CF ₃		NA	18.82 ± 1.34	-
1a	2	2-CF ₃		NA	>30	-
1b	2	3-CF ₃		NA	12.56 ± 1.79	-
1c	2	2-Cl, 4-CF ₃		NA	3.14 ± 0.07	-
1d	2	2-OMe, 4-CF ₃		NA	18.41 ± 1.26	-
2a	1	4-CF ₃		1.22 ± 0.15	>30	>24.60
2b	2	4-CF ₃		0.41 ± 0.27	>30	>73.17
3	2	4-CF ₃		NA	>30	-
4a	1	4-CF ₃		4.2 ± 0.927	>30	>7.14

Shown are EC₅₀ and CC₅₀ values in μM. Data represents mean values ± standard deviation calculated from three independent experiments and each experiment was performed in biological triplicates. NA = not active.

Table 2. Comparison of compound cytotoxicity and antiviral activity (CVB3) in different cell lines.

Compound	HelaR19			HEK293T			HAP1		
	EC ₅₀ (μM)	CC ₅₀ (μM)	SI	EC ₅₀ (μM)	CC ₅₀ (μM)	SI	EC ₅₀ (μM)	CC ₅₀ (μM)	SI
(R_S)-fluoxetine	2.70 ± 0.54	29.03 ± 1.04	11	1.41 ± 0.89	25.87 ± 1.45	18	2.40 ± 0.33	23.74 ± 1.01	10
(S)-fluoxetine	0.62 ± 0.01	27.67 ± 0.87	45	0.7 ± 0.65	24.65 ± 2.56	35	0.69 ± 0.04	24.00 ± 1.87	35
2a	2.43 ± 0.32	56.78 ± 0.03	23	2.30 ± 0.44	45.87 ± 0.45	20	2.20 ± 0.32	40.72 ± 0.61	19
2b	0.87 ± 0.98	64.99 ± 1.34	75	1.05 ± 0.02	52.98 ± 0.21	53	0.98 ± 0.21	49.39 ± 0.11	50

Shown are EC₅₀ and CC₅₀ values in μM. Data represents mean values ± standard deviation calculated from two independent experiments. Each experiment was done in biological triplicates.

SI = Selectivity Index (CC₅₀/EC₅₀). Selectivity index was calculated from the averaged EC₅₀ and CC₅₀ values of the independent experiments.

Table 3. Broad-Spectrum antiviral activity of most potent compounds.

Virus	EV-A71		CVB3		PV-1		CV-A24		EV-D68		HRV-A2		HRV-B14	
	Species	Strain	EV-B	Nancy	EV-C	Sabin1	EV-C	Joseph	EV-D	Fermon	RV-A	RV-B	RV-A	RV-B
(R_S)-fluoxetine	NA	NA	2.84 ± 0.73	NA	NA	NA	2.49 ± 0.23	NA	NA	NA	NA	NA	NA	NA
(S)-fluoxetine	NA	NA	0.70 ± 0.14	NA	NA	NA	0.63 ± 0.17	NA	6.99 ± 0.84	NA	NA	7.25 ± 0.69	NA	NA
2a	NA	NA	1.98 ± 0.68	NA	NA	NA	3.03 ± 0.48	NA	NA	NA	NA	NA	NA	NA
2b	NA	NA	0.87 ± 0.33	NA	NA	NA	0.56 ± 0.21	NA	NA	NA	NA	3.33 ± 1.05	NA	NA

Shown are EC₅₀ values in μM. Data represents mean values ± standard deviation calculated from three independent experiments. Each experiment was done in biological triplicates

NA = not active.

To investigate the broad-spectrum anti-enteroviral activity of the compounds **2a** and **2b**, Hela R19 cells were infected with representative virus serotypes of different enteroviruses species in both a multicycle CPE reduction assay (MOI 0.001 or 0.01, depending on virus, see Supplementary Information) and in a single cycle assay (MOI 1) in which virus reproduction was evaluated after 8 h or 10 h of infection (depending on virus, see Supplementary Information). Both, **2a** and **2b** inhibited CVB3 and EV-D68, but not EV-A71 or representatives of the EV-C species (poliovirus and CV-A24) (Table 3 and Figure 1). Compound **2b** showed a slightly higher potency towards CVB3 and EV-D68 compared to compound **2a**. Unlike racemic fluoxetine, **2b** also inhibited HRV-14 replication. Notably, **2b** inhibited HRV-14 even more potently than (*S*)-fluoxetine. However, unlike (*S*)-fluoxetine, **2b** did not inhibit HRV-2 (Table 3 and Figure 1).

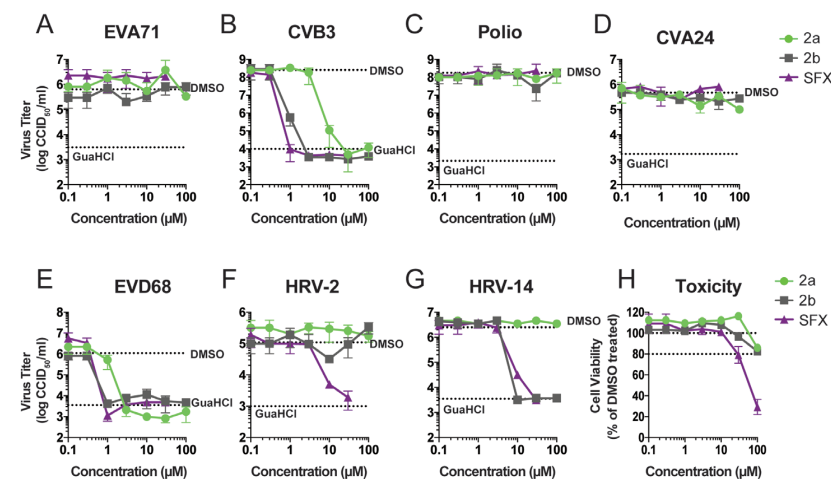


Figure 1. Antiviral effect of analogue 2a and 2b on a panel of enteroviruses. In a single cycle assay Hela R19 cells were infected with different enterovirus species (A) EV-A71 (strain BrCr) (B) CVB3 (strain Nancy) (C) poliovirus (strain Sabin). (D) CV-A24 (Strain Joseph) (E) EV-D68 (strain Fermon) (F) HRV-A2 (G) HRV-B14 at MOI 1 and treated with serial dilutions of (*S*)-fluoxetine (SFX) and the analogues **2a** and **2b**. As a control, guanidine hydrochloride (GuaHCl) was used as a pan-enterovirus inhibitor targeting 2C. At 8 or 10 hours post infection (depending on the virus, see Supplementary Information), cells were freeze-thawed three times and virus titers of lysates were determined by endpoint titration. (H) In parallel, uninfected cells were treated with compound and cell viability was determined using an MTS assay. Data represent mean values ± standard deviation from one representative of two independent experiments. Every experiment was performed in biological triplicates.

Over the last decades several structurally disparate 2C inhibitors were identified but the mode of action is poorly understood.²⁴ We previously reported the putative binding area of (*S*)-fluoxetine in a homology model of CVB3 2C, which was based on the published crystal structure of EV-A71 2C, and provided experimental support for that model through mutational analysis of potential interacting residues.^{20,25}

We demonstrated that the triple mutations A224V-I227V-A229V, which gives cross resistance towards most of the 2C inhibitors,¹⁶ as well as the single mutations I227V, C179F and F190L conferred resistance towards (*S*)-fluoxetine.²⁰ To explore if the newly synthesized compounds have a similar resistance profile, and thus potentially occupy the same binding site, we infected Hela R19 cells with viruses carrying mutations which confer resistance to (*S*)-fluoxetine. Viruses harbouring the 2C triple mutations A224V-I227V-A229V or the single mutations I227V, C179F or F190L were tested for cross-resistance towards the novel analogues **2a** and **2b** (Figure 2). HelaR19 cells were infected with mutant viruses at a MOI of 1 and virus titers were determined by endpoint titration at 8 hours post infection. The triple mutant A224V-I227V-A229V conferred a high level of resistance towards both compound **2a** and **2b** as it does to (*S*)-fluoxetine. Remarkably, the single mutation I227V showed resistance towards (*S*)-fluoxetine but not against the new analogues **2a** or **2b**. The residue C179F conferred resistance towards (*S*)-fluoxetine and **2b**, but not against **2a**. Notably, the mutation F190L did not confer resistance to either **2a** or **2b**. Summarized, the overall resistance profile for the new compounds is very similar to (*S*)-fluoxetine but not identical. This suggests that the compounds likely occupy the same binding pocket as (*S*)-fluoxetine, but the exact binding mode could be slightly different. Unfortunately, the lack of an experimental structure of the fluoxetine/2C complex does not yet allow us to generate an accurate binding model for the newly reported compounds.

Given the improved antiviral activity of the racemic mixture of **2b**, we dissected the role of the two **2b**-enantiomers. The antiviral activity of the enantiomers was evaluated in a multicycle assay. The *S*-enantiomer of **2b** showed a ~3-4 fold increased antiviral activity against CVB3, EV-D68 and HRV-14 compared to the racemic **2b** and (*S*)-fluoxetine (Figure 3A and Table 4). Additionally, the *S*-enantiomer but not the racemic mixture of **2b** also inhibited HRV-2 (Figure 3A). Remarkably, the *R*-enantiomer showed subtle antiviral activity against CVB3 and EV-D68 (Figure 3A). Both enantiomers did not inhibit EV-A71 or the representative members of the EV-C species (PV-1 and CV-A24, data not shown). Additionally, we investigated the binding of the two enantiomers to a recombinant fragment of CVB3 2C (D116) using a thermal shift assay. As reported previously, (*S*)-fluoxetine shifted the melting temperature of 2C in a dose-dependent manner.

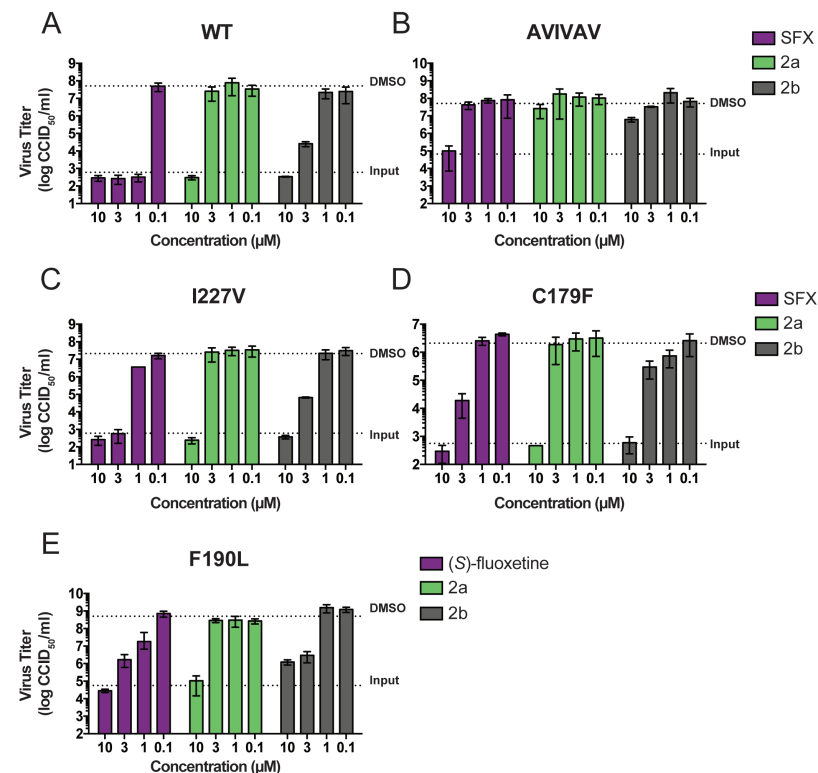


Figure 2. Mutations in the CVB3-2C protein confer resistance to compound **2a and **2b**.** Hela R19 cells were infected with a selection of CVB3 viruses harbouring previously identified mutations in the non-structural protein 2C, which confer resistance towards (*S*)-fluoxetine (SFX). (20) Hela R19 were infected with and MOI 1 of (A) CVB3 wildtype virus. (B) the AVIVAV mutant (A224V-I227V-A229V triple mutant) (C) the I227V single mutant (D) the C179F and (E) the F190L mutant. Eight hours post infection cells were freeze-thawed three times and virus titers were determined with endpoint titration. Data represented show mean values \pm standard deviation from one experiment representative of two independent experiments. Every experiment was performed in biological triplicates.

Consistent with the antiviral activity, the **2b** *S*-enantiomer caused a dose-dependent shift in the melting temperature of 2C, indicative of direct binding. Unlike (*R*)-fluoxetine, a thermal shift was also observed for the **2b** *R*-enantiomer of **2b** at higher concentrations. This suggests that the *R*-enantiomer of **2b** exerts indeed subtle antiviral activity.

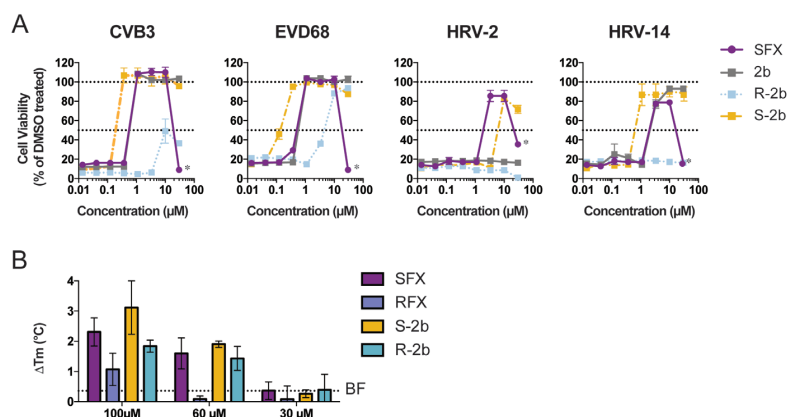


Figure 3. The *S*-enantiomer of 2b exerts potent antiviral activity concomitant with 2C binding. (A) A Multi-cycle CPE reduction assay to determine the antiviral activity of the 2b-enantiomers was performed. HeLa R19 cells were treated with serial dilutions of racemate, (*S*)-, or (*R*)- enantiomer of 2b and infected with CVB3 (strain Nancy), EVD68 (strain Fermon), HRV-2 (G) and HRV-14 at low MOI (depending on the virus, see Supplementary Information) to reach full CPE within three days. As positive control, cells were treated with (*S*)-fluoxetine. * indicates cytotoxicity of (*S*)-fluoxetine. Data shown are from one experiment representative of three independent experiments done in biological triplicates (B) The binding of the 2b-enantiomers to a recombinant fragment of CVB3-2C was determined by thermal shift assay. The thermal stabilization of 2C is represented by change in melting temperature. The dashed line represents data from the negative control BF738735, a phosphatidylinositol-4-kinase III b inhibitor, used at a concentration of 250 μM. Data shown is representative of two independent experiments, each of which was done in technical triplicates. Error bars depict standard deviation calculated from both experiments.

Table 4. Antiviral activity of the 2b enantiomers.

Compound	EV-A71	CVB3	PV-1	CV-A24	EV-D68	HR-V2	HR-V14	CC ₅₀
(<i>S</i>)-fluoxetine	>30	0.83 ± 0.29	>30	>30	0.68 ± 0.95	2.49 ± 2.5	3.76 ± 1.45	27.81 ± 0.95
2b	>30	0.81 ± 0.46	>30	>30	0.56 ± 0.77	>30	4.3 ± 2.98	60.76 ± 0.45
(<i>R</i>)-2b	>30	>30*	>30	>30	4.13 ± 1.4	>30	>30	57.95 ± 0.65
(<i>S</i>)-2b	>30	0.19 ± 0.45	>30	>30	0.11 ± 0.02	7.49 ± 1.12	0.98 ± 1.25	59.6 ± 1.45

*subtle antiviral activity observed

Shown are EC₅₀ and CC₅₀ values in μM. Data represents mean values ± standard deviation calculated from three independent experiments and each experiment was performed in biological triplicates.

In conclusion, our study established that the introduced changes on the *para*-trifluoro-phenoxy moiety of fluoxetine resulted in the loss of antiviral activity. Although it may not be possible to fully uncouple the SSRI activity from the antiviral activity, it appears that modifications on the amine moiety can increase the antiviral activity and reduce cytotoxicity. Additionally, we confirmed the importance of the chiral configuration in maintaining the antiviral activity. Similar to fluoxetine, the antiviral activity of the 2b *S*-enantiomer was higher compared to the *R*-enantiomer or the racemic mixture of 2b. Interestingly, unlike (*R*)-fluoxetine, the 2b *R*-enantiomer gained subtle antiviral activity against CV-B3 and EV-D68. In line with the antiviral activity, the *S*-enantiomer as well as high concentrations of *R*-enantiomer caused a dose-dependent thermal shift of 2C, suggestive of a direct interaction. Known resistance mutations confer cross-resistance to the analogues 2a and 2b and our data indicate that the novel compounds interact with 2C in a similar manner as (*S*)-fluoxetine. However, the observed variations in the resistance profile of the two drugs point to subtle differences in the interaction with the 2C protein.

Acknowledgements

This work was supported by research grants from the Netherlands Organisation for Scientific Research (NWO-ECHO-711.017.002 to FJMvK, NWO-VICI-91812628 to FJMvK), the European Union (Horizon 2020 Marie Skłodowska-Curie ETN 'ANTIVIRALS', grant agreement number 642434 to BC, AB and FJMvK). D.L.H. is funded from the European Union's Horizon 2020 research and innovation program under the Marie Skłodowska-Curie grant agreement (No 842333) and holds an EMBO non-stipendiary long-term Fellowship (ALTF 1172-2018). S.F. was supported by the Sêr Cymru II programme which is part-funded by Cardiff University and the European Regional Development Fund through the Welsh Government.

References

- Tapparel C, Siegrist F, Petty TJ, Kaiser L. Picornavirus and enterovirus diversity with associated human diseases. *Infect Genet Evol.* 2013;14(1):282–93.
- Pons-Salort M, Parker EPK, Grassly NC. The epidemiology of non-polio enteroviruses: Recent advances and outstanding questions. *Curr Opin Infect Dis.* 2015;28(5):479–87.
- Cassidy H, Poelman R, Knoester M, Van Leer-Buter CC, Niesters HGM. Enterovirus D68 – The New Polio? *Front Microbiol. Frontiers*; 2018 Nov;9:2677.
- Morens DM, Folkers GK, Fauci AS. Acute Flaccid Myelitis: Something Old and Something New. *MBio. American Society for Microbiology (ASM)*; 2019;10(2).
- Aw-Yong KL, NikNadia NMN, Tan CW, Sam I, Chan YF. Immune responses against enterovirus A71 infection: Implications for vaccine success. *Rev Med Virol. John Wiley & Sons, Ltd*; 2019 Sep;29(5).
- Ulferts R, Van Der Linden L, Thibaut HJ, Lanke KHW, Leyssen P, Coutard B, et al. Selective serotonin reuptake inhibitor fluoxetine inhibits replication of human enteroviruses B and D by targeting viral protein 2C. *Antimicrob Agents Chemother.* 2013;57(4):1952–6.
- Zuo J, Quinn KK, Kye S, Cooper P, Damoiseaux R, Krogstad P. Fluoxetine is a potent inhibitor of coxsackievirus replication. *Antimicrob Agents Chemother.* 2012;56(9):4838–44.
- Bauer L, Manganaro R, Zonsics B, Strating JRP, El Kazzi P, Lorenzo Lopez M, et al. Fluoxetine inhibits enterovirus replication by targeting the viral 2C protein in a stereospecific manner. *ACS Infect Dis. American Chemical Society*; 2019 Jul;acsinfecdis.9b00179.
- Mirzayan C, Wimmer E. Genetic analysis of an NTP-binding motif in poliovirus polypeptide 2C. *Virology.* 1992;189(2):547–55.
- Rodriguez PL, Carrasco L. Poliovirus protein 2C has ATPase and GTPase activities. *J Biol Chem.* 1993;268(11):8105–10.
- Mirzayan C, Wimmer E. Biochemical Studies on Poliovirus Polypeptide 2C: Evidence for ATPase Activity. *Virology. Academic Press*; 1994 Feb;199(1):176–87.
- Papageorgiou N, Coutard B, Lantez V, Gautron E, Chauvet O, Baronti C, et al. The 2C putative helicase of echovirus 30 adopts a hexameric ring-shaped structure. *Acta Crystallogr Sect D Biol Crystallogr.* 2010;66(10):1116–20.
- Xia H, Wang P, Wang GC, Yang J, Sun X, Wu W, et al. Human Enterovirus Nonstructural Protein 2C^{ATPase} Functions as Both an RNA Helicase and ATP-Independent RNA Chaperone. *PLoS Pathog.* 2015;11(7):1–29.
- Bienz K, Egger D, Pfister T, Troxler M. Structural and functional characterization of the poliovirus replication complex. *J Virol.* 1992;66(5):2740–7.
- Adams P, Kandiah E, Effantin G, Steven AC, Ehrenfeld E. Poliovirus 2C protein forms homo-oligomeric structures required for ATPase activity. *J Biol Chem.* 2009;284(33):22012–21.
- De Palma AM, Heggermont W, Lanke K, Coutard B, Bergmann M, Monforte A-M, et al. The Thiazolobenzimidazole TBZE-029 Inhibits Enterovirus Replication by Targeting a Short Region Immediately Downstream from Motif C in the Nonstructural Protein 2C. *J Virol.* 2008;82(10):4720–30.
- Sweeney TR, Cisnetto V, Bose D, Bailey M, Wilson JR, Zhang X, et al. Foot-and-mouth disease virus 2C is a hexameric AAA+ protein with a coordinated ATP hydrolysis mechanism. *J Biol Chem.* 2010;285(32):24347–59.
- Benkahla MA, Alidjinou EK, Sane F, Desailoud R, Hober D. Fluoxetine can inhibit coxsackievirus-B4 E2 in vitro and in vivo. *Antiviral Res. Elsevier*; 2018 Nov;159:130–3.
- Gofshsteyn J, Cárdenas AM, Bearden D. Treatment of Chronic Enterovirus Encephalitis With Fluoxetine in a Patient With X-Linked Agammaglobulinemia. *Pediatr Neurol. Elsevier Inc*; 2016;64:94–8.
- Bauer L, Manganaro R, Zonsics B, Strating JRP, El Kazzi P, Lorenzo Lopez M, et al. Fluoxetine Inhibits Enterovirus Replication by Targeting the Viral 2C Protein in a Stereospecific Manner. *ACS Infect Dis. American Chemical Society*; 2019 Sep;5(9):1609–23.
- Wenthur CJ, Bennett MR, Lindsley CW. Classics in chemical neuroscience: Fluoxetine (Prozac). *ACS Chem Neurosci.* 2014;5(1):14–23.
- Wenthur CJ. Classics in Chemical Neuroscience: Methylphenidate. *ACS Chem Neurosci.* 2016;7(8):1030–40.
- Pincus SE, Diamond DC, Emini EA, Wimmer E. Guanidine-selected mutants of poliovirus: mapping of point mutations to polypeptide 2C. *J Virol.* 1986;57(2):638–46.
- Bauer L, Lyoo H, van der Schaar HM, Strating JR, van Kuppeveld FJ. Direct-acting antivirals and host-targeting strategies to combat enterovirus infections. *Curr Opin Virol. Elsevier B.V.*; 2017;24:1–8.
- Guan H, Tian J, Qin B, Wojdyla JA, Wang B, Zhao Z, et al. Crystal structure of 2C helicase from enterovirus 71. *Sci Adv.* 2017;3(4):1–10.

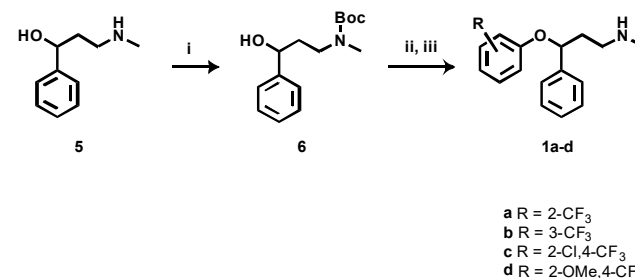
Supporting Information

General Chemistry methods

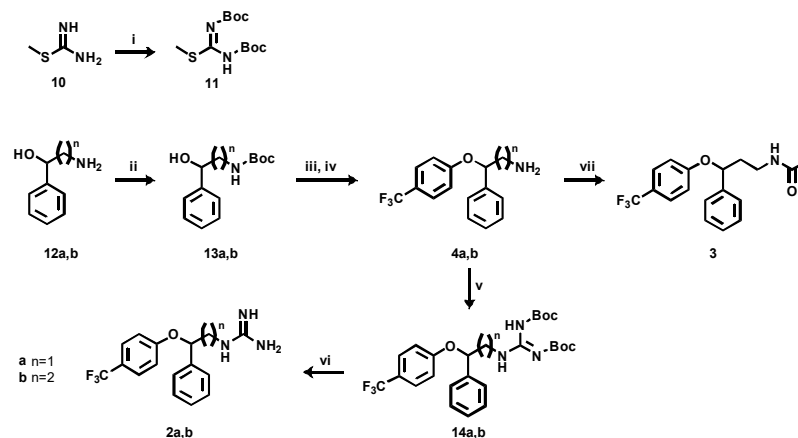
All solvents and reagents used were obtained from commercial sources unless otherwise indicated. All reactions were performed under a nitrogen atmosphere. ^1H , ^{13}C and ^{19}F NMR spectra were recorded with a Bruker Avance III HD spectrometer operating at 500 MHz for ^1H , 125 MHz for ^{13}C and 470 MHz for ^{19}F with Me_4Si as internal standard. Deuterated dimethyl sulfoxide (DMSO) was used as the solvent for NMR experiments, unless otherwise stated. ^1H chemical shifts values (δ) are referenced to the residual non-deuterated components of the NMR solvents ($\delta = 2.50$ ppm for DMSO). The ^{13}C chemical shifts (δ) are referenced to DMSO (central peak, $\delta = 39.5$ ppm). Thin layer chromatography (TLC) was performed on Silica gel plates (Merck Kieselgel 60 F254), which were developed by the ascending method. Column chromatography was performed on an Isolera Biotage system. UPLC-UV-MS analysis was conducted on a Waters UPLC system with both Diode Array detection and Electrospray (+ve and -ve ion) MS detection. The following conditions were applied: Waters Acquity UPLC BEH C18 1.7 μm 2.1x50 mm column, 0.5 mL/min, column temperature 40°C; mobile phase was LC-MS grade H_2O containing 0.1% formic acid (A) and LC-MS grade MeCN containing 0.1% formic acid (B); sample diluent: MeCN; sample concentration: 1 $\mu\text{g}/\text{mL}$; injection volume: 2 μL , gradient 90% eluent A (0.1 min), 90%-0% eluent A (1.5 min), 0% eluent A (1.4 min), 90% eluent A (0.1 min) (method 1). All compounds tested in biological assays were >95% pure. Purity of intermediates was >90%, unless otherwise stated.

Synthetic Routes

Compounds **1a-d** were synthesised starting from the commercially available 3-(methylamino)-1-phenylpropan-1-ol **5**, with the *N*-Boc protection of its amino group, to give **6**. Compound **6** was then *O*-arylated through Mitsunobu reaction using different phenols. Followed by *N*-Boc deprotection using trifluoro acetic acid (TFA) the desired products **1a-d** were obtained (scheme 1).

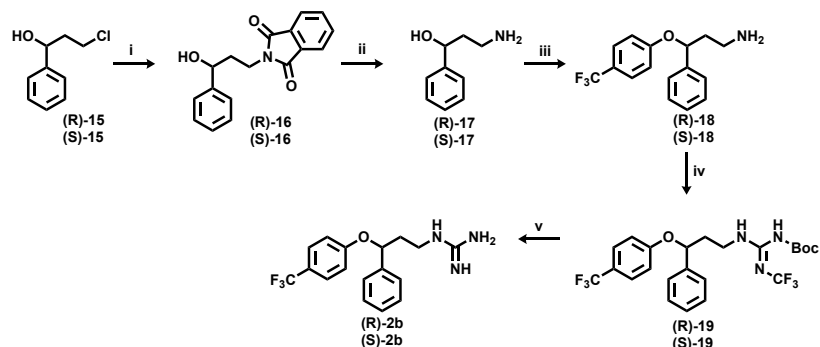


Scheme 1. Synthesis of phenoxy derivatives of fluoxetine; (i) $(\text{Boc})_2\text{O}$, DCM, rt, on, 99%; (ii) phenols, PPh_3 , DIAD, diethyl ether, rt, 2h, 60-79%; (iii) TFA, DCM, rt, on, 62-83%;



Scheme 2. Synthesis of guanidine (**2a** and **2b**) and the acetoamide (**3**) derivatives of fluoxetine; i) $(\text{Boc})_2\text{O}$, NaHCO_3 sat, DCM, rt, 48h, 47%; ii) $(\text{Boc})_2\text{O}$, DCM, rt, on, 69%; iii) 4-(trifluoromethyl)phenol, PPh_3 , DIAD, diethyl ether, rt, 3h; iv) HCl, DCM, rt, on or TFA, DCM, rt, on, 27% over two steps; v) *N,N'*-bis(*tert*-butoxycarbonyl)-*S*-methylisothiourea **11**, DIPEA, DCM, rt, on, 46-81%; vi) SnCl_4 , EtOAc, rt, 3h, 28-95%; vii) acetyl chloride, TEA, DCM, rt, 2h, 98%.

Synthesis of compounds **2a,b** and **3** starts from the commercial available 2-amino-1-phenylethan-1-ol **12a** and 3-amino-1-phenylpropan-1-ol **12b**, obtaining compound **4a** and norfluoxetine **4b** following the synthetic pathway previously adopted for the preparation of **1a-d**, as showed in scheme 2. Reaction of **4a** and **4b** with the guanidinylation reagent *N,N'*-bis(*tert*-butoxycarbonyl)-*S*-methylisothiourea **11** gives the *N,N'*-bis(Boc) protected guanidine derivatives **14a,b**, which are then converted to the desired final products **2a,b** by a mild bis-Boc deprotection using stannic chloride. Compound **3** was synthesised by acetylation of norfluoxetine **4b**.



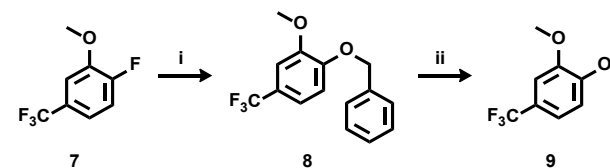
Scheme 3. Synthesis of (R)- and (S)- enantiomers of compound **2b**; i) potassium phthalimide, DMF, 90 °C, 2 h, 65-84%; ii) $\text{NH}_2\text{NH}_2 \cdot \text{H}_2\text{O}$, ethanol (EtOH), reflux, 2 h, 53-77%; iii) NaH, *p*-fluorobenzotrifluoride, DMF, 0 °C then 90 °C for 1 h, 50-54%. iv) *N,N'*-bis(*tert*-butoxycarbonyl)-*S*-methylisothiourea (**11**), DIPEA, DCM, r.t., 72h., 34-45%; v) SnCl_4 , EtOAc, 0 °C then r.t, 3h, 75-80%.

Preparation of the two single enantiomers of compound **2b** was performed adapting the method previously reported by Costa et al.⁴ The commercially available single enantiomers **15** were converted into the corresponding phthalimide derivatives **16** through a nucleophilic substitution. A hydrazinolysis reaction using hydrazine monohydrate in ethanol was exploited to obtain primary amine **17**, which were then converted through a $\text{S}_{\text{N}}\text{Ar}$ reaction to the corresponding single norfluoxetine enantiomers **18** using *p*-fluorobenzotrifluoride in DMF. Preparation of *N,N'*-bis(Boc) protected guanidine derivatives **19** and consequent deprotection-step using stannic chloride were performed, as previously reported for **2b** preparation, obtaining the desired final products (R)-**2b** and (S)-**2b** as pure single enantiomers.

Fluoxetine analogues

N-Boc-3-(methylamino)-1-phenylpropan-1-ol (**6**)

To a solution of 3-(methylamino)-1-phenylpropan-1-ol (**5**) (12.1 mmol) in anhydrous DCM (48 mL), di-*tert*-butyl dicarbonate (13.3 mmol) was added, the reaction mixture was stirred at room temperature overnight. The reaction mixture was then washed with a saturated aqueous NH_4Cl (3x30 mL), brine (3x30 mL), dried over Na_2SO_4 and the solvent was removed at reduced pressure. Compound **6** was obtained as a colourless oil which, was used without further purification. Yield: 99%. $^1\text{H NMR}$ (DMSO- d_6), δ : 7.36 – 7.29 (m, 4H), 7.30 – 7.20 (m, 1H), 5.22 (d, $J = 4.4$ Hz, 1H), 4.52 (dd, $J = 11.0, 6.2$ Hz, 1H), 3.18 (br s, 2H), 2.76 (s, 3H), 1.78 (br s, 2H), 1.35 (br s, 9H). $^{13}\text{C NMR}$ (DMSO- d_6), δ : 155.22, 146.33, 128.48, 127.17, 126.13, 78.66, 70.67, 46.03, 37.91, 34.46, 28.53. UPLC-MS: Rt: 1.883, MS (ESI)⁺: 288.1 [M+Na]⁺, 192.1[C₁₁H₁₄NO₂]⁺.



Scheme 3. Synthesis of 2-methoxy-4-(trifluoromethyl)phenol; i) NaH, benzyl alcohol, DMF, rt, 5h, Y=85%; ii) H_2 , Pd/C, EtOAc, rt, overnight;

1-(benzyloxy)-2-methoxy-4-(trifluoromethyl)benzene (**8**)

Sodium hydride (2.36 mmol) was added to a solution of benzyl alcohol (2.15 mmol) in DMF (10 mL). After thirty minutes, 1-fluoro-2-methoxy-4-(trifluoromethyl)benzene (**7**) (2.58 mmol) was added dropwise to the mixture. The reaction was stirred at room temperature for five hours. The reaction mixture was diluted in ethyl acetate (20 mL) and washed with water (3x20 mL), brine (3x20 mL). The organic layer was dried over Na_2SO_4 and the solvent was removed at reduced pressure. The crude residue was purified by flash column chromatography, eluting with n-Hexane-DCM 100:0 v/v increasing to 50:50 v/v. Compound **8** was obtained as a white powder. Yield: 85%. $^1\text{H NMR}$ (DMSO- d_6), δ : 7.48 – 7.44 (m, 2H), 7.44 – 7.38 (m, 2H), 7.35 (td, $J = 8.6, 4.5, 1.4$ Hz, 1H), 7.29 – 7.19 (m, 3H), 5.18 (s, 1H), 3.84 (s, 2H). $^{19}\text{F NMR}$ (DMSO- d_6), δ : -59.45 (s, 3F). $^{13}\text{C NMR}$ (DMSO- d_6), δ : 151.21, 149.72, 136.93, 128.95, 128.51, 128.34, 124.89 (q, $J = 271.4$ Hz), 121.82 (q, $J = 32.1$ Hz), 118.54 (q, $J = 3.5$ Hz), 113.48, 108.89 (q, $J = 3.5$ Hz), 70.40, 56.34.

2-methoxy-4-(trifluoromethyl)phenol (**9**)

A solution of 1-(benzyloxy)-2-methoxy-4-(trifluoromethyl)benzene (**8**) (1.59 mmol) in anhydrous EtOAc (0.15 M) was stirred under H_2 atmosphere in presence of Pd/C (15%). The reaction mixture was then stirred at room temperature overnight, filtered on Celite and the solvent was removed at reduced pressure. Compound **9** was obtained as a colorless oil which was used without further purification. Yield: 84%. $^1\text{H NMR}$ (DMSO- d_6), δ : 9.88 (s, 1H), 7.17 (s, 1H), 7.14 (d, $J = 8.2$ Hz, 1H), 6.93 (d, $J = 8.2$ Hz, 1H), 3.83 (s, 3H). $^{19}\text{F NMR}$ (DMSO- d_6), δ : -59.45 (s, 3F). $^{13}\text{C NMR}$ (DMSO- d_6), δ : 150.58, 148.30, 125.10 (q, $J = 270.9$ Hz), 120.11 (q, $J = 32.0$ Hz), 118.83 (q, $J = 4.2$ Hz), 115.88, 109.27 (q, $J = 3.5$ Hz), 56.30.

General method for the preparation of fluoxetine derivatives (1a-d)

To a solution of triphenylphosphine (1.70 mmol) in anhydrous diethyl ether (3.39 mL) cooled at 0 °C, diisopropyl azodicarboxylate (1.14 mmol) in anhydrous diethyl ether (0.57 mL) was added. After twenty minutes, different phenols (1.36 mmol) in anhydrous diethyl ether (2.26 mL) were added before adding the solution of *N*-Boc-3-(methylamino)-1-phenylpropan-1-ol (**5**) (1.13 mmol) in anhydrous diethyl ether (2.83 mL). The reaction was stirred at room temperature for three hours before removing the solvent in vacuo. The crude residue was purified by flash column chromatography

eluting with *n*-hexane/DCM 100:0 v/v increasing to 0:100 v/v and DCM/MeOH 100:0 v/v increasing to 97:3 v/v.

The *N*-Boc-*N*-methyl-3-phenoxy-3-phenylpropan-1-amine (0.84 mmol) were then solubilised in anhydrous DCM (4.2 mL). The reaction as cooled at 0°C before adding TFA (4.20 mmol) and the reaction mixture was stirred at room temperature for two hours. After completion of the reaction was established by TLC, the mixture was diluted with DCM (8 mL) and was washed with sat. NaHCO₃ solution (3x10 mL) and brine (3x10 mL). The organic layers were then combined, dried over Na₂SO₄ and the solvent was removed at reduced pressure. The crude residue was purified by flash column chromatography.

***N*-methyl-3-phenyl-3-(2-(trifluoromethyl)phenoxy)propan-1-amine (1a)**

Purified by flash column chromatography eluting with DCM/MeOH 100:0 v/v increasing to 90:10 v/v. Yield: 83%, yellow oil. ¹H NMR (DMSO-*d*₆), δ : 8.88 (s, 2H), 7.61 (d, *J* = 6.8 Hz, 1H), 7.48 (t, *J* = 7.4 Hz, 1H), 7.44 – 7.37 (m, 4H), 7.34 – 7.28 (m, 1H), 7.06 – 7.00 (m, 2H), 5.81 – 5.73 (m, 1H), 3.05 – 2.92 (m, 2H), 2.55 (s, 3H), 2.34 – 2.15 (m, 2H). ¹⁹F NMR (DMSO-*d*₆), δ : -60.77 (s, 3F). ¹³C NMR (DMSO-*d*₆), δ : 13C NMR (126 MHz, DMSO) δ 155.15, 140.20, 134.36, 129.34, 128.66, 127.32 (q, *J* = 5.0 Hz), 126.28, 124.36 (q, *J* = 272.4 Hz), 120.89, 117.80 (q, *J* = 30.0 Hz), 115.14, 76.57, 45.45, 34.50, 32.89. UPLC-MS: Rt: 1.733, MS (ESI)⁺: 310[M+1]⁺.

***N*-methyl-3-phenyl-3-(3-(trifluoromethyl)phenoxy)propan-1-amine (1b)**

Purified by flash column chromatography eluting with DCM/MeOH 100:0 v/v increasing to 90:10 v/v. Yield: 62%, yellow oil. ¹H NMR (DMSO-*d*₆), δ : 7.46 – 7.38 (m, 3H), 7.35 (t, *J* = 7.6 Hz, 2H), 7.27 (t, *J* = 7.3 Hz, 1H), 7.22 – 7.16 (m, 3H), 5.55 (dd, *J* = 7.7, 5.4 Hz, 1H), 2.62 – 2.54 (m, 2H), 2.28 (s, 3H), 2.15 – 2.05 (m, 1H), 1.95 – 1.85 (m, 1H). ¹⁹F NMR (DMSO-*d*₆), δ : -61.22 (s, 3F). ¹³C NMR (DMSO-*d*₆), δ : 158.46, 141.57, 131.07, 129.07, 128.16, 126.53, 120.30, 117.56 (q, *J* = 4.0 Hz), 112.86 (q, *J* = 4.0 Hz), 77.95, 47.92, 38.08, 36.36. UPLC-MS: Rt: 1.77, MS (ESI)⁺: 310[M+1]⁺.

3-(2-chloro-4-(trifluoromethyl)phenoxy)-*N*-methyl-3-phenylpropan-1-amine (1c)

Purified by flash column chromatography eluting with DCM/MeOH 100:0 v/v increasing to 90:10 v/v. Yield: 63%, colourless oil. ¹H NMR (DMSO-*d*₆), δ : 7.81 (d, *J* = 2.0 Hz, 1H), 7.54 (dd, *J* = 8.7, 1.8 Hz, 1H), 7.42 – 7.34 (m, 4H), 7.31 – 7.26 (m, 1H), 7.16 (d, *J* = 8.7 Hz, 1H), 5.71 (dd, *J* = 7.9, 5.1 Hz, 1H), 2.69 – 2.58 (m, 2H), 2.30 (s, 3H), 2.21 – 2.10 (m, 1H), 1.98 (dt, *J* = 13.8, 7.2 Hz, 1H). ¹⁹F NMR (DMSO-*d*₆), δ : -60.15 (s, 3F). ¹³C NMR (DMSO-*d*₆), δ : 156.35, 140.78, 129.19, 128.41, 127.49 (q, *J* = 3.7 Hz), 126.31, 125.98 (q, *J* = 3.9 Hz), 124.12 (q, *J* = 256.5 Hz), 122.36 (q, *J* = 32.9 Hz), 115.99, 78.95, 47.65, 37.77, 36.17. UPLC-MS: Rt: 1.631, MS (ESI)⁺: 344.2[M+1]⁺.

3-(2-methoxy-4-(trifluoromethyl)phenoxy)-*N*-methyl-3-phenylpropan-1-amine (1d)

Purified by flash column chromatography eluting with DCM/MeOH 100:0 v/v increasing to 90:10 v/v. Yield: 64%, yellow oil. ¹H NMR (DMSO-*d*₆), δ : 7.41 – 7.33 (m, 4H), 7.29 – 7.24 (m, 1H), 7.20 (d, *J* = 2.0 Hz, 1H), 7.11 (dd, *J* = 8.4, 1.2 Hz, 1H), 6.94 (d, *J* = 8.4 Hz, 1H), 5.53 (dd, *J* = 7.8, 5.1 Hz, 1H), 3.88 (s, 3H), 2.63 (s, 2H), 2.31 (s, 3H), 2.19 – 2.08 (m, 1H), 1.99 – 1.90 (m, 1H). ¹⁹F NMR (DMSO-*d*₆), δ : -59.88 (s, 3F). ¹³C NMR (DMSO-*d*₆), δ : 150.42, 150.04, 141.47, 129.06, 128.18, 126.38, 124.80 (q, *J* = 271.3 Hz), 121.71 (q, *J* = 32.2 Hz), 118.31 (q, *J* = 4.2 Hz), 114.94, 109.09 (q, *J* = 3.4 Hz), 78.41, 56.48, 47.76, 37.69, 35.97. UPLC-MS: Rt: 1.585, MS (ESI)⁺: 340.2[M+1]⁺.

***N,N'*-Bis(tert-butoxycarbonyl)-*S*-methylisothiourea (11)**

To a stirring mixture of methyl carbamimidothioate hemisulfate (7.18 mmol) in sat. NaHCO₃ (8 mL) and DCM (16 mL) a solution of di-tert-butyl decarbonate (14.37 mmol) in DCM (12 mL) was added. The reaction was stirred at room temperature for 48 hours. The mixture was diluted in DCM (8 mL) and the organic layer was separated from the aqueous. The aqueous phase was extracted with DCM (2x20 mL). The combined organic layers were dried over Na₂SO₄, filtrated and concentrated under reduced pressure. The crude was stirred in EtOH/H₂O 9:1 for 1h, the resulting precipitate was filtrated under vacuum to give compound **8** as a white powder. Yield: 55%. This compound was previously reported, and the spectral data agree with those specified in literature. ¹H NMR (CDCl₃-*d*), δ : 11.60 (s, 1H), 2.40 (s, 3H), 1.53 (s, 9H), 1.51 (s, 9H). ¹³C NMR (CDCl₃-*d*), δ : 171.46, 160.77, 150.78, 83.24, 80.97, 28.04, 14.41. UPLC-MS: Rt: 2.168, MS (ESI)⁺: 291.1[M+1]⁺, 313.1[M+Na]⁺.

***N*-Boc-2-(methylamino)-1-phenylethan-1-ol (13a)**

To a solution of 2-amino-1-phenylpropan-1-ol (**12a**) (3.64 mmol) in anhydrous DCM (14 mL), di-tert-butyl dicarbonate (4 mmol) was added, the reaction mixture was stirred at room temperature overnight. The reaction mixture was then washed with a 1M HCl solution (3x30mL), brine (3x30mL), dried over Na₂SO₄ and the solvent was removed at reduced pressure. Compound **13a** was obtained as a colourless oil which, was used without further purification. The residue was purified by flash column chromatography, eluting with *n*-Hexane-EtOAc 100:0 v/v increasing to 60:40 v/v. Compound **10a** was obtained as a white solid. Yield: 93%. ¹H NMR (DMSO-*d*₆), δ : 7.35 – 7.29 (m, 4H), 7.27 – 7.21 (m, 1H), 6.71 (t, *J* = 5.5 Hz, 1H), 5.34 (d, *J* = 4.5 Hz, 1H), 4.61 – 4.55 (m, 1H), 3.16 – 3.08 (m, 1H), 3.05 – 2.94 (m, 1H), 1.36 (s, 9H). ¹³C NMR (DMSO-*d*₆), δ : 156.09, 144.16, 128.41, 127.39, 126.50, 78.04, 71.94, 48.63, 28.71. UPLC-MS: Rt: 1.668, MS (ESI)⁺: 164.0[C₉H₁₀NO₂]⁺.

***N*-Boc-3-(methylamino)-1-phenylpropan-1-ol (13b)**

To a solution of 3-amino-1-phenylpropan-1-ol (**12b**) (1.65 mmol) in DCM (7 mL), di-tert-butyl dicarbonate (1.8 mmol) was added, the reaction mixture was stirred at

room temperature overnight. The reaction mixture was then washed with a saturated aqueous NH_4Cl (3x30ml), brine (3x30ml), dried over Na_2SO_4 and the solvent was removed at reduced pressure. Compound **13b** was obtained as a colourless oil which, was used without further purification. Yield: 87%. $^1\text{H NMR}$ (DMSO- d_6), δ : 7.40 – 7.34 (m, 4H), 7.31 – 7.24 (m, 1H), 6.82 (t, J = 5.0 Hz, 1H), 5.25 (d, J = 4.5 Hz, 1H), 4.60 (dd, J = 11.0, 6.4 Hz, 1H), 3.03 (dd, J = 13.6, 6.3 Hz, 2H), 1.75 (dd, J = 14.2, 6.8 Hz, 2H), 1.43 (s, 9H). $^{13}\text{C NMR}$ (DMSO- d_6), δ : 156.05, 146.55, 128.45, 127.11, 126.14, 77.87, 70.68, 39.79, 37.70, 28.74.

2-phenyl-2-(4-(trifluoromethyl)phenoxy)ethan-1-amine hydrochloride (4a)

To a solution of triphenylphosphine (1.9 mmol) in anhydrous diethyl ether (3.8 mL) cooled at 0°C, diisopropyl azodicarboxylate (1.28 mmol) in anhydrous diethyl ether (0.6 mL) was added. After twenty minutes, 4-(trifluoromethyl)phenol (1.52 mmol) in anhydrous diethyl ether (2.26 mL) was added before adding the solution of *N*-Boc-2-(methylamino)-1-phenylethan-1-ol (**13a**) (1.27 mmol) in anhydrous diethyl ether (3.1 mL). The reaction was stirred at room temperature for three hours before removing the solvent in vacuo. The crude residue was purified by flash column chromatography eluting with n-hexane-DCM 100:0 v/v increasing to 0:100 v/v and DCM/MeOH 100:0 v/v increasing to 97:3 v/v to give. The residue was then solubilised in anhydrous DCM (2.7 mL) was cooled to 0°C and HCl (2M) in diethyl ether (3.57 mmol) was added. The reaction was stirred overnight at room temperature. Formation of a precipitate was observed. The precipitate was filtrated under vacuum and washed with DCM to give compound **4a** as a white solid. Yield: 37% over 2 steps. $^1\text{H NMR}$ (DMSO- d_6), δ : 8.51 (s, 3H), 7.61 (d, J = 8.7 Hz, 2H), 7.48 – 7.39 (m, 4H), 7.35 (t, J = 7.2 Hz, 1H), 7.10 (d, J = 8.6 Hz, 2H), 5.76 (dd, J = 9.0, 3.7 Hz, 1H), 3.32 – 3.21 (m, 2H). $^{19}\text{F NMR}$ (DMSO- d_6), δ : -59.99 (s, 3F). $^{13}\text{C NMR}$ (DMSO- d_6), δ : 160.21, 137.23, 129.44, 129.23, 127.35 (q, J = 3.7 Hz), 126.82, 124.84 (q, J = 271.3 Hz), 122.34 (q, J = 32.1 Hz), 117.01, 76.83, 44.94. UPLC-MS: Rt: 1.7, MS (ESI) $^+$: 282.0[M+1] $^+$.

3-phenyl-3-(4-(trifluoromethyl)phenoxy)propan-1-amine (4b)

To a solution of triphenylphosphine (3 mmol) in anhydrous diethyl ether (6 mL) cooled at 0°C, diisopropyl azodicarboxylate (2 mmol) in anhydrous diethyl ether (1 mL) was added. After twenty minutes, 4-(trifluoromethyl)phenol (2.4 mmol) in anhydrous diethyl ether (4 mL) was added before adding the solution of *N*-Boc-3-(methylamino)-1-phenylpropan-1-ol (**13b**) (2.0 mmol) in anhydrous diethyl ether (5 mL). The reaction was stirred at room temperature for three hours before removing the solvent in vacuo. The crude residue was purified by flash column chromatography eluting with n-hexane-DCM 100:0 v/v increasing to 0:100 v/v and DCM/MeOH 100:0 v/v increasing to 98:2 v/v.

The residue was then solubilised in anhydrous DCM (4.2 mL) and the reaction mixture cooled at 0°C. The TFA (4.20 mmol) was added and the mixture was stirred at room temperature for two hours. The reaction mixture was diluted with DCM (8 mL)

and was washed with sat. NaHCO_3 solution (3x10 mL) and brine (3x10 mL). The organic layers were then dried over Na_2SO_4 and the solvent removed at reduced pressure. The residue was purified by flash column chromatography eluting with n-Hexane-DCM 100:0 v/v increasing to 50:50 v/v. Compound **4b** was obtained as a yellow oil. Yield: 27% over two steps. $^1\text{H NMR}$ (DMSO- d_6), δ : 7.55 (d, J = 8.7 Hz, 2H), 7.42 – 7.32 (m, 4H), 7.26 (t, J = 7.2 Hz, 1H), 7.06 (d, J = 8.6 Hz, 2H), 5.61 – 5.55 (m, 1H), 2.69 (t, J = 6.8 Hz, 2H), 2.13 – 2.03 (m, 1H), 1.93 – 1.83 (m, 1H). $^{19}\text{F NMR}$ (DMSO- d_6), δ : -59.88 (s, 3F). $^{13}\text{C NMR}$ (DMSO- d_6), δ : 160.99, 141.43, 129.10, 128.18, 127.27 (q, J = 3.7 Hz), 126.46, 124.92 (q, J = 271.1 Hz), 121.54 (q, J = 32.1 Hz), 116.61, 77.48, 41.01, 37.95.

N,N'-Bis(tert-butoxycarbonyl)-(1-(2-phenyl-2-(4-(trifluoromethyl)phenoxy)ethyl)) guanidine (14a)

A solution of *N,N'*-bis(tert-butoxycarbonyl)-*S*-methylisothiourea **8** (0.50 mmol) in anhydrous DCM (0.5 M) was added dropwise to a solution of 2-phenyl-2-(4-(trifluoromethyl)phenoxy)ethan-1-amine **4a** (0.48 mmol) and DIPEA (0.86 mmol) in anhydrous DCM (0.5 M), previously cooled at 0°C. The reaction mixture was stirred at room temperature overnight. A stream of nitrogen gas was bubbled through the reaction mixture for 1 hour to purge the gaseous by-product CH_3SH . The residue was purified by flash column chromatography eluting with hexane/ EtOAc 100:0 v/v increasing to 90:10 v/v. Compound **14a** was obtained as a white solid. Yield: 46%. $^1\text{H NMR}$ (DMSO- d_6), δ : 11.44 (s, 1H), 8.55 (t, J = 5.4 Hz, 1H), 7.59 (d, J = 8.7 Hz, 2H), 7.45 (d, J = 7.2 Hz, 2H), 7.39 (t, J = 7.5 Hz, 2H), 7.32 (t, J = 7.3 Hz, 1H), 7.15 (d, J = 8.7 Hz, 2H), 5.71 (dd, J = 7.0, 5.0 Hz, 1H), 3.84 – 3.73 (m, 2H), 1.45 (s, 9H), 1.41 (s, 9H). $^{19}\text{F NMR}$ (DMSO- d_6), δ : -60.00 (s, 3F). $^{13}\text{C NMR}$ (DMSO- d_6), δ : 163.36, 160.66, 155.98, 152.51, 138.33, 129.15, 128.82, 127.40 (q, J = 3.7 Hz), 126.89, 124.86 (q, J = 271.1 Hz), 122.05 (q, J = 31.7 Hz), 116.73, 83.67, 78.83, 77.85, 46.50, 28.42, 28.00. UPLC-MS: Rt: 2.466, MS (ESI) $^+$: 524.2[M+1] $^+$.

N,N'-Bis(tert-butoxycarbonyl)-(1-(3-phenyl-3-(4-(trifluoromethyl)phenoxy)propyl)) guanidine (14b)

A solution of *N,N'*-bis(tert-butoxycarbonyl)-*S*-methylisothiourea **8** (0.28 mmol) in DCM (0.5 M) was added dropwise to a solution of 3-phenyl-3-(4-(trifluoromethyl)phenoxy)propan-1-amine **4b** (0.31 mmol) and DIPEA (0.34 mmol) in DCM (0.5 M) at 0°C. The reaction mixture was stirred at room temperature overnight. A stream of nitrogen gas was bubbled through the reaction mixture for 1 hour to purge the gaseous by-product CH_3SH . The residue was purified by flash column chromatography, eluting with n-Hexane-EtOAc 100:0 v/v increasing to 80:20 v/v. Compound **14b** was obtained as a white solid. Yield: 81%. $^1\text{H NMR}$ (DMSO- d_6), δ : 11.46 (s, 1H), 8.49 (t, J = 5.4 Hz, 1H), 7.55 (d, J = 8.7 Hz, 2H), 7.41 (d, J = 7.2 Hz, 2H), 7.35 (t, J = 7.6 Hz, 2H), 7.27 (t, J = 7.3 Hz, 1H), 7.08 (d, J = 8.7 Hz, 2H), 5.58 (dd, J = 8.0, 4.3 Hz, 1H), 3.52 – 3.43 (m, 2H), 2.25 – 2.15 (m, 1H), 2.14 – 2.05 (m, 1H), 1.48 (s, 9H), 1.37 (s, 9H). $^{19}\text{F NMR}$ (DMSO- d_6), δ : -59.91 (s, 3F). $^{13}\text{C NMR}$ (DMSO- d_6), δ : 163.50, 160.73, 155.69, 152.44, 140.96, 129.11, 128.25,

127.16 (q, J = 3.6 Hz), 126.49, 121.60 (q, J = 31.9 Hz), 116.64, 83.32, 78.52, 78.33, 38.11, 37.34, 28.42, 28.09. **UPLC-MS:** Rt: 2.43, MS (ESI)⁺: 538.2[M+1]⁺, 560.2[M+Na]⁺.

1-(2-phenyl-2-(4-(trifluoromethyl)phenoxy)ethyl)guanidine (2a)

Tin(IV) chloride (0.29 mmol) was added to a solution of *N,N'*-bis(tert-butoxycarbonyl)-*N''*-3-phenyl-3-(4-(trifluoromethyl)phenoxy)propylguanidine (0.074 mmol) in anhydrous EtOAc (1 mL) at 0°C under a N₂ atmosphere. The reaction mixture was stirred at room temperature for three hours. The mixture was diluted in EtOAc and washed with sat. NaHCO₃ solution, dried over Na₂SO₄, filtrated and the solvent removed at reduced pressure. The resulting solid residue was poured into ice-cooled EtOAc. The resulting precipitate was filtered, washed with cold EtOAc and dried under vacuum to give compound **2a** as a white powder. Yield: 95%. ¹H NMR (DMSO-d₆), δ: 7.58 (d, J = 8.7 Hz, 2H), 7.47 (d, J = 7.3 Hz, 2H), 7.38 (t, J = 7.5 Hz, 2H), 7.31 (t, J = 7.3 Hz, 1H), 7.08 (d, J = 8.6 Hz, 2H), 5.60 – 5.52 (m, 1H), 3.62 – 3.47 (m, 2H). ¹⁹F NMR (DMSO-d₆), δ: -59.91 (s, 3F). ¹³C NMR (DMSO-d₆), δ: 160.76, 157.57, 138.57, 129.08, 128.70, 127.34 (q, J = 3.5 Hz), 127.01, 124.89 (q, J = 269.3 Hz), 121.88 (q, J = 32.8 Hz), 116.69, 78.76, 57.09. **UPLC-MS:** Rt: 1.627, MS (ESI)⁺: 324.2[M+1]⁺.

1-(3-phenyl-3-(4-(trifluoromethyl)phenoxy)propyl)guanidine (2b)

Tin(IV) chloride (0.86 mmol) was added to a solution of *N,N''*-Bis(tert-butoxycarbonyl)-(1-(3-phenyl-3-(4-(trifluoromethyl)phenoxy)propyl))guanidine (0.22 mmol) in anhydrous EtOAc (3 mL) at 0°C under a N₂ atmosphere. The reaction mixture was stirred at room temperature for three hours. The mixture was diluted in EtOAc and washed with sat. NaHCO₃ solution, dried over Na₂SO₄, filtrated and the solvent removed at reduced pressure. The resulting solid residue was poured into ice-cooled EtOAc. The resulting precipitate was filtered, washed with cold EtOAc and dried under vacuum to give compound **2b** as a white powder. Yield: 28%. ¹H NMR (DMSO-d₆), δ: 7.56 (d, J = 8.7 Hz, 2H), 7.42 (d, J = 7.5 Hz, 2H), 7.36 (t, J = 7.6 Hz, 2H), 7.28 (t, J = 7.3 Hz, 1H), 7.07 (d, J = 8.6 Hz, 2H), 5.53 (dd, J = 8.3, 4.4 Hz, 1H), 3.28 – 3.23 (m, 2H), 2.21 – 2.09 (m, 1H), 2.07 – 1.95 (m, 1H). ¹⁹F NMR (DMSO-d₆), δ: -59.90 (s, 3F). ¹³C NMR (DMSO-d₆), δ: 160.85, 160.02, 140.92, 129.18, 128.33, 127.30 (q, J = 3.7 Hz), 126.45, 124.91 (q, J = 271.1 Hz), 121.70 (q, J = 32.0 Hz), 116.66, 77.31, 38.24, 37.55. **UPLC-MS:** Rt: 1.673, MS (ESI)⁺: 338.2[M+1]⁺.

N-(3-phenyl-3-(4-(trifluoromethyl)phenoxy)propyl)acetamide (3)

Acetyl chloride was added drop-wise to a solution, previously cooled at 0°C, of 3-phenyl-3-(4-(trifluoromethyl)phenoxy)propan-1-amine (0.2 mmol), triethylamine (0.38 mmol) in anhydrous DCM (0.4 M) under nitrogen atmosphere. The reaction was allowed to warm-up to room temperature and was stirred for 2 hours. The mixture was diluted with DCM (8 ml) and extracted with 2N HCl solution (3x10ml). The organic layer was washed with brine (3x10 mL), dried over Na₂SO₄ and the solvent removed at reduced pressure. The residue was purified by flash column chromatography eluting

with DCM/MeOH 100:0 v/v increasing to DCM/MeOH 98:2 v/v. Compound **12** was obtained as a yellow oil. Yield: 98%. ¹H NMR (DMSO-d₆), δ: 7.93 (t, J = 5.0 Hz, 1H), 7.56 (d, J = 8.8 Hz, 2H), 7.41 – 7.32 (m, 5H), 7.27 (t, J = 7.2 Hz, 1H), 7.05 (d, J = 8.7 Hz, 2H), 5.47 (dd, J = 7.9, 5.0 Hz, 1H), 3.21 – 3.11 (m, 2H), 2.15 – 2.03 (m, 1H), 1.97 – 1.87 (m, 1H), 1.80 (s, 3H). ¹⁹C NMR (DMSO-d₆), δ: -59.89 (s, 3F). ¹³C NMR (DMSO-d₆), δ: 169.64, 160.91, 141.15, 129.13, 128.25, 127.29 (q, J = 3.7 Hz), 126.45, 124.92 (q, J = 271.1 Hz), 121.60 (q, J = 32.1 Hz), 116.64, 77.53, 38.20, 35.74, 23.09. **UPLC-MS:** Rt: 1.923, MS (ESI)⁺: 338.2[M+1]⁺, 176.1[C11H14NO]⁺.

General method for the preparation of (R)-2-(3-hydroxy-3-phenylpropyl)isoindoline-1,3-dione ((R)-16) and (S)-2-(3-hydroxy-3-phenylpropyl)isoindoline-1,3-dione ((S)-16)

To a stirring suspension of potassium phthalimide (1.2 mmol) in dry dimethylformamide (DMF) (5 mL) was added the corresponding 3-chloro-1-phenyl-1-propanol single enantiomer ((R)-15 and (S)-16) (1 mmol). The reaction mixture was heated to 90 °C and left stirring for 2 hours, until completion was observed by thin layer chromatography (TLC.) The reaction mixture was concentrated *in vacuo* and the resulting residue was purified by flash column chromatography using an isocratic elution *n*-hexane/diethyl ether 60:40 v/v.

(R)-2-(3-hydroxy-3-phenylpropyl)isoindoline-1,3-dione ((R)-16)

Yield: 84%, as white solid. ¹H NMR (CDCl₃), δ: 7.78 – 7.61 (m, 4H), 7.28 – 7.10 (m, 5H), 4.62-4.58 (m, 1H), 2.76 (bs, 1H, OH), 3.84-3.80 (m, 2H), 2.04-1.97 (m, 2H). This compound was previously reported and the spectral data agree with those specified in literature.⁴

(S)-2-(3-hydroxy-3-phenylpropyl)isoindoline-1,3-dione ((S)-16)

Yield: 65%, as white solid. ¹H NMR (CDCl₃), δ: 7.78 – 7.61 (m, 4H), 7.28 – 7.10 (m, 5H), 4.62-4.58 (m, 1H), 2.76 (bs, 1H, OH), 3.84-3.80 (m, 2H), 2.04-1.97 (m, 2H). This compound was previously reported and the spectral data agree with those specified in literature.⁵

General method for the preparation of (R)-3-amino-1-phenylpropan-1-ol ((R)-17) and (S)-3-amino-1-phenylpropan-1-ol ((S)-17)

To a stirred solution of the corresponding 2-(3-hydroxy-3-phenylpropyl)isoindoline-1,3-dione ((R)-16 and (S)-16) (1 mmol) in EtOH (15 mL) was added hydrazine monohydrate (3 mmol). The reaction mixture was stirred for 1 hour and then heated to reflux for 2 hours. Upon completion the reaction mixture was concentrated under reduced pressure, diluted with water (5 mL) and washed with EtOAc (3 × 15 mL). The organic layers were collected, dried over Na₂SO₄ and the solvent removed under reduced pressure. The residue was purified by flash column chromatography eluting

with DCM/MeOH 100:0 v/v increasing to DCM/MeOH 93:7 v/v then DCM/MeOH/Et₃N 80:14:6 v/v.

(R)-3-amino-1-phenylpropan-1-ol ((R)-17)

Yield: 77%, as an oil. ¹H NMR (DMSO-d₆), δ: 7.36–7.24 (m, 4H), 7.25–7.18 (m, 1H), 4.65 (dd, *J* = 7.1, 6.0 Hz, 1H), 3.88 (bs, 3H, OH, NH₂), 2.76-2.59 (m, 2H), 1.74-1.62 (m, 2H). This compound was previously reported and the spectral data agree with those specified in literature.⁴

(S)-3-amino-1-phenylpropan-1-ol ((S)-17)

Yield: 53%, as an oil. ¹H NMR (DMSO-d₆), δ: 7.36–7.24 (m, 4H), 7.25–7.18 (m, 1H), 4.65 (dd, *J* = 7.1, 6.0 Hz, 1H), 3.88 (bs, 3H, OH, NH₂), 2.76-2.59 (m, 2H), 1.74-1.62 (m, 2H). This compound was previously reported and the spectral data agree with those specified in literature.⁶

General method for the preparation of (R)-3-phenyl-3-(4-(trifluoromethyl)phenoxy)propan-1-amine ((R)-18) and (S)-3-phenyl-3-(4-(trifluoromethyl)phenoxy)propan-1-amine ((S)-18)

At 0 °C, to a stirred solution of the corresponding 3-amino-1-phenylpropan-1-ol ((R)-17 and (S)-17) (1 mmol), sodium hydride (60% in mineral oil, 1.5 mmol) in DMF (5.0 mL) was added. The reaction mixture was stirred at room temperature for 10 min and 4-fluorobenzotrifluoride (1 mmol) was added. The resulting mixture was heated for 1 hour at 90 °C, until completion was observed by TLC. The mixture was cooled to room temperature and concentrated under reduced pressure. The residue was diluted with water (10 mL), extract with EtOAc (3 × 25 mL) and the combined organic layers were dried over MgSO₄ and the solvent removed under reduced pressure. The crude product was purified by cation exchange column chromatography using a Hypersil SCX column eluting with MeOH and then methanolic ammonia (7M).

(R)-3-phenyl-3-(4-(trifluoromethyl)phenoxy)propan-1-amine ((R)-18)

Yield: 54%, as an oil. ¹H NMR (CDCl₃), δ: 7.35 (d, *J* = 8.6 Hz, 2H), 7.33–7.32 (m, 4H), 7.29-7.26 (m, 1H), 6.83 (d, *J* = 8.6 Hz, 2H), 5.31 (dd, *J* = 8.2, 4.7 Hz, 1H), 2.93-2.86 (m, 2H), 2.21-2.14 (m, 1H), 2.01-1.94 (m, 1H), 1.61 (bs, 1H, NH₂). This compound was previously reported and the spectral data agree with those specified in literature.⁷

(S)-3-phenyl-3-(4-(trifluoromethyl)phenoxy)propan-1-amine ((S)-18)

Yield: 50%, as an oil. ¹H NMR (CDCl₃), δ: 7.35 (d, *J* = 8.6 Hz, 2H), 7.33–7.32 (m, 4H), 7.29-7.26 (m, 1H), 6.83 (d, *J* = 8.6 Hz, 2H), 5.31 (dd, *J* = 8.2, 4.7 Hz, 1H), 2.93-2.86 (m, 2H), 2.21-2.14 (m, 1H), 2.01-1.94 (m, 1H), 1.61 (bs, 1H, NH₂). This compound was previously reported and the spectral data agree with those specified in literature.⁷

General procedure for the preparation of (R)- N',N''-Bis(tert-butoxycarbonyl)-(1-(3-phenyl-3-(4-(trifluoromethyl)phenoxy)propyl) guanidine ((R)-19) and (S)- N',N''-Bis(tert-butoxycarbonyl)-(1-(3-phenyl-3-(4-(trifluoromethyl)phenoxy)propyl) guanidine ((S)-19)

A solution of *N,N'*-bis(tert-butoxycarbonyl)-5-methylisothiourea **8** (2.4 mmol) in dry DCM (1.5 mL) was added drop-wise to a solution of the corresponding 3-phenyl-3-(4-(trifluoromethyl)phenoxy)propan-1-amine ((R)-18 and (S)-18) (1 mmol) and DIPEA (2 mmol) in dry DCM (1.5 mL) at 0°C. The reaction mixture was stirred at room temperature for 72h. A stream of nitrogen gas was bubbled through the reaction mixture for 1 hour to purge the gaseous by-product CH₃SH. The reaction solvent was removed under reduced pressure and the residue was purified by flash column chromatography eluting with *n*-hexane/diethyl ether 100:0 v/v increasing to 60:40 v/v.

(R)-N',N''-Bis(tert-butoxycarbonyl)-(1-(3-phenyl-3-(4-(trifluoromethyl)phenoxy)propyl) guanidine ((R)-19)

Yield: 34%, as white solid. ¹H NMR (CDCl₃), δ: 11.42 (s, 1H, NH), 8.61 (t, *J* = 4.7 Hz, 1H, NH), 7.34 (d, *J* = 8.6 Hz, 2H), 7.27-7.24 (m, 4H), 7.20-7.17 (m, 1H), 6.88 (d, *J* = 8.6 Hz, 2H), 5.24-5.21 (m, 1H), 3.63-3.48 (m, 2H), 2.21–2.07 (m, 2H), 1.44 (s, 9H), 1.42 (s, 9H). ¹⁹F NMR (CDCl₃), δ: -61.59 (s, 3F). ¹³C NMR (CDCl₃), δ: 163.5 (C=O), 160.1 (C=O), 156.1 (C=N), 153.1, 140.1 (C, C-aromatic), 128.9, 128.0 (CH, C-aromatic), 126.6 (q, *J* = 3.7 Hz, CH, C-aromatic), 125.7 (CH, C-aromatic), 123.1 (q, *J* = 32.7 Hz, C, C-aromatic), 115.8 (CH, C-aromatic), 83.1, 79.3 (C), 79.1 (CH), 38.1, 37.7 (CH₂), 28.3, 28.1 (CH₃). UPLC-MS: Rt: 2.43 min, MS (ESI)⁺: 538.2 [M+H]⁺, 560.2[M+Na]⁺.

(S)-N',N''-Bis(tert-butoxycarbonyl)-(1-(3-phenyl-3-(4-(trifluoromethyl)phenoxy)propyl) guanidine ((S)-19)

Yield: 45%, as white solid. ¹H NMR (CDCl₃), δ: 11.42 (s, 1H, NH), 8.61 (t, *J* = 4.7 Hz, 1H, NH), 7.34 (d, *J* = 8.6 Hz, 2H), 7.27-7.24 (m, 4H), 7.20-7.17 (m, 1H), 6.88 (d, *J* = 8.6 Hz, 2H), 5.24-5.21 (m, 1H), 3.63-3.48 (m, 2H), 2.21–2.07 (m, 2H), 1.44 (s, 9H), 1.42 (s, 9H). ¹⁹F NMR (CDCl₃), δ: -61.59 (s, 3F). ¹³C NMR (CDCl₃), δ: 163.5 (C=O), 160.1 (C=O), 156.1 (C=N), 153.1, 140.1 (C, C-aromatic), 128.9, 128.0 (CH, C-aromatic), 126.6 (q, *J* = 3.7 Hz, CH, C-aromatic), 125.7 (CH, C-aromatic), 123.1 (q, *J* = 32.7 Hz, C, C-aromatic), 115.8 (CH, C-aromatic), 83.1, 79.3 (C), 79.1 (CH), 38.1, 37.7 (CH₂), 28.3, 28.1 (CH₃). UPLC-MS: Rt: 2.43 min, MS (ESI)⁺: 538.2 [M+H]⁺, 560.2[M+Na]⁺.

General procedure for the preparation of (R)-1-(3-phenyl-3-(4-(trifluoromethyl)phenoxy)propyl)guanidine ((R)-2b) and (S)-1-(3-phenyl-3-(4-(trifluoromethyl)phenoxy)propyl)guanidine ((S)-2b)

Tin(IV) chloride (4 mmol) was added to a solution of the corresponding *N',N''*-bis(tert-butoxycarbonyl)-(1-(3-phenyl-3-(4-(trifluoromethyl)phenoxy)propyl)guanidine (1 mmol) in anhydrous EtOAc (5 mL) at 0°C under nitrogen atmosphere. The reaction mixture was stirred at room temperature for three hours. The reaction mixture was

diluted in EtOAc (5 mL) and washed with sat. NaHCO₃ solution (3x5 ML), dried over Na₂SO₄ and the solvent removed under reduced pressure. The resulting crude solid purified by flash column chromatography eluting with DCM/MeOH 100:0 v/v increasing to DCM/MeOH 85:15 v/v then DCM/MeOH/Et₃N 80:14:6 v/v.

(R)-1-(3-phenyl-3-(4-(trifluoromethyl)phenoxy)propyl)guanidine ((R)-2b)

Yield: 80%, as white solid. ¹H NMR (DMSO-d₆), δ: 7.56 (d, *J* = 8.6 Hz, 2H), 7.45-7.41 (m, 2H), 7.34-7.31 (m, 2H), 7.27-7.23 (m, 1H), 7.04 (d, *J* = 8.6 Hz, 2H), 5.60 (m, 1H), 3.25 – 3.19 (m, 1H), 3.16 – 2.12 (m, 1H), 2.16-2.08 (m, 1H), 2.02-1.95 (m, 1H). ¹⁹F NMR (DMSO-d₆), δ: -59.92 (s, 3F). ¹³C NMR (DMSO-d₆), δ: 160.8 (C=N), 157.6, 141.0 (C, C-aromatic), 129.1, 128.2 (CH, C-aromatic), 127.2 (d, *J* = 3.7 Hz, CH, C-aromatic), 126.4 (CH, C-aromatic), 125.9 (q, *J* = 271.1 Hz, CF₃), 121.7 (q, *J* = 32.0 Hz, C, C-aromatic), 116.6 (CH, C-aromatic), 77.2 (CH), 38.2, 37.5 (CH₂). UPLC-MS: Rt: 1.67 min, MS (ESI)⁺: 338.2 [M+H]⁺.

(S)-1-(3-phenyl-3-(4-(trifluoromethyl)phenoxy)propyl)guanidine ((S)-2b)

Yield: 75%, as white solid. ¹H NMR (DMSO-d₆), δ: 7.56 (d, *J* = 8.6 Hz, 2H), 7.45-7.41 (m, 2H), 7.34-7.31 (m, 2H), 7.27-7.23 (m, 1H), 7.04 (d, *J* = 8.6 Hz, 2H), 5.60 (m, 1H), 3.25 – 3.19 (m, 1H), 3.16 – 2.12 (m, 1H), 2.16-2.08 (m, 1H), 2.02-1.95 (m, 1H). ¹⁹F NMR (DMSO-d₆), δ: -59.92 (s, 3F). ¹³C NMR (DMSO-d₆), δ: 160.8 (C=N), 157.6, 141.0 (C, C-aromatic), 129.1, 128.2 (CH, C-aromatic), 127.2 (d, *J* = 3.7 Hz, CH, C-aromatic), 126.4 (CH, C-aromatic), 125.9 (q, *J* = 271.1 Hz, CF₃), 121.7 (q, *J* = 32.0 Hz, C, C-aromatic), 116.6 (CH, C-aromatic), 77.2 (CH), 38.2, 37.5 (CH₂). UPLC-MS: Rt: 1.67 min, MS (ESI)⁺: 338.2 [M+H]⁺.

Materials and Methods

Cells and Reagents

HAP1 cells were obtained from Horizon Discovery Group (Cambridge, UK) and cultured in Iscove's modified Dulbecco's medium (IMDM) (Lonza) containing 10% (v/v) fetal calf serum (FCS.) cells were cultured in Dulbecco's minimum essential medium (DMEM) (Lonza) supplemented with 10% (v/v) FCS. HEK293T (ATCC CRL-3216) and Hela R19 (were obtained from G. Belov) were grown at 37°C in 5% CO₂. HeLaR19 cells, University of Maryland, College Park, MD, USA. Guanidine hydrochloride (GuaHCl) was purchased from Sigma-Aldrich. Racemic mixture of fluoxetine was purchased from Sigma-Aldrich. The (S)- fluoxetine was purchased from Sigma-Aldrich. GuaHCl was dissolved in water at 2 M stock concentration and all other compounds were dissolved in DMSO at 10 mM stock concentration.

Viruses

EV-A71 (strain BrCr), PV1 (strain Sabin) and EV-D68 (strain Fermon) were obtained from the National Institute for Public Health and Environment (RIVM) in the Netherlands.

HRV-2 and HRV-14 were obtained from Joachim Seipelt from the Medical University of Vienna in Austria. CVB3 wt (strain Nancy) and CVB3 2C mutant viruses (2C[A224V/I227V/A229V], 2C[I227V], 2C[C179F], 2C[F190L], described in¹), were obtained by transfecting cells with *in vitro* transcribed RNA transcripts derived from wt and mutant full-length p53CB3/T7 infectious clones². To ensure that the introduced mutations are retained in the generated virus, viral RNA was isolated with NucleoSpin[®] RNA Virus kit (Macherey-Nagel) according to the manufacturer's protocol and the presence of the desired mutations was confirmed by Sanger sequencing. Virus titers were determined by endpoint dilution titration and calculated according to the method of Reed and Muench³ and expressed as 50% cell culture infective dose (CCID₅₀).

Single-cycle virus infection

Virus infections were performed by incubating subconfluent HeLa R19 cells with virus at a multiplicity of infection (MOI) of 1 at 37°C for 30 min. Next, the medium was removed and fresh (compound-containing) medium was added to the cells. At 8 hours (EV-A71, CVB3, Poliovirus) or 10 hours (CV-A24, EV-D68, HRV-2 and HRV-14) after infection, the medium was discarded and cells were lysed. For measurements of infectious particles, virus was released from the cells by three freeze-thawing cycles. Virus titers were determined as described above. Cell viability was determined in parallel using the Aqueous One Solution Cell Proliferation Assay (Promega) according to the manufacturer's protocol. Optical density at 490 nm was determined using a microplate reader.

Multicycle virus infection

Subconfluent layers of HeLa R19 cells were seeded in 96-wells and treated with serial dilutions of the corresponding compounds. Cells were infected with viruses at the lowest possible MOI (MOI 0.001 for EV-A71, CVB3, poliovirus, CV-A24, EV-D68 and MOI 0.01 for EV-D68, HRV-2) resulting in full CPE within 3 days. Subsequently the cells were incubated at 37°C for 3 days until full CPE was observed in the virus-infected untreated cell controls. Cell viability was determined as described above. Raw OD values were converted to percentage of untreated and uninfected cell control after subtraction of the background.

Thermal shift assays

The DNA fragment coding for CVB3 2C (amino acids 116 to 329) was cloned with an N-terminal and cleavable -hexahistidine-MBP tag. The recombinant WT protein was produced in Escherichia coli RosettaTM 2 (DE3) (Sigma-Aldrich). Protein expression was induced with the addition of 0.5 mM IPTG when cultures reach OD_{600nm} of 0.5. Protein was expressed for 16 hrs at 18 °C with shaking at 200 rpm. Protein purification was performed as described previously, with the exception that 3C protease (Sigma-Aldrich) was used instead of TEV.(Lantez et al., 2011) The final size-exclusion chromatography step was performed at 4°C with buffer containing 25mM Tris (pH 8), 300mM NaCl

and 1mM MgCl₂, using a superose® 6 increase 10/300 column GL (GE Healthcare Life Science). The binding of (S)- and (R)-fluoxetine and both 2b-enantiomers to WT CVB3 2C was monitored by the fluorescence-based thermal shift assay (TSA) using a Roche LightCycler®480. TSA plates were prepared by dispensing into each well the 2C protein (final concentration of 10 μM in 50 mM Tris, 300 mM NaCl and 1mM MgCl₂, pH 8) and a SYPRO orange solution in concentrations recommended by the manufacturer in a final volume of 25 μL. The experiments were performed under a temperature gradient ranging from 20 to 90 °C (incremental steps of 0.2 °C/12 s). The denaturation of the proteins was monitored by following the increase of the fluorescence emitted by SYPRO orange that binds exposed hydrophobic regions of the denatured protein. The melting temperature (T_m) was calculated as the mid-log of the transition phase from the native to the denatured protein. The reference unfolding temperature of proteins in 5% DMSO (T₀) was subtracted from the values in the presence of compounds (T_m) to obtain thermal shifts, ΔT_m = (T_m – T₀).

Supporting information references

1. Bauer L, Manganaro R, Zonsics B, Strating JRP, El Kazzi P, Lorenzo Lopez M, et al. Fluoxetine Inhibits Enterovirus Replication by Targeting the Viral 2C Protein in a Stereospecific Manner. *ACS Infect Dis*. American Chemical Society; 2019 Sep;5(9):1609–23.
2. Wessels E, Notebaart RA, Duijsings D, Lanke K, Vergeer B, Melchers WJG, et al. Structure-function analysis of the coxsackievirus protein 3A: Identification of residues important for dimerization, viral RNA replication, and transport inhibition. *J Biol Chem*. 2006;281(38):28232–43.
3. Reed LJ, Muench H. A simple method of estimating fifty percent endpoints. *Am J Hyg*. 1938;27(3):493–7.
4. Andrés-Costa, M.J., Proctor, K., Sabatini, M.T. et al. Enantioselective transformation of fluoxetine in water and its ecotoxicological relevance. *Sci Rep* 7, 15777 (2017). <https://doi.org/10.1038/s41598-017-15585-1>.
5. Fuller, R. W., Robertson, D. W. & Wong, D. T. Preparation and formulation of fluoxetine analog as serotonin antagonist, Eli Lilly and Co., USA, May23, EP 369685 (1990).
6. Ou Z., Xu J., Du L., Tang L., Niu Y., Cui J. Preparation of interface-assembled carbonyl reductase and its application in the synthesis of s-licarbazepine in toluene/Tris-HCL buffer biphasic system *Journal of Microbiology and Biotechnology*, Volume 28, 2018
7. John R. Cashmana, Troy Voelker, Robert Johnson, Aaron Janowsky. Stereoselective inhibition of serotonin re-uptake and phosphodiesterase by dual inhibitors as potential agents for depression. *Bioorg. Med. Chem.* 17 (2009) 337–343.
8. Lantez, V., Dalle, K., Charrel, R., Baronti, C., Canard, B., and Coutard, B. (2011). Comparative production analysis of three phlebovirus nucleoproteins under denaturing or non-denaturing conditions for crystallographic studies. *PLoS Negl Trop Dis* 5, e936.

Chapter

6

Rational design of highly potent broad-spectrum enterovirus inhibitors targeting the nonstructural protein 2C

Lisa Bauer¹, Roberto Manganaro², Birgit Zonsics², Daniel L. Hurdiss¹, Marleen Zwaagstra¹, Tim Donselaar¹, Naemi G. E. Welter³, Regina G. D. M. van Kleef³, Moira Lorenzo Lopez², Federica Bevilacqua², Thamidur Raman², Salvatore Ferla², Marcella Bassetto⁴, Johan Neyts⁵, Jeroen R. P. M. Strating¹✉, Remco H. S. Westerink³, Andrea Brancale², Frank J. M. van Kuppeveld^{1*}

¹ Virology Section, Infectious Disease and Immunology Division, Department of Biomolecular Health Sciences, Faculty of Veterinary Medicine, Utrecht University, Utrecht, The Netherlands,

² Medicinal Chemistry, School of Pharmacy & Pharmaceutical Sciences, Cardiff University, Cardiff, United Kingdom,

³ Neurotoxicology Research Group, Toxicology Division, Institute for Risk Assessment Sciences (IRAS), Faculty of Veterinary Medicine, Utrecht University, Utrecht, The Netherlands,

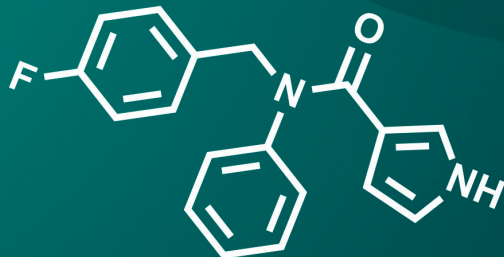
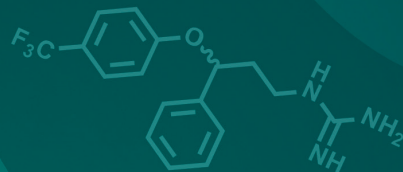
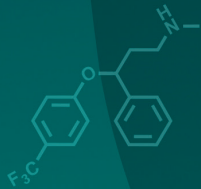
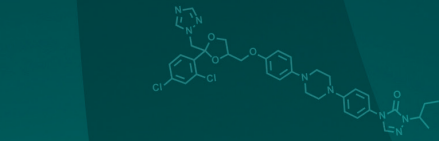
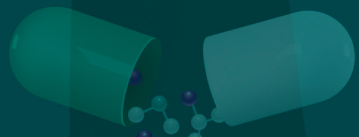
⁴ Department of Chemistry, Swansea University, Swansea, United Kingdom,

⁵ Department of Microbiology, Immunology and Transplantation, Rega Institute for Medical Research, KU Leuven, Leuven, Belgium

✉Current address: Viroclinics, Rotterdam, The Netherlands

*f.j.m.vankuppeveld@uu.nl

PLOS Biology, 2020, 18 (11), e3000904



Abstract

There is a great need for antiviral drugs to treat enterovirus (EV) and rhinovirus (RV) infections, which can be severe and occasionally life-threatening. The conserved nonstructural protein 2C, which is an AAA+ ATPase, is a promising target for drug development. Here, we present a structure-activity relationship study of a previously identified compound that targets the 2C protein of EV-A71 and several EV-B species members, but not poliovirus (PV) (EV-C species). This compound is structurally related to the Food and Drug Administration (FDA)-approved drug fluoxetine—which also targets 2C—but has favorable chemical properties. We identified several compounds with increased antiviral potency and broadened activity. Four compounds showed broad-spectrum EV and RV activity and inhibited contemporary strains of emerging EVs of public health concern, including EV-A71, coxsackievirus (CV)-A24v, and EV-D68. Importantly, unlike (S)-fluoxetine, these compounds are no longer neuroactive. By raising resistant EV-A71, CV-B3, and EV-D68 variants against one of these inhibitors, we identified novel 2C resistance mutations. Reverse engineering of these mutations revealed a conserved mechanism of resistance development. Resistant viruses first acquired a mutation in, or adjacent to, the $\alpha 2$ helix of 2C. This mutation disrupted compound binding and provided drug resistance, but this was at the cost of viral fitness. Additional mutations at distantly localized 2C residues were then acquired to increase resistance and/or to compensate for the loss of fitness. Using computational methods to identify solvent accessible tunnels near the $\alpha 2$ helix in the EV-A71 and PV 2C crystal structures, a conserved binding pocket of the inhibitors is proposed.

Introduction

The genus *Enterovirus* of the family *Picornaviridae* is a large group of nonenveloped, positive-sense, single-stranded (+) RNA viruses. Four enterovirus species (EV-A to -D) and three rhinovirus species (RV-A to -C) constitute the set of human pathogens that have large medical and socioeconomical impact, such as poliovirus (PV), coxsackievirus (CV) A and B, echoviruses, numbered EVs (e.g., EV-A71, EV-D68) and RVs (e.g., human rhinovirus [HRV]-A2, HRB-14)¹. Though often unnoticed and self-limiting, EV infections can cause serious illnesses and be associated with major complications, which can be life-threatening, especially in infants, young children, and immunocompromised individuals. Infections with EVs can cause a broad range of different clinical manifestations, including hand-foot-and-mouth disease, conjunctivitis, aseptic meningitis, myocarditis, severe neonatal sepsis-like diseases, respiratory diseases, acute flaccid paralysis (AFP), and acute flaccid myelitis (AFM). In recent years, several EVs have been considered as pathogens of increasing health concern. These include EV-A71 and EV-D68—of which large outbreaks in South East Asia and the United States, respectively, are associated with severe neurological complications—as well as CV-A24v (an EV-C species member), which causes large pandemics of a highly contagious conjunctivitis²⁻⁵. RVs are the causative agent of the common cold and can trigger exacerbations of asthma and chronic obstructive pulmonary disease (COPD)¹.

Several strategies may be used to control EV infections. One strategy involves the development of vaccines. Inactivated and life attenuated vaccines have been developed against PV, and recently, inactivated vaccines against EV-A71 were approved in China⁶. However, given the large number of serotypes (>100 nonpolio EVs and >150 HRVs), development of a pan-EV and -RV vaccine seems unfeasible. Another strategy is the development of potent antivirals. Several EV inhibitors have been identified. These include both direct-acting antivirals, most of which bind to the viral capsid or the viral protease 3C, as well as inhibitors that target host factors essential for virus replication (reviewed by Bauer and colleagues⁷). These inhibitors were tested in clinical trials, but their development was halted due to limited efficacy, poor bioavailability, or toxicity issues. At present, no antiviral against EVs is licensed for therapeutic use.

An attractive target for antivirals is the highly conserved and multifunctional nonstructural protein 2C. 2C is an ATPase associated with diverse cellular activities (AAA+ ATPase) classified within the superfamily 3 (SF3) helicases. These enzymes couple the hydrolysis of ATP to movement of protein domains which, in turn, drive the unwinding of a nucleic acid substrate. It has been shown biochemically that 2C functions as RNA helicase and ATP-independent RNA chaperone⁸⁻¹¹. 2C fulfills pleiotropic functions during the virus life cycle, including replication organelle formation, genome replication, and encapsidation¹²⁻¹⁹. Screening of drug libraries identified many structurally disparate 2C inhibitors such as the Food and Drug Administration (FDA)-approved drugs fluoxetine, dibucaine, pirlindole, and zuclopenthixol²⁰⁻²³. One of the most promising candidates is fluoxetine, a selective serotonin reuptake inhibitor (SSRI) that is approved for the

treatment of depression and anxiety disorders. Fluoxetine inhibits replication of viruses belonging to the EV-B and EV-D species and some RV, but not of viruses belonging to EV-A and EV-C species^{21,23,24}. Fluoxetine has been used off-label to successfully treat an immunocompromised child with chronic EV encephalitis²⁵. Recently, the safety and efficacy of fluoxetine for treatment of EV-D68 associated AFM was investigated in a retrospective study. The treatment with fluoxetine revealed no clinical benefit but rather suggested a worsening of the patient conditions in the fluoxetine-treated cohort²⁶. The reason for this is unknown but might be related to the drug's SSRI activity. We previously established that fluoxetine inhibits viral replication stereospecifically by directly binding 2C²⁴. Unfortunately, the chemical moiety important for the SSRI activity is essential for the antiviral activity, and thus far these two activities could not be uncoupled²⁷. This raises concerns about the therapeutic application of fluoxetine and shows that other, potent, biosafe, and broad-spectrum antiviral inhibitors are needed.

In a high-throughput screen of small molecules, the compound N-(4-fluorobenzyl)-N-(4-methoxyphenyl)furan-2-carboxamide (which will further be referred to as compound 1) was identified as a potential CV-B3 2C inhibitor²⁰. Previously, it was shown that compound 1 inhibited several viruses belonging to the EV-B species and a clinical isolate of EV-A71, but it failed to inhibit PV-1 and PV-3. Notwithstanding this, the chemical similarity to fluoxetine, as well as the absence of a chiral center and the CF₃ at the phenoxy moiety, make it an interesting candidate for the development of more potent and possibly also broad-spectrum EV inhibitors (Fig 1A). In the present study, we report the rational development of new 2C-targeting antiviral inhibitors based on the backbone of compound 1. We identified several broad-spectrum inhibitors that inhibit representative members of all human EV and RV species tested as well as contemporary isolates of EV-A71, CV-A24v, and EV-D68. Notably, unlike (S)-fluoxetine, these broad-spectrum EV inhibitors were shown to be not neuroactive. By raising EV-A71, CV-B3, and EV-D68 variants resistant against one of the broad-spectrum EV inhibitors, we identified some novel resistance mutations in 2C. Employing reverse genetics, we provide evidence for a conserved mechanism of resistance development, involving mutations in the α 2 helix of 2C. As these mutations reduced viral replication, additional mutations at distantly localized residues in 2C were acquired to compensate for the loss of fitness. A structural model for a conserved binding pocket in 2C is proposed.

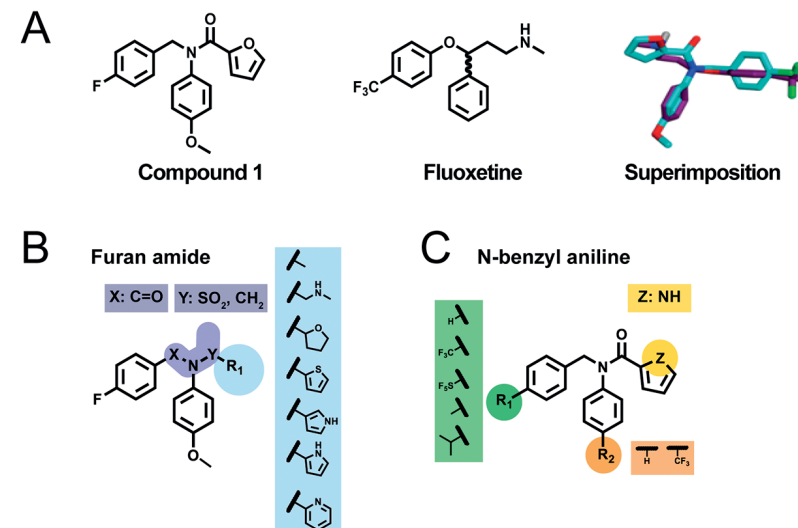


Figure 1. Structural comparison of fluoxetine and compound 1. (A) The compounds fluoxetine and compound 1, and a superimposition of them, are depicted. (B) The furan moiety (R1) is highlighted in blue and the amide moiety (X-N-Y) in purple. The substitutions that were explored are shown in the purple and blue boxes. (C) The R1 (green) and R2 (orange) moieties of the N-benzylaniline were substituted to the modifications shown in green and orange boxes. Additionally, the heteroatom (yellow) in the furan moiety was changed.

Results

Comparison of antiviral activity of (S)-fluoxetine and compound 1

We first compared the antiviral spectrum of (S)-fluoxetine and compound 1. EVs cause an observable cytopathic effect (CPE), apparent as rounding, detachment, and eventually dying of cells. Both compounds were tested side by side in a CPE-based multicycle viral replication assay to elucidate whether the compounds inhibited replication of several EV serotypes. Subconfluent HeLa R19 cells were treated with 2-fold compound dilutions in the range of 30 μ M-0.23 μ M. The cells were infected with virus at low multiplicity of infection (MOI) to reach full CPE within 3 days. As previously reported, (S)-fluoxetine inhibited EV-B (CV-B3), EV-D (EV-D68), RV-A (RV-A2), and RV-B (RV-B14), but not EV-A (EV-A71) and EV-C (PV-1 and CVA24) species members^{7,21,22}. As reported, compound 1 inhibited CV-B3 but not EV-A71 or PV-1²⁰. Additionally, we show antiviral activity of compound 1 against EV-D68 and HRV-B14 but not CV-A24 and HRV-A2. (S)-fluoxetine showed a 50% cytotoxic concentration (CC_{50}) of 21.63 ± 1.40 , whereas compound 1 did not show any adverse cytotoxic effect in the concentration range tested (Table1).

Table 1. Comparison of antiviral activity of (S)-fluoxetine and compound 1.

Virus	Species	Strain	SFX	Compound 1
EV-A71	EV-A	BrCr	>30	>30
CV-B3	EV-B	Nancy	0.50 ± 0.09	1.71 ± 0.07
PV-1	EV-C	Sabin1	>30	>30
CV-A24	EV-C	Joseph	>30	>30
EV-D68	EV-D	Fermon	0.62 ± 0.22	0.32 ± 0.06
HRV-A2	RV-A		8.92 ± 0.23	>30
HRV-B14	RV-B		6.21 ± 0.43	10.84 ± 1.27
CC₅₀			21.56 ± 0.21	>30

Multicycle viral replication assays were performed in HeLa R19 cells, and shown are EC₅₀ and CC₅₀ values in micromolar. Data represents mean ± SD calculated from at least three different experiments performed in biological triplicates.

Abbreviations: CC₅₀, 50% cytotoxic concentration; CV, coxsackievirus; EC₅₀; EV, enterovirus; HRV, human rhinovirus; PV, poliovirus; RV, rhinovirus; SFX, (S)-fluoxetine

Synthesis of compound 1 analogues

Different structural modifications of compound 1 were planned in order to investigate whether its antiviral activity could be enhanced and its antiviral spectrum broadened. An initial effort was focused on replacing the original furan with different heteroaromatic rings and diverse heterocyclic/aliphatic groups (Fig 1B). The role of the amide bond was also explored by replacing it with either a sulfonamide bond or a methylene bridge. Different substituents on the 4-position on both rings of the *N*-benzylaniline moiety were also investigated (Fig 1C). Preparation of compound 1 analogues, in which the furan ring and the amide bond were modified, was performed through an efficient two-step synthetic pathway in which compound 4, prepared by reductive amination between 4-fluorobenzaldehyde 2 and *p*-anisidine 3, was used as common synthetic intermediate. The synthesis routes are displayed in S1 Fig and S2 Fig, and the synthesis route is described in S1 Text. Derivatives 5a–d were synthesized reacting 4 with different acyl or sulfonyl chloride in dichloromethane using trimethylamine as base. Compound 1 and derivatives 5e and 5f—presenting a pyridine and a tetrahydrofuran ring in place of furan, respectively—were obtained through an amide coupling reaction between 4 and the corresponding carboxylic acid in dimethylformamide, using diisopropylethylamine (DIPEA) as base and 2-(1*H*-benzotriazole-1-yl)-1,1,3,3-tetramethyluronium tetrafluoroborate (TBTU) as a coupling agent. Reductive amination between 4 and furan-2-carbaldehyde yield compound 5g, whereas preparation of compound 6 was achieved by 2 steps: amide bond formation reacting 4 and 2-bromoacetyl chloride, followed by nucleophilic displacement of the bromine atom by methyl amine. Different attempts were made for the preparation of compounds 12a–b, in which the *N*-(4-fluoro) benzylaniline portion is bound to position 3

of a pyrrole ring. A coupling reaction either using TBTU or 1,1'-Carbonyldiimidazole (CDI) as coupling agent did not give the desired product, with formation of several undesired species. After failing in converting the pyrrole-3-carboxylic acid to the corresponding acyl chloride using thionyl chloride in dichloromethane, a different approach was applied as reported in S1 Fig synthesis route B. The pyrrole-3-carboxylic acid nitrogen was selectively *tert*-butoxycarbonyl (Boc)-protected through a 3-step synthesis, and the resulting compounds 10a–b were then converted into 11a–b via TBTU-assisted coupling reaction. Removal of the Boc protecting group using trifluoroacetic acid (TFA) in dichloromethane gave compounds 12a–b in a very high yield. Reductive amination between 4-methoxyaniline 3 and furan-2-carbaldehyde 13, followed by the reaction with 4-fluorobenzoyl chloride, gave the final product 15 in a quantitative yield. Analogues 19a–i, bearing different substituents in 4-position of the *N*-benzylaniline moiety, were prepared following the same synthetic pathway adopted for derivatives 5a–d. Reductive amination between differently substituted benzaldehydes and anilines yielded the intermediates 18a–i in a high yield, which were then converted into the corresponding final compounds 19a–i by reaction with furan-2-carbonyl chloride in dichloromethane and trimethylamine as base. 1*H*-pyrrole-2-carbonyl chloride 21, required for the preparation of compound 22, was prepared in situ by refluxing 1*H*-pyrrole-2-carboxylic acid 20 with thionyl chloride, as reported in S2 Fig.

Antiviral activity of the newly synthesized compounds against CV-B3

We first evaluated the antiviral activity of the synthesized compounds in a multicycle viral replication assay using CV-B3. Substituting the furan amide with a methyl group (5a), a tetrahydrofuran group (5f), or a methyl amine group⁶ resulted in a loss of antiviral activity suggesting that the aromatic furan ring is essential for the antiviral activity (S1 Table). Substituting the amide in position Y into a SO₂ (5b) or CH₂ (5g) also resulted in loss of antiviral activity, suggesting that the amide in position Y is also essential. Changing the methyl group in position X into a carbonyl group and substituting Y into a CH₂¹⁵ also abolished antiviral activity. To explore the possibility of changing the furan ring, we substituted the R1 position with several aromatic heterocyclic moieties like thiophene (5d), pyridine (5e), or pyrrole (5c, 12a) (Fig 1B). The thiophene-2-carboxamide (5d: 50% effective concentration [EC₅₀] = 0.51 ± 0.05 μM, CC₅₀ ≥ 30 μM) and especially the pyrrole-3-carboxamide substitution (12: EC₅₀ = 0.08 ± 0.08 μM, CC₅₀ > 30 μM) increased the antiviral activity against CV-B3 (approximately 4- and 25-fold, respectively) (S1 Table). Taken together, these data indicated that the amide bond and the furan ring are essential for the antiviral activity, but the modification on the furan moiety can vary.

Next, we explored the substituents R1 and R2 of the *N*-benzylaniline moiety (Fig 1C). Removal of the R1 substituent (19c), the R2 substituent (19b), or both (19a) had only small effects (i.e., less than 3-fold increase or decrease) on the antiviral activity (S2 Table). Similarly, substitution of R1 to a tri-fluoro moiety (19d, 19e), a methyl group (19g), or a bulky and highly lipophilic electron withdrawing pentafluorosulfanyl (19f),

with or without removing the R2 substituent, only marginally affected antiviral activity. Substitution of R2 to a tri-fluoro moiety (19i) also had little effect. Together, this suggests that the substituents in R1 and R2 are not essential for the antiviral activity and can be modified. Only introduction of a branched alkyl group in R1 and removing the R2 substituent (19h) decreased the antiviral activity to a larger extent. Substitution of the R1 group with a CF₃ group, removal of the R2 substituent, and substituting the heteroatom in the furan ring to an N²² also had little, if any, effect on antiviral activity. Taken together, exploring R1 and R2 of the N-benzylaniline moiety results in active compounds in which the antiviral activity is not drastically increased or decreased compared to compound 1.

Antiviral effect and cytotoxicity of active analogues in different cell lines

Next, we tested the active compounds for their antiviral effect and cytotoxicity in different cell lines. A CPE-based multicycle viral replication assay using CV-B3 was performed in HeLa R19, HAP1, and Buffalo Green Monkey (BGM) cells. The highest concentration of compounds used was 100 μ M. The furan analogues 5c, 12a, and 5e showed no cytotoxicity. Of these compounds, 12a had the most potent antiviral activity, independent of the cell line (S3 Table). The N-benzylaniline analogues 19a, 19b, 19c, 19g, and 22 also did not show any cytotoxicity or very minimal cytotoxicity (19d). The other compounds (5d, 19e, 19f, 19h, 19i) showed cytotoxicity in a similar range as the parental compound 1. Remarkably, 19h showed antiviral activity in the human cell lines HeLa R19 and HAP1 but not in monkey BGM cells. The reason for this is unknown. One explanation is that the drug must be metabolized and that the corresponding enzyme is absent in BGM. Alternatively, the compound may be inactivated or degraded in BGM cells. Overall, compounds 12a, 19b, and 19d showed less cytotoxicity and the strongest increase in selectivity index, which determines the window between antiviral activity and host cell toxicity, in all cell lines tested relative to compound 1.

Antiviral effect of active compounds against other EVs

To evaluate their spectrum of antiviral activity, we screened the active compounds against a panel of different EVs representative of each of the 4 human EV and of 2 RV species. Many compounds showed a similar antiviral spectrum as the parental compound 1. For some compounds, an extended spectrum of activity was observed. Compounds 19a and 19g showed anti-EV activity but not anti-RV activity. Importantly, compounds 12a, 19b, and 19d inhibited all representative EVs and RVs (Table 2). We also tested the spectrum of activity of 12a and 19d in a single-cycle viral replication assay. Consistent with the results in the multicycle viral replication assay, compounds 12a and 19d inhibited all representative viruses in a single-cycle viral replication assay (Fig 2A), and none of them showed any cytotoxic effect (Fig 2B). Notably, 12a showed higher potency against all viruses tested except against EV-A71.

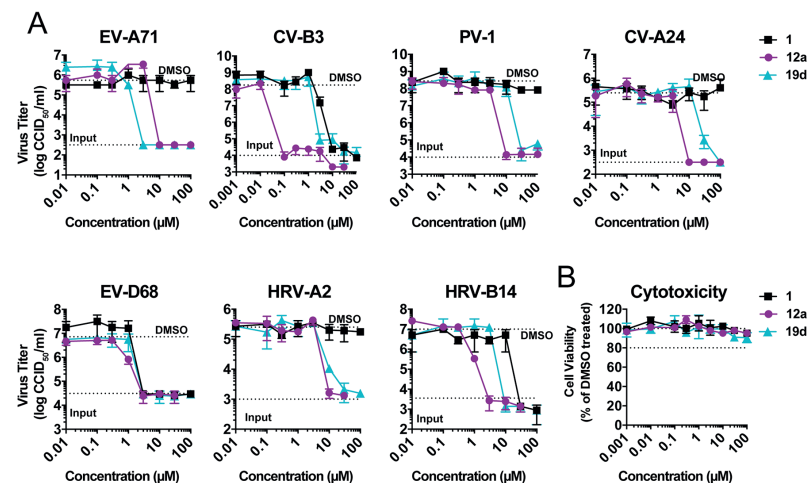


Figure 2. Antiviral efficacy of compound 1, 12a, and 19d against a panel of EVs. (A) In a single-cycle viral replication assay, HeLa R19 cells were infected with EV-A71 (strain BrCr), CV-B3 (strain Nancy), PV-1 (strain Sabin), CV-A24 (strain Joseph), EV-D68 (strain Fermon), HRV-A2, and HRV-B14 at MOI 1. At 30 minutes after infection, the cells were treated with serial dilutions of the parental compound 1 and the analogues 12a and 19d. Eight hours (EV-A71, CV-B3, PV-1, CV-A24) or ten hours (EV-D68, HRV-2, HRV-14) post infection, cells were freeze-thawed three times, and virus titers of lysates were determined by endpoint dilution. (B) In parallel, uninfected cells were treated with compounds only, and cell viability was determined using an MTS assay. Data represent mean \pm SD from one representative experiment. Every experiment was performed in biological triplicates, and two independent experiments were performed. CCID₅₀, cell culture infectious dose; CV, coxsackievirus; EV-A71, enterovirus A71; EV-D68, enterovirus D68; HRV, human rhinovirus; MOI, multiplicity of infection; 3-(4,5-dimethylthiazol-2-yl)-5-(3-carboxymethoxyphenyl)-2-(4-sulfophenyl)-2H-tetrazolium, MTS; PV-1, poliovirus 1

The broad-spectrum EV and RV inhibitors 12a, 19b, and 19d were further profiled for their broad-range antiviral activity against several contemporary isolates of EV-A71 (isolates derived from an outbreak of hand-foot-and-mouth disease in Taiwan), CV-A24v (isolates derived from an outbreak in Malaysia 2002–2003), and EV-D68 (isolated from patients with respiratory infection in the Netherlands 2009–1010)^{4,28,29}. As expected, the parental compound 1 only inhibited the contemporary strains of EV-D68 (Table 3). (S)-fluoxetine also inhibited contemporary strains of EV-D68 and some, but not all, contemporary EV-A71 strains. Importantly, 12a, 19b, and 19d inhibited all clinical isolates of EV-A71, CV-A24v, and EV-D68 tested (Table 3). Taken together, we identified three compounds—12a, 19b, and 19d—that inhibited all EVs, all RVs, and all clinical isolates of the serotypes EV-A71, CV-A24, and EV-D68.

Table 2. Antiviral activity of active compounds against representative EV species.

Compound	EV-A71	PV-1	CV-A24	EV-D68	HRV-A2	HRV-B14
1	>30	>30	>30	1.13 ± 0.82	>30	12.36 ± 1.51
5c	>30	>30	>30	3.47 ± 0.08	>30	>30
5d	>30	>30	>30	2.82 ± 0.40	>30	9.29 ± 0.36
5e	>30	>30	>30	10.45 ± 1.37	>30	>30
12a	4.03 ± 0.73	3.71 ± 0.18	3.51 ± 0.22	1.08 ± 0.20	8.51 ± 0.22	1.45 ± 0.21
19a	3.50 ± 0.31	32.58 ± 1.08	21.48 ± 0.03	1.34 ± 0.45	>30	>30
19b	0.89 ± 0.09	9.08 ± 0.54	6.39 ± 0.74	0.50 ± 0.26	22.21 ± 0.61	10.51 ± 0.61
19c	>30	>30	>30	8.94 ± 0.82	>30	>30
19d	0.27 ± 0.12	21.54 ± 0.54	19.53 ± 0.55	1.37 ± 0.02	15.15 ± 1.13	4.19 ± 0.58
19e	4.08 ± 0.99	>30	>30	4.47 ± 0.26	>30	8.38 ± 0.48
19f	4.37 ± 0.50	>30	>30	14.50 ± 0.86	>30	5.22 ± 0.54
19g	0.60 ± 0.14	17.50 ± 1.00	10.16 ± 0.87	1.49 ± 0.08	>30	12.51 ± 1.05
19h	1.89 ± 0.21	>30	>30	>30	>30	4.64 ± 0.92
19i	>30	>30	>30	3.35 ± 0.19	>30	>30
22	1.27 ± 0.49	>30	>30	12.40 ± 0.81	>30	>30

Multicycle virus replication assays were performed in HeLa R19 cells, and shown are EC₅₀ values in micromolar. Data represent mean ± SD calculated from 2 different experiments performed in biological triplicates.

Abbreviations: CV, coxsackievirus; EC₅₀, 50% effective concentration; EV, enterovirus; HRV, human rhinovirus, PV-1, poliovirus 1

Table 3. Antiviral activity of active compounds against different clinical isolates of EV-A71, EV-D68, and CV-A24v.

Virus	Strain	Cluster	SFX	1	12a	19b	19d
EV-A71	BrCr	A	>30	>30	4.48 ± 0.42	1.12 ± 0.15	1.68 ± 0.62
	TW/70811/08	B5	>30	>30	8.18 ± 0.61	0.92 ± 0.17	0.754 ± 0.01
	TW/96016/08	B5	>30	>30	9.47 ± 0.04	1.89 ± 0.02	1.94 ± 0.82
	TW/72232/04	C4	6.20 ± 1.45	>30	6.41 ± 2.09	3.83 ± 0.25	2.54 ± 1.72
	TW/2728/04	C4	4.93 ± 0.57	>30	8.33 ± 0.65	2.10 ± 0.08	2.33 ± 1.23
EV-D68	TW/2945/98 ^a	NA	4.65 ± 1.11	>30	9.17 ± 0.41	2.02 ± 0.15	2.9 ± 1.03
	Fermon		0.74 ± 0.12	0.65 ± 0.20	1.23 ± 0.16	0.58 ± 0.10	1.36 ± 0.22
	4311000742	A	0.66 ± 0.14	3.83 ± 0.40	1.86 ± 0.16	1.31 ± 0.90	3.91 ± 0.13
	4310901348	A	1.24 ± 0.32	4.47 ± 0.13	2.72 ± 0.96	1.71 ± 0.68	3.55 ± 0.43
	4310902042	B	0.57 ± 0.30	4.05 ± 0.65	1.44 ± 0.23	0.91 ± 0.92	3.53 ± 0.41
CV-A24	4310900947	B	0.95 ± 0.27	3.65 ± 0.34	1.84 ± 0.40	1.85 ± 0.18	4.60 ± 0.37
	4310902284	C	1.46 ± 0.36	2.23 ± 0.12	2.31 ± 0.82	1.29 ± 0.21	1.82 ± 0.57
	Joseph		>30	>30	3.45 ± 0.42	4.99 ± 0.61	18.65 ± 0.67
	110386		>30	>30	1.94 ± 0.07	2.53 ± 0.45	15.66 ± 1.32
	110389		>30	>30	3.77 ± 0.32	5.65 ± 0.23	18.55 ± 0.44
CV-A24v	110390		>30	>30	1.91 ± 0.55	4.16 ± 0.17	16.75 ± 0.33
	110392		>30	>30	2.32 ± 0.23	4.35 ± 0.18	19.06 ± 0.97

Multicycle viral replication assay was performed in HeLa R19 cells, and shown are EC₅₀ values in micromolar. Data represent mean ± SD calculated from 2 different experiments performed in biological triplicates. ^a provided by Steve Oberste from the Center of Disease Control and Prevention [20].

Abbreviations: CV, coxsackievirus; EC₅₀, 50% effective concentration; EV, enterovirus; NA, not available; SFX, (S)-flouxetine

Sensitivity of CV-B3 2C mutants to the broad-spectrum EV and RV compounds

Previously, it was shown that compound 1-resistant CV-B3 viruses had acquired 2C mutations S58N, C179F, I227V, and N257D. Subsequently, it was shown that C179F alone could provide protection against compound 1 (other mutants were not tested)²⁰. Moreover, mutations C179F, I227V, and the triple-mutant A224V-I227V-A229V, as well as F190L, conferred resistance to (*S*)-fluoxetine^{20,24}. This likely suggests that both compounds target a common binding pocket. We investigated whether these mutations conferred cross-resistance to 12a and 19b. For this, we used a recombinant CV-B3 virus encoding a *Renilla* luciferase reporter gene (Rluc-CV-B3) upstream of the capsid coding region. Cells were infected with Rluc-CV-B3 viruses harboring 2C mutations and treated with serial dilutions of compound. Eight hours post infection, *Renilla* luciferase was determined as a sensitive and quantitative read-out for virus replication. As previously reported, the mutation C179F conferred resistance to compound 1²⁰. Additionally, we observed that all other common 2C resistance mutations (C179Y, F190L, I227V, and A224V-I227V-A229V) conferred compound 1 resistance (Fig 3A). The resistance profile of 12a resembled that of the parental compound 1 and (*S*)-fluoxetine (Fig 3B). Remarkably, I227V and A224V-I227V-A229V did not confer resistance to 19d, whereas C179F and F190L provided only a low level of resistance.

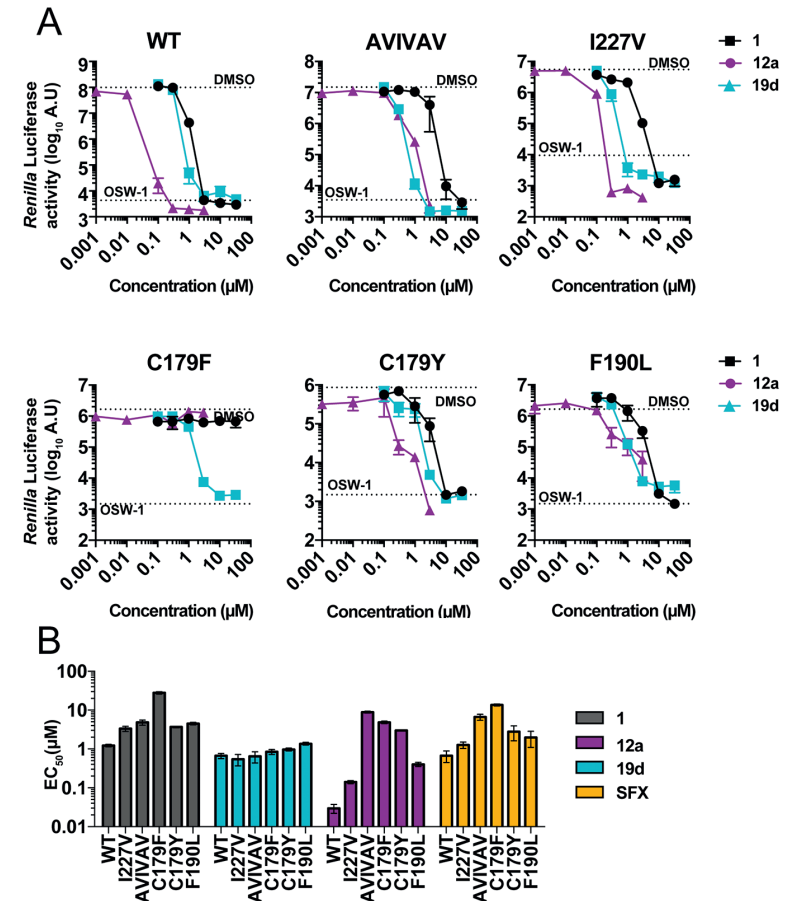


Figure 3. Mutations in the CV-B3 protein 2C confer resistance to compound 1 and 12a but not 19d. In a single-cycle viral replication assay, HeLa R19 cells were infected with a selection of Rluc-CV-B3 reporter viruses containing previously identified mutations in the nonstructural protein 2C conferring resistance to (*S*)-fluoxetine [24]. (A) HeLa R19 were infected with a MOI 0.1 of Rluc-CV-B3 WT virus, the triple mutant (A224V-I227V-A229V, designated as AVIVAV), the I227V single mutant, the C179F or the C179Y mutant, and the F190L mutant. At 30 minutes post infection, the cells were treated with serial dilutions of compound 1, 12a, 19d, as well as 10nM OSW-1 as a control replication inhibitor that acts via the host protein OSBP. Eight hours post infection, cells were lysed, and virus titers were determined by measuring Rluc activity as a quantitative measurement for viral replication. Data represent mean \pm SD from one experiment representative of three independent experiments performed in biological triplicates. (B) The EC₅₀ values of the three independent experiments were calculated for each mutant Rluc-CV-B3 virus and each compound. (*S*)-fluoxetine was used as a positive control. A.U., arbitrary units; AVIVAV, CV-B3 virus harboring the triple mutation A224V-I227V-A229V; EC₅₀, 50% effective concentration; CV, coxsackievirus; MOI, multiplicity of infection; Rluc, *Renilla* luciferase; WT, wild type

Raising resistant viruses against compound 19d

As known 2C mutations only marginally provided resistance to 19d, we raised 19d-resistant virus variants of EV-A71, CV-B3, and EV-D68 via a clonal resistance selection procedure described previously³⁰.

CV-B3. Two 19d-resistant CV-B3 virus pools were obtained. Both contained a mutation at position F190 (F190L or F190V) together with other mutations (Table 4). The first CV-B3 virus pool acquired the mutation F190V and three additional 2C mutations: A220P, S233P, and D234N (Table 4 and Fig 4A). A220P is located close to the motif C that is part of the ATPase domain and structurally immediately followed by the 224AGSINA229 loop, a hotspot for resistance mutations toward 2C inhibitors^{31,32}. The second CV-B3 virus pool contained the mutations F190L and H243R (Table 4). The latter amino acid is located near the arginine finger (which is formed by 240R and R241) of 2C. Both resistant virus pools are cross-resistant to 12a, 19b, and (S)-fluoxtetine. We reverse engineered the single mutations observed in pool 2 (F190L and H243R), either alone or in combination, into the RLuc-CV-B3 reporter virus. Viruses were characterized for their 19d sensitivity in a single-cycle viral replication assay, and replication kinetics were analyzed using *Renilla* luciferase as read-out. Mutation F190L conferred a low level of resistance to 19d, whereas H243R did not provide any resistance. Remarkably, introducing both mutations F190L/H243R conferred a high level of resistance (Fig 4B). Replication analysis showed that each of the single mutations caused a delay in replication kinetics but that the double mutation restored replication kinetics to wild-type levels (Fig 4C). Mapping of the mutations on the CV-B3 2C homology model that we previously published²⁴ showed that residue F190 is located in the $\alpha 2$ helix, whereas residue H243 is localized more distantly (Fig 4D and S3 Fig). Together, these data suggest that CV-B3 first acquired a mutation at position F190, which gives a low level of resistance and maps in the conserved part of the $\alpha 2$ helix of the CV-B3 homology model³³. However, mutation of this position resulted in a loss of viral fitness. Other mutations in more distantly located residues (e.g., H243R) were then acquired that further increased resistance and restored the replication fitness of the virus.

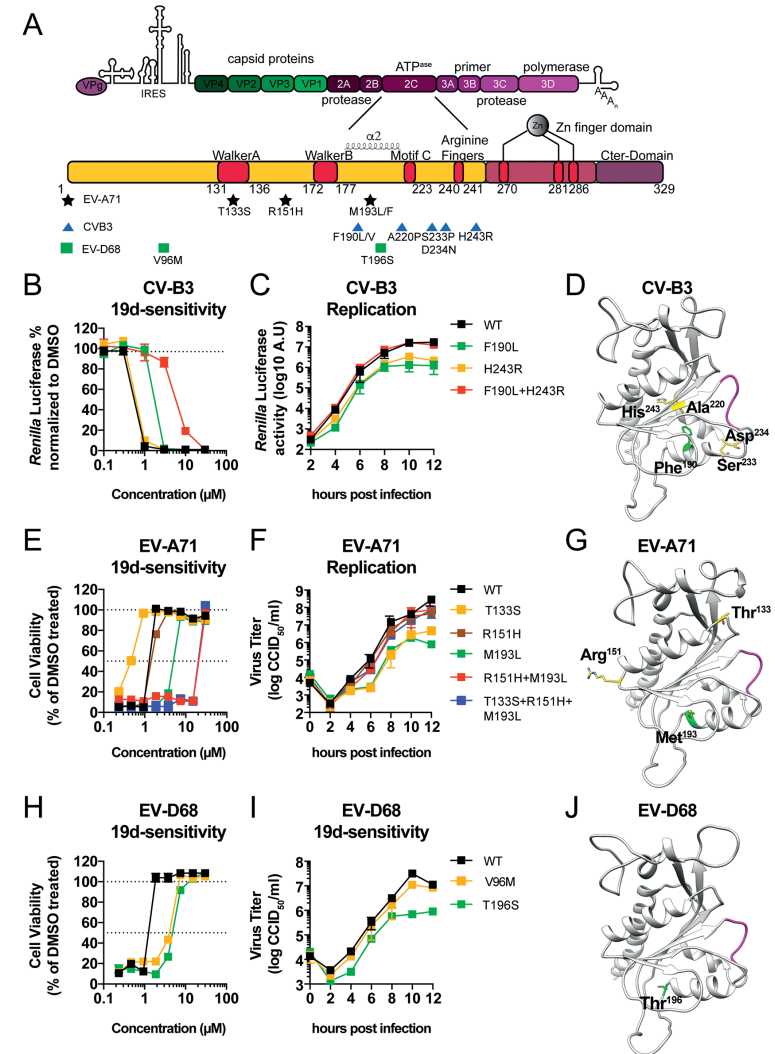


Figure 4. Effect of reverse-engineered 2C mutations on 19d sensitivity and replication fitness. (A) Schematic representation of the viral genome with a focus on the 2C protein and the functional domains. The resistance mutations for EV-A71 are highlighted with black stars, CV-B3 resistance mutations are depicted in blue triangles, and EV-D68 resistance mutations in green squares. (B) Single-cycle viral replication assay to determine 19d sensitivity of RLuc-CV-B3 reporter viruses harboring 2C mutations. HeLa R19 cells were infected with MOI 0.1 of RLuc-CV-B3 reporter virus and treated with serial dilutions of 19d. RLuc activity was determined at 8 hours post infection as a quantitative measure of replication. (C) Replication of RLuc-CV-B3 2C mutant viruses. HeLa R19 cells were infected at MOI 0.1 with the RLuc-CV-B3 viruses, and at the

indicated time points, the cells were lysed and luciferase activity was determined. (D) The 2C mutations of CV-B3 2C which were acquired during resistance selection are mapped onto the previously published homology model of CV-B3 2C [24]. The amino acid F190 is highlighted in green, the amino acids H243 and A220P in yellow, and the amino acids S233 and D234 in red. (E) Multicycle viral replication assay to determine 19d sensitivity of reverse-engineered EV-A71 2C mutant viruses. HeLa R19 cells were treated with serial dilutions of 19d and infected with MOI of 0.001 of the reverse-engineered EV-A71 mutant viruses. After 3 days, the cells' viability was determined using an MTS assay. (F) Replication of EV-A71 reverse-engineered viruses. After infection for 30 minutes at MOI 5, cells were incubated for the indicated time points. Cells were freeze-thawed three times to harvest infectious virus particles. Total virus titers were determined by endpoint dilution. (G) The 2C mutations of EV-A71 2C which were acquired during resistance selection are mapped onto the EV-A71 2C crystal structure PDB: 5GRB [33]. The amino acid M193 is depicted in green, the amino acid R151 in yellow, and T133 in red. (H) Multicycle viral replication assay to determine 19d resistance of reverse-engineered EV-D68 2C mutant viruses. The experiment was done similar to (E), and cells were infected with MOI 0.1 to reach full CPE within 3 days. (I) Growth curves of reverse-engineered EV-D68 viruses. Growth kinetics was assessed similar to in (C). (J) The amino acid T196 of EV-D68 2C is highlighted in green and mapped onto a homology model of EV-D68 2C which was built similar to the CV-B3 homology model based on the crystal structure of EV-A71 (PDB: 5GRB). The primary mutation T196S is highlighted in green. Data represent mean \pm SD from one experiment representative of at least two independent experiments performed in biological triplicates. A.U., arbitrary units; CCID50, 50% cell culture infective dose; CV, coxsackievirus; EV, enterovirus; IRES, internal ribosomal entry side; MOI, multiplicity of infection; MTS, 3-(4,5-dimethylthiazol-2-yl)-5-(3-carboxymethoxyphenyl)-2-(4-sulfophenyl)-2H-tetrazolium; PDB, protein database; Rluc, *Renilla* luciferase; WT, wild type

Table 4. Phenotypic characterization of 19d-resistant virus pools.

Virus	Genotype 2C	19d	Fold	12a	Fold	19b	Fold	SFX	Fold
EV-A71	WT	0.66 \pm 0.09	1	4.65 \pm 0.27	1	0.82 \pm 0.12	1	>30	ND
EV-A71 pool 1	M193L	3.14 \pm 0.36	5	3.34 \pm 0.20	1	2.27 \pm 0.1	3	>30	ND
EV-A71 pool 2	R151H, M193L	7.64 \pm 0.27	12	20.48 \pm 1.74	4	10.74 \pm 0.40	13	>30	ND
EV-A71 pool 3	R151H, M193F	6.97 \pm 0.07	11	23.85 \pm 1.34	5	11.10 \pm 0.46	14	>30	ND
EV-A71 pool 4	T133S, R151H, M193L	8.24 \pm 0.16	12	25.34 \pm 0.90	5	11.59 \pm 2.01	14	>30	ND
CV-B3	WT	1.26 \pm 0.15	1	0.02 \pm 0.01	1	0.29 \pm 0.05	1	0.43 \pm 0.16	1
CV-B3 pool 1	F190V, A220P, S233P, D234N	7.44 \pm 0.49	5	0.34 \pm 0.12	18	1.46 \pm 0.31	5	4.58 \pm 0.31	11
CV-B3 pool 2	F190L, H243R	12.40 \pm 1.13	9	0.26 \pm 0.03	14	2.18 \pm 0.03	8	4.13 \pm 1.94	10
EV-D68	WT	1.55 \pm 0.17	1	1.25 \pm 0.09	1	0.83 \pm 0.09	1	0.65 \pm 0.16	1
EV-D68 pool 1	T196S	3.79 \pm 0.18	2	3.12 \pm 0.32	2	1.75 \pm 0.10	2	10.21 \pm 0.01	16
EV-D68 pool 2	V96M	4.35 \pm 0.09	3	4.18 \pm 0.03	3	2.76 \pm 0.14	4	10.05 \pm 0.45	15

Multicycle viral replication assays were performed in HeLa R19 cells, and shown are EC₅₀ values in micromolar and fold resistance. Data represent mean \pm SD calculated from three different experiments all performed in biological triplicates. All underlying experimental data are displayed in S1 Data.

Abbreviations: CV, coxsackievirus; EC₅₀, 50% effective concentration; EV, enterovirus; ND, not determined; SFX, (S)-fluoxtetine; WT, wild type

EV-A71. Four different 19d-resistant EV-A71 virus pools were obtained. All contained a mutation at position M193, either M193L or M193F, alone or in combination with additional mutations (Table 4 and Fig 4A). M193L was previously reported to provide resistance to guanidine hydrochloride (GuaHCl), a well-known 2C inhibitor³⁴. Two virus pools contained a second mutation, R151H, and displayed a further increase in resistance. The fourth virus pool contained M193L, R151H, and a third mutation in the Walker A motif, T133S. This pool exhibited only a slight increase in 19d resistance. Similar profiles were observed when these virus pools were tested for their resistance to inhibitors 12a and 19b (Table 4). To obtain more insight into the effects of the mutations on 19d sensitivity and virus growth, we introduced them—either individually or in combination—into the infectious clone of EV-A71 by reverse genetics. The mutant viruses were characterized for their 19d resistance in a multicycle viral replication assay (Fig 4E). Moreover, we determined single-cycle replication kinetics of these viruses in the absence of inhibitor (Fig 4F). The single mutation M193L, but not T133S or R151H, conferred 19d resistance. Whereas R151H alone did not confer resistance, the double mutation (M193L/R151H) further increased the resistance. Introduction of a third mutation, T133S (M193L/R151H/T133S), slightly further increased resistance (Fig 4E). In the replication kinetics analysis, we observed that replication of viruses carrying single mutations M193L or T133S, but not R151H, was impaired (Fig 4F). Remarkably, viruses carrying double mutation M193L/R151H or triple mutation M193L/R151H/T133S showed wild-type replication kinetics. These resistance mutations were mapped on the EV-A71 2C crystal structure (PDB: 5GRB) (Fig 4G). The data are in line with those observed for CV-B3 in that a primary mutation in the a2 helix of EV-A71 2C (M193L) was acquired that provided resistance to 19d but which was at the expense of virus fitness. Additional mutations (R151H and T133S) were then acquired which compensated for the loss of fitness and further increased resistance.

EV-D68. Two 19d-resistant EV-D68 pools were obtained. One pool contained the single mutation V96M, while the other contained the single mutation T196S (Fig 4A). Both resistant virus pools conferred 19d resistance and cross-resistance to 12a, 19b, and (S)-flouxetine (Table 4). Both mutations were reverse engineered into an EV-D68 infectious clone and tested for their 19d sensitivity in a multicycle viral replication assay as well as for their replication kinetics. Both V96M and T196S provided 19d resistance, although resistance was rather moderate (Fig 4H). The V96M mutant virus grew comparably to wild-type, whereas the replication kinetics of T196S was impaired (Fig 4I). Mapping of the mutations on an EV-D68 2C homology model that we built on the 2C crystal structure of EV-A71 showed that residue T196 is located very close to the a2 helix (Fig 4J). Unfortunately, we cannot draw any conclusions on the position and/or role of residue V96 since structural data of the first 116 amino acids of 2C are missing.

In summary, we observed a common pattern that 19d-resistant EV-A71, CV-B3, and EV-D68 variants acquired a mutation in the a2 helix or very close to it. Acquiring these mutations came with a fitness cost for the virus. Additional mutations in more

distantly localized residues were obtained that increased resistance and improved the viral fitness. Together, this suggests that the a2 helix may form a part of the compound binding site.

In silico identification of a putative solvent accessible tunnel in 2C

To strengthen the hypothesis that the a2 helix is likely part of the binding pocket, we used computational methods to identify solvent accessible tunnels within the EV-A71 2C crystal structure (PDB: 5GRB)³⁵⁻³⁸. Using the amino acid M193 in the a2 helix of EV-A71 2C as starting coordinate, and an origin radius of 5 Å, we identified three solvent accessible tunnels surrounding the a2 helix in EV-A71 (Fig 5A). These tunnels connect the interior of the molecule with the surrounding environment and provide a possible entry side for compounds to bind 2C.

Next, we explored the occurrence of solvent accessible tunnels in the 2C protein of PV, of which also a crystal structure has been solved (PDB: 5Z3Q)³³. Previous studies have identified 2C mutations F164Y, N179G/A, and M187L in PV to confer resistance to the 2C inhibitors GuaHCl or MRL-1237³⁵⁻³⁹. These residues localize very close to the a2 helix (Fig 5B). We mapped the mutations on the 2C crystal structure of PV (PDB: 5Z3Q) and looked for solvent accessible tunnels using M187 amino acid as starting coordinate and an origin radius of 5 Å. We were able to identify a tunnel at the a2 helix of 2C PV, and this tunnel shows similarities to the tunnel we observed in EV-A71 2C. The same tunnel was predicted when residues F164 (S4 Fig Panel A) or N179 (S4 Fig Panel B) were used as starting coordinate. Additionally, other programs also predicted very similar solvent-accessible tunnels or cavities within 2C of EV-A71 and PV-1 (S4 Fig Panel C-F). Taken together, we propose that the a2 helix in 2C is part of the binding pocket of inhibitors and that mutations in this helix disrupt binding of these inhibitors, thereby providing a first layer of resistance.

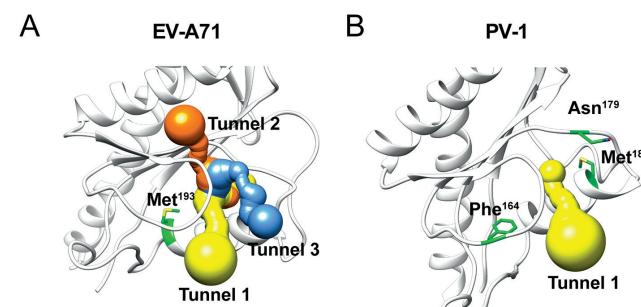


Figure 5. In silico prediction of solvent accessible tunnels reveals a binding pocket surrounding the a2 helix of 2C. (A) The MOLE tool was used to identify solvent exposed tunnels surrounding the a2 helix of 2C [40]. For EV-A71 the 2C crystal structure PDB: 5GRB was used, and the amino acid M193 was used as starting point [33]. (B) For PV the 2C crystal structure PDB: 5Z3Q with the amino acid M187 as starting point [41]. The primary mutations of EV-A71 and PV-1 are highlighted in green and the in silico predicted tunnels are colored in yellow, blue, and orange. Asn, asparagine; EV, enterovirus; Met, ; PDB, protein database; Phe, phenylalanine; PV, poliovirus

To test the hypothesis that the 2C a2 helix mutation disrupted compound binding, we performed thermal shift assays with (*S*)-fluoxetine and 19d. We expressed recombinant fragments of CV-B3 2C lacking the first 116 amino acids and the corresponding 2C fragment of the single mutant F190L. Both (*S*)-fluoxetine and 19d caused a dose-dependent shift in the melting temperature of the wild-type 2C protein, indicative of a direct binding of the wild-type protein to the compounds (Fig 6A and 6B). No shift was observed upon testing the F190L mutant, indicating that the binding of the compounds was disrupted by the a2 helix mutation. These data provide the first evidence that mutations in the a2 helix of 2C disrupt compound binding.

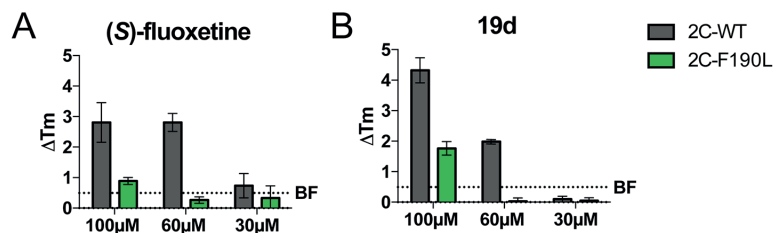


Figure 6. Resistance mutations in the a2 helix of CV-B3 2C disrupt compound binding. The binding of (A) (*S*)-fluoxetine and (B) 19d to a recombinant fragment of the CV-B3 2C protein and the CV-B3 2C a2 helix mutant F190L was assessed by thermal shift assays. The thermal shift of 2C is represented by change in melting temperature (ΔT_m). The dashed line represents data from the negative control BF738735, an inhibitor of the pan-EV host factor phosphatidylinositol-4-III b, used at a concentration of 100 μM . Data shown are representative of one out of two experiments which were performed in technical triplicates. Error bars depict SD calculated from technical triplicates of the representative experiment. All underlying experimental data that are displayed can be found in S2 Data. CV, coxsackievirus; EV, enterovirus; Tm, melting temperature; WT, wild type

Combination of 12a and 19b reveals most potent broad-spectrum EV and RV inhibitor

Our data suggest that 12a and 19b as well as 19d target the same common druggable binding pocket in the 2C proteins of CV-B3, EV-A71, and EV-D68. Next, we were wondering whether a combination of the chemical features of the broad-spectrum EV and RV inhibitors 12a and 19b could increase the antiviral activity. Therefore, we synthesized a new compound with the combined chemical moieties of the furan amide analogue 12a with the fluoride moiety of the N-benzylaniline analogues 19b (Fig 7A). The antiviral activity and the antiviral spectrum of the new combined analogue 12b was tested in a multicycle viral replication assay against the panel of prototypic EV and RV species. Compound 12b showed an improved antiviral profile against all tested viruses compared to the parental compound 1 and the analogue 12a (Fig 7B). The antiviral activity against the serotypes CV-B3, EV-D68, and HRV-B14 is in the nM range, whereas its activity is in the sub- μM or low μM range against EV-A71, PV-1, CV-A24, and HRV-2. These data show that broad-spectrum 2C inhibitors can be developed in the therapeutically relevant nM range.

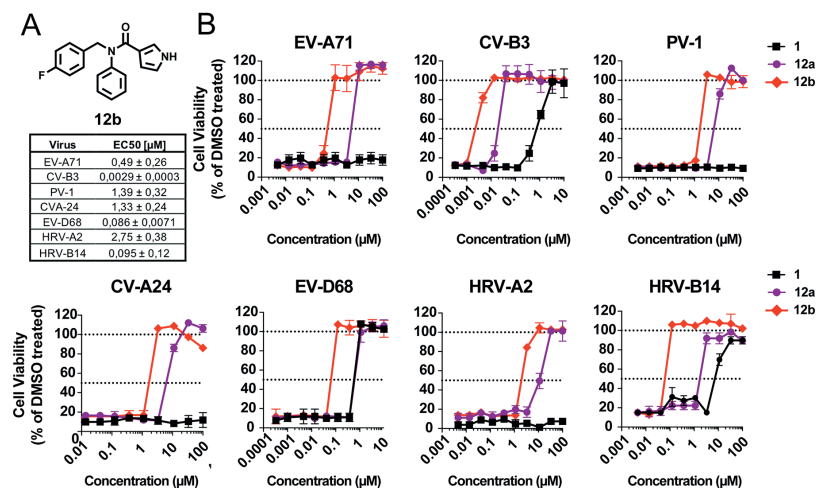


Figure 7. Combination of compound 12a and 19b reveals the most potent broad-spectrum EV and RV inhibitor 12b. (A) The chemical backbone of 12b is shown. The table represents the EC₅₀ values in $\mu\text{M} \pm \text{SD}$ of compound 12b. EC₅₀ is calculated for the panel of representative EV and RV. EC₅₀ values represent mean values that are calculated from three independent experiments which were performed in biological triplicates. (B) A multicycle viral replication assay was performed to determine the antiviral activity of compound 12b. HeLa R19 cells were treated with serial dilutions of parental compound 1, the furan amide analogue 12a and 12b. Immediately thereafter, cells were infected with EV-A71 (BrCr), CV-B3 (Nancy), PV-1, CV-A24 (Joseph), EV-D68 (Fermon), HRV-A2, and HRV-B14 at low MOI (depending on the virus, see Material and Methods) to reach full CPE within 3 days. Data are shown from one representative experiment out of three independent experiments which were performed in biological triplicate. All underlying experimental data that are displayed can be found in S2 Data. CPE, cytopathic effect; CV, coxsackievirus; EC₅₀, 50% effective concentration; EV, enterovirus; HRV, human rhinovirus; PV, poliovirus; RV, rhinovirus

Broadly active EV inhibitors do not affect serotonin, dopamine, or norepinephrine transporter activity and neural activity

Fluoxetine is an SSRI, and both enantiomers are equipotent in SSRI activity. Given the structural similarity of the compound 1 analogues to fluoxetine, we wanted to exclude that these analogues also exhibit the same undesirable neurological effects. To do this, we investigated whether the compounds inhibit the monoamine reuptake of serotonin, dopamine, and norepinephrine through inhibition of their corresponding transporters serotonin transporter (SERT), dopamine transporter (DAT) and norepinephrine transporter (NET). Previously, it was shown using the Neurotransmitter Transporter Uptake Assay that human embryonic kidney (HEK) 293 cells transfected with human DAT, NET, and SERT show a stable and near linear increase in fluorescence indicating proper transporter function (Fig 8A)⁴². Exposure of HEK293 cells expressing human SERT to fluoxetine (1 and 100 μM) resulted in complete inhibition of SERT-mediated uptake (Fig 8B). These results are in line with fluoxetine acting as an SSRI and with

previous results showing concentration-dependent inhibition of human SERT by fluoxetine (50% inhibitory concentration [IC_{50}] = 0.3 μ M, full inhibition at $\geq 1 \mu$ M⁴²). As reported, fluoxetine promiscuously inhibited also the DAT and NET activity at 100 μ M. In contrast, neither 12a, 19b, 19d, nor the combined compound 12b inhibited SERT, DAT, or NET function at 1 μ M or 100 μ M, respectively. We also used a multiwell micro-electrode array (mwMEA) to assess effects of fluoxetine and the compound 1 analogues on spontaneous neuronal activity to determine their neurotoxic potential (for review see⁴³ and overview of methods see S5 Fig). Unlike fluoxetine—which inhibited the mean spike rate (MSR), mean burst rate (MBR), and mean network burst rate (MNBR) in a concentration-dependent manner—none of the compound 1 analogues affected neuronal activity (S6 Fig).

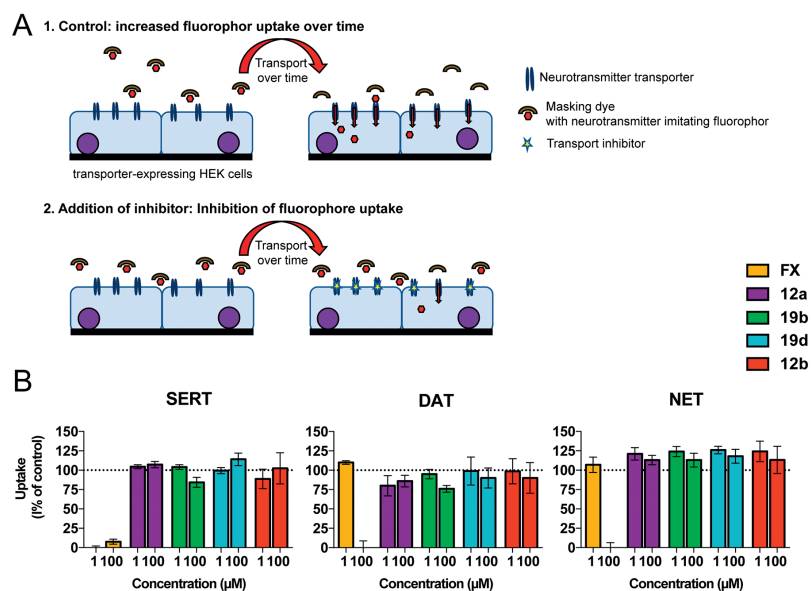


Figure 8. Broadly active EV inhibitors do not affect SERT, DAT, or NET activity. (A) Overview of the principle of the fluorescent measurements of neurotransmitter transporter function. Cells expressing human monoamine transporters (SERT, DAT, or NET) are incubated with a fluorescent transporter substrate and a cell-impermeable masking dye that extinguishes only extracellular fluorescence (left). Cells gain fluorescence following uptake of the substrate, and the increase in fluorescence is a measure for transporter function (top right). Cells with impaired transporter function will take up less substrate, resulting in lower fluorescence (bottom right). (B) Effects of fluoxetine and compounds 12a, 12b, 19b, and 19d on inhibition of SERT-, DAT-, and NET-mediated uptake of fluorescent substrate. Uptake is shown as mean \pm SEM as percentage compared to control (DMSO) wells ($n = 7$ –16 wells, derived from 2 independent cultures). All underlying experimental data that are displayed can be found in S2 Data. DAT, dopamine transporter; EV, enterovirus; FX, racemic fluoxetine; NET, norepinephrine transporter; SERT, serotonin transporter;

Discussion

EVs, especially EV-A71, EV-D68, and CV-A24v, impose serious public health threats. Currently, there are no antiviral therapies licensed to treat EV infections. The highly conserved nonstructural protein 2C fulfills pleiotropic functions during the viral life cycle. Hence, it represents an interesting target for the development of broad-spectrum anti-EV inhibitors. The FDA-approved drug fluoxetine, which is an SSRI, was an attractive candidate for the treatment of EV infections, but several recent studies raised concerns about its clinical application. One retrospective study revealed adverse effects when using fluoxetine as treatment option for EV-D68-associated paralysis. The data suggested a worsening of patient condition, possibly due to its SSRI activity²⁶. Additionally, our previous work showed that the antiviral activity of fluoxetine is unlikely to be decoupled from its SSRI activity^{24,27}. This clearly demonstrates that more potent and safer molecules are needed for treatment of EV infections.

In a high-throughput screen, compound 1 was identified as a CV-B3 inhibitor²⁰. The chemical structure is reminiscent of fluoxetine but lacks a chiral center and the trifluoro moiety important for the SSRI activity of fluoxetine. In this study, we investigated the pharmacophoric features of compound 1 which underpin its antiviral activity. An important focus was to explore the furan amide moiety and the substituents of the N-benzylaniline moiety. First, the synthesized analogues were screened for their antiviral activity against CV-B3. The structure-activity relationship study revealed that the furan amide, but not the N-benzylaniline moiety, was essential for the antiviral activity. Even though the furan amide was essential, different modifications can be introduced. Subsequently, compounds that inhibited CV-B3 were evaluated for their ability to inhibit representatives of four human EV and two RV species. Several compounds showed an increased potency and broadened antiviral spectrum relative to parental compound 1. Four of these compounds—the furan analogues 12a and 12b and the N-benzylaniline analogues 19b and 19d—inhibited all representative EVs and RVs, suggesting broad-spectrum EV and RV activity. Moreover, SERT/DAT/NET experiments suggest that the compounds, unlike (*S*)-fluoxetine, are not neuroactive.

Several structurally disparate 2C inhibitors have already been identified. With the exception of fluoxetine, dibucaine, pirlindole, and several other 2C inhibitors presented at a conference, the anti-enteroviral spectrum of most 2C-targeting compounds has not been systematically characterized^{7,22,44}. The FDA-approved drugs fluoxetine (racemic mixture), dibucaine, and pirlindole and the parental compound 1 showed a limited antiviral spectrum and low potency²⁰. We speculate that the broader antiviral spectrum of 2C inhibitors correlates with an increased antiviral activity and potency. Our previous finding that higher antiviral activity of (*S*)-fluoxetine resulted in a broader antiviral spectrum than the less active racemic mixture lends support to this hypothesis²⁴. In our study, we identified several compounds that showed higher antiviral potency as well as a broader spectrum. The 4 compounds that showed the highest antiviral activity (i.e., 12a, 12b, 19b, and 19d) showed broad-spectrum EV and RV activity. These data

lend further support to the proposed correlation between the antiviral potency of 2C inhibitors and the broadness of their antiviral spectrum.

To validate the broad-spectrum EV antiviral activity of 12a, 19b, and 19d, several clinical isolates of the serotypes EV-A71, CV-A24v, and EV-D68 were tested. Indeed, the compounds inhibited all clinical isolates, albeit with subtle differences. We reported previously that (*S*)-fluooxetine does not inhibit EV-A71 strain BrCr. Interestingly, several EV-A71 clinical isolates were inhibited by (*S*)-fluooxetine^{20,24}. The differences in the antiviral spectrum could be due to very minor intrinsic genetic differences between the clinical isolates of EV-A71. However, the observation that all isolates are inhibited by compounds 12a, 19b, and 19d but not the parental compound 1 makes it more likely that there is a correlation between antiviral potency and antiviral spectrum.

Combining the chemical moieties of 12a with 19b resulted in the most potent broad-spectrum EV and RV inhibitor. This compound, 12b, inhibited CV-B3, EV-D68, and HRV-B14 in the nM range, EV-A71 in the sub- μ M range, and EV-C and HRV-A2 in the low μ M range. The selectivity index, a parameter to express a compound's *in vitro* efficacy in the inhibition of virus replication, showed therapeutically relevant values in the range of 100 up to 3,000 and even higher against CV-B3 for the broad-spectrum EV and RV inhibitors (S3 Table). Together, these data show that 2C is an excellent target for highly potent antiviral drugs and that broad-spectrum 2C inhibitors can be developed in the therapeutically relevant nM range.

Raising compound-resistant viruses can reveal important insights into the mode of action of these compounds and their binding site. It was previously shown that mutation C179F conferred resistance to compound 1, whereas mutations I227V and A224V-I227V-A229V provided resistance to the thiazolobenzimidazol TBZE-029 and (*S*)-fluooxetine^{20,23,24,31}. We tested each of these mutations for their resistance toward compound 1, 12a, 19d, and (*S*)-fluooxetine. Compound 1 and 12 showed a similar resistance profile as (*S*)-fluooxetine. The resistance profile of 19d was slightly different. Unlike to the other compounds, mutations C179F and F190L provided some 19d resistance, but mutations I227V and A224V-I227V-A229V did not provide any resistance. These subtle differences in the resistant profiles of compound 1 and 12a on the one hand and 19d on the other hand may be explained by small differences in the interaction between the compounds and 2C, but the exact reason remains to be determined.

To gain more insight in how EVs can develop resistance, we raised 19d-resistant pools of EV-A71, CV-B3, and EV-D68. The importance of the mutations that were observed in these pools was evaluated by introducing them, alone or in combination, in recombinant viruses using reverse genetics. The recovered viruses were characterized for resistance as well as virus fitness. We observed a common mechanism in resistance development toward 19d in the serotypes EV-A71 and CV-B3. First, mutations in the α 2 helix of 2C, or very close to it, were acquired that conferred 19d resistance but at the same time reduced viral fitness. Second, resistant EV-A71 and CV-B3 virus pools acquired additional mutations that are distant from the α 2 helix. These distal mutations alone provided little if any resistance. But the combination of α 2 helix mutations

together with the distal mutations increased 19d resistance and additionally restored viral fitness. In addition, we raised 19d-resistant EV-D68 viruses. Similar to EV-A71 and CV-B3, a resistance mutation—T196S—arose close to the α 2 helix. Interestingly, we also identified an EV-D68 virus pool that carried the mutation V96M. To our knowledge, this is the first mutation against a 2C inhibitor that is located outside the known structure. This suggests that the ATPase domain works in concert with the enigmatic N-terminal domain of 2C. We propose that mutations in, or in proximity to, the α 2 helix of 2C disrupt compound binding, which results in loss of viral fitness. Additional distant mutations are required to compensate for the fitness defects and to further increase resistance.

2C is an SF3 helicase, which typically form hexameric assemblies. Such proteins have Walker A, B, and C motifs which form the catalytic site for ATPase activity. The energy produced by ATP hydrolysis induces a series of conformational changes that drive unwinding of RNA or DNA by SF3 helicases⁴⁵. To support the hypothesis that the α 2 helix of 2C forms part of the compound binding pocket, we predicted solvent accessible tunnels in the 2C proteins of EV-A71 and PV-1. We identified several tunnels that intersect at the α 2 helix of EV-A71 2C. One of these tunnels was also present in the PV-1 2C. On basis of these observations, we propose that there is a common druggable binding pocket close to the α 2 helix of 2C that is conserved in all the EVs and RVs. In support of this, 19d-resistant virus pools conferred cross-resistance to the broad-spectrum EV and RV inhibitors 12a and 19b. Additionally, CV-B3 and EV-D68 virus pools also conferred cross-resistance to (*S*)-fluooxetine. Furthermore, the compounds (*S*)-fluooxetine and 19d caused a dose-dependent shift in the melting temperature of recombinant CV-B3 2C protein suggestive of direct binding. Both compounds did not cause a shift in melting temperature of the F190L 2C mutant. This lends further support that the α 2 helix is part of the binding pocket and that mutations in the α 2 helix disrupt compound binding.

All predicted tunnels are very close to the Walker B domain but on the opposite side from where ATP is coordinated. This indicates that the compounds likely inhibit the 2C protein allosterically and do not directly occupy the ATP binding site (S2 Fig Panel E). Several possibilities for allosteric inhibition of the 2C protein can be proposed. Inhibitor binding could prevent the proper assembly of the functional 2C oligomer, or conversely, the inhibitors might stabilize the 2C protein and prevent conformational changes during ATP hydrolysis. This mechanism has already been shown for a small molecule inhibitor of the human AAA+ ATPase, p97⁴⁶. The allosteric p97 inhibitor binds at the interface of two adjacent protein domains and thereby prevents propagation of the conformational changes that are necessary for proper p97 ATPase function. The lack of oligomeric 2C structures makes it difficult to elucidate whether the compounds would stabilize or destabilize the quaternary structure, or inhibit the enzymatic activities of 2C. Crystallographic or cryo-EM structures of oligomeric 2C in complex with inhibitors are needed to clarify the binding site and the mode of action of 2C inhibitors.

In conclusion, we identified several novel, highly potent inhibitors with broad-spectrum EV and RV activity. Our data suggest that the 2C proteins of EV and RV share

a common, druggable binding pocket. Additionally, these compounds are less cytotoxic compared to the parental compound 1. The structure of the novel analogues resembles that of fluoxetine, but importantly, they lack the tri-fluoro moiety that is required for the SSRI activity of fluoxetine. This suggests that the novel inhibitors do not act as SSRIs, but this remains to be experimentally proven *in vivo*. Since the compounds are not FDA approved, pharmacological, pharmacokinetics, and toxicological data are required. Given the broad-spectrum activity of these novel compounds, we believe these to be promising candidates for further preclinical assessment. Eventually, these compounds could be developed into urgently needed broad-spectrum antivirals to combat EV and RV infections.

Materials and methods

Ethics statement

All experimental procedures involving animals were in accordance with Dutch law and approved by the Ethical Committee for Animal Experimentation of Utrecht University and the Central Committee Animal Experimentation (CCD; #AVD108002016443-1). Animals were treated humanely, and all efforts were made to minimize the number of animals used and their suffering.

Cells

BGM cells (purchased from European Cell Culture Collection [ECACC]), Rhabdomyosarcoma (RD) cells (American Type Culture Collection [ATCC]) and HeLa R19 cells (ATCC) were cultured in Dulbecco's Modified Eagle Medium (DMEM; Lonza, Switzerland) supplemented with 10% (vol/vol) fetal calf serum (FCS; Lonza). HAP1 cells were obtained from Horizon Discovery Group plc (Cambridge, UK) and cultured in Iscove's Modified Dulbecco's Medium (IMDM; Lonza) containing 10% (vol/vol) FCS. Huh7-Lunet 7/T7, a stable cell pool expressing T7 RNA polymerase and blasticidin S-deaminase⁴⁷, were kindly provided by Volker Lohmann (Universitätsklinikum Heidelberg, Germany) and cultured in DMEM supplemented with 10% FCS and 10 µg/mL blasticidin (Sigma-Aldrich, Zwijndrecht, The Netherlands). All cell lines were grown at 37 °C in 5% CO₂. HEK293 cells expressing human DAT, NET, or SERT (kindly provided by Dr. Hoener from F. Hoffmann-La Roche Ltd., Basel, Switzerland) were cultured as described previously^{42,48}. Briefly, transfected HEK cells were cultured in T75 flasks (Thermo Fisher Scientific, Massachusetts) at 37 °C and 5% CO₂. DMEM high glucose (41965-039) was supplemented with 10% dialyzed fetal bovine serum (FBS), 2 mM L-glutamine, 1% 5,000 U/mL–5,000 µg/mL penicillin/streptomycin, 1 mM sodium pyruvate, 1% minimum essential medium non-essential amino acids solution (MEM-NEAA) solution, and 5 µL/mL geneticin selective antibiotic. Trypsin-EDTA (0.05%) was prepared by diluting trypsin-EDTA (0.5%) in phosphate-buffered saline (PBS). All cell culture materials were obtained from Gibco (Life Technologies, Breda, The Netherlands). Medium was refreshed every 2–4 days, and cells were passaged at >80% confluence with the use of PBS and trypsin-

EDTA (0.05%) for up to 10 passages. The cell lines were routinely tested for mycoplasma contamination.

Synthesized compounds and reagents

GuaHCl and (S)-fluoxetine were purchased from Sigma-Aldrich. GuaHCl was dissolved in water at 2 M stock concentration, and all other compounds were dissolved in DMSO at 10 mM stock concentration. Neurobasal-A medium, penicillin–streptomycin (5,000 U/mL–5,000 µg/mL), B27 plus supplement, N2 supplement, and L-glutamine are obtained from Life Technologies (Bleiswijk, The Netherlands). Polyethyleneimine (PEI) solution (50%), sodium borate, boric acid, and all other chemicals (unless stated otherwise) are obtained from Sigma-Aldrich (Zwijndrecht, The Netherlands). General chemical synthesis route and NMR spectra of the compounds are listed in S1 Text.

Viruses

EV-A71 (strain BrCr), PV-1 (strain Sabin, ATCC), and the EV-D68 strains Fermon, 431100074, 4310901348, 4310902042, 4310900947, and 4310902284 were obtained from the National Institute for Public Health and Environment (RIVM) in the Netherlands. HRV-2 and HRV-14 were obtained from Joachim Seipelt from the Medical University of Vienna in Austria. CV-B3 (strain Nancy) was obtained by transfecting BGM cells with RNA transcripts derived from the full-length infectious clones p53CB3/T7 as described by Wessels and colleagues⁴⁹. EV-A71 clinical isolates TW/70811/08, TW/96016/08, TW/72232/04, TW/2639/04, and TW/2728/04 were kindly provided by Johan Neyts, REGA Institute for medical research, KU Leuven, Belgium.

Resistance selection and phenotyping of resistant virus variants

We raised compound 13-resistant EV-A71, CV-B3, and EV-D68 viruses as described earlier³⁰. In short, the lowest concentration of 19d and the highest virus input that showed reproducible inhibition of viral CPE was determined. Next, three 96-well plates containing HeLa R19 cells were treated with the lowest determined compound concentration and the highest virus input to select for viruses outgrowing the compound. CPE development was monitored daily, and 3 days post infection, samples showing CPE were harvested after three freeze-thawing cycles. The harvested virus isolates were titrated in the presence of same concentration of 19d. After 3 days, the lysates of the highest virus dilution showing full CPE was harvested, and the isolates were expanded in a 25 cm² flask in the presence of 19d. In parallel, virus without compound was taken along and used as a reference. The virus titers from the obtained virus variants were determined by endpoint dilution, and the P2 and P3 regions were sequenced. The resistance and cross-resistance phenotype of the virus variants was determined with a multicycle viral replication assay.

Reverse engineering of resistance virus variants

The CV-B3 mutations 2C[C179F], 2C[C179Y], 2C[F190L], 2C[I227V], and 2C[A224V/I227V/A229V] were previously introduced into the p53CB3/T7 infectious clone²⁴. To obtain RLuc-CV-B3 reporter viruses, which contains the *Renilla* luciferase gene upstream of the capsid coding region, the 2C mutations were cloned into pRLuc-53CB3/T7 using BssHII (nt 4239) and XbaI (nt t4948)⁵⁰. Mutations 2C[H243R] and 2C[F190L/H243R] were introduced into the pRLuc-53CB3/T7 backbone with the Q5 site-directed mutagenesis kit (New England Biolabs, Bioké, Leiden, The Netherlands). After site-directed mutagenesis, the plasmids were subjected to Sanger sequencing to ensure the existence of the introduced mutation. RLuc-CV-B3 wild-type and 2C mutant viruses were obtained by transfection of MluI-linearized plasmid DNA into the Huh7-Lunet 7/T7 cells as described earlier^{47,50}.

The EV-A71 mutations 2C[T133S], 2C[R151H], 2C[M193L], 2C[M193L/R151H], and 2C[M193L/R151H/T133S] and the EV-D68 mutations 2C[V96M] and 2C[T196S] were introduced into the pEV-A71 backbone (kindly provided by Johan Neyts)⁵¹ and pRib-EVD68 Fermon⁵², respectively, using the Q5 site-directed mutagenesis kit (New England Biolabs, Bioké, Leiden, The Netherlands). After site-directed mutagenesis, the plasmids were subjected to Sanger sequencing to ensure the existence of the introduced mutation. The corresponding primers used for site-directed mutagenesis of the aforementioned viruses are reported in S4 Table. To obtain virus, the plasmids were linearized with MluI, and RNA was in vitro transcribed using the T7 RiboMAX Express Large Scale RNA production system (Promega, Leiden, The Netherlands) according to the manufacturer's protocol and transfected into HeLa R19 and RD cells. To ensure that the introduced mutations were retained in the generated virus, viral RNA was isolated with the NucleoSpin RNA Virus kit (Macherey-Nagel, Leiden, The Netherlands) according to the manufacturer's protocol, and the presence of the desired mutations was confirmed by Sanger sequencing. Virus titers were determined by endpoint dilution titration and calculated according to the method of Reed and Muench and expressed as 50% cell culture infective dose (CCID₅₀)⁵³.

Single-cycle virus infection

Virus infections were performed by incubating subconfluent HeLa R19 cells with virus at the indicated MOI at 37 °C for 30 minutes. Next, the inoculum was removed, and fresh control medium or compound-containing medium was added to the cells. At the indicated time points, cells were frozen. For measurements of infectious particles, virus was released from the cells by three freeze-thawing cycles. Virus titers were determined by endpoint dilution assay and calculated by the method of Reed and Muench and expressed as 50% tissue culture infectious dose (TCID₅₀) [53]. In the case of RLuc-CV-B3 infection, cells were lysed at the indicated time points post infection, and the *Renilla* luciferase Assay System (Promega, Leiden, The Netherlands) was used to determine the luciferase activity. Cell viability was determined in parallel using the AQueous One Solution Cell Proliferation Assay (Promega, Leiden, The Netherlands) according to the

manufacturer's protocol. Optical density at 490 nm was determined using a microplate reader.

Multicycle virus infection

Subconfluent layers of HeLa R19 cells were seeded in 96 wells and treated with serial dilutions of the corresponding compounds. Cells were infected with viruses at the lowest possible MOI resulting in full CPE within 3 days (MOI 0.001 for EV-A71, EV-A71 clinical isolates, CV-B3, and PV-1; MOI 0.01 for CV-A24, CV-A24v and HRV-14; MOI 0.1 for EV-D68, EV-D68 clinical isolates, and HRV-2). Subsequently the cells were incubated at 37 °C for 3 days until full CPE was observed in the virus-infected untreated cell controls. Cell viability was determined using the AQueous One Solution Cell Proliferation Assay (Promega, Leiden, The Netherlands) according to the manufacturer's protocol. The optical density at 490 nm was determined using a microplate reader. Raw OD values were converted to percentage of untreated and uninfected cell control after subtraction of the background. The concentration of compound that inhibits virus-induced cell death or expression of *Renilla* luciferase by 50% (EC₅₀) was calculated by nonlinear regression analysis with GraphPad Prism Version 6. We set the threshold for compound activity at concentration of 10 μM or less since low μM range is typical for antivirals in clinical use. Cytotoxicity of the compounds was assessed in a similar set-up, and CC₅₀ values were derived from cell viability values determined with an MTS assay.

Thermal shift assays

The DNA fragment encoding residues 116 to 329 of CV-B3 2C (strain Nancy) was cloned into a pET28b plasmid, downstream of an N-terminal, and 3C protease cleavable, hexahistidine-MBP tag. The F190L mutation was introduced using a Q5 site-directed mutagenesis kit (New England Biolabs, Bioké, Leiden, The Netherlands). The recombinant WT protein, and F190L variant, were produced in *Escherichia coli* RosettaTM 2 (DE3) (Sigma-Aldrich, Zwijndrecht, The Netherlands). When cultures reached OD_{600nm} of 0.5, protein expression was induced by the addition of 0.5 mM IPTG. Subsequently, protein was expressed for 16 hrs at 18 °C, with shaking at 200 rpm. Further protein purification steps were performed essentially as described previously²⁷, with the exception that TEV protease was replaced with 3C protease (Sigma-Aldrich). The final size-exclusion chromatography step was performed at 4°C with buffer containing 25mM Tris (pH 8), 300mM NaCl and 1mM MgCl₂, using a superose® 6 increase 10/300 column GL (GE Healthcare Life Science, Eindhoven, The Netherlands). The binding of (S)- and (R)-fluoxetine and both 2b-enantiomers to WT CV-B3 2C, and the F190L variant, was monitored by the fluorescence-based thermal shift assay (TSA) using a Roche LightCycler®480, as described previously²⁷. Each well of the TSA plates contained WT or F190L 2C protein (final concentration of 10 μM in 50 mM Tris, 300 mM NaCl and 1mM MgCl₂, pH 8) and a SYPRO orange solution in concentrations recommended by the manufacturer, in a final volume of 25 μL. All TSA experiments were performed using a temperature gradient ranging from 20 to 90 °C (incremental steps of 0.2 °C/12 s). Protein

denaturation was monitored by following the increase of the fluorescence emitted by SYPRO orange, which binds to exposed hydrophobic regions of the denatured protein. The mid-log of the transition phase from the native to the denatured protein was used to calculate the melting temperature (T_m). The reference unfolding temperature of proteins in 5% DMSO (T_0) was subtracted from the values in the presence of compounds (T_m) to obtain thermal shifts, $\Delta T_m = (T_m - T_0)$.

Rat neuronal cell culture preparation for recording of neuronal activity

Primary rat cortical cells were isolated from PND0-1 Wistar rat pups as described previously^{54,55}. Briefly, PND0-1 pups are decapitated, and cortices were rapidly dissected on ice and were kept in serum-free dissection medium (Neurobasal-A supplemented with 25 g/L sucrose, 450 μ M l-glutamine, 30 μ M glutamate, 1% penicillin/streptomycin, and 2% B27 plus supplement [pH 7.4]) during the entire procedure. Cortices were dissociated to a single-cell suspension by mincing with scissors, trituration, and filtering through a 100 μ m mesh (EASYstrainer, Greiner Bio-one, Solingen Germany). The cell suspension was diluted to a 2×10^6 cells/mL solution, after which droplets of 50 μ L were placed on the electrode fields in wells of pre-coated 48-well MEA plates (Axion BioSystems, Atlanta, GA). All cell culture surfaces were pre-coated with 0.1% PEI solution diluted in borate buffer (24 mM sodium borate/50 mM boric acid in Milli-Q adjusted to pH 8.4). After plating, cells were left to adhere for approximately 2 hours before adding 450 μ L serum-free dissection medium. Rat primary cortical cells were maintained at 37 °C in a humidified 5% CO₂ incubator. At DIV4, 90% of the serum-free dissection medium was replaced with serum-free culture medium (Neurobasal-A supplemented with 25 g/L sucrose, 450 μ M l-glutamine, 1% penicillin/streptomycin, and 2% B27 plus supplement [pH 7.4]). Rat primary cortical neurons were used for neurotoxicity assessment at DIV15.

MEA recordings of spontaneous neuronal activity in rat primary cortical cultures

Each well of a 48-well MEA plate contains 16 nanotextured gold micro-electrodes (approximately 40–50 μ m diameter; 350 μ m spacing) with 4 integrated ground electrodes, yielding a total of 768 channels for simultaneous recording (for review see⁴³). Spontaneous electrical activity was recorded as described previously^{54,55} (S3_Fig). Briefly, signals were recorded at the day of experiments (DIV15) using a Maestro 768-channel amplifier with integrated heating system, temperature controller, and a data acquisition interface (Axion BioSystems, Atlanta, GA). Data acquisition was managed with Axion's Integrated Studio (AxIS version 2.4.2.13) and recorded as .RAW files. All channels were sampled simultaneously with a gain of 1,200 \times and a sampling frequency of 12.5 kHz/channel, using a 200–5,000 Hz band-pass filter.

Prior to the recording, MEA plates were allowed to equilibrate for 5–10 minutes in the Maestro. Following a 30-minute baseline recording, wells were exposed to the test

compounds or the DMSO control, and activity was recorded for another 30 minutes to determine the acute effects of test compounds on neuronal activity. Stock solutions of compounds dissolved in DMSO (10 mM) were diluted (1:100) in serum-free culture medium to obtain 100 μ M solutions, which were used for exposure of cells in the MEA (dilution 1:10; final concentration 10 μ M/0.1% DMSO). In order to prevent receptor (de)sensitization, each well was exposed only to a single concentration.

To determine (modulation of) spontaneous activity, RAW data files were re-recorded to obtain Alpha Map files for further data analysis. In this re-recording, spikes were detected using the AxIS spike detector (Adaptive threshold crossing, Ada BandFit version 2) with a variable threshold spike detector set at 7 \times SD of internal noise level (rms) on each electrode. Post/pre-spike duration was set to 3.6/2.4 ms. For further data analysis, spike files were loaded in NeuralMetric Tool (version 2.2.4, Axion BioSystems). Only active electrodes (MSR \geq 6 spikes/min) in active wells (\geq 1 active electrode) were included in the data analysis. The (network) bursting behavior was analyzed using the Poisson Surprise method⁵⁶ with a minimal surprise of 10 and a minimum bursting frequency of 0.3 bursts/min. Network bursts were extracted with the adaptive threshold algorithm. Effects of test compounds on the spontaneous activity pattern were determined by comparing activity during exposure to baseline activity. To prevent inclusion of exposure artefacts, the window of 20–30 minutes post exposure was used for analysis of effects. A custom-made Microsoft Excel macro was used to calculate treatment ratios (TRs) per well for the different metric parameters (MSR, MBR, and MNBR) by: $(\text{parameter}_{\text{exposure}} / \text{parameter}_{\text{baseline}}) \times 100\%$. Hereafter, TRs will be normalized to DMSO control. Wells that show effects 2 \times SD above or below average were considered outliers (5.1%) and were removed for further data analysis.

Inhibition of uptake by monoamine transporters

Uptake activity of hNET, hDAT, and hSERT was measured using the Neurotransmitter Transporter Uptake Assay Kit from MDS Analytical Technologies (Sunnyvale, CA) as described previously^{42,48}. Briefly, the kit contained a mix consisting of a fluorescent substrate, which resembles the biogenic amine neurotransmitters, and a masking dye that extinguishes extracellular fluorescence. The fluorescent substrate solution was prepared by dissolving the mix in HBSS according to the manufacturer's instructions and stored at –18 °C for a maximum of 4 days. Uptake of the fluorescent substrate increases intracellular fluorescence, while extracellular fluorescence is blocked by the masking dye (Fig 8)⁵⁷.

On day 0, HEK 293 cells were seeded at a density of approximately 60,000 cells/well in clear-bottom, black-walled, 96-well plates (Greiner Bio-one, Solingen Germany) coated with PLL buffer (50 mg/L). Cells were allowed to proliferate overnight in a humidified 5% CO₂/95% air atmosphere at 37 °C. Experiments were performed the next day (day 1). Cells were pre-incubated with the fluorescent substrate for 12 minutes ($t = -12$ to $t = 0$) prior to a 30-minute drug exposure. Culture medium was replaced by 100 μ L/well fluorescent substrate solution, and uptake measurements were started. At $t = 0$, 100 μ L/

well HBSS with 0.1% DMSO (control) or with test compound (final concentration 1–100 μM) was added to each well, and uptake was measured continuously for 30 minutes. Background wells were pre-incubated with 100 μL /well HBSS without fluorescent substrate solution and exposed at $t = 0$ min to 100 μL /well HBSS.

Fluorescence was recorded every 3 minutes, starting directly after addition of the fluorescent substrate solution ($t = -12$) using a microplate reader (Tecan Infinite M200 microplate; Tecan Trading Männedorf, Switzerland) at 37 °C at 430/515 nm excitation/emission wavelength in bottom-reading mode using optimal gain values for each cell type (number of cycles: 21; time interval: 3 minutes; number of flashes: 19; integration time: 20 μs , no lid). Cell attachment was visually examined following experiments.

The fluorescence of each well was background corrected (time- and plate-matched). First, uptake of the fluorescent substrate was first determined per well by calculating the change in fluorescence (ΔFU) at 12 minutes after exposure to the test compound ($t = 12$) compared to the fluorescence prior to exposure (i.e., the fluorescence following 12-minute pre-incubation with the fluorescent substrate at $t = 0$), as a percentage of the fluorescence prior to exposure. Second, the percentage uptake in control wells of all plates was averaged, and wells that showed values $2\times$ SD above or below average were considered outliers and were excluded from further analysis. Uptake in compound-exposed wells was expressed as a percentage of control wells, outliers in exposed groups (effects $2\times$ SD above or below average) were removed (approximately 1%), and all uptake values were scaled between 0% and 100%.

Prediction of solvent accessible tunnels

For prediction of solvent accessible tunnels, we used the crystal structure of EV-A71 2C PDB: 5GRB/Chain B and PV 2C PDB 5Z3Q/Chain A. As a starting point for the tunnel prediction, the amino acid of 2C of EV-A71 M193 and PV-1 2C F164—N179 and M187, respectively—were used. We used the MOLEonline web interface⁴⁰, CAVER 3.0PyMol plugin⁵⁸, and CASTp⁵⁹ to generate solvent accessible tunnels or surfaces^{40,58,59}. Figures were generated using UCSF Chimera and PyMol (The PYMOL Molecular Graphics system Version 234932948 Schrödinger, LLC).

Statistical analysis

Each experiment was performed at least in technical duplicates, and all experiments were performed in biological triplicates. Statistical significance of the MEA data and transporter inhibition was determined using one-way ANOVA and, if applicable, a post hoc Tukey test. $P \leq 0.05$ was considered significant. Statistical analysis, nonlinear regression, and the graphs were made with GraphPad Prism Version 6 or R version 3.6.0 (R core team 2019).

Acknowledgement

We thank Prof. Friedrich Förster for providing access to equipment used for purification of recombinant 2C proteins.

References

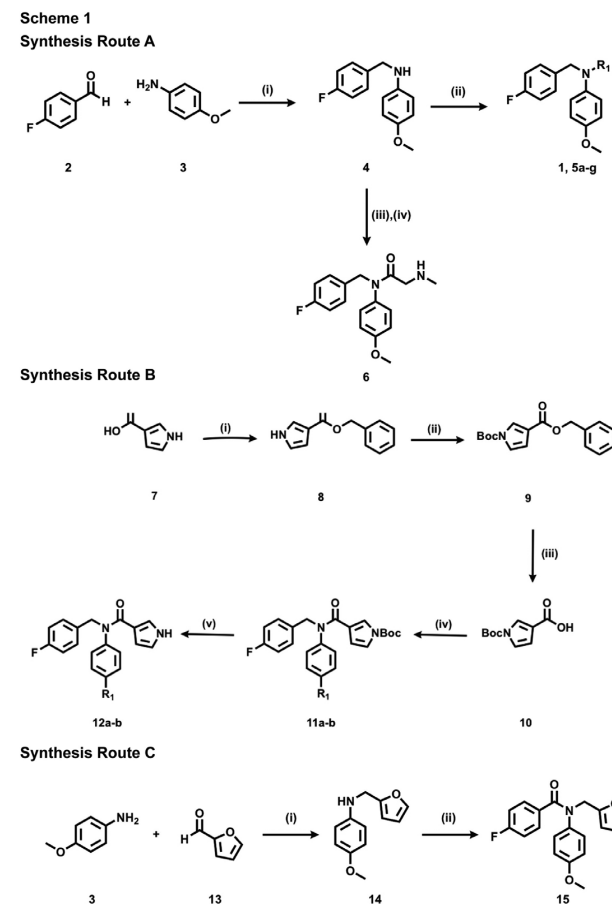
1. Tapparel C, Siegrist F, Petty TJ, Kaiser L. Picornavirus and enterovirus diversity with associated human diseases. *Infect Genet Evol.* 2013;14:282-93.
2. Holm-Hansen CC, Midgley SE, Fischer TK. Global emergence of enterovirus D68: a systematic review. *Lancet Infect Dis.* 2016;16(5):e64-e75.
3. Puenpa J, Wanlapakorn N, Vongpunsawad S, Poovorawan Y. The History of Enterovirus A71 Outbreaks and Molecular Epidemiology in the Asia-Pacific Region. *J Biomed Sci.* 2019;26(1):75.
4. Ghazali O, Chua KB, Ng KP, Hooi PS, Pallansch MA, Oberste MS, et al. An outbreak of acute haemorrhagic conjunctivitis in Melaka, Malaysia. *Singapore Med J.* 2003;44(10):511-6.
5. Kurokawa M, Rai SK, Ono K, Gurung R, Ruit S. Viral investigation of acute hemorrhagic conjunctivitis outbreak (2003) in Nepal using molecular methods. *Southeast Asian J Trop Med Public Health.* 2006;37(5):904-10.
6. Aw-Yong KL, NikNadia NMN, Tan CW, Sam IC, Chan YF. Immune responses against enterovirus A71 infection: Implications for vaccine success. *Rev Med Virol.* 2019;29(5):e2073.
7. Bauer L, Lyoo H, van der Schaar HM, Strating JR, van Kuppeveld FJ. Direct-acting antivirals and host-targeting strategies to combat enterovirus infections. *Current Opinion in Virology.* 2017;24:1-8.
8. Klein M, Eggers HJ, Nelsen-Salz B. Echovirus 9 strain barty non-structural protein 2C has NTPase activity. *Virus Res.* 1999;65(2):155-60.
9. Pfister T, Wimmer E. Characterization of the nucleoside triphosphatase activity of poliovirus protein 2C reveals a mechanism by which guanidine inhibits poliovirus replication. *The Journal of Biological Chemistry.* 1999;274(11):6992-7001.
10. Rodriguez PL, Carrasco L. Poliovirus protein 2C has ATPase and GTPase activities. *The Journal of Biological Chemistry.* 1993;268(11):8105-10.
11. Xia H, Wang P, Wang GC, Yang J, Sun X, Wu W, et al. Human Enterovirus Nonstructural Protein 2CATPase Functions as Both an RNA Helicase and ATP-Independent RNA Chaperone. *PLoS Pathog.* 2015;11(7):e1005067.
12. Cho MW, Teterina N, Egger D, Bienz K, Ehrenfeld E. Membrane rearrangement and vesicle induction by recombinant poliovirus 2C and 2BC in human cells. *Virology.* 1994;202(1):129-45.
13. Aldabe R, Carrasco L. Induction of membrane proliferation by poliovirus proteins 2C and 2BC. *Biochem Biophys Res Commun.* 1995;206(1):64-76.
14. Teterina NL, Gorbalenya AE, Egger D, Bienz K, Ehrenfeld E. Poliovirus 2C protein determinants of membrane binding and rearrangements in mammalian cells. *Journal of Virology.* 1997;71(12):8962-72.
15. Suhy DA, Giddings TH, Jr., Kirkegaard K. Remodeling the endoplasmic reticulum by poliovirus infection and by individual viral proteins: an autophagy-like origin for virus-induced vesicles. *Journal of Virology.* 2000;74(19):8953-65.
16. Vance LM, Moscufo N, Chow M, Heinz BA. Poliovirus 2C region functions during encapsidation of viral RNA. *Journal of Virology.* 1997;71(11):8759-65.
17. Verlinden Y, Cuconati A, Wimmer E, Rombaut B. The antiviral compound 5-(3,4-dichlorophenyl) methylhydantoin inhibits the post-synthetic cleavages and the assembly of poliovirus in a cell-free system. *Antiviral Research.* 2000;48(1):61-9.
18. Wang C, Ma HC, Wimmer E, Jiang P, Paul AV. A C-terminal, cysteine-rich site in poliovirus 2C(ATPase) is required for morphogenesis. *J Gen Virol.* 2014;95(Pt 6):1255-65.

19. Liu Y, Wang C, Mueller S, Paul AV, Wimmer E, Jiang P. Direct interaction between two viral proteins, the nonstructural protein 2C and the capsid protein VP3, is required for enterovirus morphogenesis. *PLoS Pathog.* 2010;6(8):e1001066.
20. Zuo J, Kye S, Quinn KK, Cooper P, Damoiseaux R, Krogstad P. Discovery of Structurally Diverse Small-Molecule Compounds with Broad Antiviral Activity against Enteroviruses. *Antimicrobial Agents and Chemotherapy.* 2015;60(3):1615-26.
21. Zuo J, Quinn KK, Kye S, Cooper P, Damoiseaux R, Krogstad P. Fluoxetine Is a Potent Inhibitor of Coxsackievirus Replication. *Antimicrobial Agents and Chemotherapy.* 2012;56(9):4838-44.
22. Ulferts R, de Boer M, van der Linden L, Bauer L, Lyoo HR, Mate MJ, et al. Screening of a library of FDA-approved drugs identifies several enterovirus replicaton inhibitors that target viral protein 2C. *Antimicrobial Agents and Chemotherapy.* 2016.
23. Ulferts R, van der Linden L, Thibaut HJ, Lanke KH, Leyssen P, Coutard B, et al. Selective serotonin reuptake inhibitor fluoxetine inhibits replication of human enteroviruses B and D by targeting viral protein 2C. *Antimicrobial Agents and Chemotherapy.* 2013;57(4):1952-6.
24. Bauer L, Manganaro R, Zonsics B, Strating J, El Kazzi P, Lorenzo Lopez M, et al. Fluoxetine inhibits enterovirus replication by targeting the viral 2C protein in a stereospecific manner. *ACS Infectious Diseases.* 2019.
25. Gofshsteyn J, Cardenas AM, Bearden D. Treatment of Chronic Enterovirus Encephalitis With Fluoxetine in a Patient With X-Linked Agammaglobulinemia. *Pediatr Neurol.* 2016.
26. Messacar K, Sillau S, Hopkins SE, Otten C, Wilson-Murphy M, Wong B, et al. Safety, tolerability, and efficacy of fluoxetine as an antiviral for acute flaccid myelitis. *Neurology.* 2018.
27. Manganaro R, Zonsics B, Bauer L, Lorenzo Lopez M, Donselaar T, Zwaagstra M, et al. Synthesis and antiviral effect of novel fluoxetine analogues as enterovirus 2C inhibitors. *Antiviral Research.* 2020:104781.
28. Meijer A, van der Sanden S, Snijders BE, Jaramillo-Gutierrez G, Bont L, van der Ent CK, et al. Emergence and epidemic occurrence of enterovirus 68 respiratory infections in The Netherlands in 2010. *Virology.* 2012;423(1):49-57.
29. Chang SC, Li WC, Chen GW, Tsao KC, Huang CG, Huang YC, et al. Genetic characterization of enterovirus 71 isolated from patients with severe disease by comparative analysis of complete genomes. *J Med Virol.* 2012;84(6):931-9.
30. Delang L, Segura Guerrero N, Tas A, Querat G, Pastorino B, Froeyen M, et al. Mutations in the chikungunya virus non-structural proteins cause resistance to favipiravir (T-705), a broad-spectrum antiviral. *J Antimicrob Chemother.* 2014;69(10):2770-84.
31. De Palma AM, Heggermont W, Lanke K, Coutard B, Bergmann M, Monforte AM, et al. The thiazolobenzimidazole TBZE-029 inhibits enterovirus replication by targeting a short region immediately downstream from motif C in the nonstructural protein 2C. *Journal of Virology.* 2008;82(10):4720-30.
32. Klein M, Hadaschik D, Zimmermann H, Eggers HJ, Nelsen-Salz B. The picornavirus replication inhibitors HBB and guanidine in the echovirus-9 system: the significance of viral protein 2C. *J Gen Virol.* 2000;81(Pt 4):895-901.
33. Guan H, Tian J, Qin B, Wojdyla JA, Wang B, Zhao Z, et al. Crystal structure of 2C helicase from enterovirus 71. *Sci Adv.* 2017;3(4):e1602573.
34. Sadeghipour S, Bek EJ, McMinn PC. Selection and characterisation of guanidine-resistant mutants of human enterovirus 71. *Virus Res.* 2012;169(1):72-9.
35. Shimizu H, Agoh M, Agoh Y, Yoshida H, Yoshii K, Yoneyama T, et al. Mutations in the 2C region of poliovirus responsible for altered sensitivity to benzimidazole derivatives. *Journal of Virology.* 2000;74(9):4146-54.
36. Tolskaya EA, Romanova LI, Kolesnikova MS, Gmyl AP, Gorbalenya AE, Agol VI. Genetic studies on the poliovirus 2C protein, an NTPase. A plausible mechanism of guanidine effect on the 2C function and evidence for the importance of 2C oligomerization. *J Mol Biol.* 1994;236(5):1310-23.
37. Pincus SE, Wimmer E. Production of guanidine-resistant and -dependent poliovirus mutants from cloned cDNA: mutations in polypeptide 2C are directly responsible for altered guanidine sensitivity. *Journal of Virology.* 1986;60(2):793-6.
38. Baltera RF, Jr., Tershak DR. Guanidine-resistant mutants of poliovirus have distinct mutations in peptide 2C. *Journal of Virology.* 1989;63(10):4441-4.
39. Pincus SE, Diamond DC, Emini EA, Wimmer E. Guanidine-selected mutants of poliovirus: mapping of point mutations to polypeptide 2C. *Journal of Virology.* 1986;57(2):638-46.
40. Pravda L, Sehnal D, Tousek D, Navratilova V, Bazgier V, Berka K, et al. MOLEonline: a web-based tool for analyzing channels, tunnels and pores (2018 update). *Nucleic Acids Res.* 2018;46(W1):W368-W73.
41. Guan H, Tian J, Zhang C, Qin B, Cui S. Crystal structure of a soluble fragment of poliovirus 2CATPase. *PLoS Pathog.* 2018;14(9):e1007304.
42. Zwartsen A, Verboven AHA, van Kleef R, Wijnolts FMJ, Westerink RHS, Hondebrink L. Measuring inhibition of monoamine reuptake transporters by new psychoactive substances (NPS) in real-time using a high-throughput, fluorescence-based assay. *Toxicol In Vitro.* 2017;45(Pt 1):60-71.
43. Johnstone AF, Gross GW, Weiss DG, Schroeder OH, Gramowski A, Shafer TJ. Microelectrode arrays: a physiologically based neurotoxicity testing platform for the 21st century. *Neurotoxicology.* 2010;31(4):331-50.
44. Thibaut HJ LC, Coutard J, Van der Linden L, Canard B, De Palma AM, Van Kuppeveld F, Jung YS and Neyts J. A novel class of highly potent small molecule inhibitors of entero/rhinovirus replication that target the non structural protein 2C [Poster]. 2013. Available from: https://rega.kuleuven.be/cmt/jn/poster/2013/2013_ht/Poster%20ICAR%202013%20MOA%20KRICT.pdf. [12.11.2020].
45. Singleton MR, Dillingham MS, Wigley DB. Structure and mechanism of helicases and nucleic acid translocases. *Annual review of biochemistry.* 2007;76:23-50.
46. Banerjee S, Bartesaghi A, Merk A, Rao P, Bulfer SL, Yan Y, et al. 2.3 Å resolution cryo-EM structure of human p97 and mechanism of allosteric inhibition. *Science.* 2016;351(6275):871-5.
47. Backes P, Quinkert D, Reiss S, Binder M, Zayas M, Rescher U, et al. Role of annexin A2 in the production of infectious hepatitis C virus particles. *Journal of virology.* 2010;84(11):5775-89.
48. Zwartsen A, Verboven AHA, van Kleef R, Wijnolts FMJ, Westerink RHS, Hondebrink L. Corrigendum to “Measuring inhibition of monoamine reuptake transporters by new psychoactive substances (NPS) in real-time using a high-throughput, fluorescence-based assay” [Toxicology in Vitro (2017) 60-71]. *Toxicol In Vitro.* 2020;62:104631.
49. Wessels E, Duijsings D, Lanke KH, van Dooren SH, Jackson CL, Melchers WJ, et al. Effects of picornavirus 3A Proteins on Protein Transport and GBF1-dependent COP-I recruitment. *Journal of virology.* 2006;80(23):11852-60.

50. Lanke KH, van der Schaar HM, Belov GA, Feng Q, Duijsings D, Jackson CL, et al. GBF1, a guanine nucleotide exchange factor for Arf, is crucial for coxsackievirus B3 RNA replication. *Journal of virology*. 2009;83(22):11940-9.
51. Sun L, Lee H, Thibaut HJ, Lanko K, Rivero-Buceta E, Bator C, et al. Viral engagement with host receptors blocked by a novel class of tryptophan dendrimers that targets the 5-fold-axis of the enterovirus-A71 capsid. *PLoS Pathog*. 2019;15(5):e1007760.
52. Baggen J, Liu Y, Lyoo H, van Vliet ALW, Wahedi M, de Bruin JW, et al. Bypassing pan-enterovirus host factor PLA2G16. *Nature communications*. 2019;10(1):3171.
53. Reed LJ, Muench H. A simple method of estimating fifty percent endpoints *American Journal of Epidemiology*. 1938;27(3):493-7.
54. Dingemans MM, Schutte MG, Wiersma DM, de Groot A, van Kleef RG, Wijnolts FM, et al. Chronic 14-day exposure to insecticides or methylmercury modulates neuronal activity in primary rat cortical cultures. *Neurotoxicology*. 2016;57:194-202.
55. Tukker AM, de Groot MW, Wijnolts FM, Kasteel EE, Hondebrink L, Westerink RH. Is the time right for in vitro neurotoxicity testing using human iPSC-derived neurons? *ALTEX*. 2016;33(3):261-71.
56. Legendy CR, Salzman M. Bursts and recurrences of bursts in the spike trains of spontaneously active striate cortex neurons. *J Neurophysiol*. 1985;53(4):926-39.
57. Jorgensen S, Nielsen EO, Peters D, Dyhring T. Validation of a fluorescence-based high-throughput assay for the measurement of neurotransmitter transporter uptake activity. *J Neurosci Methods*. 2008;169(1):168-76.
58. Jurcik A, Bednar D, Byska J, Marques SM, Furmanova K, Daniel L, et al. CAVER Analyst 2.0: analysis and visualization of channels and tunnels in protein structures and molecular dynamics trajectories. *Bioinformatics*. 2018;34(20):3586-8.
59. Tian W, Chen C, Lei X, Zhao J, Liang J. CASTp 3.0: computed atlas of surface topography of proteins. *Nucleic Acids Res*. 2018;46(W1):W363-W7.

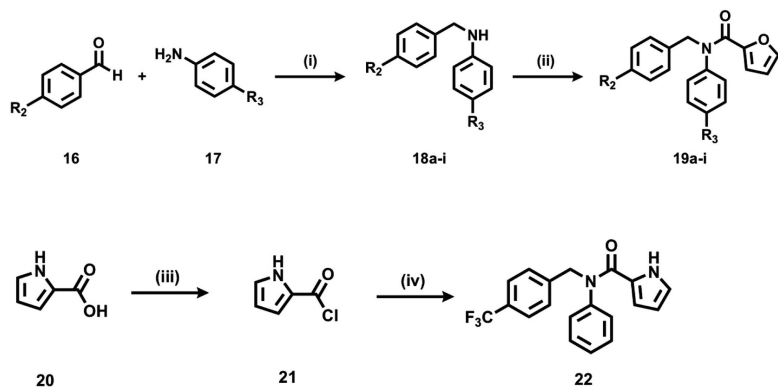
Supplemental Information

Supplement Figures

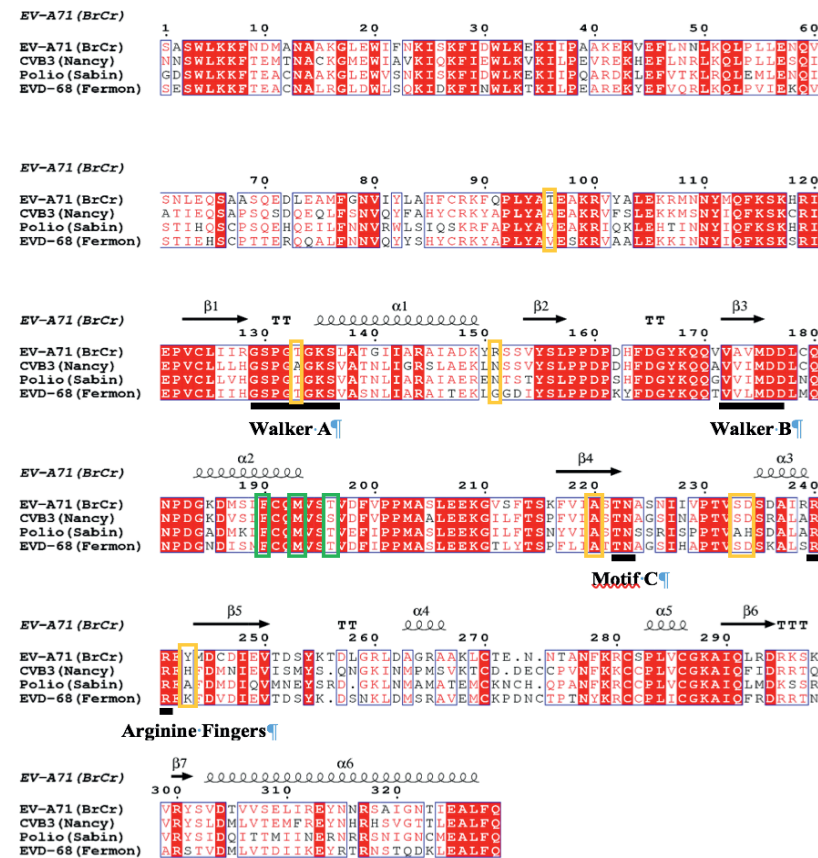


Supplementary Figure 1. Synthesis routes of compound 1 analogues to explore the furan ring and the amide bond. Synthetic route a): (i) NaBH₄, MeOH/THF (4:1), rt, 6 h, quantitative; (ii) Compounds 5a–5d: corresponding acyl chloride or sulphonyl chloride, TEA, DCM, rt, 3h, 63%–98%; Compounds 1, 5e–f: corresponding carboxylic acids, TBTU, DIPEA, DMF, rt, on, 37%–69%; Compounds 5g: Na(AcO)₃BH, MeOH, rt, on, 30%; (iii) 2-bromoacetyl chloride, TEA, DCM, rt, 1h, 68%; (iv) methylamine, EtOH, rt, on, 66%; Synthetic route b): (i) K₂CO₃, benzyl bromide, DMF, rt, 18h 68%; (ii) Boc, DMAP, TEA, THF, rt, 18h, 90%; (iii) Pd/C 10%, H₂ atmosphere, EtOAc/MeOH (1:1, rt, 20h, 93%; (iv) compound 4 or compound 18b, TBTU, DIPEA, DMF, 45 °C, 48-72h, 79%-45%; (v) DCM/TFA (1:1), rt, 4h, 91%-89%. Synthetic route c): (i) NaBH₄, MeOH/THF (4:1), rt, 6 h, 88%; (ii) 4-fluorobenzoyl chloride, TEA, DCM, rt, 3h, quantitative.

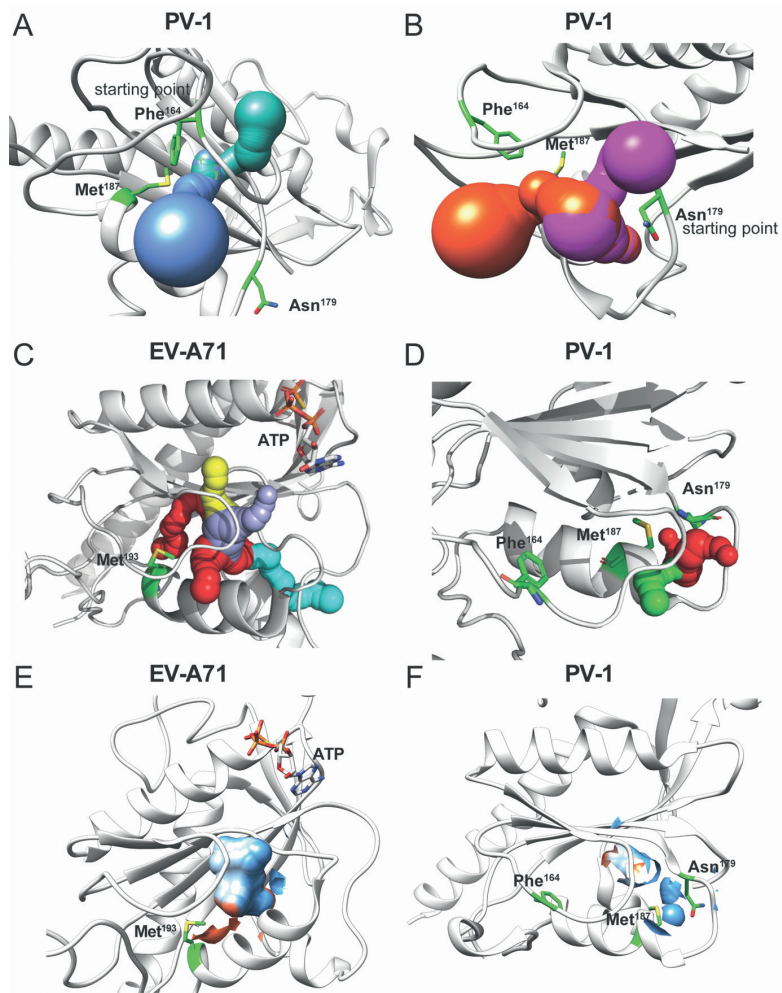
Scheme 2



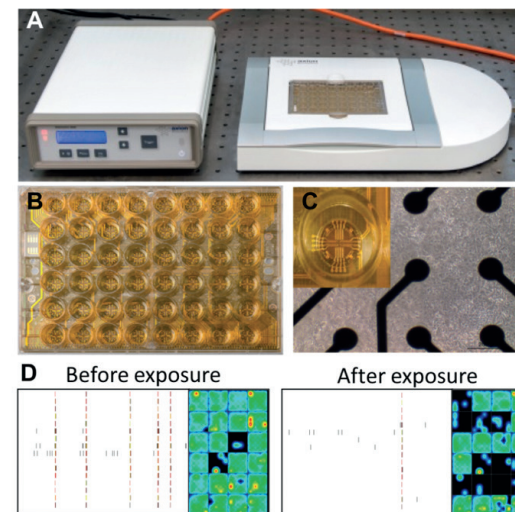
Supplementary Figure 2. Synthesis routes of compound 1 analogues to explore the 4-positions of the N-benzyl aniline moiety. (i) NaBH₄, MeOH/THF (4:1), rt, 6 h, 40%–99%; (ii) furan-2-carbonyl chloride, TEA, DCM, rt, 3 h, Y = 56%–99%; (iii) thionyl chloride, DCM, reflux, 2h; (iv) compound 18d, TEA, DCM, rt, 3h, 75%.



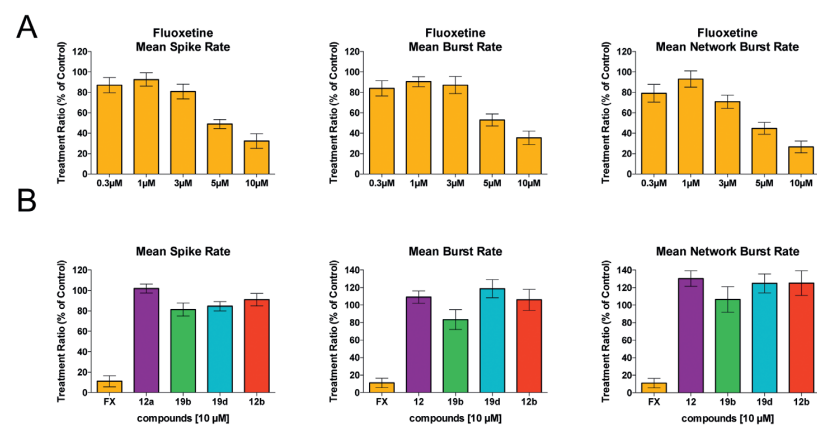
Supplementary Figure 3. Structure-based multiple sequence alignment of 2C proteins. Multiple sequence alignment of EV-A71 (strain BrCr), CV-B3 (strain Nancy), PV (strain Sabin), and EV-D68 (strain Fermon) was performed with Clustal Omega. Invariant amino acids are highlighted in red. Secondary structural elements are shown on top of the alignment and are based on the EV-A71 crystal structure (PDB: 5GRB)¹. Functional motifs are indicated in black. The green box indicates resistance mutations which are located at or close by the $\alpha 2$ helix. The yellow boxes highlight distal mutations.



Supplementary Figure 4. In silico prediction of a possible binding pocket around the $\alpha 2$ helix of 2C. The mole online version ² was used to calculate solvent exposed tunnels in 2C of PV-1 (PDB: 5Z3Q, ref. ³) from different starting points. (A) The starting point for calculation was the amino acid F164, and in (B) the starting point for the tunnel prediction was N179. The Pymol plug-in CAVER 3.0.3 ⁴ was used to calculate solvent accessible tunnel in the nonstructural protein 2C. (A) The EV-A71 2C crystal structure PDB: 5GRB (ref. ¹), chain B was used. The amino acid M193 in the $\alpha 2$ helix of 2C is depicted in green and represents the starting point to identify solvent accessible tunnels. The identified tunnels are shown red, blue, green, and yellow. (B) For PV, the 2C crystal structure 5Z3Q, chain B was used to identify solvent accessible tunnels using the amino acid M187 as starting point. The identified tunnels are depicted in red, green, and blue. The CASTp online tool was used to predict cavities on the protein surfaces of the 2C nonstructural proteins of (C) EV-A71 and (D) PV ⁵. The cavities are highlighted in blue.



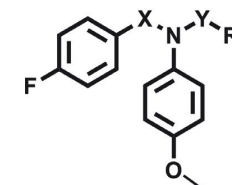
Supplementary Figure 5. Overview of the microelectrode array (MEA) recordings used to measure changes in neuronal activity. Photographs of the Maestro 768-channel amplifier (A) and 48-well MEA plate (B). Each well contains 16 nanotextured gold micro-electrodes on top of which neuronal cells can be cultures for recording of spontaneous electrical activity (C). Baseline activity recorded before exposure (D, left) is compared to activity following exposure to a (inhibitory) test compound (D, right) to determine a TR that describes the changes in neuronal activity due to exposure to the test compounds. Modified after Tukker and colleagues, 2016 ⁶. TR, treatment ratio.



Supplementary Figure 6. Modulation of spontaneous neuronal activity anti-EV inhibitors. (A) Modulation of spontaneous neuronal activity by fluoxetine. Concentration–response curves for inhibition of MSR (left), MBR (middle), and MNBR (right) following acute exposure to fluoxetine. Neuronal activity is depicted as the mean TR \pm SEM as percent of control (DMSO) wells ($n = 12$ – 16 wells, derived from 2 independent cultures, $*P < 0.05$). (B) Modulation of spontaneous neuronal activity by fluoxetine and antiviral compounds. When tested at a single, high concentration (10 μ M), fluoxetine induced a profound inhibition of MSR (left), MBR (middle), and MNBR (right), whereas the antiviral compounds 12a, 12b, 19b, and 19d were without effect. Neuronal activity is depicted as the mean TR \pm SEM as percent of control (DMSO) wells ($n = 8$ – 16 wells, derived from 2 independent cultures, $*P < 0.05$).

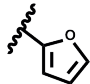
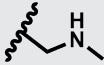
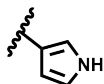
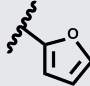
Supplement Table

Supplementary Table 1. Antiviral activity of the furan amide moiety analogues against CV-B3.



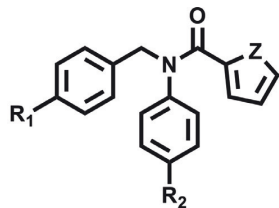
Compound	X	Y	R ₁	EC ₅₀ (μM)	CC ₅₀ (μM)
1	CH ₂	CO		1.92 \pm 0.04	>30
5a	CH ₂	CO		>30	>30
5b	CH ₂	SO ₂		>30	>30
5c	CH ₂	CO		3.01 \pm 0.2	>30
5d	CH ₂	CO		0.51 \pm 0.04	>30
5e	CH ₂	CO		6.44 \pm 0.42	>30
5f	CH ₂	CO		>30	>30



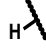

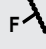

Supplementary Table 1. Continued

Compound	X	Y	R ₁	EC ₅₀ (μ M)	CC ₅₀ (μ M)
5g	CH ₂	CH ₂		>30	>30
6	CH ₂	CO		>30	>30
12a	CH ₂	CO		0.08 \pm 0.02	>30
15	C=O	CH ₂		>30	>30

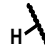

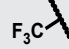

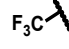
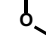
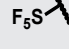
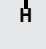



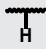
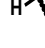
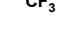

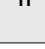
Multicycle viral replication assays were performed in HeLa R19 cells, and shown are EC₅₀ and CC₅₀ values in μ M. Data represent mean \pm SD calculated from two different experiments both performed in biological triplicates.

Supplementary Table 2. Antiviral activity of the N-benzylaniline moiety analogues against CV-B3.



Compound	R ₁	R ₂	Z	EC ₅₀ (μ M)	CC ₅₀ (μ M)
1			O	1.92 \pm 0,28	>30
19a			O	0.91 \pm 0.03	>30
19b			O	0.83 \pm 0.10	>30

Supplementary Table 2. Continued

Compound	R ₁	R ₂	Z	EC ₅₀ (μ M)	CC ₅₀ (μ M)
19c			O	4.07 \pm 0.25	>30
19d			O	0.79 \pm 0.06	>30
19e			O	0.86 \pm 0.12	>30
19f			O	3.10 \pm 0.42	>30
19g			O	0.88 \pm 0.02	>30
19h			O	7.03 \pm 0.92	>30
19i			O	2.45 \pm 0.10	>30
22			NH	1.50 \pm 0.08	>30

Multicycle viral replication assays were performed in HeLa R19 cells, and shown are EC₅₀ and CC₅₀ values in μ M. Data represents mean \pm SD calculated from two different experiments both performed in biological triplicates.

Supplementary Table 3. Antiviral efficacy against CV-B3 and cytotoxicity of the active compounds in different cell lines.

Compound	Hela		HAP1		BGM				
	EC ₅₀	SI	EC ₅₀	SI	EC ₅₀	SI			
1	1.76 ± 0.11	43.92 ± 3.52	25	1.57 ± 0.08	45.59 ± 0.50	29	1.66 ± 0.23	50.65 ± 0.32	32
5c	4.82 ± 0.14	>100	>20	2.52 ± 0.47	>100	>40	4.18 ± 0.39	>100	>25
5d	0.42 ± 0.11	53.05 ± 1.45	127	0.25 ± 0.08	53.94 ± 0.04	216	0.63 ± 0.14	66.05 ± 1.05	105
5e	8.87 ± 0.45	>100	>12	15.85 ± 1.65	>100	>6	17.82 ± 1.13	>100	>6
12a	0.01 ± 0.01	>100	>1000	0.02 ± 0.02	>100	>3000	0.04 ± 0.02	>100	>2900
19a	1.62 ± 0.37	>100	>50	0.73 ± 0.25	>100	>130	1.84 ± 0.06	>100	>55
19b	0.68 ± 0.22	>100	>150	0.35 ± 0.20	>100	>250	0.14 ± 0.04	>100	>750
19c	4.42 ± 0.36	>100	>23	2.12 ± 0.03	>100	>45	4.30 ± 0.35	>100	>25
19d	0.77 ± 0.14	93.68 ± 1.34	107	0.75 ± 0.06	97.77 ± 0.32	117	0.38 ± 0.06	92.59 ± 1.51	217
19e	0.93 ± 0.06	54.00 ± 1.00	58	2.85 ± 0.71	54.89 ± 0.44	19	2.41 ± 0.36	55.92 ± 0.95	23
19f	3.28 ± 0.74	32.87 ± 2.00	10	2.10 ± 0.20	62.54 ± 1.55	30	2.60 ± 0.38	31.92 ± 1.41	12
19g	1.36 ± 0.35	>100	>75	2.38 ± 0.30	>100	>35	1.70 ± 0.26	>100	>60
19h	7.62 ± 0.93	42.75 ± 1.75	6	4.13 ± 0.15	48.74 ± 0.35	12	>100	46.83 ± 1.48	ND
19i	2.75 ± 0.25	68.53 ± 0.47	25	1.75 ± 0.29	>100	>55	1.71 ± 0.28	55.40 ± 0.05	32
22	2.60 ± 0.09	>100	>40	2.69 ± 0.19	>100	>35	2.28 ± 0.27	>100	>45

Multicycle viral replication assay was performed in HeLa R19, HAP1, and BGM cells. Shown are EC₅₀ and CC₅₀ values in μM. Data represent mean ± SD calculated from two independent experiments both performed in biological triplicates. SI = selectivity index (CC50/EC50).

Supplementary Table 4. Primers used for site-directed mutagenesis.

Virus	2C mutations		5'-3' sequence
CVB3	H234R	FW	AAGGAGATTTcgCTTTGACATGAAC
		REV	GCCAAGGCTCTGCTATCT
EV-A71	M193L	FW	ATTTTGTCAActgGTTTCTACAGTAG
		REV	AGGGACATGTCTTTTCCG
	R151H	FW	TGACAAGTAcacTCTAGTGATAC
		REV	GCAATGGCTCTAGCTATAATG
	T133S	FW	TTCCCCAGGAtcgGGCAAATCGC
		REV	CCTCTGATGATCAAGCATAACAGTTTC
EVD-68	V96M	FW	ACTTTACGCAatgGAATCAAAAAG
		REV	GGTGCCTACTTCTACAG
	T196S	FW	TTCCCCAGGAtcgGGCAAATCGC
		REV	CCTCTGATGATCAAGCATAACAGTTTC

Primers used for introducing mutations in CV-B3, EV-A71, and EV-D68. Mutations introduced are shown in small characters in the primer sequence.

Chemical Synthesis

Synthesis of compound 1 analogues

Different structural modifications of compound **1** were planned in order to investigate whether its antiviral activity could be enhanced and its antiviral spectrum could be broadened. An initial effort was focused on replacing the original furan with different heteroaromatic rings and diverse heterocyclic/aliphatic groups (Fig 1B). The role of the amide bond was also explored by replacing it with either a sulfonamide bond or a methylene bridge. Different substituents on the 4-position on both rings of the *N*-benzylaniline moiety were also investigated (Fig 1C). Preparation of compound **1** analogues, in which the furan ring and the amide bond were modified, was performed through an efficient two-step synthetic pathway in which compound **4**, prepared by reductive amination between 4-fluorobenzaldehyde **2** and *p*-anisidine **3**, was used as common synthetic intermediate. Derivatives **5a-d** were synthesized reacting **4** with different acyl or sulfonyl chloride in dichloromethane using trimethylamine as base. Compound **1** and derivatives **5e** and **5f**, presenting a pyridine and a tetrahydrofuran ring in place of furan respectively, were obtained through an amide coupling reaction between **4** and the corresponding carboxylic acid in dimethylformamide, using DIPEA as base and TBTU as coupling agent, Reductive amination between **4** and furan-2-carbaldehyde yield compound **5g**, whereas preparation of compound **6** was achieved by two steps: amide bond formation reacting **4** and 2-bromoacetyl chloride, followed by nucleophilic displacement of the bromine atom by methyl amine. Different attempts

were made for the preparation of compounds **12a-b**, in which the *N*-(4-fluoro)benzylaniline portion is bound to position three of a pyrrole ring. Coupling reaction either using TBTU or CDI as coupling agent did not give the desired product, with formation of several undesired species. After failing in converting the pyrrole-3-carboxylic acid to the corresponding acyl chloride using thionyl chloride in dichloromethane, a different approach was applied as reported in S1_Fig route **b**. The pyrrole-3-carboxylic acid nitrogen was selectively Boc-protected through a 3-step synthesis, and the resulting compounds **10a-b** were then converted into **11a-b** via TBTU-assisted coupling reaction. Removal of the Boc protecting group using TFA in dichloromethane gave compounds **12a-b** in a very high yield. Reductive amination between 4-methoxyaniline **3** and furan-2-carbaldehyde **13**, followed by the reaction with 4-fluorobenzoyl chloride gave the final product **15** in a quantitative yield. Analogues **19a-i**, bearing different substituents in 4-position of the *N*-benzylaniline moiety, were prepared following the same synthetic pathway adopted for derivatives **5a-d**. Reductive amination between differently substituted benzaldehydes and anilines yielded the intermediates **18a-l** in a high yield, which were then converted into the corresponding final compounds **19a-i** by reaction with furan-2-carbonyl chloride in dichloromethane and trimethylamine as base. 1*H*-pyrrole-2-carbonyl chloride **21**, required for the preparation of compound **22**, was prepared *in situ* by refluxing 1*H*-pyrrole-2-carboxylic acid **20** with thionyl chloride, as reported in S2 Fig.

General chemistry methods

All solvents and reagents used were obtained from commercial sources unless otherwise indicated. All reactions were performed under a nitrogen atmosphere. ¹H, ¹³C and ¹⁹F NMR spectra were recorded with a Bruker Avance III HD spectrometer operating at 500 MHz for ¹H, 125 MHz for ¹³C and 470 MHz for ¹⁹F with Me₄Si as internal standard. Deuterated dimethyl sulfoxide (DMSO) and deuterated chloroform (CDCl₃) were used as solvents for NMR experiments, unless otherwise stated. ¹H chemical shifts values (δ) are referenced to the residual non-deuterated components of the NMR solvents (δ = 2.50 ppm for DMSO and 7.26 for CHCl₃). Thin layer chromatography (TLC) was performed on Silica gel plates (Merck Kieselgel 60 F254), which were developed by the ascending method. Column chromatography was performed on an Isolera Biotage system. UPLC-UV-MS analysis was conducted on a Waters UPLC system with both Diode Array detection and Electrospray (+ve and -ve ion) MS detection. The following conditions were applied: Waters Acquity UPLC BEH C18 1.7 μm 2.1x50 mm column, 0.5 mL/min, column temperature 40°C; mobile phase was LC-MS grade H₂O containing 0.1% formic acid (A) and LC-MS grade MeCN containing 0.1% formic acid (B); sample diluent: MeCN; sample concentration: 1 μg/mL; injection volume: 2 μL, gradient 90% eluent A (0.1 min), 90%-0% eluent A (1.5 min), 0% eluent A (1.4 min), 90% eluent A (0.1 min) (method 1).

All compounds tested in biological assays were >95% pure. Purity of intermediates was >90%, unless otherwise stated.

General procedure A: Reductive amination for the preparation of compounds **4**, **14**, **18a-i**

A solution of the corresponding aniline (1.1 equiv) in a mix of anhydrous methanol (24 mL) and anhydrous tetrahydrofuran (6 mL) was treated with the corresponding benzaldehyde (1 equiv) under nitrogen atmosphere. The reaction was stirred at room temperature for 6 hours. The mixture was then cooled to 0°C and sodium borohydride (2 equiv) was added in small portions. The reaction was stirred at room temperature overnight. The reaction was concentrated under reduced pressure and the crude product was purified by automated flash column chromatography (*n*-hexane:EtOAc 100:0 v/v increasing to 60:40 v/v).

N-(4-Fluorobenzyl)-4-methoxyaniline (**4**)

Reagents: *p*-anisidine and 4-fluorobenzaldehyde. Yield quantitative, brown solid. ¹H-NMR (CDCl₃): δ 7.37-7.32 (m, 2H, H-aromatic), 7.03 (apparent t, J₁=8.7 Hz, 2H, H-aromatic), 6.79 (d, J=9.0 Hz, 2H, H-aromatic), 6.60 (d, J=9.0 Hz, 2H, H-aromatic), 4.26 (s, 2H, CH₂), 3.78 (bs, 1H, NH), 3.75 (s, 3H, CH₃). This compound was previously reported and the spectral data agree with those specified in literature.³

N-(Furan-2-ylmethyl)-4-methoxyaniline (**14**)

Reagents: *p*-anisidine and furfural. Yield 88%, orange waxy solid. ¹H-NMR (CDCl₃): δ 7.36 (dd, J₁=1.8 Hz, J₂=0.8 Hz, 1H, H-aromatic), 6.79 (d, J=9.0 Hz, 2H, H-aromatic), 6.65 (d, J=9.0 Hz, 2H, H-aromatic), 6.31 (dd, J₁=3.1 Hz, J₂=1.8 Hz, 1H, H-aromatic), 6.21 (dd, J₁=3.1 Hz, J₂=0.8 Hz, 1H, H-aromatic), 4.27 (s, 2H, CH₂), 3.76 (bs, 1H, NH), 3.74 (s, 3H, CH₃). This compound was previously reported and the spectral data agree with those specified in literature.⁴

N-Benzylaniline (**18a**)

Reagents: aniline and benzaldehyde. Yield 96%, white waxy solid. ¹H-NMR (CDCl₃): δ 7.40-7.34 (m, 4H, H-aromatic), 7.29 (tt, J₁=7.1 Hz, J₂=1.6 Hz, 1H, H-aromatic), 7.21-7.17 (m, 2H, H-aromatic), 6.74 (tt, J₁=7.1 Hz, J₂=1.1 Hz, 1H, H-aromatic), 6.67-6.64 (m, 2H, H-aromatic), 4.35 (s, 2H, CH₂), 4.03 (bs, 1H, NH). This compound was previously reported and the spectral data agree with those specified in literature.⁵

N-(4-Fluorobenzyl)aniline (**18b**)

Reagents: aniline and 4-fluorobenzaldehyde. Yield 40%, dark orange oil. ¹H-NMR (CDCl₃): δ 7.36-7.32 (m, 2H, H-aromatic), 7.18 (dd, J₁=8.6 Hz, J₂=7.3 Hz, 2H, H-aromatic), 7.06-7.00 (m, 2H, H-aromatic), 6.74 (tt, J₁=7.7 Hz, J₂=7.3 Hz, 1H, H-aromatic), 6.65-6.62

(m, 2H, H-aromatic), 4.31 (s, 2H, CH₂), 4.01 (bs, 1H, NH). This compound was previously reported and the spectral data agree with those specified in literature.⁵

***N*-Benzyl-4-methoxyaniline (18c)**

Reagents: *p*-anisidine and benzaldehyde. Yield 99%, yellow solid. ¹H-NMR (CDCl₃): δ 7.41-7.31 (m, 4H, H-aromatic), 7.27 (tt, J₁=7.9 Hz, J₂=7.1 Hz, 1H, H-aromatic), 6.82-6.74 (m, 2H, H-aromatic), 6.65-6.58 (m, 2H, H-aromatic), 4.29 (s, 2H, CH₂), 3.78 (bs, 1H, NH), 3.74 (s, 3H, CH₃). This compound was previously reported and the spectral data agree with those specified in literature.⁵

***N*-(4-(trifluoromethyl)benzyl)aniline (18d)**

Reagents: aniline and 4-trifluoromethylbenzaldehyde. Yield 94%, pale-yellow oil. ¹H-NMR (CDCl₃): δ 7.59 (d, J=8.2 Hz, 2H, H-aromatic), δ 7.49 (d, J=8.2 Hz, 2H, H-aromatic), δ 7.20-7.16 (m, 2H, H-aromatic), δ 6.74 (tt, J₁=7.3 Hz, J₂=1.06 Hz, 1H, H-aromatic), δ 4.42 (s, 2H, CH₂), δ 4.15 (s, 1H, NH). This compound was previously reported and the spectral data agree with those specified in literature.⁶

4-Methoxy-*N*-(4-(trifluoromethyl)benzyl)aniline (18e)

Reagents: *p*-anisidine and 4-trifluoromethylbenzaldehyde. Yield 92%, pale-yellow oil. ¹H-NMR (CDCl₃): δ 7.58 (d, J=8.0 Hz, 2H, H-Aromatic), δ 7.47 (d, J=8.0 Hz, 2H, H-Aromatic), δ 6.77 (d, J=8.9 Hz, 2H, H-Aromatic), δ 6.57 (d, J=8.9 Hz, 2H, H-Aromatic), δ 4.36 (s, 2H, CH₂), δ 3.88 (bs, 1H, NH), δ 3.74 (s, 3H, CH₃). This compound was previously reported and the spectral data agree with those specified in literature.⁷

***N*-(4-(Pentafluorosulfaneyl)benzyl)aniline (18f)**

Reagents: aniline and 4-pentafluorosulfanylbenzaldehyde. Yield 74%, pale-yellow oil. ¹H-NMR (CDCl₃): δ 7.72 (d, J=8.7 Hz, 2H, H-Aromatic), δ 7.46 (d, J=8.7 Hz, 2H, H-Aromatic), 7.21-7.16 (m, 2H, H-Aromatic), 6.77-6.74 (m, 1H, H-Aromatic), δ 6.60 (d, J=7.6 Hz, 2H, H-Aromatic), δ 4.42 (s, 2H, CH₂), δ 4.14 (bs, 1H, NH). ¹³C-NMR (CDCl₃): δ 152.7-152.6 (m, C), 147.5 (C), 143.7 (C), 129.3 (CH), 127.2 (CH), 126.3-126.2 (m, CH), 118.1 (CH), 112.9 (CH), 47.4 (CH₂). ¹⁹F-NMR (CDCl₃): δ 63.1(d, J=150.0 Hz, 4F), 84.8 (q, J=147.4 Hz, 1F).

***N*-(4-Methylbenzyl)aniline (18g)**

Reagents: aniline and *p*-tolualdehyde. Yield 94%, white solid. ¹H-NMR (CDCl₃): δ 7.28 (d, J=7.9 Hz, 2H, H-aromatic), 7.21-7.15 (m, 4H, H-aromatic), 6.73 (tt, J₁=7.6 Hz, J₂=7.3 Hz, 1H, H-aromatic), 6.67-6.28 (m, 2H, H-aromatic), 4.29 (s, 2H, CH₂), 3.98 (bs, 1H, NH), 2.36 (s, 3H, CH₃). This compound was previously reported and the spectral data agree with those specified in literature.⁵

***N*-(4-Isopropylbenzyl)aniline (18h)**

Reagents: aniline and 4-isopropylbenzaldehyde. Yield 97%, yellow oil. ¹H-NMR (CDCl₃): 7.34-7.28 (m, 2H, H-aromatic), 7.24-7.14 (m, 4H, H-aromatic), 6.75-6.69 (m, 1H,

H-aromatic), 6.65 (d, J=8.2 Hz, 2H, H-aromatic), 4.29 (s, 2H, CH₂), 3.98 (bs, 1H, NH), 2.97-2.85 (m, 1H, CH), 1.26 (dd, J₁=6.9 Hz, J₂=0.7 Hz, 6H, 2 · CH₃). This compound was previously reported and the spectral data agree with those specified in literature.⁸

***N*-benzyl-4-(trifluoromethyl)aniline (18i)**

Reagents: benzaldehyde and 4-trifluoromethylaniline. Yield 43%, white solid. ¹H-NMR (DMSO-d₆): δ 7.39 – 7.29 (m, 6H, H-aromatic), 7.27 – 7.22 (m, 1H, H-aromatic), 6.99 (t, J = 6.0 Hz, 1H, H-aromatic), 6.67 (d, J = 8.6 Hz, 2H, H-aromatic), 4.33 (d, J = 6.0 Hz, 2H, CH₂). ¹³C NMR (DMSO-d₆): δ 152.07 (C), 139.85 (C), 128.86 (CH), 127.59 (CH), 127.56 (C), 127.28 (CH), 126.65 (q, J_{C-F} = 3.8 Hz, C), 112.06 (CH), 46.33 (CH₂). ¹⁹F NMR (DMSO-d₆): δ -58.88 (s, 3F).⁹

General procedure B: Preparation of compounds 5a-d, 15, 19a-19i, 22

The corresponding compound prepared using general procedure A (1 equiv) was dissolved using dry DCM (12 mL). Triethylamine (2 equiv) was added to the mixture and the reaction cooled to 0°C. The corresponding acyl or sulphonyl chloride (1.6 equiv) was added drop-wise and the reaction mixture was allowed to warm to room temperature and then left stirring for 3 hours. After completion, the reaction mixture was concentrated under reduced pressure and purified by automated flash column chromatography.

***N*-(4-fluorobenzyl)-*N*-(4-methoxyphenyl)acetamide (5a)**

Purification by automated flash column chromatography (*n*-hexane:EtOAc 100:0 v/v increasing to 60:40 v/v). Yield: 83%, colourless oil. ¹H-NMR (DMSO-d₆): δ 7.20 (dd, J₁ = 8.5 Hz, J₂ = 5.7 Hz, 2H, H-aromatic), 7.10 (t, J = 8.9 Hz, 2H, H-aromatic), 7.06 (d, J = 8.9 Hz, 2H, H-aromatic), 6.91 (d, J = 8.9 Hz, 2H, H-aromatic), 4.78 (s, 2H), 3.73 (s, 3H), 1.79 (s, 3H). ¹³C-NMR (DMSO-d₆): δ 170.0 (C), 161.7 (d, J_{C-F} = 242.6 Hz, C), 158.7 (C), 135.6 (C), 134.4 (d, J_{C-F} = 3.0 Hz, C), 130.5 (d, J_{C-F} = 8.1 Hz, CH), 129.6 (CH), 115.4 (CH), 115.0 (d, J_{C-F} = 21.2 Hz), 55.7 (CH₃), 51.5 (CH₂), 22.7 (CH₃). ¹⁹F-NMR (DMSO-d₆): δ -115.7 (s, 1F). **UPLC-MS:** Rt: 1.81 min, MS (ESI)⁺: 274.1[M+1]⁺.

***N*-(4-fluorobenzyl)-*N*-(4-methoxyphenyl)furan-2-sulfonamide (5b)**

Purification by automated flash column chromatography (*n*-hexane:EtOAc 100:0 v/v increasing to 70:30 v/v). Yield: 99%, white solid. ¹H-NMR (DMSO-d₆): δ 8.09 (dd, J₁ = 1.8 Hz, J₂ = 0.9 Hz, 1H, H-aromatic), 7.29 – 7.24 (m, 2H, H-aromatic), 7.15 – 7.08 (m, 3H, H-aromatic), 6.97 – 6.93 (m, 2H, H-aromatic), 6.85 – 6.81 (m, 2H, H-aromatic), 6.75 (dd, J₁ = 3.5 Hz, J₂ = 1.8 Hz, 1H, H-aromatic), 4.81 (s, 2H, CH₂), 3.70 (s, 3H, CH₃). ¹³C-NMR (DMSO-d₆): δ 162.2 (d, J_{C-F} = 243.5 Hz, C), 159.1 (C), 148.2 (CH), 147.4 (C), 132.8 (d, J_{C-F} = 3.0 Hz, C), 130.8 (C), 130.7 (d, J_{C-F} = 8.3 Hz, CH), 130.5 (CH), 118.1 (CH), 115.7 (d, J_{C-F} = 21.4

H₂, 114.7 (CH), 112.2 (CH), 55.7 (CH₃), 54.2 (CH₂). ¹⁹F-NMR (DMSO-d₆): δ -114.88 (s, 1F). **UPLC-MS**: Rt: 1.98 min, MS (ESI)⁺: 362.3[M+1]⁺.

***N*-(4-fluorobenzyl)-*N*-(4-methoxyphenyl)-1H-pyrrole-2-carboxamide (5c)**

Purification by automated flash column chromatography (*n*-hexane:EtOAc 100:0 v/v increasing to 70:30 v/v). Yield: 63%, white solid. ¹H-NMR (DMSO-d₆): δ 11.53 (s, 1H, H-aromatic), 7.28 (dd, J₁ = 8.7 Hz, J₂ = 5.6 Hz, 2H, H-aromatic), 7.12 (t, J = 8.7 Hz, 2H, H-aromatic), 7.02 (d, J = 9.0 Hz, 2H, H-aromatic), 6.93 (d, J = 9.0 Hz, 2H, H-aromatic), 6.80 (td, J₁ = 2.8 Hz, J₂ = 1.4 Hz, 1H, H-aromatic), 5.81 (dt, J₁ = 3.8 Hz, J₂ = 2.5 Hz, 1H, H-aromatic), 4.92 (s, 2H, CH₂), 4.80 (td, J₁ = 3.7 Hz, J₂ = 1.4 Hz, 1H, H-aromatic), 3.76 (s, 3H, CH₃). ¹³C-NMR (DMSO-d₆): δ 161.7 (d, J_{C-F} = 242.6 Hz, C) (C), 161.4 (C), 159.1 (C), 135.6 (C), 134.6 (d, J_{C-F} = 2.9 Hz, C), 130.7 (d, J_{C-F} = 8.2 Hz, CH), 130.4 (CH), 124.9 (C), 122.0 (CH), 115.5 (d, J_{C-F} = 21.3 Hz, CH), 115.0 (CH), 113.7 (CH), 109.2 (CH), 55.7 (CH₃), 52.91 (CH₂). ¹⁹F-NMR (DMSO-d₆): δ -115.63 (s, 1F). **UPLC-MS**: Rt: 1.92 min, MS (ESI)⁺: 325.2[M+1]⁺.

***N*-(4-Fluorobenzyl)-*N*-(4-methoxyphenyl)thiophene-2-carboxamide (5d)**

Purification by automated flash column chromatography (*n*-hexane:EtOAc 100:0 v/v increasing to 40:60 v/v). Yield 79%, solid. ¹H-NMR (CDCl₃): δ 7.30 (dd, J₁ = 4.9 Hz, J₂ = 1.2 Hz, 1H, H-aromatic), 7.26-7.22 (m, 2H, H-aromatic), 6.97-6.91 (m, 4H, H-aromatic), 6.85-6.82 (m, 3H, H-aromatic), 6.81-6.79 (m, 1H, H-aromatic), 4.96 (s, 2H, CH₂), 3.81 (s, 3H, CH₃). ¹³C-NMR (CDCl₃): δ 163.2-162.2 (d, J_{C-F} = 246.5 Hz, C), 162.4 (C=O), 159.5 (C), 137.9 (C), 134.8 (C), 133.1 (C), 132.7 (CH), 131.1 (CH), 130.9-130.8 (d, J_{C-F} = 8.1 Hz, CH), 130.3 (CH), 126.7 (CH), 115.3-115.1 (d, J_{C-F} = 21.3 Hz, CH), 114.7 (CH), 55.4 (CH₃), 54.0 (CH₂). ¹⁹F-NMR (CDCl₃): δ -114.9 (s, 1F). **UPLC-MS**: Rt: 1.99 min, MS (ESI)⁺: 342.2 [M+H]⁺.

4-Fluoro-*N*-(furan-2-ylmethyl)-*N*-(4-methoxyphenyl)benzamide (15)

Purification by automated flash column chromatography (*n*-hexane:DCM 75:25 v/v increasing to 0:100 v/v). Yield quantitative, orange oil. ¹H-NMR (CDCl₃): δ 7.34 (dd, J₁ = 1.8 Hz, J₂ = 0.8 Hz, 1H, H-aromatic), 7.34-7.28 (m, 2H, H-aromatic), 6.89-6.81 (m, 4H, H-aromatic), 6.69 (d, J = 8.9 Hz, 2H, H-aromatic), 6.28 (dd, J₁ = 3.2 Hz, J₂ = 1.8 Hz, 1H, H-aromatic), 6.22 (collapsed, 1H, H-aromatic), 5.01 (s, 2H, CH₂), 3.73 (s, 3H, CH₃). ¹³C-NMR (CDCl₃): δ 169.3 (C=O), 163.1 (d, J_{C-F} = 250.2 Hz, C), 158.2 (C), 150.7 (C), 142.1 (CH), 136.0 (m, C), 131.8 (d, J_{C-F} = 3.3 Hz, C), 131.0 (d, J_{C-F} = 8.5 Hz, CH), 128.9 (CH), 114.7 (d, J_{C-F} = 21.7 Hz), 114.3 (CH), 110.4 (CH), 109.1 (CH), 55.3 (CH₃), 46.9 (CH₂). ¹⁹F-NMR (CDCl₃): δ -114.9 (s, 1F). **UPLC-MS**: Rt: 1.91 min, MS (ESI)⁺: 326.2 [M+H]⁺.

***N*-Benzyl-*N*-phenylfuran-2-carboxamide (19a)**

Purification by automated flash column chromatography (*n*-hexane:EtOAc 100:0 v/v increasing to 0:100 v/v). Yield 84%, white solid. ¹H-NMR (CDCl₃): δ 7.33-7.29 (m, 4H, H-aromatic), 7.29-7.26 (m, 4H, H-aromatic), 7.25-7.21 (m, 1H, H-aromatic), 7.04-6.99 (m,

2H, H-aromatic), 6.17 (dd, J₁ = 3.5 Hz, J₂ = 1.7 Hz, 1H, H-aromatic), 5.72 (d, J = 3.5 Hz, 1H, H-aromatic), 5.04 (s, 2H, CH₂). ¹³C-NMR (CDCl₃): δ 159.0 (C=O), 146.8 (C), 144.3 (CH), 142.3 (C), 137.0 (C), 129.3 (CH), 128.8 (CH), 128.4 (CH), 128.3 (CH), 127.9 (CH), 127.3 (CH), 116.4 (CH), 110.8 (CH), 53.9 (CH₂). **UPLC-MS**: Rt: 2.21 min, MS (ESI)⁺: 278.1 [M+H]⁺.

***N*-(4-Fluorobenzyl)-*N*-phenylfuran-2-carboxamide (19b)**

Purification by automated flash column chromatography (*n*-hexane:EtOAc 100:0 v/v increasing to 0:100 v/v). Yield 92%, white solid. ¹H-NMR (CDCl₃): δ 7.35-7.30 (m, 4H, H-aromatic), 7.25-7.21 (m, 2H, H-aromatic), 7.05-6.97 (m, 2H, H-aromatic), 6.99-6.94 (m, 2H, H-aromatic), 6.17 (dd, J₁ = 3.5 Hz, J₂ = 1.7 Hz, 1H, H-aromatic), 5.71 (d, J = 3.4 Hz, 1H, H-aromatic), 5.00 (s, 2H, CH₂). ¹³C-NMR (CDCl₃): δ 162.2 (d, J_{C-F} = 245.7 Hz, C), 159.1 (C=O), 146.8 (C), 144.5 (CH), 142.1 (C), 132.8 (d, J_{C-F} = 3.2 Hz, C), 130.7 (d, J_{C-F} = 8.1 Hz, CH), 129.5 (CH), 128.5 (CH), 128.2 (CH), 116.6 (CH), 115.2 (d, J_{C-F} = 21.3 Hz, CH), 110.0 (CH), 53.3 (CH₂). ¹⁹F-NMR (CDCl₃): δ -114.9 (s, 1F). **UPLC-MS**: Rt: 1.90 min, MS (ESI)⁺: 296.0 [M+H]⁺.

***N*-Benzyl-*N*-(4-methoxyphenyl)furan-2-carboxamide (19c)**

Purification by automated flash column chromatography (*n*-hexane:DCM 75:25 v/v increasing to 0:100 v/v). Yield 90%, white solid. ¹H-NMR (CDCl₃): δ 7.36 (dd, J₁ = 1.7 Hz, J₂ = 0.7 Hz, 1H, H-aromatic), 7.28-7.26 (m, 4H, H-aromatic), 7.25-7.21 (m, 1H, H-aromatic), 6.91 (d, J = 9.0 Hz, 2H, H-aromatic), 6.81 (d, J = 9.0 Hz, 2H, H-aromatic), 6.18 (dd, J₁ = 3.5 Hz, J₂ = 1.7 Hz, 1H, H-aromatic), 5.63 (bs, 1H, H-aromatic), 4.99 (s, 2H, CH₂), 3.80 (s, 3H, CH₃). ¹³C-NMR (CDCl₃): δ 159.3 (C=O), 159.2 (C), 146.9 (C), 144.4 (CH), 137.2 (C), 134.9 (C), 129.7 (CH), 129.1 (CH), 128.3 (CH), 127.4 (CH), 116.4 (CH), 114.5 (CH), 111.0 (CH), 55.4 (CH₃), 54.1 (CH₂). **UPLC-MS**: Rt: 2.17 min, MS (ESI)⁺: 308.1 [M+H]⁺.

***N*-phenyl-*N*-(4-(trifluoromethyl)benzyl)furan-2-carboxamide (19d)**

Purification by automated flash column chromatography (*n*-hexane:EtOAc 100:0 v/v increasing to 70:30 v/v). Yield 88%, yellow solid. ¹H-NMR (DMSO-d₆): δ 7.72 – 7.64 (m, 3H, H-aromatic), 7.50 (d, J = 8.0 Hz, 2H, H-aromatic), 7.41 – 7.30 (m, 3H, H-aromatic), 7.20 (d, J = 7.0 Hz, 2H, H-aromatic), 6.40 (dd, J₁ = 3.5 Hz, J₂ = 1.7 Hz, 1H, H-aromatic), 5.89 (d, J = 3.3 Hz, 1H, H-aromatic), 5.11 (s, 2H, CH₂). ¹³C-NMR (DMSO-d₆): δ 159.1 (C=O), 146.8 (C), 142.5 (C), 129.9 (CH), 129.1 (CH), 128.3 (CH), 128.3 (CH), 125.7 (q, J_{C-F} = 3.7 Hz, CH), 117.0 (CH), 111.8 (CH), 53.1 (CH₂). ¹⁹F-NMR (DMSO-d₆): δ -60.86 (s, 3F). **UPLC-MS**: Rt: 2.03 min, MS (ESI)⁺: 346.2[M+1]⁺.

***N*-(4-Methoxyphenyl)-*N*-(4-(trifluoromethyl)benzyl)furan-2-carboxamide (19e)**

Purification by automated flash column chromatography (*n*-hexane:EtOAc 100:0 v/v increasing to 20:80 v/v). Yield 66%, pale-yellow oil. ¹H-NMR (CDCl₃): δ 7.52 (d, J = 8.2 Hz, 2H, H-aromatic), 7.40 (d, J = 8.2 Hz, 2H, H-aromatic), 7.38-7.37 (m, 1H, H-aromatic), 6.92 (d, J = 8.9 Hz, 2H, H-aromatic), 6.84 (d, J = 8.9 Hz, 2H, H-aromatic), 6.20 (dd, J₁ = 3.5 Hz, J₂ = 1.7 Hz, 1H, H-aromatic), 5.69-5.65 (m, 1H, H-aromatic), 5.04 (s, 2H, CH₂), 3.81 (s,

3H, CH₃). ¹³C-NMR (CDCl₃): δ 159.4 (C), 159.3 (C=O), 146.6 (C), 144.7 (CH), 141.3-141.2 (m, C), 134.7 (C), 129.8 (q, J_{C-F} = 32.3 Hz, C), 129.5 (CH), 129.3 (CH), 125.3 (q, J_{C-F} = 3.7 Hz, CH), 125.2 (q, J_{C-F} = 271.9 Hz, C), 116.7 (CH), 114.7 (CH), 111.1 (CH), 55.4 (CH₃), 53.8 (CH₂). ¹⁹F-NMR (CDCl₃): δ -62.49 (s, 3F). **UPLC-MS**: Rt: 2.02 min, MS (ESI)⁺: 376.3 [M+H]⁺.

N-(4-(Pentafluorosulfaneyl)benzyl)-N-phenylfuran-2-carboxamide (19f)

Purification by automated flash column chromatography (*n*-hexane:DCM 100:0 v/v increasing to 0:100 v/v). Yield 56%, pale-yellow oil. ¹H-NMR (CDCl₃): δ 7.66 (d, J=8.8 Hz, 2H, H-aromatic), 7.40 (d, J=8.8 Hz, 2H, H-aromatic), 7.38-7.35 (m, 3H, H-aromatic), 7.34 (dd, J₁=1.7 Hz, J₂=0.9 Hz, 1H, H-aromatic), 7.08-7.03 (m, 2H, H-aromatic), 6.21 (dd, J₁=3.5 Hz, J₂=1.7 Hz, 1H, H-aromatic), 5.79 (d, J=3.5 Hz, 1H, H-aromatic), 5.06 (s, 2H, CH₂). ¹³C-NMR (CDCl₃): δ 159.3 (C=O), 153.0 (m, C), 146.5 (C), 144.7 (CH), 142.2 (C), 141.0 (C), 129.7 (CH), 129.0 (CH), 128.3 (CH), 128.2 (CH), 126.1-126.0 (m, CH), 117.0 (CH), 111.1 (CH), 53.4 (CH₃). ¹⁹F-NMR (CDCl₃): δ 62.8(d, J=150.0 Hz, 4F), 84.6 (q, J=147.4 Hz, 1F). **UPLC-MS**: Rt: 2.06 min, MS (ESI)⁺: 404.2 [M+H]⁺.

N-(4-Methylbenzyl)-N-phenylfuran-2-carboxamide (19g)

Purification by automated flash column chromatography (*n*-hexane:DCM 75:25 v/v increasing to 0:100 v/v). Yield 67%, white solid. ¹H-NMR (CDCl₃): δ 7.35-7.29 (m, 4H, H-aromatic), 7.16 (d, J=7.9 Hz, 2H, H-aromatic), 7.06 (d, J=7.9 Hz, 2H, H-aromatic), 7.04-6.98 (m, 2H, H-aromatic), 6.17 (dd, J₁=3.5 Hz, J₂=1.7 Hz, 1H, H-aromatic), 5.70 (d, J=3.5 Hz, 1H, H-aromatic), 5.00 (s, 2H, CH₂), 2.30 (s, 3H, CH₃). ¹³C-NMR (CDCl₃): δ 159.1 (C=O), 147.0 (C), 144.4 (CH), 142.4 (C), 137.1 (C), 134.0 (C), 129.3 (CH), 129.0 (CH), 128.9 (CH), 128.5 (CH), 128.0 (CH), 116.4 (CH), 110.9 (CH), 53.7 (CH₂), 21.1 (CH₃). **UPLC-MS**: Rt: 1.98 min, MS (ESI)⁺: 292.0 [M+H]⁺.

N-(4-Isopropylbenzyl)-N-phenylfuran-2-carboxamide (19h)

Purification by automated flash column chromatography (*n*-hexane:DCM 75:25 v/v increasing to 0:100 v/v). Yield 99%, white solid. ¹H-NMR (CDCl₃): δ 7.37-7.28 (m, 4H, H-aromatic), 7.19 (d, J=8.2 Hz, 2H, H-aromatic), 7.12 (d, J=8.2 Hz, 2H, H-aromatic), 7.06-7.00 (m, 2H, H-aromatic), 6.17 (dd, J₁=3.3 Hz, J₂=1.7 Hz, 1H, H-aromatic), 5.71 (d, J=3.3 Hz, 1H, H-aromatic), 5.00 (s, 2H, CH₂), 2.92-2.80 (m, 1H, CH), 1.21 (d, J=6.9 Hz, 6H, 2 · CH₃). ¹³C-NMR (CDCl₃): δ 159.1 (C=O), 148.1 (C), 147.0 (C), 144.3 (CH), 142.6 (C), 134.4 (C), 129.3 (CH), 128.9 (CH), 128.5 (CH), 127.9 (CH), 126.4 (CH), 116.4 (CH), 110.9 (CH), 53.8 (CH₂), 33.8 (CH), 24.0 (2 · CH₃). **UPLC-MS**: Rt: 2.12 min, MS (ESI)⁺: 320.2 [M+H]⁺.

N-benzyl-N-(4-(trifluoromethyl)phenyl)furan-2-carboxamide (19i)

Purification by automated flash column chromatography (*n*-hexane:DCM 100:0 v/v increasing to 0:100 v/v). Yield 99%, yellow solid. ¹H-NMR (DMSO-d₆): δ 8.70 (d, J = 8.4 Hz, 2H, H-aromatic), 7.66 (dd, J₁ = 1.7 Hz, J₂ = 0.8 Hz, 1H, H-aromatic), 7.38 (d, J = 8.2 Hz, 2H, H-aromatic), 7.33 – 7.20 (m, 5H, H-aromatic), 6.47 (dd, J₁ = 3.5 Hz, J₂ = 1.7 Hz, 1H, H-aromatic), 6.35 (dd, J₁ = 3.5 Hz, J₂ = 0.7 Hz, 1H, H-aromatic), 5.10 (s, 2H, CH₂). ¹³C-NMR

(DMSO-d₆): δ 159.1 (C=O), 147.0 (C), 146.4 (C), 145.9 (CH), 137.3 (C), 128.9 (CH), 128.5 (CH), 128.3 (CH), 127.8 (q, J_{C-F} = 32.1 Hz, C), 127.8 (CH), 126.7 (q, J_{C-F} = 3.7 Hz, CH), 124.4 (q, J_{C-F} = 272.2 Hz, C), 117.5 (CH), 112.0 (CH), 53.1 (CH₂). ¹⁹F-NMR (DMSO-d₆): δ -60.81 (s, 3F). **UPLC-MS**: Rt: 2.059 min, MS (ESI)⁺: 346.2[M+1]⁺.

N-Phenyl-N-(4-(trifluoromethyl)benzyl)-1H-pyrrole-2-carboxamide (22)

The required 1H-pyrrole-2-carbonyl chloride (**21**) was prepared *in situ* by refluxing 1H-pyrrole-2-carboxylic acid (**20**) (1 equiv) with thionyl chloride (1 equiv) in dry dichloromethane (6 mL) for two hours. After removing the solvent, the obtained chloride was used without any further purification for the preparation of compound 22. Purification by automated flash column chromatography (*n*-hexane:EtOAc 100:0 v/v increasing to 40:60 v/v). Yield 75%, pale-yellow oil. ¹H-NMR (CDCl₃): δ 9.61 (s, 1H, NH), 7.54 (d, J=8.0 Hz, 2H, H-aromatic), 7.43-7.37 (m, 5H, H-aromatic), 7.12-7.0 (m, 2H, H-aromatic), 6.84-6.83(m, 1H, H-aromatic), 5.92-5.90 (m, 1H, H-aromatic), 5.07 (s, 2H, CH₂), 4.88-4.87 (m, 1H, H-aromatic). ¹³C-NMR (CDCl₃): δ 148.3 (C=O), 142.4 (C), 141.5 (m, C), 129.7 (CH), 129.5 (C), 129.9 (CH), 128.8 (CH), 128.6 (CH), 125.4 (q, J_{C-F} = 3.7 Hz, CH), 125.2 (q, J_{C-F} = 271.1 Hz, C), 124.6 (C), 121.2 (CH), 114.1 (CH), 109.9 (CH), 53.8 (CH₂). ¹⁹F-NMR (CDCl₃): δ -62.48 (s, 3F). **UPLC-MS**: Rt: 2.05 min, MS (ESI)⁺: 345.2 [M+H]⁺.

General procedure C: Preparation of compounds 1, 5e-f

The corresponding compound prepared using general procedure A (1 equiv) and TBTU (1.2 equiv) were suspended in dry DMF (5 mL) under nitrogen atmosphere. The corresponding acid (1.1 equiv) was added. The reaction mixture was cooled to 0° C in an-ice bath and then DIPEA (3.5 equiv) was added. The reaction was stirred at room temperature overnight. After completion, the reaction mixture was concentrated under vacuum and the residue dissolved with EtOAc (35 mL) and washed with HCl 1M (25 mL), NaHCO₃ (25 mL) and brine (25 mL). The organic phase was dried over Na₂SO₄, concentrated under vacuum and the crude product purified by automated flash column chromatography (*n*-hexane:DCM 75:25 v/v increasing to 0:100 v/v).

N-(4-fluorobenzyl)-N-(4-methoxyphenyl)furan-2-carboxamide (1)

Purification by automated flash column chromatography (*n*-hexane:EtOAc 100:0 v/v increasing to 70:30 v/v). Yield 60%, white solid. ¹H-NMR (DMSO-d₆): δ 7.71 – 7.67 (m, 1H, H-aromatic), 7.27 (dd, J₁ = 8.7 Hz, J₂ = 5.6 Hz, 2H, H-aromatic), 7.12 (t, J = 8.7 Hz, 2H, H-aromatic), 7.03 (d, J = 8.9 Hz, 2H, H-aromatic), 6.91 (d, J = 8.9 Hz, 2H, H-aromatic), 6.39 (dd, J₁ = 3.5 Hz, J₂ = 1.7 Hz, 1H, H-aromatic), 5.72 (apparent s, 1H, H-aromatic), 4.93 (s, 2H, CH₂), 3.74 (s, 3H, CH₃). ¹³C-NMR (DMSO-d₆): δ 161.8 (d, J_{C-F} = 242.9 Hz, C), 159.0 (C=O), 158.9 (C), 146.9 (CH), 145.6 (C), 134.9 (C), 133.9 (d, J_{C-F} = 3.0 Hz, C), 130.8 (d, J_{C-F} = 8.2 Hz, CH), 129.8 (CH), 116.6 (CH), 115.6 (d, J_{C-F} = 21.3 Hz, CH), 115.0 (CH), 111.7 (CH), 55.7 (CH₃), 52.8 (CH₂). ¹⁹F-NMR (DMSO-d₆): δ -115.39 (s, 1F). **UPLC-MS**: Rt: 1.92 min, MS (ESI)⁺: 326.2[M+1]⁺, 348.2[M+Na]⁺.

***N*-(4-fluorobenzyl)-*N*-(4-methoxyphenyl)picolinamide (5e)**

Purification by automated flash column chromatography (DCM:MeOH 100:0 v/v increasing to 99:1 v/v). Yield 37%, white solid. ¹H-NMR (DMSO-*d*₆): δ 8.32 (s, 1H, H-aromatic), 7.71 (t, *J* = 6.9 Hz, 1H, H-aromatic), 7.45 (d, *J* = 7.4 Hz, 1H, H-aromatic), 7.33 (dd, *J*₁ = 8.4 Hz, *J*₂ = 5.7 Hz, 2H, H-aromatic), 7.23 (s, 1H, H-aromatic), 7.15 (t, *J* = 8.5 Hz, 2H, H-aromatic), 6.89 (d, *J* = 8.0 Hz, 2H, H-aromatic), 6.67 (d, *J* = 8.0 Hz, 2H, H-aromatic), 5.03 (s, 2H, CH₂), 3.61 (s, 3H, CH₃). ¹³C-NMR (DMSO-*d*₆): δ 168.8 (C=O), 161.8 (d, *J*_{C-F} = 242.9 Hz, C), 157.9 (C), 155.0 (C), 148.7 (CH), 136.9 (CH), 135.0 (C), 133.9 (d, *J*_{C-F} = 3.0 Hz, C), 130.5 (d, *J*_{C-F} = 8.0 Hz, CH), 129.4 (CH), 124.2 (CH), 123.5 (CH), 115.6 (d, *J*_{C-F} = 21.3 Hz, CH), 114.2 (CH), 55.5 (CH₃), 52.0 (CH₂). ¹⁹F-NMR (DMSO-*d*₆): δ -115.44 (s, 1F). **UPLC-MS**: Rt: 1.806 min, MS (ESI)⁺: 337.3[M+1]⁺, 359.3[M+Na]⁺

***N*-(4-Fluorobenzyl)-*N*-(4-methoxyphenyl)tetrahydrofuran-2-carboxamide (5f)**

Yield 69%, yellow oil. ¹H-NMR (CDCl₃): δ 7.14 (dd, *J*₁ = 6.5 Hz, *J*₂ = 5.4 Hz, 2H, H-aromatic), 6.95-6.90 (m, 2H, H-aromatic), 6.85 (d, *J* = 9.0 Hz, 2H, H-aromatic), 6.81 (d, *J* = 9.1 Hz, 2H, H-aromatic), 4.91 (d, *J* = 14.0 Hz, 1H, CH₂), 4.65 (d, *J* = 14.0 Hz, 1H, CH₂), 4.25 (dd, *J*₁ = 11.0 Hz, *J*₂ = 6.0 Hz, 1H, CH₂), 4.08-4.01 (m, 1H, CH₂), 3.85-3.78 (m, 1H, CH), 3.78 (s, 3H, CH₃), 2.08-1.91 (m, 2H, CH₂), 1.85-1.67 (m, 2H, CH₂). ¹³C-NMR (CDCl₃): δ 173.0 (C=O), 162.1 (d, *J*_{C-F} = 245.5 Hz, C), 159.1 (C), 133.6 (C), 133.1 (d, *J*_{C-F} = 3.2 Hz, C), 130.7 (d, *J*_{C-F} = 8.1 Hz, CH), 129.7 (CH), 115.1 (d, *J*_{C-F} = 21.3 Hz, CH), 114.6 (CH), 75.0 (CH), 69.59 (CH₂), 55.4 (CH₃), 52.6 (CH₂), 30.3 (CH₂), 25.9 (CH₂). ¹⁹F-NMR (CDCl₃): δ -115.0 (s, 1F). **UPLC-MS**: Rt: 1.84 min, MS (ESI)⁺: 330.2 [M+H]⁺.

Preparation of *N*-(4-fluorobenzyl)-*N*-(furan-2-ylmethyl)-4-methoxyaniline (5g)

N-(4-fluorobenzyl)-4-methoxyaniline (**4**) (1.8 equiv) was dissolved in methanol:tetrahydrofuran (4:1, 2 mL). Furan-2-carbaldehyde (1 equiv) was added and the mixture was stirred at room temperature for 3 hours. The reaction mixture was cooled to 0°C before adding sodium triacetoxyborohydride (2 equiv). The reaction was allowed to warm-up to room temperature and stirred overnight. After completion, the reaction mixture was concentrated under vacuum, water (30 mL) was added and the mixture was extracted with DCM (3x20 mL). The combined organic layers were washed with brine (3x20 mL), dried over Na₂SO₄ and concentrated under vacuum. The crude product was purified by automated flash column chromatography (*n*-hexane:EtOAc 100:0 v/v increasing to 60:40 v/v).

Yield 30%, yellow oil. ¹H-NMR (DMSO-*d*₆): δ 7.57 (dd, *J*₁ = 1.8 Hz, *J*₂ = 0.8 Hz, 1H, H-aromatic), 7.29 – 7.23 (m, 2H, H-aromatic), 7.11 (ddd, *J*₁ = 9.6, 5.9 Hz, *J*₂ = 2.6 Hz, 2H, H-aromatic), 6.74 (s, 4H, H-aromatic), 6.37 (dd, *J*₁ = 3.2 Hz, *J*₂ = 1.8 Hz, 1H, H-aromatic), 6.25 (dd, *J*₁ = 3.2 Hz, *J*₂ = 0.7 Hz, 1H, H-aromatic), 4.49 (s, 2H, CH₂), 4.47 (s, 2H, CH₂), 3.63 (s, 3H, CH₃). ¹³C-NMR (DMSO-*d*₆): δ 161.5 (d, *J*_{C-F} = 242.0 Hz, C), 152.9 (C), 151.9 (C), 142.7 (C), 142.6 (CH), 135.7 (d, *J*_{C-F} = 2.8 Hz, C), 129.2 (d, *J*_{C-F} = 8.0 Hz, CH), 115.6 (CH), 115.5 (d,

*J*_{C-F} = 21.2 Hz, CH), 114.8 (CH), 110.7 (CH), 108.2 (CH), 55.6 (CH₃), 54.3 (CH₂), 48.6 (CH₂). ¹⁹F-NMR (DMSO-*d*₆): δ -116.47 (s, 1F). **UPLC-MS**: Rt: 2.13, MS (ESI)⁺: 312.1[M+1]⁺.

Preparation of *N*-(4-fluorobenzyl)-*N*-(4-methoxyphenyl)-2-(methylamino)acetamide (6)

2-bromoacetyl chloride (1 equiv) was added drop-wise to a solution of *N*-(4-fluorobenzyl)-4-methoxyaniline (**4**) (1.1 equiv) and TEA (2 equiv) in anhydrous DCM (0.2 M) at 0°C. The resulting mixture was stirred at room temperature for 3 hours. The reaction mixture was diluted in DCM and washed with a 1M HCl solution (20 mL), brine (20 mL), dried over Na₂SO₄ and concentrated under vacuum. The crude product purified by automated flash column chromatography (DCM:MeOH 100:0 v/v increasing to 99:1 v/v).

Yield 87%, yellow oil. ¹H-NMR (DMSO-*d*₆): δ 7.25 – 7.18 (m, 2H, H-aromatic), 7.18 – 7.08 (m, 4H, H-aromatic), 6.95 – 6.84 (m, 2H, H-aromatic), 4.81 (s, 2H, CH₂), 4.04 (s, 2H, CH₂), 3.74 (s, 3H, CH₃).

2-bromo-*N*-(4-fluorobenzyl)-*N*-(4-methoxyphenyl)acetamide (1 equiv) was dissolved in absolute EtOH and methylamine in EtOH (2 equiv) was added. The mixture was stirred at room temperature overnight. The solvent was evaporated under reduced pressure and the crude product was purified by automated flash column chromatography (DCM:MeOH 100:0 v/v increasing to 95:5 v/v).

Yield: 66%, yellow oil. ¹H-NMR (DMSO-*d*₆): δ 7.21 (dd, *J*₁ = 8.5 Hz, *J*₂ = 5.7 Hz, 2H, H-aromatic), 7.11 (t, *J* = 8.9 Hz, 2H, H-aromatic), 7.05 (d, *J* = 8.9 Hz, 2H, H-aromatic), 6.92 (d, *J* = 8.9 Hz, 2H, H-aromatic), 4.81 (s, 2H, CH₂), 3.74 (s, 3H, CH₃), 3.03 (s, 2H, CH₂), 2.22 (s, 3H, CH₃). ¹³C-NMR (DMSO-*d*₆): δ 170.7 (C=O), 161.8 (d, *J*_{C-F} = 242.8 Hz, CH), 159.0 (C), 134.1 (d, *J*_{C-F} = 3.0 Hz, C) 133.9 (C), 130.6 (d, *J*_{C-F} = 8.2 Hz, CH), 129.7 (CH), 115.5 (d, *J*_{C-F} = 21.3 Hz, CH), 115.1 (CH), 55.7 (CH₃), 52.5 (CH₂), 51.8 (CH₂), 35.9 (CH₃). ¹⁹F-NMR (DMSO-*d*₆): δ -115.53 (s, 1F). **UPLC-MS**: Rt: 1.45, MS (ESI)⁺: 303.2[M+1]⁺.

Preparation of Benzyl 1*H*-pyrrole-3-carboxylate (8)

Pyrrole-3-carboxylic acid (**7**) (1 equiv) was dissolved in dimethylformamide (10 mL). K₂CO₃ (1.5 equiv) and benzyl bromide (1.05 equiv) were added and the mixture was stirred eighteen hours at room temperature. After completion, the reaction mixture was concentrated under vacuum, water (30 mL) was added and the mixture was extracted with EtOAc (3x40 mL). The combined organic layers were washed with water (50 mL) and brine (40 mL), dried over MgSO₄ and concentrated under vacuum. The crude product purified by automated flash column chromatography (*n*-hexane:EtOAc 100:0 v/v increasing to 60:40 v/v).

Yield 68%, yellow oil. ¹H-NMR (CDCl₃): δ 8.61 (bs, 1H, NH), 7.48-7.43 (m, 1H, H-aromatic), 7.43-7.40 (m, 2H, H-aromatic), 7.39-7.34 (m, 2H, H-aromatic), 7.33-7.29 (m, 1H, H-aromatic), 6.77-6.73 (m, 1H, H-aromatic), 6.71-6.67 (m, 1H, H-aromatic), 5.29 (s, 2H, CH₂). ¹³C-NMR (CDCl₃): δ 164.8 (C=O), 136.7 (C), 128.5 (CH), 128.0 (CH), 127.9 (CH), 123.7 (CH), 118.8 (CH), 116.3 (C), 109.9 (CH), 65.5 (CH₂).

Preparation of 3-Benzyl 1-(*tert*-butyl) 1*H*-pyrrole-1,3-dicarboxylate (9)

Benzyl 1*H*-pyrrole-3-carboxylate (8) (1 equiv), di-*tert*-butyl dicarbonate (1.15 equiv), 4-Dimethylaminopyridine (0.09 equiv) and triethylamine (1.1 equiv) were dissolved in tetrahydrofuran (10 mL). The mixture was stirred at room temperature for eighteen hours. After completion, the reaction was concentrated under vacuum and the residue was dissolved with EtOAc (70 mL) and the organic layer was washed with HCl 0.1 N (40 mL), water (40 mL) and brine (40 mL). The organic layer was dried over Na₂SO₄, concentrated under vacuum and the crude product purified by automated flash column chromatography (*n*-hexane:EtOAc 100:0 v/v increasing to 60:40 v/v).

Yield 90%, transparent oil. ¹H-NMR (CDCl₃): δ 7.85 (dd, J₁=2.1 Hz, J₂=1.6 Hz, 1H, H-aromatic), 7.44-7.39 (m, 2H, H-aromatic), 7.39-7.35 (m, 2H, H-aromatic), 7.35-7.30 (m, 1H, H-aromatic), 7.20 (dd, J₁=3.3 Hz, J₂=2.1 Hz, 1H, H-aromatic), 6.63 (dd, J₁=3.3 Hz, J₂=1.6 Hz, 1H, H-aromatic), 5.29 (s, 2H, CH₂), 1.60 (s, 9H, 3 · CH₃). ¹³C-NMR (CDCl₃): δ 163.9 (C=O), 148.1 (C=O), 136.3 (C), 128.5 (CH), 128.1 (CH), 125.0 (CH), 120.7 (CH), 119.2 (C), 112.0 (CH), 85.0 (C), 65.9 (CH₂), 27.9 (3 · CH₃).

Preparation of 1-(*tert*-Butoxycarbonyl)-1*H*-pyrrole-3-carboxylic acid (10)

3-Benzyl 1-(*tert*-butyl) 1*H*-pyrrole-1,3-dicarboxylate (9) was dissolved in mixture of ethylacetate:methanol (1:1, 11 mL). Pd/C 10% was added as catalyst and the reaction was stirred for twenty-four hours under H₂ atmosphere. The catalyst was removed by filtration through celite pad, using a mixture of ethylacetate:methanol (1:1) to wash the pad. The filtrate was concentrated under reduced pressure and the crude product purified by automated flash column chromatography (*n*-hexane:EtOAc 100:0 v/v increasing to 0:100 v/v).

Yield 93%, yellow oil. ¹H-NMR (CDCl₃): δ 10.03 (bs, 1H, COOH), 7.90-7.89 (m, 1H, H-aromatic), 7.21 (dd, J₁=3.2 Hz, J₂=2.1 Hz, 1H, H-aromatic), 4.62 (dd, J₁=4.9 Hz, J₂=1.6 Hz, 1H, H-aromatic), 1.61 (s, 9H, 3 · CH₃). ¹³C-NMR (CDCl₃): δ 166.1 (C=O), 148.1 (C=O), 118.8 (CH), 116.1 (CH), 109.8 (C), 103.1 (CH), 84.5 (C), 27.9 (3 · CH₃).

Preparation of *tert*-Butyl-3-((4-fluorobenzyl)(4-methoxyphenyl) carbamoyl)-1*H*-pyrrole-1-carboxylate (11a)

Prepared according to general procedure C. The reaction was left stirring at 45°C for 48 hours. HCl 0.5M (25 mL) was used for the work-up. Purification by automated flash column chromatography (*n*-hexane:EtOAc 100:0 v/v increasing to 50:50 v/v). Yield 79%, orange oil. ¹H-NMR (CDCl₃): δ 7.25-7.21 (m, 2H, H-aromatic), 6.97-6.87 (m, 6H, H-aromatic), 6.82 (d, J=9.0 Hz, 2H, H-aromatic), 5.83 (dd, J₁=3.3 Hz, J₂=1.6 Hz, 1H, H-aromatic), 4.95 (s, 2H, CH₂), 3.79 (s, 3H, CH₃), 1.50 (s, 9H, 3 · CH₃). ¹³C-NMR (CDCl₃): δ 164.3 (C=O), 162.1 (d, J_{C-F}=245.3 Hz, C), 159.1 (C), 148.1 (C), 135.4 (C), 133.4 (d, J_{C-F}=3.2 Hz, C), 130.6 (d, J_{C-F}=8.0 Hz, CH), 129.9 (CH), 124.3 (CH), 122.2 (C), 119.1 (CH), 115.1 (d, J_{C-F}=21.3 Hz, CH), 114.5 (CH), 113.1 (CH), 84.3 (C), 55.4 (CH₃), 53.3 (CH₂), 27.8 (3 · CH₃). ¹⁹F-NMR (CDCl₃): δ -115.0 (s, 1F). UPLC-MS: Rt: 2.53 min, MS (ESI)⁺: 425.3[M+H]⁺.

Preparation of *tert*-Butyl-3-((4-fluorobenzyl)(phenyl)carbamoyl)-1*H*-pyrrole-1-carboxylate (11b)

Prepared according to general procedure C. The reaction was left stirring at 45°C for 72 hours. HCl 0.5M (25 mL) was used for the work-up. Purification by automated flash column chromatography (*n*-hexane:diethylether 100:0 v/v increasing to 60:40 v/v). Yield 45%, orange oil. ¹H-NMR (CDCl₃): δ 7.33-7.30 (m, 3H, H-aromatic), 7.25-7.22 (m, 2H, H-aromatic), 7.03-7.01 (m, 2H, H-aromatic), 6.97-6.92 (m, 3H, H-aromatic), 6.88-6.87 (m, 1H, H-aromatic), 5.82 (dd, J₁=3.3 Hz, J₂=1.6 Hz, 1H, H-aromatic), 5.00 (s, 2H, CH₂), 1.50 (s, 9H, 3 · CH₃). ¹³C-NMR (CDCl₃): δ 165.9 (C=O), 163.1 (d, J_{C-F}=246.3 Hz, C), 148.0 (C), 142.8 (C), 134.2 (C), 133.3 (d, J_{C-F}=3.2 Hz, C), 130.5 (d, J_{C-F}=8.0 Hz, CH), 129.4 (CH), 128.7 (CH), 127.9 (CH), 124.3 (CH), 122.1 (C), 119.0 (CH), 115.1 (d, J_{C-F}=21.3 Hz, CH), 113.0 (CH), 84.4 (C), 53.2 (CH₂), 27.8 (3 · CH₃). ¹⁹F-NMR (CDCl₃): δ -115.2 (s, 1F). UPLC-MS: Rt: 2.58 min, MS (ESI)⁺: 395.0[M+H]⁺.

General procedure D: Preparation of compounds 12a-b

Compounds 11a-b were dissolved in dichloromethane (2.5 mL) and the mixture was cooled to 0°C in an ice-bath. A solution of dichloromethane:trifluoroacetic acid (TFA) (1:1, 2 mL) was added drop-wise and stirring at room temperature for four hours. After completion, the reaction mixture was concentrated under vacuum and the excess of TFA removed by co-evaporation with dichloromethane. The crude compound was purified by cation exchange column chromatography eluting with MeOH and then ammonia (7M in methanol).

N-(4-Fluorobenzyl)-*N*-(4-methoxyphenyl)-1*H*-pyrrole-3-carboxamide (12a)

Yield 91%, brown solid. ¹H-NMR (CDCl₃): δ 8.27 (bs, 1H, NH), 7.26-7.21 (m, 2H, H-aromatic), 6.97-6.90 (m, 4H, H-aromatic), 6.82 (d, J=8.9 Hz, 2H, H-aromatic), 6.58-6.55 (m, 1H, H-aromatic), 6.49 (m, 1H, H-aromatic), 5.86-5.83 (m, 1H, H-aromatic), 4.97 (s, 2H, CH₂), 3.80 (s, 3H, CH₃). ¹³C-NMR (CDCl₃): δ 165.3 (C=O), 162.0 (d, J_{C-F}=242.3 Hz, C), 158.9 (C), 136.1 (C), 133.8 (d, J_{C-F}=3.2 Hz, C), 130.6 (d, J_{C-F}=8.1 Hz, CH), 130.0 (CH), 123.1 (CH), 119.2 (C), 117.3 (CH), 115.1 (d, J_{C-F}=21.2 Hz, CH), 114.4 (CH), 110.8 (CH), 55.4 (CH₃), 53.3 (CH₂). ¹⁹F-NMR (CDCl₃): δ -115.5 (s, 1F). UPLC-MS: Rt: 2.08 min, MS (ESI)⁺: 295.0 [M+H]⁺.

N-(4-Fluorobenzyl)-*N*-phenyl-1*H*-pyrrole-3-carboxamide (12b)

Yield 89%, brown solid. ¹H-NMR (CDCl₃): δ 8.38 (bs, 1H, NH), 7.25-7.15 (m, 5H, H-aromatic), 6.99-6.95 (m, 2H, H-aromatic), 6.89-6.84 (m, H-aromatic), 6.49-6.46 (m, 1H, H-aromatic), 6.40-6.38 (m, 1H, H-aromatic), 5.74-5.71 (m, 1H, H-aromatic), 4.93 (s, 2H, CH₂). ¹³C-NMR (CDCl₃): δ 165.2 (C=O), 163.0 (d, J_{C-F}=245.0 Hz, C), 143.5 (C), 133.7 (d, J_{C-F}=3.2 Hz, C), 130.5 (d, J_{C-F}=8.0 Hz, CH), 129.3 (CH), 128.9 (CH), 127.6 (CH), 123.8 (CH),

119.1 (C), 117.4 (CH), 115.2 (d, $J_{C-F} = 21.3$ Hz, CH), 110.6 (CH), 53.3 (CH₂). ¹⁹F-NMR (CDCl₃): δ -115.5 (s, 1F). **UPLC-MS**: Rt: 1.77 min, MS (ESI)⁺: 325.1 [M+H]⁺.

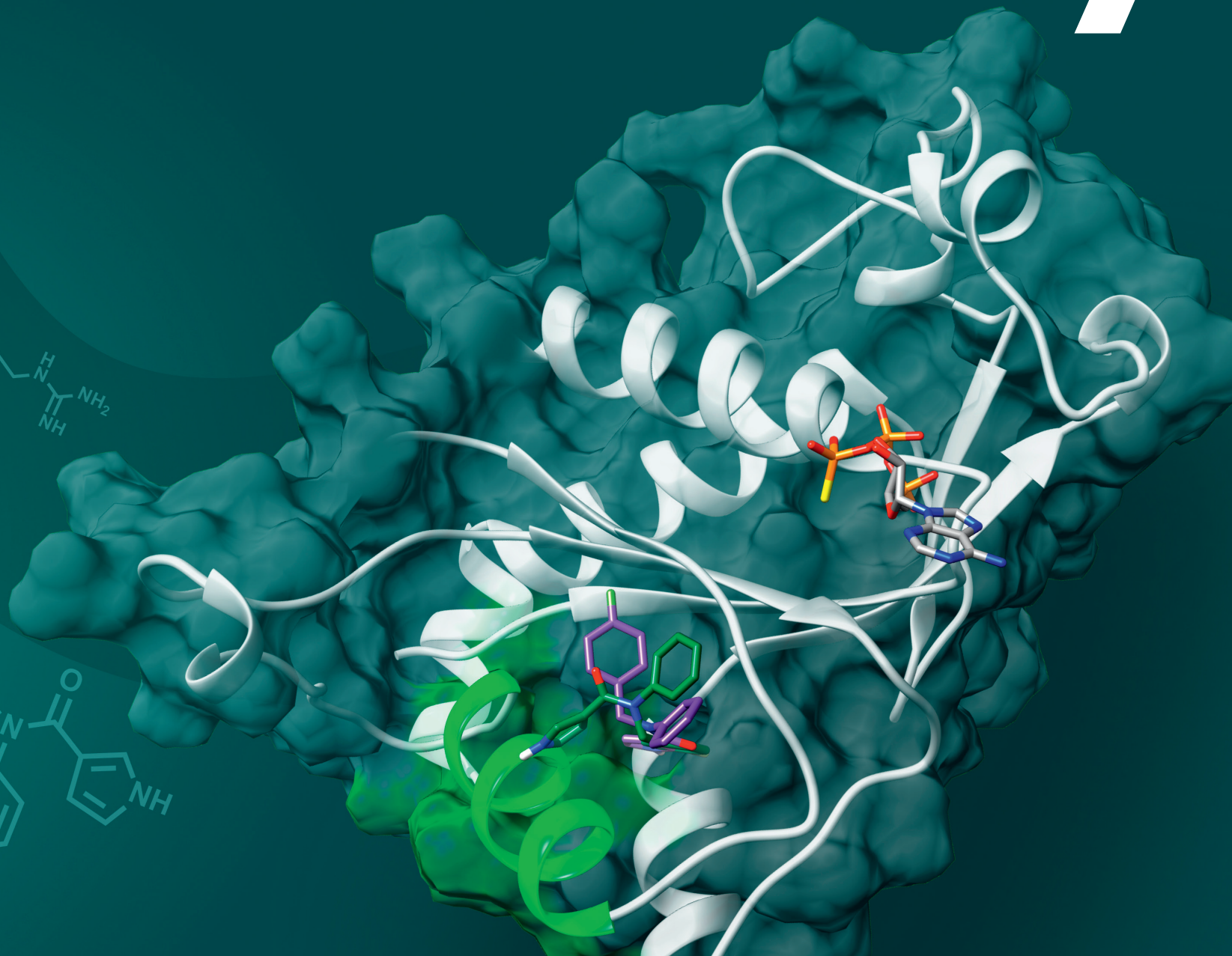
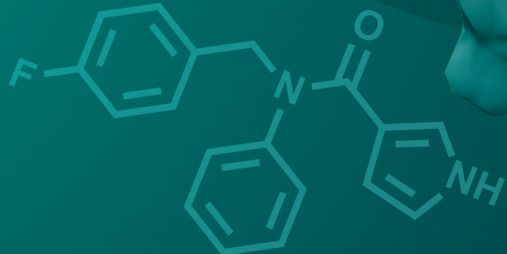
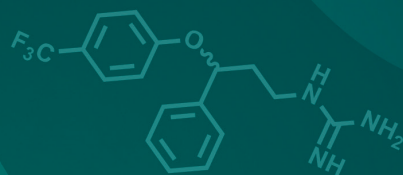
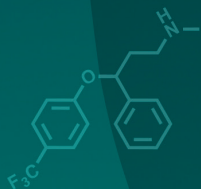
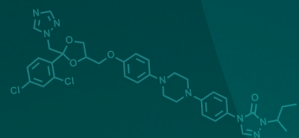
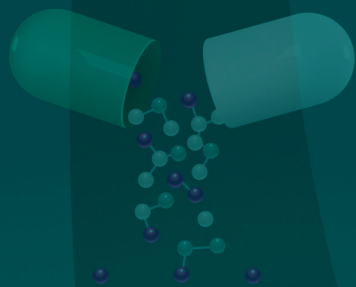
References

1. Guan, H. *et al.* Crystal structure of 2C helicase from enterovirus 71. *Sci Adv* 3, e1602573, doi:10.1126/sciadv.1602573 (2017).
2. Pravda, L. *et al.* MOLEonline: a web-based tool for analyzing channels, tunnels and pores (2018 update). *Nucleic Acids Res* 46, W368-W373, doi:10.1093/nar/gky309 (2018).
3. Guan, H., Tian, J., Zhang, C., Qin, B. & Cui, S. Crystal structure of a soluble fragment of poliovirus 2CATPase. *PLoS pathogens* 14, e1007304, doi:10.1371/journal.ppat.1007304 (2018).
4. Jurcik, A. *et al.* CAVER Analyst 2.0: analysis and visualization of channels and tunnels in protein structures and molecular dynamics trajectories. *Bioinformatics* 34, 3586-3588, doi:10.1093/bioinformatics/bty386 (2018).
5. Tian, W., Chen, C., Lei, X., Zhao, J. & Liang, J. CASTp 3.0: computed atlas of surface topography of proteins. *Nucleic Acids Res* 46, W363-W367, doi:10.1093/nar/gky473 (2018).
6. Tukker, A. M. *et al.* Is the time right for in vitro neurotoxicity testing using human iPSC-derived neurons? *ALTEX* 33, 261-271, doi:10.14573/altex.1510091 (2016).

Chapter

General Discussion

7



1. Summary

The genus *Enterovirus* (EV), belonging to the *Picornaviridae* family, includes many important human pathogens (eg. poliovirus, EV-A71, coxsackievirus, EV-D68, rhinovirus). These viruses are the causative agents of several mild diseases but can also cause more severe neurological complications, especially in young children and immunocompromised people. The symptoms include hand-foot-and-mouth disease, conjunctivitis, aseptic meningitis, severe neonatal sepsis-like disease and acute flaccid paralysis, whereas infections with rhinoviruses (RV) can cause the common cold and exacerbations of asthma and COPD. Despite the clinical importance, tools to fight these diseases are limited. Vaccines only exist against poliovirus and EV-A71 and currently, no antiviral treatment is licensed.

Over the years, several different direct-acting and host-directed inhibitors against EV were developed. Capsid binders were the most advanced group in clinical development. Some showed good activity against a number of EV species, while other species were naturally resistant. Another drawback of capsid binders is that resistant viruses emerge rapidly. Inhibitors targeting the 3C protease were developed but also failed in clinical trials due to poor bioavailability and limited efficacy. Several inhibitors of the 3D polymerase were identified but these compounds never entered clinical trials. A number of structurally disparate inhibitors, as well as FDA-approved drugs, were identified to target the non-structural protein, 2C. However, these compounds were never tested in clinical trials. EV critically depends on specific host factors to ensure genome replication. The search for inhibitors of viral replication revealed several essential host factors important for the virus, including the lipid kinase PI4KB and the lipid shuttling protein OSBP. Up to now, the PI4KB inhibitor Enviroxime was the only host-targeting compound under clinical development as a treatment option for RV infections. However, Enviroxime showed toxicity and the clinical development was suspended. **Chapter 2** summarizes the inhibitors that have been developed against EVs.

Drug discovery and development is a very costly and time-consuming process. Advances in structural biology and computational modelling accelerated the development of structure-based and ligand-based drug design. These developments sparked the emergence of drug repurposing as an alternative to costly *de-novo* drug design. This concept uses drugs which are already approved for the treatment of a specific disease to potentially treat a different condition. It offers an attractive advantage to *de-novo* drug design, since profound pharmacological and toxicological profiles are readily available which allows for the bypass of expensive preclinical development.

Drug repurposing screens identified several FDA-approved drugs that inhibit EV replication. One of the identified compounds is the antifungal itraconazole (ITZ) which is currently also under clinical development for its anticancer activity. ITZ exerts its anticancer activity through several pathways, independent of its antifungal activity. The known targets of ITZ did not explain its antiviral activity. Instead, OSBP, a lipid shuttling protein, was identified as the novel ITZ target.¹ In **chapter 3** we investigate

a structure-activity relationship (SAR) study on the chemical properties underlying the antiviral activity in order to decouple the different pharmacological features of ITZ. The backbone structure of ITZ consists of a core of five linear linked rings (dioxolanyl-methoxyphenyl-piperaziny-phenyl-triazolone). The dioxolane ring carries a dichlorophenyl and a triazole moiety and the triazolone ring carries the *sec*-butyl chain. The triazole ring, important for the antifungal activity, is dispensable for the antiviral activity, thus these two pharmacological functions can be decoupled. The branching of the *sec*-butyl chain, which is an important feature for the anticancer activity, is essential for the antiviral activity. Finally, the core structure of five rings is also essential for the antiviral activity. Changing the core structure or removing one or more rings results in a loss of antiviral activity. Thus, the antifungal activity and partially the anticancer activity can be decoupled from the antiviral activity. Additionally, we provide *in silico* studies which explore how ITZ possibly binds to oxysterol-binding protein (OSBP). Therefore, the gained knowledge allows for the development of ITZ-derived antivirals with increased OSBP specificity and fewer side effects.

Drug repurposing screens identified the FDA-approved drug fluoxetine (Prozac®, a selective serotonin reuptake inhibitor (SSRI)), which is clinically used for the treatment of depression and anxiety disorders, as EV inhibitor.^{2,3} **Chapter 4** investigates the mode-of-action of fluoxetine. Fluoxetine has a chiral center resulting in two enantiomers. We identified that the *S*-enantiomer, but not the *R*-enantiomer, has potent antiviral activity. Additionally, (*S*)-fluoxetine showed an increase in the antiviral spectrum. This indicates that there is a correlation between a higher potency and a broad spectrum of antiviral activity which will be further discussed in Section II. 1. In-line with the observed antiviral effect, the *S*-enantiomer of fluoxetine, but not the *R*-enantiomer, showed binding to a recombinant coxsackievirus B3 (CV-B3) 2C protein. Based on a recently elucidated structure of 2C of the fluoxetine-insensitive EV-A71, we predicted a possible binding mechanism using a homology model of 2C of the fluoxetine-sensitive CV-B3. We used the model to investigate 2C mutations in the predicted binding pocket which were either previously identified resistance mutations to structurally disparate 2C inhibitors or designed by a structure-guided approach. Several of these mutations conferred fluoxetine resistance and disrupted binding of fluoxetine. Thus, this study provided insight into the mode-of-action of fluoxetine.

To dissect the pharmacophoric features of fluoxetine that are important for its antiviral activity we conducted a SAR study in **chapter 5**. We explored changes in the *para* trifluoro-phenoxy moiety, which is essential for the SSRI activity, and in the amino moiety of fluoxetine. Changes in the *para*-trifluoro-phenoxy moiety resulted in a loss of antiviral activity. Substitutions in the amino moiety resulted in a racemic amino-analogue that had a similar antiviral activity compared to (*S*)- fluoxetine. Remarkably, the *R*-enantiomer of the new fluoxetine analogue slightly gained in antiviral activity against CV-B3 and EV-D68. In-line with the antiviral effect, the *S*-enantiomer displayed stronger binding to the recombinant 2C protein compared to the *R*-enantiomer. Thus, we identified that the SSRI activity and the antiviral activity cannot be decoupled.

Furthermore, one analogue was shown to be as potent as the (*S*)-enantiomer of fluoxetine, which confirmed the importance of the chiral conformation for the antiviral activity.

In **chapter 4** and **5**, we established that fluoxetine inhibits viral replication stereospecifically by directly binding 2C. However, the chemical moiety important for the SSRI activity is essential for the antiviral activity, and thus far, these two activities are unlikely to be uncoupled. This raised concerns about the therapeutic application of fluoxetine and shows that other potent, biosafe and broad-spectrum antiviral inhibitors are needed. In **chapter 6** we conducted a SAR study on the molecule *N*-(4-fluorobenzyl)-*N*-(4-methoxyphenyl)furan-2-carboxamide which was identified in a small molecule screen as a potent CV-B3 inhibitor.⁴ This compound was of interest because it is structurally similar to fluoxetine but lacks the tri-fluoro moiety and the chiral center. The SAR study revealed several highly potent pan-EV 2C inhibitors with a similar resistance profile as (*S*)-fluoxetine. One compound showed a distinct resistance profile. We raised EV-A71, CV-B3 and EV-D68 resistant virus pools against this pan-EV and -RV inhibitor against which common 2C mutations did not confer cross-resistance. Analysis of the virus genotypes revealed a common mechanism of resistance development which is likely similar to most of the 2C inhibitors. All resistant viruses acquired a mutation in the $\alpha 2$ helix of 2C, or came very close. *In silico* predictions revealed at least one solvent accessible tunnel close to the resistance mutation in EV-A71 and poliovirus 1 (PV-1). Taken together, this study revealed several new broad spectrum EV and RV inhibitors. The molecular and virological data provided the first evidence that EV and RV share a common druggable binding pocket in the non-structural protein 2C.

2. Enterovirus non-structural protein 2C; the target of many small molecule inhibitors

The highly conserved non-structural protein 2C, which is an AAA+ ATPase, is a promising target for drug development. Several structurally disparate 2C inhibitors have already been identified. Most of the 2C inhibitors directly interfere with viral replication, but the mode-of-action and the antiviral spectrum of these inhibitors are poorly studied. In this thesis we investigated the mode-of-action of the FDA-approved drug fluoxetine and the compound *N*-(4-fluorobenzyl)-*N*-(4-methoxyphenyl)furan-2-carboxamide, both of which are 2C inhibitors directly targeting viral replication. Studying the mode-of-action of these 2C inhibitors revealed several common features which will be discussed below.

Correlation of potency with broad-spectrum antiviral activity of 2C inhibitors

The racemic mixture of fluoxetine and several other 2C inhibitors showed strong antiviral activity against EV-B and EV-D species, but not against EV-A and EV-C or RVs.³⁻¹¹ **Chapter 4** revealed that the *S*-enantiomer, but not the *R*-enantiomer of fluoxetine, inhibits viral replication. We tested the *S*-enantiomer separately against a broad

spectrum of clinically important EV. These experiments revealed that the antiviral spectrum of the *S*-enantiomer increased compared to the racemic mixture. A similar profile was also observed with the compound *N*-(4-fluorobenzyl)-*N*-(4-methoxyphenyl)furan-2-carboxamide (compound **1**) in **chapter 6**. Compound **1** showed a limited anti-EV spectrum and only inhibited prototypic members of EV-B and EV-D species and RV-B14. We identified several chemically modified analogues with increased potency that inhibited the whole spectrum of EV and RV. Together, these studies underline the potential of 2C inhibitors to be developed into pan-EV and RV inhibitors.

The pan-EV inhibitors identified in **chapter 6** and (*S*)-fluoxetine were also tested on numerous clinical isolates of the serotypes EV-A71, CV-A24v and EV-D68. Pan-EV and RV compounds indeed inhibited all clinical isolates, albeit with subtle differences. Remarkably, we identified that (*S*)-fluoxetine inhibited several clinical isolates of EV-A71, but not the prototypical strain EV-A71 BrCr. This is reminiscent of the class of tryptophan dendrimer entry inhibitors which are also only active against clinical isolates of EV-A71. In this case, subtle genetic variations made strains sensitive or insensitive.¹² We aligned the 2C proteins of EV-A71 clinical isolates to determine differences in the amino acid sequence which could explain the insensitivity towards (*S*)-fluoxetine. We introduced these mutations into the insensitive EV-A71 BrCr strain, but none of the mutations revealed a fluoxetine sensitive virus (Bauer et al, unpublished results). These experiments ruled out minor intrinsic genetic differences between the clinical EV-A71 isolates as the reason for differences in sensitivity to (*S*)-fluoxetine. This suggests that the potency of the compound likely determines the antiviral spectrum of 2C inhibitors.

The ideal antiviral compound shows low cytotoxic effects, even at very high concentrations, but exerts the antiviral activity at very low concentrations. Racemic fluoxetine, as well as compound **1**, inhibited a limited range of EV and RV species. In **chapter 4**, we observed that (*S*)-fluoxetine showed increased potency compared to racemic fluoxetine. This resulted in a broader anti-EV and RV spectrum. Similarly, in **chapter 6**, three compound **1** analogues that showed the highest antiviral activity exerted pan-EV and pan-RV activity. Together, this again indicates that there is a correlation of antiviral potency and antiviral spectrum of 2C inhibitors, because only highly potent 2C inhibitors exert pan-EV and RV activity. Interestingly, in a recently published SAR study of dibucaine, which is another FDA-approved drug targeting 2C, several analogues showed an increased potency.¹³ Unfortunately, these dibucaine analogues were only tested against clinical isolates of EV-D68, but not against other serotypes. Further analysis of the activity of these dibucaine analogues against the whole spectrum of EVs and RVs could confirm the hypothesis that high potency of 2C inhibitors results in pan-EV activity. The differences in compound sensitivity of EV and RV species to 2C inhibitors can potentially be attributed to the structural accessibility of the 2C binding pocket. It is viable that the 2C binding pocket is slightly easier accessible in EV-B and EV-D species and therefore, these species are inhibited by less potent 2C inhibitors compared to EV-A, EV-C and RV species.

Insight into the binding site of 2C inhibitors

The 2C protein is poorly soluble, which greatly complicates structural studies of 2C alone or in complex with its inhibitors. We therefore made use of computational methods to discover potential drug-ligand interaction sites. We focused on 2C of CV-B3, especially the loop region comprised of the residues A224, G225, S226, I227, N228 and A229 (designated as 224AGSINA229) which is a hot spot for resistance mutations against structurally disparate 2C inhibitors.^{10,14,15} The triple mutant A224V-I227V-A229V (AVIVAV mutant) in CV-B3 2C conferred high levels of resistance towards several 2C inhibitors and also to (*S*)-fluoxetine (**chapter 4**).^{2,10,11,14,16} In **chapter 4**, we generated a homology model of the fluoxetine-sensitive CV-B3 2C based on the crystal structure of the fluoxetine-insensitive EV-A71 2C, since structural data from fluoxetine-sensitive viruses (e.g. CV-B3 or EV-D68) were not available. Molecular dynamics simulations, mutational studies with virological and biochemical assays, provided support for the proposed location of the binding pocket. For the first time, these experiments indicated the location of a conserved, common druggable binding pocket for 2C inhibitors in all EVs and RVs as well as three possible entrances towards the pocket.

The compound **1** analogue **19d** only showed very little, if any, cross-resistance to the common 2C mutations that provide cross-resistance to (*S*)-fluoxetine, compound **1** and analogues thereof (**chapter 6**). Raising resistance against **19d** in the serotypes EV-A71, CV-B3 and EV-D68 combined with computational methods and virological assays allowed us to define the binding pocket and its accessibility more precisely. All resistant viruses in the different serotypes acquired a mutation in the $\alpha 2$ helix of 2C, or came very close. This suggested that the entrance to the predicted binding pocket might be close to the $\alpha 2$ helix. Additionally, this entrance was also predicted in the CV-B3 model in **chapter 4**. A common solvent accessible tunnel in the 2C protein of EV-A71 and PV-1 supported the predicted location of the common druggable binding pocket. The common tunnel suggested that the $\alpha 2$ helix is involved in compound binding. *In vitro* evidence for this hypothesis was obtained by mutating the $\alpha 2$ helix residues in the infectious clones of the different serotypes which conferred drug resistance. Additionally, the resistance mutation in the $\alpha 2$ helix of CV-B3 disrupted the binding to 2C inhibitors. Similar resistance profiles in different serotypes suggest, that the druggable pocket and the entrance at the $\alpha 2$ helix is a common feature in EVs 2C proteins.

Mutations that provide resistance to antiviral compounds targeting viral polymerases, viral helicases or the viral protease can result in decreased viral fitness.¹⁷⁻¹⁹ This was also found for 2C resistance mutations in **chapter 6**. Acquiring a resistance mutation in the $\alpha 2$ helix in 2C resulted in a reduction of viral fitness in all different investigated EV serotypes. Interestingly, several resistant virus pools gained additional mutations located distal from the $\alpha 2$ helix. These compensatory mutations increased the compound resistance and additionally restored the fitness defect. Since structural data are not available, it is challenging to speculate what effects these compensatory mutations would have on the confirmation and stability of 2C. The observation that a virus becomes resistant to a drug at the cost of fitness and that compensatory mutations

are then obtained that increase viral fitness is a common feature. For instance, it has also been observed in resistant virus pools raised against several viral polymerase inhibitors²⁰⁻²² and it was also previously observed for the 2C inhibitor guanidium chloride (GuaHCl) in EV-A71²³

Mechanistic insight into the MOA of 2C inhibitors

2C is an ATP-dependent helicase and forms higher oligomeric structures that are necessary for proper function.²⁴⁻²⁷ Based on the structural information from the previous section 2, all predicted tunnels represent possible entrances to the binding pocket. These tunnels are very close to the Walker B domain but distantly located from the catalytic ATP binding site (Figure 1). This suggests that the 2C inhibitors likely do not occupy the ATP binding site, but rather bind the 2C protein allosterically in a common druggable pocket in 2C.

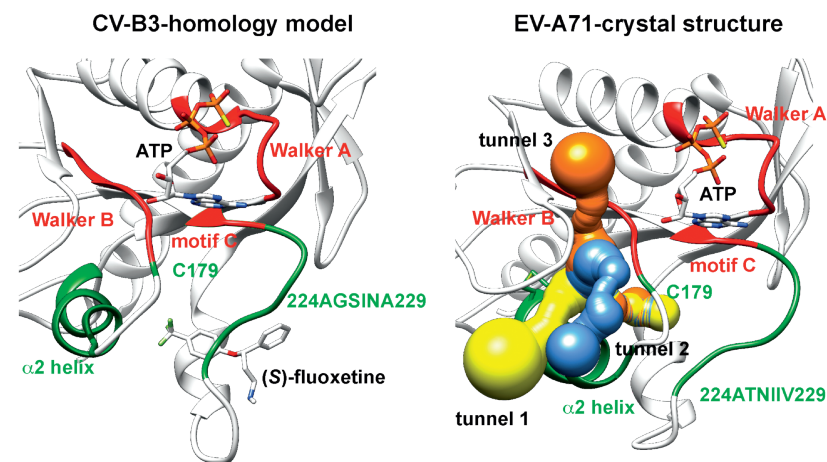


Figure 1. 2C inhibitors likely do not bind in the catalytic center of 2C. On the left panel (*S*)-fluoxetine is docked into the homology model of CV-B3 2C. The binding mode indicates that (*S*)-fluoxetine does not bind in the catalytic center. In the right panel, the predicted tunnels are overlaid with the EV-A71 2C crystal structure (PDB 5GRB, chain A). The entrance to the binding site is located differently compared to the docked (*S*)-fluoxetine. These tunnels indicate that novel compound **1** analogues do not bind in the catalytic center.

The 224AGSINA229 loop is a hotspot for resistance development against TBZE-029¹⁰ and (*S*)-fluoxetine (Bauer et al., unpublished results). Remarkably, when raising resistance against compound **19d**, resistance mutation occurred in the $\alpha 2$ helix of 2C and not in the 224AGSINA229 loop. This is a surprising observation for which no explanation can be given unless structural information becomes available. Based on our modelling data, it can be speculated that the 224AGSINA229 loop and the $\alpha 2$ -helix are interconnected with tunnels that overlap at the Walker B domain where the putative

binding pocket is also located. The differences in acquiring resistance mutation in the 224AGSINA229 loop or the α 2-helix may be due to different binding modes of (S)-fluoxetine compared to compound **19d**.

Several mechanisms of inhibition of the studied 2C inhibitors can be proposed. 2C likely oligomerizes in hexameric structures. 2C inhibitors could prevent the proper assembly of the functional 2C oligomer. However, this possibility is rather unlikely since the proposed binding pocket is not close to the hypothetical oligomerization pocket. ATPases undergo several conformational changes that allow ATP hydrolyses. Conversely, inhibitors might stabilize the 2C oligomer and thus, prevent the necessary conformational changes important for ATP hydrolyses. A similar mechanism has already been identified for an inhibitor of the human AAA+ ATPase, p97.²⁸ The allosteric p97 inhibitor binds at the interface of two adjacent protein domains which prevents the conformational changes that are necessary for the proper p97 ATPase function.²⁸ The lack of oligomeric 2C structures makes it difficult to elucidate whether the compounds stabilize or destabilize the quaternary structure, or inhibit the enzymatic activities of 2C. Crystallographic or cryo-EM structures of oligomeric 2C in complex with inhibitors are needed to clarify the binding site and the mode-of-action of 2C inhibitors.

Clinical perspectives of fluoxetine and compound **1** analogues

Out of the several 2C inhibitors derived from repurposing drug screens, fluoxetine showed a promising potential for clinical application as antiviral. Fluoxetine is licensed for its antidepressant activity as racemic mixture (1:1 mixture of S- and R-enantiomer) and it was found to inhibit EV-B and EV-D species *in vitro*.²⁹ Fluoxetine has been used off-label to treat an immunocompromised child with chronic EV-B induced encephalitis.³⁰ The treatment with fluoxetine eliminated the virus and led to the recovery of the patient. Additionally, intraperitoneally administered fluoxetine proved to be effective in a pancreatitis mouse model and its racemic mixture reduced the CV-B4 levels in heart and pancreas. However, it should be emphasized that in this experimental setting, fluoxetine was administered prior to CV-B4 infection as well as after infection as daily treatment.³¹

The latest outbreaks of EV-D68 in the USA are associated with severe neurological complications, particularly acute flaccid myelitis (AFM). Currently, there is no antiviral therapy licensed for EV-related AFM and treatment relies on supportive care. Pediatricians used off-label treatment with fluoxetine to treat patients after the onset of AFM.³² Even though fluoxetine was well-tolerated, this study revealed no beneficial effect of fluoxetine to treat AFM, but rather suggested that the fluoxetine treated cohort had somewhat more severe symptoms.³² Several limitations of the retrospective study make it difficult to draw definite conclusions on why fluoxetine treatment was not effective. Patients have been treated with different dosing of fluoxetine after the onset of AFM in small cohort groups. Furthermore, the onset of AFM may be indicative of accumulating irreversible neuronal damage, rather than the result of active virus replicating in the neurons. Fluoxetine has also been evaluated as a treatment option

in a neonatal mouse model of EV-D68-induced paralysis.³³ In this setting, fluoxetine was administered intraperitoneally at the time of infection but did not reduce virus titers in the muscle and spinal cord and seemed to slightly aggravate the disease.³³ Together, these data suggest that fluoxetine has a negative effect on AFM outcome. The reasons for this are unknown but are possibly due to side effects of the SSRI activity. To circumvent the problem of the SSRI activity's side effect, we attempted to decouple the antiviral effect from the SSRI activity. **Chapter 5** revealed that it is very unlikely that these functions can be decoupled. In **chapter 6** we described that the most potent pan-EV and RV compound **1** analogues are devoid of SSRI activity and are no longer neuroactive, unlike fluoxetine.

The efficacy of the replication inhibitor fluoxetine *in vivo* might depend on the time of administration and on which EV-induced disease is treated. It is likely that it will have little beneficial effect when it is administered to treat clinical symptoms when hardly any replicating virus is left. It also may depend on the affected tissue as the bioavailability of fluoxetine may vary between organs. The lack of beneficial effect of fluoxetine administered to patients suffering from EV-D68-induced AFM is unlikely due to poor bioavailability in the brain. This is supported by the fact that fluoxetine was successfully used to treat an immunocompromised child with coxsackievirus-B induced encephalitis. Differences in sensitivity to fluoxetine may also account for the observation that fluoxetine may be beneficial to treat some, but not all, EV-induced diseases. Obviously, a more potent inhibitor would be highly beneficial. Despite the more favorable antiviral profile of (S)-fluoxetine described in **chapter 4**, the direct translation to clinical application is not possible, since only the racemic mixture is FDA-approved. Thus, it would be of greater advantage to develop other more potent and safer pan-EV and RV inhibitors. The novel broadly active 2C inhibitors identified in this thesis (**chapter 6**) could be of importance for anti-EV therapy development.

In **chapter 6**, we investigated the important chemical moieties of compound **1** in a SAR study, which was originally identified as CV-B3 2C inhibitor targeting 2C.⁴ The compound is structurally similar to fluoxetine, but lacks a chiral center and the *para*-trifluoro group important for the SSRI activity. Unlike fluoxetine, compound **1** and analogues thereof did not indicate neuroactivity that potentially underlie the adverse effect. Compared to (S)-fluoxetine and derivatives thereof, the novel compound **1** analogues showed highly improved antiviral activity (against some EVs even in the nM range) and a pan-EV and RV spectrum. These novel inhibitors were also active against several clinical isolates of emerging serotypes EV-A71, EV-D68 and CVA-24v. In summary, the compound **1** analogues show a much better *in vitro* profile compared to fluoxetine and derivatives thereof. Pharmacological studies and *in vivo* efficacy of the new inhibitors would be required to evaluate their potential for clinical application.

Future perspectives

Fluoxetine and compound **1** analogues target the same binding pocket in 2C. It would be desirable to develop 2C inhibitors so that they can be combined with an

inhibitor with a different mode-of-action for combination therapy. The recently elucidated EV-A71 and PV 2C crystal structures raised several vulnerable features for antiviral drug development.^{34,35} A potential strategy is the pharmacological inhibition of the ATPase domain, which would result in novel antivirals with a different mode-of-action (Figure 2).^{24,25,27} We aimed to target 2C's ATPase domain with a computer aided structure-based drug development approach. We conducted molecular dynamics on the bipartite binding pocket and observed the movement of the ATP molecule within the active site. Several frames were selected for the ensembled docking to perform vHTS. Ensembled docking corresponds to the generation of an ensemble of binding sites within a drug target. It uses molecular dynamics of a ligand and its protein to generate binding site conformations that can be used for SBDD.³⁶ Based on this docking approach several compounds were selected for *in vitro* tests. Of the synthesized compounds, one inhibited EV-A71 and CV-B3 in the high μM range (Figure 2). Investigating the mode-of-action and enhancing the antiviral activity with medicinal chemistry could lead to a highly potent compound with a new mechanism of 2C inhibition.

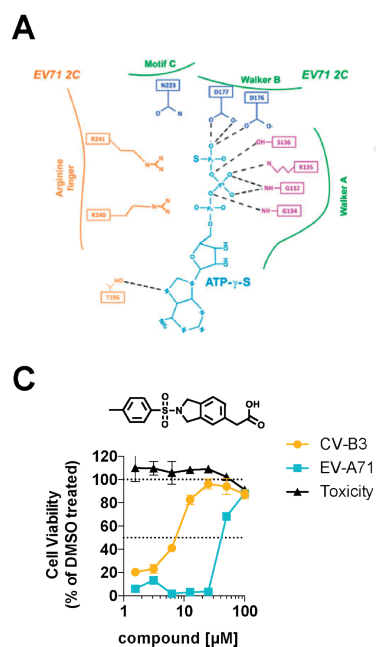


Figure 2. The ATP-enssembled docking revealed a new EV inhibitor. (A) The binding site of ATP is shown based on the EV-A71 crystal structure (with permission from Science Advances). (B) Results of the molecular dynamics indicate the movement of ATP within the bipartite binding pocket. Different frames of the molecular dynamic simulation were used for virtual high-throughput compound screening. (C) The active compound which was identified with the ATP-enssembled docking inhibits CV-B3 and EV-A71 *in vitro*.

The crystal packing of both EV-A71 2C and PV 2C revealed a C-terminal oligomerization mechanism in which the α -helical C-terminus of a monomer dips into a hydrophobic pocket in the adjacent monomer in order to oligomerize (Figure 3).^{34,35} This indicates another potentially druggable feature of 2C. Not only the disrupting or stabilizing of host-viral protein-protein interaction, but also disruption/stabilization of viral intra- and inter-protein interactions have become promising new strategies for antiviral drug development against RNA viruses.³⁷⁻⁴¹ Small molecules as modulators of protein-protein interactions may have the drawback that the oligomerization pocket is broad and shallow. Hence, small molecules might not be large enough to occupy broad and shallow pockets to inhibit/stabilize the oligomerization.⁴² Alternatively, to disrupt the protein-protein interaction/oligomerization of 2C, small cell-permeating synthetic proteins (e.g. Alphabodies) mimicking an α -helix scaffold may be developed and applied to disrupt 2C oligomerization.⁴³

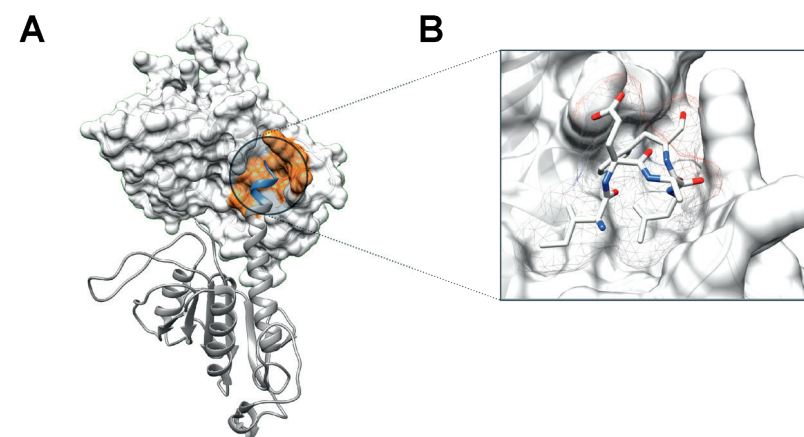


Figure 3. 2C-Selfoligomerization as potential drug target. (A) C-terminal oligomerization in the EV-A71 2C crystal structure (PDB: 5GRB chain A and chain F were used) (B) Close-up of the C-terminal residues which are mediating the C-terminal oligomerization according to the crystal structure. The shape of the last amino acids is shown in a mesh grid and represents the conformation used for virtual high-throughput screening.

An alternative approach for the development of antiviral drugs is a ligand-based strategy. Information of existing 2C inhibitors were used to generate a pharmacophore model indicating similarities in the steric and electronic features of published 2C inhibitors^{4,10,11,14}. Unfortunately, this preliminary approach did not reveal any new inhibitors (Bauer et al, unpublished results). This strategy most likely failed as the structures of the 2C inhibitors were very diverse and the pharmacophore model was not based on the crystallized structure-ligand complex. A ligand-protein complex would allow to consider the exact pharmacophoric features facilitating the ligand-protein interaction. The most successful example for this approach in antiviral drug development is the anti-influenza compound zanamivir.⁴⁴

The 2C inhibitors identified in this thesis show highly potent broad-spectrum inhibition of EV and RV *in vitro*. The development of resistance against the 2C inhibitors studied in this thesis *in vitro*, suggests that monotherapy with 2C inhibitors might not be a viable approach for clinical application. A similar problem was observed with the rapid resistance development, or even naturally resistance strains, against capsid binders.⁴⁵⁻⁴⁸ Antiviral combination therapy against several chronic viruses (e.g. human immunodeficiency virus, hepatitis B virus and hepatitis C virus) have been proven to be very successful.⁴⁹ Currently, combined strategies are being investigated in the frame of the global polio eradication campaign which may also be applicable to the treatment of other EV and RV infections (<http://polioeradication.org/tools-and-library/current-research-areas/antivirals/>). A combination of a capsid binder (Pocapavir) with protease inhibitors (AG-7404/V-7404) is under clinical development. Both compounds have some drawbacks, e.g. rapid development of resistance and varying potency against different EV and therefore, better compounds targeting conserved proteins of EV (e.g. 3D and 2C) are eagerly awaited.

3. Host-directed antivirals and possible new antiviral targets

All positive-strand RNA viruses create novel intracellular membranous structures on which viral replication takes place. To create replication organelles (RO), the virus hijacks host proteins to manipulate the cellular environment and the lipid metabolism so that it is favorable for the virus. Several evolutionary unrelated viruses (e.g. the flavivirus Hepatitis C virus and several picornaviruses) harness the PI4K-PI4P-OSBP axis to rewire the host cell membrane landscape and lipid metabolism. First, viruses recruit the lipid kinase PI4K (different isoforms are recruited by different viruses) that leads to a local increase of PI4P lipids. The high levels of PI4P serve as a recruitment platform for the lipid shuttling protein OSBP and possibly also other proteins that bind PI4P. Hence, pharmacological inhibition of the host factors PI4K and OSBP results in broad spectrum antiviral activity.

Itraconazole, an antifungal going antiviral

A drug repurposing screen identified the FDA-approved antifungal ITZ as a novel inhibitor of EV replication.¹ ITZ is also under clinical development for its potent anticancer activity. This multifunctionality is likely explained by the structure of the drug. ITZ is a very lipophilic molecule consisting of a core structure of five linked rings and substituents on each side of the core. The diaxolane ring containing the triazole moiety determines the antifungal activity.^{50,51} The anticancer activity is achieved by antagonizing hedgehog signaling which is linked to the *sec*-butyl chain of ITZ.⁵² ITZ also has potent antiangiogenic properties, which are exerted by interfering with vascular endothelial growth factor receptor 2 (VEGFR2) trafficking and glycosylation, as well as mTOR signaling.^{52,53} The *sec*-butyl chain is the underlying chemical moiety for interfering

with VEGFR2 trafficking and glycosylation, while mTOR signaling is inhibited by direct binding of ITZ to VDAC1 and NPC1.⁵²⁻⁵⁷ However, the inhibition of OSBP mediated lipid trafficking -underlying its antiviral activity- has not yet been linked to any particular moiety of ITZ.

In **chapter 3** we determined that the core-ring structure, together with the *sec*-butyl chain, but not the triazole moiety, is necessary for the antiviral activity. This implies that the antifungal activity can be decoupled from the antiviral activity. The triazole moiety strongly inhibits the liver enzyme CYP3A4, which is associated with hepatotoxicity.⁵⁸ The inhibition of the drug metabolizing enzyme CYP3A4 by ITZ also has a negative effect on the metabolism of other drugs.^{59,60} Based on our data, ITZ analogues devoid of the triazole moiety would have a more favorable profile for clinical application against EV. Novel ITZ analogs may be developed that retain the antiviral activity but lack the triazole moiety, thereby reducing hepatotoxicity and allowing for metabolism of drugs by CYP3A4. This would allow the use of ITZ analogues in combination with other medication, which could be antiviral drugs or medication for certain comorbidities.

We identified the *sec*-butyl chain, which is important for inhibition of hedgehog signaling and VEGFR2 glycosylation, as also being essential for the antiviral activity. Introduction of bulkier moieties, such as phenol rings, increased the antiviral activity. This is in contrast to the inhibition of hedgehog signaling, which does not allow for the introduction of bulkier residues. Shortening the five core-ring structure results in a loss of antiviral activity, whereas hedgehog activity is still sustained.⁶¹ This indicates that the antiviral activity can also be decoupled from hedgehog signaling. The core structures' five consecutive rings are responsible for the low solubility of ITZ. The length of the core-ring structure is essential for the antiviral activity, but changing the properties within these aromatic rings can lead to more soluble and less lipophilic molecules.

Our data indicate that inhibition of OSBP mediated lipid shuttling correlates with changes in VEGFR2 glycosylation. Possibly, this is linked to disruption of lipid homeostasis at the Golgi and thus, it is unlikely these two activities can be uncoupled. Strong support for this hypothesis is provided by the OSBP inhibitor OSW-1, which also alters the VEGFR2 glycosylation (Head, Strating, van Kuppeveld, and Beachy, unpublished). Interestingly, TTP-8307, which likely inhibits OSBP in a different manner⁶², does not alter VEGFR2 glycosylation (Head et al, unpublished). One possible explanation is that the affinity of TTP-8307 towards OSBP is lower and, as a consequence, TTP-8307 does not inhibit lipid shuttling as potently as OSW-1 and ITZ. Alternatively, it cannot be excluded that inhibition of other lipid shuttling proteins, such as OSBP-related proteins (ORP) or ceramide transfer protein (CERT), also contribute to disruption of cholesterol homeostasis and hence, an altered pattern in VEGFR2 glycosylation. Another possibility is that ITZ and OSW-1, but not TTP-8307, share a similar target which affects VEGFR2 glycosylation. Taken together, this implies that VEGFR2 glycosylation and OSBP mediated lipid shuttling are unlikely to be uncoupled. It remains to be established if the effect on VEGFR2 glycosylation is dependent on the disruption of lipid homeostasis induced

by OSBP inhibition. Currently, it is unknown if a changed VEGFR2 glycosylation during short term antiviral treatments would result in adverse effects.

OSBP belongs to a large family of lipid shuttling proteins. These proteins accommodate lipids in a hydrophobic pocket and transport them between two organelles at membrane contact sites or through cells.⁶³ In **chapter 3**, we elucidated the chemical moieties underlying the inhibition of OSBP mediated lipid shuttling. For a better understanding of the OSBP-itraconazole interaction we used modelling studies. We created a homology model of the OSBP-related domain (ORD) domain of OSBP and investigated possible binding modes of ITZ. In-line with the observed data, docking studies suggested that ITZ and OSW-1 bind into the ORD of OSBP, which usually accommodates cholesterol. This finding was supported by previous observations that ITZ and OSW-1 inhibited cholesterol and PI4P shuttling. In contrast, a recent study suggested that ITZ binds the ORD domain allosterically and thus, does not directly compete with the cholesterol binding as we proposed.⁶⁴ The exact binding mode of any OSBP inhibitor to the ORD of OSBP remains to be established in structural studies in order to draw conclusions on the exact binding mode.

Inhibition of OSBP causes a disturbance of cholesterol and PI(4)P lipids, and thereby affects lipid and sterol homeostasis. It is also possible that by inhibiting other lipid shuttling proteins, ITZ may contribute to a perturbed lipid homeostasis. For example, ITZ, OSW-1 and TTP-8307 inhibit the lipid transport of the ceramide transporter CERT.⁶² Other possible targets of OSBP inhibitors are the ORP family proteins. These proteins transport a wide variety of different lipids throughout the cell.⁶³ Previously, we observed that overexpression of ORP2 could rescue the inhibitory effect of OSW-1 on EV replication (Bauer and Strating et al., data not shown).^{1,65,66} ORP2 has been proposed to be a lipid droplet (LD) regulatory protein that shuttles cholesterol from LD to the ER.⁶⁷ During virus replication, LDs cluster around the ROs and possibly build membrane contact sites (MCS) with the viral RO to allow cholesterol flux. We hypothesized that the cholesterol transport from LD to the RO may be mediated by ORP2.^{68,69} We assessed the possibility of ORP2 as novel host factor for EV replication with siRNAs knock-down and CRISPR-Cas9 KO experiments. However, a link between ORP2 and the effect on EV replication could not be established in several ORP2 CRISPR knock-out cells (Bauer et al., unpublished results). Only later was it shown that ORP2 is rarely found at LD and, instead, acts in concert with ORP1L at late endosomes/ER contact sites and mediates cholesterol transfer at membrane contact sites from late endosomes to the ERs.⁷⁰

A general drawback of targeting OSBP and ORPs is cytotoxicity as lipid shuttling is often essential for cellular functions. The toxicity of OSW-1 and ITZ possibly rather relate to the inhibition of ORP4 than OSBP. ORP4 plays an essential role in cell proliferation and survival. This likely explains the high cytotoxicity of siRNA targeting ORP4 in knock-down experiments and drugs inhibiting ORP4.⁷¹ Thus, a pharmacological inhibition of ORP4 is unfavorable. This appears to be different for OSBP. Depletion of OSBP does not compromise cellular activity to a similar extent as shown for ORP4. This is likely due to redundant lipid shuttling proteins which can take over the function of OSBP. The

design of novel OSBP inhibitors that do not target ORP4 will allow for a more favorable toxicity profile, while maintaining the broad spectrum antiviral activity. Simultaneously, compounds inhibiting several different lipid shuttling proteins may be valuable tools in deciphering biological activities of lipid transport proteins.

The antiviral activity of ITZ has also been demonstrated *in vivo*. In this study, a nasal spray containing ITZ was shown to provide prophylactic protection against RV-B1 in a mouse model.⁷² This is different to the FDA-approved administration route in humans which is either topical or oral. Thus, applying ITZ as a nasal spray would require an FDA-approval of the new application route and hence, new clinical studies. Given the need for FDA-approval of the new formulation it is advisable to increase the antiviral activity of ITZ. The SAR study and the computational prediction of the binding site of OSBP may facilitate medicinal chemistry to synthesize more potent ITZ-based inhibitors, which can be tailored towards antiviral activity.

Besides EVs and coronaviruses, which both rely on OSBP, ITZ also inhibited human parechovirus 3, but not other parechovirus isolates.⁷³ However, parechoviruses are likely not dependent on the PI4KB-PI4P-OSBP axis because pharmacological inhibition of PI4KB does not inhibit virus replication.⁷⁴ This suggests that ITZ has a different mode-of-action for parechovirus 3. Indeed, it was shown that ITZ acts as entry inhibitor rather than as a replication inhibitor.⁷⁵ ITZ was also shown to inhibit feline coronavirus, likely through the inhibition of cholesterol transport, however the exact mechanism remains to be established.^{76,77} This indicates that the antiviral activity of ITZ is not limited to picornaviruses.

Targeting the PI4KB-PI4P-OSBP axis

The formation of RO is mediated by the concerted action of viral proteins (2B, 2C and 3A) and hijacked host proteins such as PI4K and OSBP.^{78,79} Pharmacological inhibition of the PI4K-PI4P-OSBP pathway indicates broad-spectrum anti-EV activity and thereby represents an interesting target for antiviral drug development. Over the last decade, several PI4KB inhibitors (e.g., PIK93, GW5074, T-00127-HEV1 and BF738735) have been identified. However, some showed lethal toxicity in mice and effected lymphocyte function, which stalled the clinical development of PI4KB inhibitors.^{80,81}

It is believed that viruses do not easily develop resistance against a host-directed antiviral. However, PI4KB resistant EV could be obtained. These viruses acquired a mutation in the non-structural protein 3A (e.g. H57Y).^{82,83} Interestingly, the same mutation provided cross-resistance towards OSBP inhibitors.^{1,62,65,84} Even though the mode-of-action of PI4KB inhibitors and OSBP inhibitors are different, cross-resistance makes it unlikely that a combination therapy thereof is a viable strategy. However, having one host-directed antiviral targeting the PI4KB-PI4P-OSBP axis in combination with a direct acting antiviral could be a possible approach. This was already successfully tested *in vitro*; where ITZ was combined with the 3C protease inhibitor rupintrivir. Resistance viruses against this combination therapy were not observed.⁸⁵

Similar to EV, the flavivirus hepatitis C virus converges on the PI4K-OSBP pathway. Besides the important function of recruiting OSBP to the RO, PI4P lipids can serve as a precursor for PI(4,5)P₂ lipids. Utilizing the host protein PIP5KA, hepatitis C virus accumulates PI(4,5)P₂ at its RO where the amphipathic helix of the non-structural protein NS5A interacts with PI(4,5)P₂. Interestingly, the EV protein 2C contains an N-terminal amphipathic helix which shares structural similarities of NS5A for PI(4,5)P₂ binding.⁸⁶ Additionally, the EV proteins 3CD and 3C are implicated in binding PI(4,5)P₂ and enhancing the concentration of PI(4,5)P₂ in the RO.^{87,88} Since PI4KB inhibitors indicate broad spectrum antiviral activity, we wondered whether PIP5K, which would act downstream of the PI4K-PI4P axis, is an important host factor for EV replication. There are two major pools of PI(4,5)P₂ lipids; one at the plasma membrane and the other in nuclear speckles, which can be discriminated against by different staining protocols.^{89,90} Upon CV-B3 infection, we observed that the nuclear speckle pools of PI(4,5)P₂ lipids disappeared. Unfortunately, we could not link the disappearance of the speckles to an effect of PI5PK, as siRNA knock-down experiments and CRISPR-Cas9-mediated KO of PIP5KA and PIP5KC showed no effect on viral replication in several cell lines (Bauer et al, unpublished results). One possible explanation for the disappearance of the nuclear speckle PI(4,5)P₂ lipids is the virus-induced nucleocytoplasmic traffic disorder. This is typically observed during EV replication and describes the increase in bidirectional permeability of the nuclear envelop due to cleavage of nuclear pore complex components by 2A^{pro}.⁹¹ Another study indicated that overexpression of EV proteins induces PI(4,5)P₂ lipid accumulation, but the exact mechanism is unknown.⁸⁸ Clearly, more research is needed to better understand the possible downstream changes in the PI4KB-PI4P-OSBP axis for EV replication, as well the suitability for targeting by antiviral compounds.

4. Concluding remarks

Currently, antiviral therapy for the treatment of EV infections is not available, while treatment options for hepatitis C virus, another positive-strand RNA virus with a similar replication strategy, are highly successful and can eliminate the virus from chronically infected patients. The overall low incidence of severe manifestations of EV infections compared to hepatitis C virus makes the drug market smaller and thus, impedes extensive industrial efforts. However, recent outbreaks of EV-A71, EV-D68 and CV-A24v with neurological complications increase the recognition of the clinical importance of non-polio EV (and RV). Antiviral drugs are necessary since EV infections can be life-threatening, especially for children and immunocompromised persons. Additionally, antiviral drugs will play a crucial role in the polio eradication campaign and the post-eradication era. This thesis focused on compounds which were identified in drug repurposing screens. This approach revealed several inhibitors eligible for the treatment of EV infections, such as the FDA-approved antifungal, itraconazole. In this thesis, the chemical backbone and the chemical moieties contributing to the

antiviral activity of itraconazole were studied. We also identified potential routes for the improvement of the chemical backbone. For example, modifications of the *sec*-butyl chain can result in compounds with improved antiviral activity and less side effects.

This thesis provides valuable insight into the mode-of-action of 2C inhibitors and underscores the large potential of 2C as an antiviral drug target. The studies revealed how fluoxetine targets the 2C protein on a molecular level. Furthermore, based on the N-(4-fluorobenzyl)-N-(4-methoxyphenyl)furan-2-carboxamide backbone, a previously described inhibitor targeting CV-B3 2C, several novel and highly potent pan-EV and RV compounds were identified. These compounds resemble the structure of fluoxetine, but lack the chemical features of an SSRI inhibitor and the chiral center. Mutations of resistant viruses of several EV serotypes point to a common druggable binding pocket for 2C inhibitors in EVs and RVs. The identified broad-spectrum inhibitors, together with the modeling studies, provide a basis for future development of highly potent 2C inhibitors targeting the predicted common druggable binding pocket. The identified pan-EV and RV compounds show very promising and highly potent antiviral efficacy without obvious cytotoxic effects *in vitro*. It would be desirable to develop these compounds further and prove their safety and efficacy in mouse models. Taken together, we demonstrated that host-targeting antiviral ITZ and direct-acting 2C inhibitors are promising candidates for the development of broad spectrum anti-EV therapy.

References

1. Strating, J. R. *et al.* Itraconazole inhibits enterovirus replication by targeting the oxysterol-binding protein. *Cell reports* 10, 600-615, doi:10.1016/j.celrep.2014.12.054 (2015).
2. Ulferts, R. *et al.* Selective serotonin reuptake inhibitor fluoxetine inhibits replication of human enteroviruses B and D by targeting viral protein 2C. *Antimicrobial agents and chemotherapy* 57, 1952-1956, doi:10.1128/AAC.02084-12 (2013).
3. Zuo, J. *et al.* Fluoxetine Is a Potent Inhibitor of Coxsackievirus Replication. *Antimicrobial agents and chemotherapy* 56, 4838-4844, doi:10.1128/Aac.00983-12 (2012).
4. Zuo, J. *et al.* Discovery of Structurally Diverse Small-Molecule Compounds with Broad Antiviral Activity against Enteroviruses. *Antimicrobial agents and chemotherapy* 60, 1615-1626, doi:10.1128/AAC.02646-15 (2015).
5. Tamm, I. *et al.* Relationship between structure of benzimidazole derivatives and selective virus inhibitory activity. Inhibition of poliovirus multiplication and cytopathic effects by 2-(alpha-hydroxybenzyl)-benzimidazole, and its 5-chloroderivative. *J Exp Med* 113, 625-656, doi:10.1084/jem.113.4.625 (1961).
6. Loddo, B., Ferrari, W., Brotzu, G. & Spanedda, A. In vitro inhibition of infectivity of polio viruses by guanidine. *Nature* 193, 97-98, doi:10.1038/193097a0 (1962).
7. Hollinshead, A. C. & Smith, P. K. Effects of certain purines and related compounds on virus propagation. *J Pharmacol Exp Ther* 123, 54-62 (1958).
8. Tamm, I. & Eggers, H. J. Differences in the selective virus inhibitory action of 2-(alpha-hydroxybenzyl)-benzimidazole and guanidine HCl. *Virology* 18, 439-447, doi:10.1016/0042-6822(62)90034-x (1962).
9. De Palma, A. M. *et al.* Anti-enterovirus activity and structure-activity relationship of a series of 2,6-dihalophenyl-substituted 1H,3H-thiazolo[3,4-a]benzimidazoles. *Biochem Biophys Res Commun* 353, 628-632, doi:10.1016/j.bbrc.2006.12.063 (2007).
10. De Palma, A. M. *et al.* The thiazolobenzimidazole TBZE-029 inhibits enterovirus replication by targeting a short region immediately downstream from motif C in the nonstructural protein 2C. *Journal of virology* 82, 4720-4730, doi:10.1128/JVI.01338-07 (2008).
11. Ulferts, R. *et al.* Screening of a library of FDA-approved drugs identifies several enterovirus replicon inhibitors that target viral protein 2C. *Antimicrobial agents and chemotherapy*, doi:10.1128/AAC.02182-15 (2016).
12. Sun, L. *et al.* Viral engagement with host receptors blocked by a novel class of tryptophan dendrimers that targets the 5-fold-axis of the enterovirus-A71 capsid. *PLoS pathogens* 15, e1007760, doi:10.1371/journal.ppat.1007760 (2019).
13. Musharrafieh, R. *et al.* Discovery of Quinoline Analogues as Potent Antivirals against Enterovirus D68 (EV-D68). *Journal of medicinal chemistry* 62, 4074-4090, doi:10.1021/acs.jmedchem.9b00115 (2019).
14. Klein, M., Hadaschik, D., Zimmermann, H., Eggers, H. J. & Nelsen-Salz, B. The picornavirus replication inhibitors HBB and guanidine in the echovirus-9 system: the significance of viral protein 2C. *J Gen Virol* 81, 895-901, doi:10.1099/0022-1317-81-4-895 (2000).
15. Hadaschik, D., Klein, M., Zimmermann, H., Eggers, H. J. & Nelsen-Salz, B. Dependence of echovirus 9 on the enterovirus RNA replication inhibitor 2-(alpha-Hydroxybenzyl)-benzimidazole maps to nonstructural protein 2C. *Journal of virology* 73, 10536-10539 (1999).
16. Klein, M., Eggers, H. J. & Nelsen-Salz, B. Echovirus 9 strain barty non-structural protein 2C has NTPase activity. *Virus Res* 65, 155-160 (1999).
17. Shimakami, T. *et al.* Protease inhibitor-resistant hepatitis C virus mutants with reduced fitness from impaired production of infectious virus. *Gastroenterology* 140, 667-675, doi:10.1053/j.gastro.2010.10.056 (2011).
18. Pfeiffer, J. K. & Kirkegaard, K. A single mutation in poliovirus RNA-dependent RNA polymerase confers resistance to mutagenic nucleotide analogs via increased fidelity. *Proceedings of the National Academy of Sciences of the United States of America* 100, 7289-7294, doi:10.1073/pnas.1232294100 (2003).
19. Yang, C. C. *et al.* A novel dengue virus inhibitor, BP13944, discovered by high-throughput screening with dengue virus replicon cells selects for resistance in the viral NS2B/NS3 protease. *Antimicrobial agents and chemotherapy* 58, 110-119, doi:10.1128/AAC.01281-13 (2014).
20. Abdelnabi, R. *et al.* Understanding the Mechanism of the Broad-Spectrum Antiviral Activity of Favipiravir (T-705): Key Role of the F1 Motif of the Viral Polymerase. *Journal of virology* 91, doi:10.1128/JVI.00487-17 (2017).
21. Lu, L., Mo, H., Pilot-Matias, T. J. & Molla, A. Evolution of resistant M414T mutants among hepatitis C virus replicon cells treated with polymerase inhibitor A-782759. *Antimicrobial agents and chemotherapy* 51, 1889-1896, doi:10.1128/AAC.01004-06 (2007).
22. Delang, L. *et al.* Mutations in the chikungunya virus non-structural proteins cause resistance to favipiravir (T-705), a broad-spectrum antiviral. *J Antimicrob Chemother* 69, 2770-2784, doi:10.1093/jac/dku209 (2014).
23. Sadeghipour, S., Bek, E. J. & McMinn, P. C. Selection and characterisation of guanidine-resistant mutants of human enterovirus 71. *Virus Res* 169, 72-79, doi:10.1016/j.virusres.2012.07.005 (2012).
24. Xia, H. *et al.* Human Enterovirus Nonstructural Protein 2CATPase Functions as Both an RNA Helicase and ATP-Independent RNA Chaperone. *PLoS pathogens* 11, e1005067, doi:10.1371/journal.ppat.1005067 (2015).
25. Adams, P., Kandiah, E., Effantin, G., Steven, A. C. & Ehrenfeld, E. Poliovirus 2C protein forms homo-oligomeric structures required for ATPase activity. *The Journal of biological chemistry* 284, 22012-22021, doi:10.1074/jbc.M109.031807 (2009).
26. Sweeney, T. R. *et al.* Foot-and-mouth disease virus 2C is a hexameric AAA+ protein with a coordinated ATP hydrolysis mechanism. *The Journal of biological chemistry* 285, 24347-24359, doi:10.1074/jbc.M110.129940 (2010).
27. Papageorgiou, N. *et al.* The 2C putative helicase of echovirus 30 adopts a hexameric ring-shaped structure. *Acta Crystallogr D Biol Crystallogr* 66, 1116-1120, doi:10.1107/S090744491002809X (2010).
28. Banerjee, S. *et al.* 2.3 A resolution cryo-EM structure of human p97 and mechanism of allosteric inhibition. *Science* 351, 871-875, doi:10.1126/science.aad7974 (2016).
29. Perez-Caballero, L., Torres-Sanchez, S., Bravo, L., Mico, J. A. & Berrocoso, E. Fluoxetine: a case history of its discovery and preclinical development. *Expert Opin Drug Discov* 9, 567-578, doi:10.1517/17460441.2014.907790 (2014).
30. Gofshsteyn, J., Cardenas, A. M. & Bearden, D. Treatment of Chronic Enterovirus Encephalitis With Fluoxetine in a Patient With X-Linked Agammaglobulinemia. *Pediatr Neurol*, doi:10.1016/j.pediatrneurol.2016.06.014 (2016).

31. Benkahla, M. A., Alidjinou, E. K., Sane, F., Desaillood, R. & Hober, D. Fluoxetine can inhibit coxsackievirus-B4 E2 in vitro and in vivo. *Antiviral research* 159, 130-133, doi:10.1016/j.antiviral.2018.10.002 (2018).
32. Messacar, K. *et al.* Safety, tolerability, and efficacy of fluoxetine as an antiviral for acute flaccid myelitis. *Neurology*, doi:10.1212/WNL.0000000000006670 (2018).
33. Hixon, A. M., Clarke, P. & Tyler, K. L. Evaluating Treatment Efficacy in a Mouse Model of Enterovirus D68-Associated Paralytic Myelitis. *J Infect Dis* 216, 1245-1253, doi:10.1093/infdis/jix468 (2017).
34. Guan, H. *et al.* Crystal structure of 2C helicase from enterovirus 71. *Sci Adv* 3, e1602573, doi:10.1126/sciadv.1602573 (2017).
35. Guan, H., Tian, J., Zhang, C., Qin, B. & Cui, S. Crystal structure of a soluble fragment of poliovirus 2CATPase. *PLoS pathogens* 14, e1007304, doi:10.1371/journal.ppat.1007304 (2018).
36. Amaro, R. E. *et al.* Ensemble Docking in Drug Discovery. *Biophys J* 114, 2271-2278, doi:10.1016/j.bpj.2018.02.038 (2018).
37. Lin, S. M. *et al.* Structure-Based Stabilization of Non-native Protein-Protein Interactions of Coronavirus Nucleocapsid Proteins in Antiviral Drug Design. *Journal of medicinal chemistry* 63, 3131-3141, doi:10.1021/acs.jmedchem.9b01913 (2020).
38. Lingappa, U. F. *et al.* Host-rabies virus protein-protein interactions as druggable antiviral targets. *Proceedings of the National Academy of Sciences of the United States of America* 110, E861-868, doi:10.1073/pnas.1210198110 (2013).
39. Muratore, G. *et al.* Small molecule inhibitors of influenza A and B viruses that act by disrupting subunit interactions of the viral polymerase. *Proceedings of the National Academy of Sciences of the United States of America* 109, 6247-6252, doi:10.1073/pnas.1119817109 (2012).
40. Takahashi, H. *et al.* Establishment of a robust dengue virus NS3-NS5 binding assay for identification of protein-protein interaction inhibitors. *Antiviral research* 96, 305-314, doi:10.1016/j.antiviral.2012.09.023 (2012).
41. Voter, A. F. & Keck, J. L. Development of Protein-Protein Interaction Inhibitors for the Treatment of Infectious Diseases. *Adv Protein Chem Struct Biol* 111, 197-222, doi:10.1016/bs.apcsb.2017.07.005 (2018).
42. Mabonga, L. & Kappo, A. P. Protein-protein interaction modulators: advances, successes and remaining challenges. *Biophys Rev* 11, 559-581, doi:10.1007/s12551-019-00570-x (2019).
43. Desmet, J. *et al.* Structural basis of IL-23 antagonism by an Alphabody protein scaffold. *Nature communications* 5, 5237, doi:10.1038/ncomms6237 (2014).
44. von Itzstein, M. *et al.* Rational design of potent sialidase-based inhibitors of influenza virus replication. *Nature* 363, 418-423, doi:10.1038/363418a0 (1993).
45. Hayden, F. G. *et al.* Intranasal pirodavir (R77,975) treatment of rhinovirus colds. *Antimicrobial agents and chemotherapy* 39, 290-294, doi:10.1128/aac.39.2.290 (1995).
46. Liu, H. M. *et al.* Characterization of poliovirus variants selected for resistance to the antiviral compound V-073. *Antimicrobial agents and chemotherapy* 56, 5568-5574, doi:10.1128/AAC.00539-12 (2012).
47. Sun, L. *et al.* Antiviral Activity of Broad-Spectrum and Enterovirus-Specific Inhibitors against Clinical Isolates of Enterovirus D68. *Antimicrobial agents and chemotherapy* 59, 7782-7785, doi:10.1128/AAC.01375-15 (2015).
48. Collett, M. S. *et al.* Antiviral Activity of Pocopavir in a Randomized, Blinded, Placebo-Controlled Human Oral Poliovirus Vaccine Challenge Model. *J Infect Dis* 215, 335-343, doi:10.1093/infdis/jiw542 (2017).
49. Hofmann, W. P., Soriano, V. & Zeuzem, S. Antiviral combination therapy for treatment of chronic hepatitis B, hepatitis C, and human immunodeficiency virus infection. *Handb Exp Pharmacol*, 321-346, doi:10.1007/978-3-540-79086-0_12 (2009).
50. Trosken, E. R. *et al.* Comparison of lanosterol-14 alpha-demethylase (CYP51) of human and *Candida albicans* for inhibition by different antifungal azoles. *Toxicology* 228, 24-32, doi:10.1016/j.tox.2006.08.007 (2006).
51. Lamb, D. C. *et al.* Characteristics of the heterologously expressed human lanosterol 14alpha-demethylase (other names: P45014DM, CYP51, P45051) and inhibition of the purified human and *Candida albicans* CYP51 with azole antifungal agents. *Yeast* 15, 755-763, doi:10.1002/(SICI)1097-0061(19990630)15:9<755::AID-YEA417>3.0.CO;2-8 (1999).
52. Shi, W. *et al.* Itraconazole side chain analogues: structure-activity relationship studies for inhibition of endothelial cell proliferation, vascular endothelial growth factor receptor 2 (VEGFR2) glycosylation, and hedgehog signaling. *Journal of medicinal chemistry* 54, 7363-7374, doi:10.1021/jm200944b (2011).
53. Nacev, B. A., Grassi, P., Dell, A., Haslam, S. M. & Liu, J. O. The antifungal drug itraconazole inhibits vascular endothelial growth factor receptor 2 (VEGFR2) glycosylation, trafficking, and signaling in endothelial cells. *The Journal of biological chemistry* 286, 44045-44056, doi:10.1074/jbc.M111.278754 (2011).
54. Head, S. A. *et al.* Antifungal drug itraconazole targets VDAC1 to modulate the AMPK/mTOR signaling axis in endothelial cells. *Proceedings of the National Academy of Sciences of the United States of America* 112, E7276-7285, doi:10.1073/pnas.1512867112 (2015).
55. Chong, C. R. *et al.* Inhibition of angiogenesis by the antifungal drug itraconazole. *ACS chemical biology* 2, 263-270, doi:10.1021/cb600362d (2007).
56. Kim, J. *et al.* Itraconazole, a commonly used antifungal that inhibits Hedgehog pathway activity and cancer growth. *Cancer cell* 17, 388-399, doi:10.1016/j.ccr.2010.02.027 (2010).
57. Head, S. A. *et al.* Simultaneous Targeting of NPC1 and VDAC1 by Itraconazole Leads to Synergistic Inhibition of mTOR Signaling and Angiogenesis. *ACS chemical biology* 12, 174-182, doi:10.1021/acscchembio.6b00849 (2017).
58. Li, Y. *et al.* Novel Tetrazole-Containing Analogues of Itraconazole as Potent Antiangiogenic Agents with Reduced Cytochrome P450 3A4 Inhibition. *Journal of medicinal chemistry* 61, 11158-11168, doi:10.1021/acs.jmedchem.8b01252 (2018).
59. Isoherranen, N., Kunze, K. L., Allen, K. E., Nelson, W. L. & Thummel, K. E. Role of itraconazole metabolites in CYP3A4 inhibition. *Drug metabolism and disposition: the biological fate of chemicals* 32, 1121-1131, doi:10.1124/dmd.104.000315 (2004).
60. Guengerich, F. P. Cytochrome P-450 3A4: regulation and role in drug metabolism. *Annu Rev Pharmacol Toxicol* 39, 1-17, doi:10.1146/annurev.pharmtox.39.1.1 (1999).
61. Wen, J., Chennamadhavuni, D., Morel, S. R. & Hadden, M. K. Truncated Itraconazole Analogues Exhibiting Potent Anti-Hedgehog Activity and Improved Drug-like Properties. *ACS Med Chem Lett* 10, 1290-1295, doi:10.1021/acsmchemlett.9b00188 (2019).
62. Albuлесcu, L. *et al.* Uncovering oxysterol-binding protein (OSBP) as a target of the anti-enteroviral compound TTP-8307. *Antiviral research* 140, 37-44, doi:10.1016/j.antiviral.2017.01.008 (2017).
63. Olkkonen, V. M. OSBP-Related Protein Family in Lipid Transport Over Membrane Contact Sites. *Lipid insights* 8, 1-9, doi:10.4137/LPI.S31726 (2015).

64. Roberts, B. L. *et al.* Differing activities of oxysterol-binding protein (OSBP) targeting anti-viral compounds. *Antiviral research* 170, 104548, doi:10.1016/j.antiviral.2019.104548 (2019).
65. Albulescu, L. *et al.* Broad-range inhibition of enterovirus replication by OSW-1, a natural compound targeting OSBP. *Antiviral research* 117, 110-114, doi:10.1016/j.antiviral.2015.02.013 (2015).
66. Burgett, A. W. *et al.* Natural products reveal cancer cell dependence on oxysterol-binding proteins. *Nature chemical biology* 7, 639-647, doi:10.1038/nchembio.625 (2011).
67. Hynynen, R. *et al.* OSBP-related protein 2 is a sterol receptor on lipid droplets that regulates the metabolism of neutral lipids. *Journal of lipid research* 50, 1305-1315, doi:10.1194/jlr.M800661-JLR200 (2009).
68. Melia, C. E. *et al.* Origins of Enterovirus Replication Organelles Established by Whole-Cell Electron Microscopy. *mBio* 10, doi:10.1128/mBio.00951-19 (2019).
69. Roulin, P. S. *et al.* Rhinovirus uses a phosphatidylinositol 4-phosphate/cholesterol counter-current for the formation of replication compartments at the ER-Golgi interface. *Cell host & microbe* 16, 677-690, doi:10.1016/j.chom.2014.10.003 (2014).
70. Koponen, A. *et al.* ORP2 interacts with phosphoinositides and controls the subcellular distribution of cholesterol. *Biochimie* 158, 90-101, doi:10.1016/j.biochi.2018.12.013 (2019).
71. Charman, M., Colbourne, T. R., Pietrangelo, A., Kreplak, L. & Ridgway, N. D. Oxysterol-binding protein (OSBP)-related protein 4 (ORP4) is essential for cell proliferation and survival. *The Journal of biological chemistry* 289, 15705-15717, doi:10.1074/jbc.M114.571216 (2014).
72. Shim, A. *et al.* Therapeutic and prophylactic activity of itraconazole against human rhinovirus infection in a murine model. *Scientific reports* 6, 23110, doi:10.1038/srep23110 (2016).
73. Rhoden, E., Nix, W. A., Weldon, W. C. & Selvarangan, R. Antifungal azoles itraconazole and posaconazole exhibit potent in vitro antiviral activity against clinical isolates of parechovirus A3 (Picornaviridae). *Antiviral research* 149, 75-77, doi:10.1016/j.antiviral.2017.11.011 (2018).
74. Lanko, K., Ma, Y., Delang, L., Mirabelli, C. & Neyts, J. Antiviral effects of selected nucleoside analogues against human parechoviruses A1 and A3. *Antiviral research* 162, 51-53, doi:10.1016/j.antiviral.2018.12.009 (2019).
75. Rhoden, E. *et al.* Antifungal Triazole Posaconazole Targets an Early Stage of the Parechovirus A3 Life Cycle. *Antimicrobial agents and chemotherapy* 64, doi:10.1128/AAC.02372-19 (2020).
76. Takano, T., Akiyama, M., Doki, T. & Hohdatsu, T. Antiviral activity of itraconazole against type I feline coronavirus infection. *Vet Res* 50, 5, doi:10.1186/s13567-019-0625-3 (2019).
77. Takano, T. *et al.* The cholesterol transport inhibitor U18666A inhibits type I feline coronavirus infection. *Antiviral research* 145, 96-102, doi:10.1016/j.antiviral.2017.07.022 (2017).
78. van der Schaar, H. M., Dorobantu, C. M., Albulescu, L., Strating, J. R. & van Kuppeveld, F. J. Fat(al) attraction: Picornaviruses Usurp Lipid Transfer at Membrane Contact Sites to Create Replication Organelles. *Trends in microbiology* 24, 535-546, doi:10.1016/j.tim.2016.02.017 (2016).
79. Baggen, J., Thibaut, H. J., Strating, J. & van Kuppeveld, F. J. M. The life cycle of non-polio enteroviruses and how to target it. *Nat Rev Microbiol* 16, 368-381, doi:10.1038/s41579-018-0005-4 (2018).
80. Lamarche, M. J. *et al.* Anti-hepatitis C virus activity and toxicity of type III phosphatidylinositol-4-kinase beta inhibitors. *Antimicrobial agents and chemotherapy* 56, 5149-5156, doi:10.1128/AAC.00946-12 (2012).
81. van der Linden, L., Wolthers, K. C. & van Kuppeveld, F. J. Replication and Inhibitors of Enteroviruses and Parechoviruses. *Viruses* 7, 4529-4562, doi:10.3390/v7082832 (2015).
82. van der Schaar, H. M. *et al.* Coxsackievirus mutants that can bypass host factor PI4KIIIbeta and the need for high levels of PI4P lipids for replication. *Cell research* 22, 1576-1592, doi:10.1038/cr.2012.129 (2012).
83. Arita, M. Mechanism of Poliovirus Resistance to Host Phosphatidylinositol-4 Kinase III beta Inhibitor. *ACS infectious diseases* 2, 140-148, doi:10.1021/acsinfecdis.5b00122 (2016).
84. Arita, M. *et al.* Oxysterol-binding protein family I is the target of minor enviroxime-like compounds. *Journal of virology* 87, 4252-4260, doi:10.1128/JVI.03546-12 (2013).
85. Wang, Y. *et al.* In Vitro Assessment of Combinations of Enterovirus Inhibitors against Enterovirus 71. *Antimicrobial agents and chemotherapy* 60, 5357-5367, doi:10.1128/AAC.01073-16 (2016).
86. Cho, N. J. *et al.* Phosphatidylinositol 4,5-bisphosphate is an HCV NS5A ligand and mediates replication of the viral genome. *Gastroenterology* 148, 616-625, doi:10.1053/j.gastro.2014.11.043 (2015).
87. Shengjuler, D. *et al.* The RNA-Binding Site of Poliovirus 3C Protein Doubles as a Phosphoinositide-Binding Domain. *Structure* 25, 1875-1886 e1877, doi:10.1016/j.str.2017.11.001 (2017).
88. Banerjee, S. *et al.* Hijacking of multiple phospholipid biosynthetic pathways and induction of membrane biogenesis by a picornaviral 3CD protein. *PLoS pathogens* 14, e1007086, doi:10.1371/journal.ppat.1007086 (2018).
89. van den Bout, I. & Divecha, N. PIP5K-driven PtdIns(4,5)P2 synthesis: regulation and cellular functions. *Journal of cell science* 122, 3837-3850, doi:10.1242/jcs.056127 (2009).
90. Hammond, G. R., Schiavo, G. & Irvine, R. F. Immunocytochemical techniques reveal multiple, distinct cellular pools of PtdIns4P and PtdIns(4,5)P(2). *The Biochemical journal* 422, 23-35, doi:10.1042/BJ20090428 (2009).
91. Belov, G. A. *et al.* Bidirectional increase in permeability of nuclear envelope upon poliovirus infection and accompanying alterations of nuclear pores. *Journal of virology* 78, 10166-10177, doi:10.1128/JVI.78.18.10166-10177.2004 (2004).

Chapter 8

Addendum

8

Nederlandse samenvatting

Een mens wordt blootgesteld aan vele verschillende ziekteverwekkers, zoals bacteriën, schimmels, wormen, helmithen en virussen. Virussen zijn obligate, intracellulaire parasieten die uit genetisch materiaal bestaan - DNA of RNA - dat omgeven en beschermd wordt door een laag bestaande uit eiwitten en/of vetten. Virussen kunnen een grote verscheidenheid aan ziekten veroorzaken. De familie *Picornaviridae* is een van de grootste families van virussen en in het bijzonder het geslacht Enterovirus herbergt talrijke virussen die mensen en/of dieren kunnen aantasten.

Tot de enterovirussen behoren vele virussen die wereldwijd voor komen regelmatig infecties veroorzaken, zoals de poliovirussen, genummerde enterovirussen (EV), echovirussen, coxsackievirussen (CV) en rhinovirussen (RV). Deze virussen kunnen zich in verscheidene klinische symptomen uiten, zoals bijvoorbeeld kinderverlamming (poliomyelitis), hand-voet-mond-ziekte, gastroenteritis, conjunctivitis, myocarditis, pericarditis, encefalitis en meningitis. Ook verschillende ziektes van de bovenste luchtwegen kunnen door deze virussen worden veroorzaakt. RV veroorzaken voornamelijk een loopneus en verkoudheid, maar kunnen ook tot een verergering van astma en chronische obstructieve longziekte (COPD) leiden. Hoewel deze virussen klinisch relevant zijn, zijn er maar beperkte bestrijdingswijzen. Om virusinfecties te vermijden tegen sommige virussen zijn vaccins beschikbaar. Wanneer men al een infectie met een virus heeft opgelopen, zijn soms behandelingen mogelijk met tegen het virus gerichte antilichamen die het virus onschadelijk maken of met antivirale geneesmiddelen die de vermeerdering of verspreiding van het virus tegengaan.

Ter bestrijding van enterovirussen bestaan er nu alleen tot de markt toegelaten vaccins tegen poliovirus en EV-A71. Voor alle andere enterovirussen zijn er op dit moment geen goedgekeurde vaccins. Omdat er veel verschillende soorten enterovirussen en rhinovirussen bestaan (>250 typen), is het heel onwaarschijnlijk dat vaccins die het hele geslacht van enterovirussen onschadelijk maken ontwikkeld kunnen worden.

Een alternatieve aanpak is de ontwikkeling van antivirale geneesmiddelen die een breed-spectrum, wellicht het hele spectrum aan enterovirussen, kunnen remmen. Op dit moment bestaan er geen antivirale geneesmiddelen ter bestrijding van enterovirussen.

De ontwikkeling van antivirale geneesmiddelen is een onderzoeksproces dat op de ontdekking van nieuwe chemische verbindingen berust. Antivirale geneesmiddelen kunnen een virus-specifieke werking hebben, wat betekent dat zij het virus zelf aanvallen. Andere antivirale geneesmiddelen zijn gericht tegen de onderdelen van de gastheercel die voor het virus essentieel zijn.

De klassieke basis om nieuwe antivirale geneesmiddelen te ontwikkelen is het fenotypisch screenen van grote bibliotheken van chemische stoffen. Deze methode kan enerzijds worden toegepast op gastheerspecifieke assays, speciaal voor virussen die de gastheercel in het proces van virusrepliatie doden. Aan de andere kant kunnen assays

worden ingezet die de enzymfuncties van virale eiwitten meten. Heden ten dage worden fenotypische screeningsmethoden geautomatiseerd uitgevoerd, waardoor duizenden tot miljoenen chemische stoffen op hun antivirale activiteit getest kunnen worden.

Vooruitgang op het gebied van structurele biologie heeft de molecuulstructuren gebaseerde ontwikkeling van antivirale geneesmiddelen gestimuleerd. Voor het proces van de geneesmiddelontwikkeling gebruikt deze methode de informatie van 3D eiwitstructuren, waardoor chemische stoffen geïdentificeerd kunnen worden die specifiek op een bepaald eiwit werken. Indien geen structuur beschikbaar is van het eiwit waar men in geïnteresseerd is kan als alternatief een ligand-gebaseerde methode worden gehanteerd. De ligand-gebaseerde methode gebruikt de structurele informatie van verscheidende liganden die allemaal een bepaald eiwit remmen. Alle deze methoden behoren tot de klassieke *de novo* geneesmiddelenontwikkeling, die vooral zeer kostbaar en tijdrovend is. In de laatste jaren is de methode van *drug repurposing* ('*geneesmiddel herbestemming*') in opmars. Bij deze methode wordt onderzocht of bestaande stoffen die al als geneesmiddel toegepast worden of in ontwikkeling zijn (geweest) nieuwe medicinale toepassingen hebben. Dit heeft het voordeel dat farmacologische en toxicologische profielen van deze geneesmiddelen vaak al voorhanden zijn. Als door *drug repurposing* geneesmiddelen ontdekt worden die een goed activiteitsprofiel tonen, kan goedkeuring van het medicijn sneller en goedkoper gebeuren, aangezien men de preklinische fase en de klinische Fase I ontwikkeling meestal kan overslaan, mits de toegediende dosering van het geneesmiddel hetzelfde of geringer is.

Door de jaren heen zijn meerdere antivirale geneesmiddelen tegen enterovirussen ontwikkeld. Het verst gevorderd in klinische studies is de klasse van zogenaamde *capside-binders*, stoffen die zich aan de oppervlaktestructuur van deze virussen binden en daarbij het binnendringen van het virus in de gastheercel belemmeren. Veel stoffen in deze klasse tonen een goede antivirale activiteit tegen een breed spectrum aan enterovirussen, maar er bestaan ook klinische isolaten die van nature resistent zijn. Een ander nadeel van *capside-binders* is dat enterovirussen in het algemeen zeer snel resistentie tegen deze stoffen ontwikkelen. Naast de oppervlakstructuren van de virussen zijn er ook nog andere virale eiwitten die goede aanknopingspunten voor geneesmiddelenontwikkeling kunnen vormen. Deze eiwitten hebben verschillende activiteiten tijdens de virale replicatie binnen de gastheercel. Er zijn stoffen ontwikkeld die het eiwit proteïne 3C^{pro} (een viraal protease dat het virale polyproteïne verwerkt), het virale polymerase 3D^{pol} of het multifunctionele virale eiwit 2C remmen. Verder zijn ook klassen van stoffen ontwikkeld die gastheereiwitten remmen. Veel van deze moleculen zijn ook in klinische studies getest, maar zijn gestrand vanwege een gebrek aan antivirale activiteit. In **hoofdstuk 2** is een samenvatting van de enterovirus-remmers en hun status in klinische studies te vinden.

In een *drug repurposing* screening zijn verscheidene goedgekeurde geneesmiddelen gevonden die de replicatie van enterovirussen remmen. Een van deze geneesmiddelen is itraconazol (ITZ; Sporanox®), een antimycoticum (antischimmel medicijn) uit de groep van de triazolen die bij schimmelinfecties oraal of intraveneus gegeven kunnen

worden. Daarnaast blijkt ITZ ook antikankeractiviteit te hebben die onafhankelijk is van de antischimmelactiviteit, waarvoor het in klinische studies getest wordt. Studies in andere labs hebben eiwitten geïdentificeerd die door ITZ geremd worden en wat zowel de antischimmelactiviteit als de antikankeractiviteit kan verklaren. Al deze doeleiwitten verklaarden echter niet hoe itraconazole enterovirussen kan remmen. Bij vervolgonderzoek in ons lab is het oxysterol-bindende eiwit (oxysterol-binding protein; OSBP), wat fosfolipiden en cholesterol bindt en transporteert, als aangrijpingspunt geïdentificeerd. In **hoofdstuk 3** zijn de resultaten van een studie naar de relatie tussen structuur en activiteit beschreven waarbij het doel was om de andere farmacologische activiteiten van ITZ te scheiden van de antivirale activiteit.

De chemische structuur van het zeer lipofiele ITZ molecuul bestaat uit vijf lineair verknoopte ringen (dioxo-lanyl-methoxyfenyl-piperaziny-fenyl-triazolon). De diaxonale ring aan het molecuuleinde beschikt over een dichlorofenyl en een triazol-groep. De triazol-groep is belangrijk voor de antischimmelactiviteit omdat betrokken is bij het remmen van een belangrijk schimmelenzym en daardoor de integriteit van de celwand van de schimmel verstoort. Een bijwerking van deze triazol-groep is echter dat deze ook betrokken is bij een nevenactiviteit van ITZ, namelijk het remmen van een belangrijk enzym in menselijke cellen dat geneesmiddelen kan metaboliseren. De triazol-ring aan de andere kant van het molecuul beschikt over een *sec*-butyl keten. De antikankeractiviteit is geassocieerd met de vertakte *sec*-butyl keten. De studie in **hoofdstuk 3** heeft aangetoond dat de triazol-groep – hoofdverantwoordelijk voor de antischimmelactiviteit – niet noodzakelijk voor de antivirale activiteit is. Daarom kan men deze twee farmacologische activiteiten van elkaar scheiden. De vertakking van de *sec*-butyl keten, die essentieel is voor de antikankeractiviteit, is ook essentieel voor de antivirale activiteit. Echter kunnen in plaats van de vertakte *sec*-butyl keten verschillende andere chemische groepen worden toegevoegd die een scheiding van deze activiteiten toestaan. De chemische kernstructuur van ITZ bestaat uit vijf lineair geschakelde ringen die allemaal voor de antivirale activiteit essentieel zijn. Verkortingen van deze keten van ringen leidt tot verlies van de antivirale activiteit. Interessant is dat de ringen zelf kunnen worden aangepast om de lipofiliciteit van het molecuul te verminderen. Deze studie toonde aan, dat men de antischimmelactiviteit en deels ook de antikankeractiviteit door verandering van de chemische structuur kan loskoppelen van de antivirale activiteit. Verder hebben wij met een *in silico* studie onderzocht hoe itraconazole aan het doeleiwit OSBP zou kunnen binden. Deze studie vormt een basis waarop de ontwikkeling van itraconazole-afgeleide moleculen voor virusbestrijdingstoepassingen voortgezet kan worden.

In een andere *drug repurposing* screen werd fluoxetine (Prozac®) als remmer van de replicatie van enterovirussen ontdekt. Fluoxetine werd op 29 december 1987 door de Amerikaanse Food and Drug Administration (FDA) toegelaten op de Amerikaanse markt en was de eerste grote doorbraak in de behandeling van depressies. Het was het eerst toegelaten medicijn van de nieuw ontwikkelde groep selectieve serotonineheropnameremmers (selective serotonin reuptake inhibitors; SSRI). In

hoofdstuk 4 is het antivirale werkingsmechanisme van fluoxetine bestudeerd. De chemische structuur van fluoxetine herbergt een chiraal centrum, wat ertoe leidt dat er twee fluoxetine enantiomeren bestaan. Deze enantiomere structuren hebben dezelfde empirische formule, maar hun ruimtelijke conformatie is anders en ze gedragen zich als een niet-congruent spiegelbeeld. In **hoofdstuk 4** is beschreven dat de (S)-enantiomeer, maar niet de (R)-enantiomeer, verantwoordelijk is voor de antivirale activiteit. Verder is aangetoond dat het racemische fluoxetine (een 1:1-mengsel van de (S)-enantiomeer en (R)-enantiomeer) alleen EV-B en EV-D types remt, maar niet EV-A, EV-C of RV. Bij deze studie is ook het (S)-enantiomeer tegen prototypische serotypen van verschillende enterovirussen en rhinovirussen getest. Het (S)-enantiomeer toonde een hogere antivirale activiteit tegen EV-B en EV-D types en ook RV types werden geremd. Dit duidt op een correlatie tussen een hogere antivirale activiteit en een breder antiviraal spectrum. Als eiwit waarop fluoxetine aangrijpt werd het multifunctionele virale eiwit 2C - een ATPase - geïdentificeerd. In overeenstemming met de antivirale activiteit van het (S)-enantiomeer is aangetoond dat alleen het (S)-enantiomeer maar niet het (R)-enantiomeer aan recombinant 2C eiwit bindt. Om het mechanisme van de interactie tussen fluoxetine en het doeleiwit 2C verder te bestuderen is een homologiemodel gemaakt van een fluoxetine-gevoelig coxsackievirus-B3 (behorend bij de soort EV-B) gegenereerd, waarbij gebruikt gemaakt is van een eerder gepubliceerde structuur van een fluoxetine-ongevoelig 2C eiwit van EV-A71 (behorend bij de soort EV-A). Dit model is gebruikt om mutaties in 2C op mogelijke bindingsplaatsen van fluoxetine aan 2C, waarvan al bekend is dat ze resistentie tegen fluoxetine veroorzaken, te bestuderen. Door deze studie konden resistentiemutaties van 2C-remmers met verschillende molecuulstructuren worden verklaard.

Verder werd het model gebruikt om de nieuwe aminozuren in de bindingsplekken te identificeren die betrokken zijn bij de binding van fluoxetine. Samengevat verschaft deze studie de eerste moleculaire inzichten in het antivirale werkingsmechanisme van fluoxetine via het doeleiwit 2C.

Fluoxetine wordt ter behandeling van depressies, diverse dwang- en angststoornissen en boulimia gebruikt. De bijwerkingen lopen uiteen van hoofdpijn, duizeligheid, diarree, tremoren, lichtgevoeligheid en seksuele disfunctie tot een verhoogd suïciderisico. Veel van deze bijwerkingen zijn te wijten aan de SSRI-activiteit van fluoxetine. Om de farmacologische eigenschappen van fluoxetine die voor de antivirale activiteit verantwoordelijk zijn te ontdekken is in **hoofdstuk 5** een studie naar de relatie tussen structuur en activiteit uitgevoerd. Het uitgangspunt van deze studie waren de resultaten zoals beschreven in **hoofdstuk 4**, waarin aangetoond werd dat het *N*-Methyl-3-(4-(trifluoromethyl)fenoxy)propan-1-amine-fragment matige antivirale activiteit heeft. Dit resultaat laat zien dat de structurele eigenschappen van de trifluorofenoxyl-groep en die van de amino-groep aan het andere einde van het molecuul voor de antivirale activiteit belangrijk zijn, terwijl de 3-fenyl-groep niet noodzakelijk is. In de trifluorofenoxyl-groep van fluoxetine bevindt de trifluoro-substituent die verantwoordelijk is voor de SSRI-activiteit van fluoxetine zich op de

para-positie. We hebben aangetoond dat veranderingen in deze groep de affiniteit van fluoxetine met de serotonine-receptor veranderen en hierdoor mogelijk ook de bijwerkingen reduceren. Daarom hebben we ook fluoxetine-analogen gesynthetiseerd die veranderingen in de trifluoro-groep hebben. Alle veranderingen in deze chemische groep leidden tot verlies van de antivirale activiteit. Substituties voor de aminogroep zijn ook gesynthetiseerd. Dit resulteerde in een racemische fluoxetine-analoog met vergelijkbare antivirale activiteit als (S)-fluoxetine. Om uit te zoeken of de analogen een vergelijkbaar resistentieprofiel vertoonden als fluoxetine, waaruit af te leiden is dat ze waarschijnlijk op dezelfde plekken aan het 2C eiwit binden, zijn een aantal van de in **hoofdstuk 3** gevonden virussen met verschillende mutaties in 2C op hun resistentie tegen de nieuwe fluoxetine-analogen getest. Daarbij hebben we gezien dat de virussen met 2C-mutaties niet alleen resistent zijn tegen fluoxetine, maar ook tegen de nieuwe fluoxetine-analogen. Net als bij fluoxetine heeft ook de meest potente analoog **2b** een chiraal centrum. In **hoofdstuk 5** is de stereochemie van dit nieuwe molecuul bestudeerd. Het S-enantiomeer had een verhoogde antivirale activiteit en een verbreed antiviraal spectrum in vergelijking met het racemische mengsel. Interessant is dat ook het R-enantiomeer van deze fluoxetine-analoog ook enige antivirale activiteit toonde tegen soorten EV-B en EV-D, terwijl de R-enantiomeer van fluoxetine zelf niet actief was tegen EV-B en EV-D. Vergelijkbaar met fluoxetine, had ook de (S)-enantiomeer van deze fluoxetine-analoog **2b** een sterkere binding aan recombinant 2C eiwit. In **hoofdstuk 5** laten we ook zien dat een racemisch mengsel van deze fluoxetine-analoog met een verandering in de aminogroep vergelijkbare antivirale activiteit heeft als (S)-fluoxetine. Samenvattend hebben we kunnen aantonen dat de chirale conformatie van fluoxetine en fluoxetine-analogen belangrijke is voor de antivirale activiteit, aangezien de (S)-enantiomeren een beduidend hogere antivirale activiteit hebben dan de (R)-enantiomeren. Uit deze studie kunnen we ook concluderen dat de SSRI-activiteit en de antivirale activiteit van fluoxetine niet van elkaar losgekoppeld kunnen worden. De in **hoofdstuk 4** en **5** beschreven resultaten laten zien dat antivirale activiteit van fluoxetine afhangt van een stereospecifieke directe binding aan het virale eiwit 2C. Anderzijds kon worden vastgesteld dat dezelfde chemische groepen die van belang zijn voor de SSRI-activiteit van fluoxetine ook essentieel zijn voor de antivirale activiteit, waardoor beide activiteiten niet losgekoppeld kunnen worden. Dit vormt een uitdaging voor een mogelijke therapeutische toepassing van fluoxetine en laat zien dat nieuwe geneesmiddelen met een hogere antivirale activiteit en idealiter ook met een pan-enterovirus en -rhinovirus spectrum nodig zijn.

In **hoofdstuk 6** is een van een studie naar de relatie tussen structuur en activiteit uitgevoerd met het molecuul N-(4-fluorobenzyl)-N-(4-methoxyfenyl)furan-2-carboxamide, wat recent als remmer voor leden van de soort EV-B is geïdentificeerd. Dit molecuul was om meerdere redenen interessant. Enerzijds toont het structurele overeenkomsten met fluoxetine, maar mist het de trifluoromethylgroep en heeft het daardoor hoogstwaarschijnlijk geen SSRI-activiteit. Anderzijds is het een planaar molecuul zonder chiraal centrum. De studie leverde meerdere hoogpotente pan-EV

en RV-remmers op. De meeste hiervan hadden een vergelijkbaar resistentieprofiel als (S)-fluoxetine, met uitzondering van één analoog, welke een ander profiel toonde. Virussen die resistent zijn tegen (S)-fluoxetine en de andere nieuwe analogen hadden nauwelijks resistentie tegen molecuul **19d** zien. Daarom hebben wij **19d**-resistente EV-A71, CV-B3 en EV-D68 virussen geproduceerd. Wij hebben mutaties in het virale eiwit 2C geïdentificeerd die deze resistentie kunnen veroorzaken. Alle resistente virussen ontwikkelden minstens één mutatie in of dichtbij de $\alpha 2$ -helix van het 2C eiwit. *In silico* modellering toonde enkele tunnels binnen de kristalstructuren van 2C voor EV-A71 en poliovirus die de binding van moleculen aan 2C toelaten. Deze tunnels overlappen met de potentiële bindingsplek voor fluoxetine als beschreven in **hoofdstuk 4**. Daarnaast is gevonden dat de antivirale activiteit van sommige moleculen in het therapeutisch relevante bereik ligt en dat de eigenschappen van neuronen niet veranderden door deze moleculen, in tegenstelling tot fluoxetine. Ook de opname van dopamine, serotonine en norepinefrine werden niet beïnvloed. Deze studie toonde aan dat het virale eiwit 2C een uitstekend doelwit voor pan-enterovirus en -rhinovirus remmers is. Moleculair-biologische en virologische data leveren ook de eerste inzichten dat enterovirussen en rhinovirussen een vergelijkbare bindingsplek voor remmers hebben die in alle enterovirussen en rhinovirussen geconserveerd is.

Deutsche Zusammenfassung

Der menschliche Organismus ist verschiedensten Krankheitserregern ausgesetzt; darunter fallen Bakterien, Pilze, Würmer, Helminthen und Viren. Viren sind obligate, intrazelluläre Parasiten, bestehend aus einem genetischen Material, entweder DNS oder RNS, welches von Proteinstrukturen umgeben und geschützt wird. Viren können unterschiedliche Organsysteme befallen und eine Vielzahl an Krankheiten verursachen. Die Familie *Picornaviridae* zählt zu einer der größten Virenfamilien und speziell die Gattung der Enteroviren beinhaltet zahlreiche Viren, die sowohl Menschen als auch Tiere befallen können. Für den Menschen besonders bedeutsam sind Polioviren, Enteroviren (EV), Coxsackieviren (CV) und Rhinoviren (RV), die jedes Jahr weltweit virale Infektionen verursachen. Diese Viren können unterschiedliche klinische Symptome hervorrufen, wie zum Beispiel Kinderlähmung (Poliomyelitis), Hand-Fuß-Mund-Krankheit, Gastroenteritis, Konjunktivitis, Myokarditis, Perikarditis, Enzephalitis und Meningitis. Auch unterschiedliche Erkrankungen des oberen Respirationstraktes können durch diese Viren verursacht werden. RV verursachen hauptsächlich Schnupfen und Erkältungen, können aber auch bei Verschlimmerungen zu Asthma und chronisch obstruktiver Lungenerkrankungen (COPD) führen. Obwohl diese Viren klinisch relevant sind, gibt es nur bedingte Bekämpfungsmethoden. Um Vireninfektionen vorzubeugen gibt es präventive Impfungen. Kommt es jedoch zu einer viralen Erkrankung, erfolgt die Behandlung häufig mit gegen das Virus gerichteten Antikörpern, die den Virus unschädlich machen, oder mittels antiviralen Medikamenten. Zur Bekämpfung der EV gibt es zurzeit nur zugelassene Impfstoffe gegen das Poliovirus und EV-A71, jedoch für alle anderen EV gibt es derzeit keine zugelassenen Impfstoffe. Da EV und RV eine Vielzahl verschiedener Serotypen – unterschiedliche Variationen von EV und RV-besitzen (>250 Serotypen), ist die Entwicklung von Impfstoffen, die die gesamte Gattung der EV unschädlich macht, sehr unwahrscheinlich. Eine alternative Behandlungsmethode ist die Entwicklung von hochwirksamen antiviralen Medikamenten, die ein großes Spektrum, wenn nicht sogar das komplette Spektrum an EV inhibieren kann. Zurzeit sind antivirale Medikamente zur Bekämpfung von EV jedoch nicht vorhanden.

Die Herstellung antiviraler Arzneimittel ist ein Forschungsprozess, der auf der Entwicklung und der Entdeckung neuer chemischer Verbindungen beruht. Antivirale Medikamente können virusspezifisch sein, das bedeutet, dass sie den Virus selber angreifen. Andere antivirale Medikamente sind wirtsspezifisch und richten sich gegen die Strukturen des Wirts, die essentiell für den Virus sind. Die Grundlage für neu zu entwickelnde antivirale Medikamente, ist das phenotypische Screening von großen Bibliotheken chemischer Stoffe. Diese Methode kann auf wirtszellen-basierenden Assays speziell für Viren, die die Wirtszelle im Zuge der Virenreplikation töten angewendet werden.

Andererseits können Assays verwendet werden, die die enzymatischen Funktionen viraler Eiweiße (Proteine) messen. Heutzutage werden phenotypische Screeningsmethoden von automatisierten Plattformen durchgeführt, die bis zu

Tausende, wenn nicht sogar Millionen chemischer Stoffe gleichzeitig für ihre antivirale Aktivität evaluieren können. Zusätzlich haben Fortschritte im Feld der Strukturbiologie die Entwicklung von struktur-basierten antiviralen Medikamenten gefördert. Für den Prozess der Medikamentenentwicklung verwendet diese Methode die Information von 3D-Proteinstrukturen, wodurch chemische Stoffe identifiziert werden können, die sich gegen dieses spezifische Protein richten. Wenn keine Struktur des gewünschten Proteins vorhanden ist, kann als Alternative eine Ligand-basierende Entwicklungsmethode verwendet werden. Die Ligand-basierte Methode verwendet die strukturelle Information verschiedener Liganden, die ein spezifisches Protein hemmen. All diese Methoden zählen zur klassischen *De-novo* Medikamentenentwicklung, die vor allem sehr kostspielig und langwierig ist. Als Alternative dazu wurde das *Drug repurposing* („Medikamenten Wiederverwendung“) entwickelt. Bei dieser attraktiven Methode wird versucht, existierende Arzneistoffe vielfältiger zu verwenden. Dies hat den Vorteil, dass pharmakologische und toxikologische Profile dieser Medikamente schon vorhanden sind. Wenn durch *Drug repurposing* Arzneimittel gefunden werden, die eine gute Wirksamkeit aufweisen, kann die Zulassung des Medikamentes schneller und kostengünstiger erfolgen, da man prä-klinische Testphasen und die klinische Phase I überspringen kann, sofern das Medikament in gleicher oder sogar in geringerer Dosierung verabreicht werden kann.

Über die Jahre hinweg wurden mehrere antivirale Medikamente gegen EV entwickelt. Die Klasse der *Capsid-Binder*, Stoffe, die an die Oberflächenstrukturen dieser Viren binden und dabei die Bindung des Virus an den Rezeptor der Wirtszelle verhindern, sind in klinischen Studien am meisten fortgeschritten. Viele Stoffe dieser Klasse zeigen eine gute antivirale Aktivität gegen ein großes Spektrum an EV, jedoch gibt es einige klinische Isolate, die von Natur aus resistent sind. Ein weiterer Nachteil der *Capsid-Binder* besteht darin, dass EV generell sehr schnell Resistenz gegen diese Stoffe entwickeln. Neben den Oberflächenstrukturen der Viren gibt es auch weitere Proteine, die gute Ziele für Medikamentenentwicklung sind. Diese Proteine haben unterschiedliche Aktivitäten und sind während der viralen Replikation innerhalb der Wirtszelle konstant im Einsatz. Es wurden Substanzen entwickelt, die das virale Protein 3C (virale Protease, prozessiert das Polyprotein), die virale Polymerase 3D oder das multifunktionale Protein 2C inhibieren. Des Weiteren wurden auch Stoffklassen entwickelt, die Wirtspoteine hemmen (Kinasehemmer). Viele dieser chemischen Verbindungen wurden in klinischen Studien getestet, wurden jedoch aufgrund mangelnder antiviraler Aktivität nicht verwendet. In **Kapitel 2** ist eine Zusammenfassung der Enterovirus-Inhibitoren und deren Status in den klinischen Studien zu finden.

In einem *Drug repurposing* Screening wurden verschiedene zugelassene Medikamente gefunden, die die Enterovirusreplikation inhibieren. Eines dieser Medikamente ist Itraconazol (ITZ), ein Antimykotikum aus der Gruppe der Triazole, das bei Pilzkrankungen entweder oral oder intravenös verabreicht wird. Des Weiteren wird ITZ zurzeit aufgrund seiner Antikrebsaktivität, welche unabhängig von der antimykotischen Aktivität ist, in klinischen Studien getestet. Andere

Studien identifizierten Proteine, welche durch ITZ inhibiert werden und sowohl der antimykotischen Aktivität als auch der Antikrebsaktivität zuzuschreiben ist. All diese Zielproteine erklärten jedoch nicht den Mechanismus, auf welche Art und Weise ITZ EV inhibieren konnte. Letztendlich wurde das Protein oxysterol-binding protein (OSBP), welches Phospholipide und Cholesterin bindet und transportiert, als Zielprotein identifiziert. In **Kapitel 3** wurde eine Struktur-Wirkungsbeziehung studiert, mit dem Ziel, die pharmakologischen Eigenschaften und die diversen pharmakologischen Aktivitäten von ITZ aufzutrennen.

Die chemische Struktur des sehr lipophilen Moleküls besteht aus fünf linear verknüpften Ringen. Die sogenannte Triazol-Gruppe ist für die antimykotische Aktivität hauptverantwortlich indem es ein wichtiges Pilzenzym inhibiert und damit die Zellwandintegrität des Pilzes stört. Eine Nebenwirkung dieser Triazole-Gruppe ist allerdings, dass es auch ein für den Menschen wichtiges Enzym ist, welches Medikamente metabolisiert. Auf der anderen Seite des Moleküls ist eine *Sec*-butyl Kette zu finden, welche mit einer Antikrebsaktivität assoziiert ist. Die Studie in **Kapitel 3** hat ergeben, dass die Triazole-Gruppe - hauptverantwortlich für die antimykotische Aktivität - entbehrlich für die antivirale Aktivität ist. Daher kann man diese zwei pharmakologischen Aktivitäten voneinander trennen. Die Verzweigung der *Sec*-butyl Kette, welche essentiell für die Antikrebsaktivität ist, ist auch essentiell für die antivirale Aktivität. Allerdings können anstatt der verzweigt *Sec*-butyl-Kette verschiedene, andere chemische Gruppen angebracht werden. Dies erlaubt eine Trennung der antikrebs und antiviralen Aktivitäten. Die chemische Struktur besteht aus fünf linearen Ringen, wobei alle Ringe für die antivirale Aktivität essentiell sind. Jegliche Verkürzung dieser Ringe führt zum Verlust der antiviralen Aktivität. Interessanterweise können die Ringe selbst modifiziert werden, um die Lipophilizität des Moleküls zu verringern. Diese Studie zeigte, dass die antimykotische und teilweise auch die Antikrebsaktivität durch Veränderungen der chemischen Struktur von der antiviralen Aktivität entkoppelt werden kann. Des Weiteren haben wir in einer *in silico* Studie gezeigt, wie Itraconazole an das Zielprotein OSBP bindet. Diese Studie legte ein Basiswissen, um die Entwicklung von Itraconazol-abgeleiteten Molekülen zur Virusbekämpfung zu ermöglichen.

In einem weiteren *Drug Repurposing* Screen wurde Fluoxetine (Prozac®) als Hemmer der Enterovirenreplikation entdeckt. Fluoxetine wurde am 29. Dezember 1987 von der Food and Drug Administration (FDA) zugelassen und war der große Durchbruch in der Behandlung von Depressionen. Es war das erste zugelassene Medikament der neu entwickelten Gruppe der Selektiven Serotonin Wiederaufnahmehemmern (SSRI). In **Kapitel 4** wurde der Wirkungsmechanismus von Fluoxetine studiert. Die chemische Struktur von Fluoxetine beinhaltet ein chirales Zentrum welches in zwei Enantiomeren resultiert. Enantiomerstrukturen weisen dieselbe Summenformel auf, jedoch ist ihre räumliche Konformation unterschiedlich und sie verhalten sich wie ein nicht-deckungsgleiches Spiegelbild zueinander. In **Kapitel 4** wurde herausgefunden, dass das (*S*)-Enantiomer, jedoch nicht das (*R*)-Enantiomer, für die antivirale Aktivität verantwortlich ist. Des Weiteren wurde gezeigt, dass das racemische Fluoxetine (1:1

Gemisch von (*S*)-Enantiomer zu (*R*)-Enantiomer) nur EV-B und EV-D Spezies, jedoch nicht EV-A und EV-C oder RV hemmt. Im Zuge dieser Studie wurde auch das (*S*)-Enantiomer gegen verschiedene EV und RV Serotypen getestet. Das (*S*)-Enantiomer zeigte eine höhere antivirale Aktivität gegenüber EV-B und EV-D Spezies und auch RV Spezies wurden gehemmt. Dies deutet auf eine Korrelation zwischen einer höheren antiviralen Aktivität und einem breiteren antiviralen Spektrum hin. Als Zielmolekül wurde das multifunktionale virale Protein 2C - eine ATPase - identifiziert. In Übereinstimmung mit der antiviralen Aktivität des (*S*)-Enantiomer wurde gezeigt, dass nur das (*S*)-Enantiomer jedoch nicht das (*R*)-Enantiomer an das rekombinant exprimierte 2C Protein bindet. Um den genauen Mechanismus der Interaktion zwischen Molekül mit Zielprotein 2C zu studieren, wurde ein Homologiemodell eines Fluoxetine-sensitiven CV-B3 (der EV-B Spezies zugehörig) generiert, dessen Strukturen analog einer kürzlich veröffentlichten Struktur eines Fluoxetine-insensitiven 2C Proteins von EV-A71 (der EV-A Spezies zugehörig) entwickelt wurden. Dieses Modell wurde verwendet um 2C Mutationen in hypothetischen Bindungstaschen zu simulieren. Aufgrund dieser Bindungstaschen konnten Resistenzmutationen verschiedener struktureller 2C Inhibitoren erklärt werden.

Außerdem wurde das Modell verwendet um neue Aminosäuren in der Bindungstasche zu identifizieren, die die Bindung zu Fluoxetine verändern. Zusammenfassend ergab diese Studie die ersten molekularen Einsichten in den Wirkungsmechanismus von Fluoxetine mit dem Zielmolekül 2C.

Wie bereits erwähnt, wird Fluoxetine zur Behandlung von Depressionen, diversen Zwangs- und Angststörungen und Bulimie verwendet. Allerdings ist die Einnahme mit Nebenwirkungen verbunden, die von Kopfweh, Schwindel, Durchfall, Tremors, Photosensitivität und sexueller Dysfunktion bis zu erhöhter Suizidgefahr reichen. Viele dieser Nebenwirkungen können der SSRI-Aktivität von Fluoxetine zugeschrieben werden. Um die pharmakologischen Eigenschaften von Fluoxetine, die für die antivirale Aktivität verantwortlich ist, herauszufinden, wurde in **Kapitel 5** eine Struktur-Wirkungsbeziehung studiert. Den Anfangspunkt der Studie setzten die Ergebnisse aus **Kapitel 4**, in dem gezeigt wurde, dass ein kleines Fragment von Fluoxetine (*N*-Methyl-3-(4-(trifluoromethyl)phenoxy)propan-1-amine-) moderate antivirale Aktivität besitzt. Dieses Resultat zeigt, dass zwei strukturellen Eigenschaften, nämlich die Trifluorophenoxy-Gruppe und die der Amino-Gruppe am anderen Ende des Moleküls für die antivirale Aktivität wichtig sind. Die Trifluoro-phenoxy-Gruppe von Fluoxetine ist für die SSRI-Aktivität, von verantwortlich. Es wurde gezeigt, dass Veränderungen an dieser Gruppe die Affinität von Fluoxetine zu Serotonin verändert und dadurch möglicherweise auch die Nebenwirkungen reduziert. Aus diesen Gründen wurden Fluoxetine-Analoga synthetisiert, die Veränderungen an dieser Gruppe aufweisen. Alle Veränderungen führten zum Verlust der antiviralen Aktivität. Des Weiteren wurden Substitutionen an der Amino-Gruppe synthetisiert. Dies resultierte in einen racemischen Fluoxetine-Analog, welches eine ähnlich antivirale Aktivität hat als (*S*)-Fluoxetine. Um herauszufinden, ob die Analoga ein ähnliches Resistenzprofil wie Fluoxetine selbst

zeigen, und dadurch vermutlich in dieselbe Bindungstasche binden, wurde eine Vielzahl der in *Kapitel 3* gefundenen Viren mit verschiedenen Mutationen in 2C gegen ihre Resistenz getestet. Dies zeigte, dass die Viren mit 2C Mutationen kreuz-resistent gegen die neuen Fluoxetine-Analoga sind. Ähnlich wie Fluoxetine, besitzt auch das potenteste Analog **2b** ein chirales Zentrum. In *Kapitel 5* wurde die Stereochemie dieses Moleküls studiert. Das (S)-Enantiomer zeigte eine erhöhte antivirale Aktivität und ein verbreitertes antivirales Spektrum im Vergleich zu dem racemischen Gemisch. Interessanterweise zeigte auch das (R)-Enantiomer dieses Fluoxetine-Analogs moderate antivirale Aktivität gegen EV-B und EV-D Spezies. Vergleichbar der antiviralen Aktivität von Fluoxetine, zeigte auch das S-Enantiomer des Fluoxetine-Analogs eine stärkere Bindung an künstlich hergestelltes 2C Protein. In *Kapitel 5* zeigten wir, dass ein racemisches Gemisch eines Fluoxetine Analog mit einer Veränderungen an der Amino-Gruppe, eine ähnliche antivirale Aktivität aufwies wie (S)-Fluoxetine. Zusammenfassend konnten wir zeigen, dass die chirale Konformation von Fluoxetine und dessen synthetisierten Analoga, eine wichtige Rolle für die antivirale Aktivität spielen, da das S-Enantiomer eine erheblich höhere antivirale Aktivität aufweist als das R-Enantiomer. Diese Studie zeigte auch, dass es sehr unwahrscheinlich ist, dass die SSRI-Aktivität und die antivirale Aktivität entkoppelt werden können.

Die Ergebnisse beschrieben in *Kapitel 4* und *5* zeigten, dass Fluoxetine die virale Aktivität stereospezifisch durch direkte Bindung an das virale Protein 2C hemmt. Andererseits konnte gezeigt werden, dass die SSRI-Aktivität essentiell ist für die antivirale Aktivität, so dass beide Aktivitäten nicht entkoppelt werden können. Dies kann problematisch für eine therapeutische Anwendung von Fluoxetine sein, und zeigt, dass Medikamente mit einer höheren antiviralen Aktivität und idealerweise mit einem pan-EV- und RV-Spektrum benötigt werden. In *Kapitel 6* wurde eine Struktur-Wirkungsbeziehung an dem Molekül N-(4-fluorobenzyl)-N-(4-methoxyphenyl)furan-2-carboxamide durchgeführt, welches kürzlich als EV-B Spezies-Inhibitor identifiziert wurde. Dieses Molekül war aus mehreren Gründen interessant: einerseits zeigt es strukturelle Ähnlichkeiten zu Fluoxetine, besitzt jedoch keine Trifluoromethyl-Gruppe und somit höchstwahrscheinlich auch keine SSRI-Aktivität, und andererseits ist es ein planares Molekül ohne chirales Zentrum. Die Struktur-Wirkungsbeziehung ergab mehrere hoch potente pan-EV- und RV-Hemmer. Die Meisten wiesen ein mit dem (S)-Fluoxetine vergleichbaren Resistenzprofil auf, mit Ausnahme eines Analogs, das ein verändertes Profil zeigte. Viren, die resistent gegen (S)-Fluoxetine und die anderen neuen Analoga sind, zeigten kaum Kreuz-Resistenz gegen das Molekül 19d. Aus diesem Grund erzeugten wir 19d-resistente EV-A71, CV-B3 und EV-D68 Viren. Wir analysierten die viralen Genome und identifizierten einige Mutationen im viralen Protein 2C, die zur Resistenz führten. Alle resistenten Viren entwickelten mindestens eine Mutationen in oder sehr nahe der α 2-Helix des 2C Proteins. *In silico* Modellierung zeigte einige Tunnel innerhalb der Strukturen des 2C Moleküls von EV-A71 und Poliovirus, welche die Bindung der Moleküle an 2C zulassen. Diese Tunnel überlappen mit der in *Kapitel 4* beschriebenen, potenziellen Bindungstasche. Des Weiteren wurde festgestellt, dass

die antivirale Aktivität einiger Moleküle im therapeutisch relevanten Bereich lagen und dabei die Eigenschaften von Neuronen nicht veränderten. Auch die Dopamin, Serotonin- und Norepinephrinaufnahme, wichtige Botenstoffe des Gehirns, die bei Depressionen und Gefühlen eine Rolle spielen, wurde nicht beeinflusst. Diese Studie zeigte, dass das virale Protein ein ausgezeichnetes Ziel für pan-EV- und RV-Inhibitoren ist. Molekularbiologische und virologische Daten geben auch die ersten Erkenntnisse, dass EV und RV eine gemeinsame Bindungstasche haben, die in allen EV und RV konserviert sind.

Diese Doktorarbeit verschaffte wichtige Einsichten in die Wirkungsweise verschiedener Inhibitoren, die die Replikation von Enteroviren stören. Einerseits wurde gezeigt, dass Wirts-spezifische Inhibitoren ein Potential für therapeutische Anwendung haben. Allerdings, speziell geprägt hat diese Doktorarbeit das therapeutische Potential von 2C Inhibitoren. Die identifizierten Inhibitoren zeigten sehr hohe antivirale Effektivität ohne ersichtliche Toxizität. Aufgrund der Erkenntnis aus dieser Arbeit, dass EV und RV eine gemeinsame konservierte Bindungstasche in 2C haben, kann die Entwicklung von 2C spezifischen Inhibitoren vorangetrieben werden.

Acknowledgements

Sitting in front of my computer and thinking about the last few pages is accompanied by an unusual set of feelings. A lot of memories and experiences that have changed and shaped me during the last years are currently going through my head. A wise person once told me that everything will be fine, also your PhD and apparently, he was right even though I never believed him (by the way, it was not the Career guy from the Network Meeting).

This work could not have happened without my supervisor Frank. During my first Skype interview you asked me if I had read any papers from your lab. Apparently, I had not and you only answered: "That is a pity". Despite this, you offered me the position. I am very grateful and thankful that you gave me the opportunity to join your lab and the Marie Curie Network Antivirals. The amount of time you invest in your students and being open to discussing everything (personal matters, music, science, feedback sessions) is very inspiring and should not be taken for granted! I figured out quickly that I was very privileged in terms of supervision. I really admire that you gave me the freedom to set up collaborations within the Antiviral Network. Thank you very much for all your hard work on improving my skills!

Jeroen, thank you for staying by my side and supporting me through all the meetings, the hours of feedback sessions, endless project discussions, professional counselling and the every now and then whisky/schnaps shots. You showed me how to perform experiments in the lab, how to organize my time better and how to be somewhat less pessimistic. Only when you left, did I realize how many skills I had learned from you in managing and finishing my PhD. I wish you all the best for your future!

A PhD thesis is not the achievement of a person alone but rather the achievement of fruitful collaborations. I was lucky to have the possibility to interact with so many brilliant people. My biggest gratitude goes to Andrea Brancale. Thank you for letting me be a part of your lab for three weeks and introducing me to the world of computer-aided drug design. I would also like to thank Bruno Coutard and Priscilla El-Kazzi for the pleasant collaboration and valuable input. Thierry Langer, thank you for teaching me the basics of ligand-based drug development. I also want to thank Sarah Head and Jun O. Liu for the nice collaboration on the itraconazole project. Lastly, I want to thank Johan Neyts, my mentor of the Antivirals Network, thank you for fruitful discussions and for your encouraging optimism.

Further, I want to thank my reading committee, Juliette Legler, Kim Benschop, Sasha Gorbalenya, Jos van Putten and Emmanuel Wiertz for constructive suggestions which improved my thesis.

Floor, Linda, Huib, Malte, Esther and Daniel you brought so much joy for me to the lab. Dancing through the lab, singing Lion King or any other Walt Disney songs in the cell culture, providing kilograms of chocolate and Gummibärchen, bike rides, dinners, sausage parties and going to the movies are just some of the activities we did together. Floor, thanks for your positive vibes, you always had incredibly calming words. Sitting

without you in the cell culture was very hard until my very last day. Linda, thank you for adopting Betsy our coffee machine with me and for all the hours we spent on paardje kijken. Huib, thank you for your eagerness to help with anything, especially with improving/shortening my protocols. Malte, after sitting alone in an office for 7 months, I was happy that you and Erhard joined my office. Thank you for listening to my complaints, for drowning my sorrows and the failed experiments in beer and Gummibärchen. Esther, thank you for consuming tons of chocolate with me. Last but not least, Daniel. Your dark British and my dark Austrian humor immediately hit it off. Apparently, we were not only having fun, but we also managed a little bit of awesome "sosip" science. It was a delight to work and collaborate with you. There has never been a moment where you were not willing to help. I really admire you and your attitude. Please, stay who you are. It is a pity that our paths did not cross earlier, but who knows what the future may bring. Guys, you all made my life in the lab so enjoyable, thanks to all of you.

Every lab should be grateful to have such nice and supportive shadow workers aka technicians like Nancy and Arno. Arno, you are just the coolest and I already miss making fun of and with you and all the dancing and high-fiving in the lab. Nancy, thank you for being so understanding and listening to my personal problems. Especially singing to Florence and the Machines with in you in the lab will be dearly missed. I really enjoyed working with you both. Arno and Nancy, your kindness and your patience, especially if we once again screwed things up in the lab, is admirable. You do the best job in keeping the lab together and functioning, without you we all would be totally lost.

Raoul, I want to express my dearest gratitude for your guidance and mentoring throughout these years. You helped me a lot with your expertise and kindness. I wish everyone could have a person/mentor like you, who is eager to help! I really enjoyed our scientific and sometimes random discussions a lot.

I would like to thank other colleagues for whatever help you provided in making the stay in the virology department so nice: Ruben, Cristina, Lucian, Jim, Hendrik, Yifei, Wentao, Hongbo, Meiling, Chunyan, Erik, Xander, Anja, Fiona, Berend-Jan, Vera, Kelly, Tengfeng, Maryam, Hilde, Erion, Chiara, Ieva, Ivy, Herman, Brenda, Wenjuan, Shan. I am sorry if you are reading this part and I forgot you to mention. I also want to especially thank you, Marleen, for taking on the burden of being my first student. You helped a lot with finishing my thesis. Good luck in your future.

As part of the EU Marie Curie Network Antiviral I was very lucky to meet so many wonderful and intelligent characters. I enjoyed all the traveling, the unofficial meetings, the scientific exchange and I cherished all the moments we had together. Clazien Oomen, thank you for organizing all the Network meetings so smoothly. Roberto and Birgit, thank you for jumping on the 2C train with me so enthusiastically. Without your help I would have never managed to finish! Marion, remember you are not a sheep. Your company was a real joy and I hope I will see you again soon. Same holds for you Krissy. Your happy attitude was apparent everywhere and made most assignments acceptable and funny like the Virovet assignment. It does not happen often that you cry because

of so much laughing and with that annoy a whole drug developing biotech company. Kristina, before I thank you I have to tell you, just stop talking in the morning before I've had my coffee. You were very lucky to survive that many meetings in a room with me! Thank you for considering my suggestion to critically listen to the now not so bad singer from Nightwish and for sharing this special concert with me. Your trait to always ask critical, rhetorical and sarcastic questions is mind blowing. Thank you for your humor, your helpfulness and especially your ability to make me somewhat smile, even in the darkest of hours. These pleiotropic characteristics of yours made me survive several conferences, network meetings and eventually my PhD. Apparently, there is not only suffering in a PhD.

Moving to a different country is not always easy but my new family made it a fantastic experience. Thanks to the International Neighbor Group of the University of Utrecht (UU-ING) for all the Wednesday Borrels which I was allowed to organize. I met a lot of inspiring people with interesting life stories. Victor, no words can describe how happy I am to have met you. You are a brother from another mother with the same passion for food, drinks and martial arts. I really enjoyed boxing with you and at some point, I promise you that I will fill you in on the fine art of (ballroom) dancing. Thank you for taking care of me, supporting me and trusting in me. I cherish all the moments we had together and all the events we planned together with and for or the ING and especially all the last beers we shared. I hope we soon can start working on our Vietnam farm project. Antonello and Marina, you brought so much happiness into my life especially in form of dancing, pizzas and board games (especially the one which must not be named). Even though hugging is not my thing, I always felt safe and I did not mind hugging either of you. Antonello and Marina, thank you for introducing me to Sofia, Pietro and Koen. Sofia, you are just soo sweet, please stay true to yourself. Pietro thank you, for your incredible talent to make ugly figures pretty and for designing my thesis cover. Kristhell (and of course also Ivan), my special friend(s). Bonding over a gallbladder-less life and the passion for Tarja, Tuomas and especially Sharon is the reason to never let it go. Joao, thank you for being a metal-head too and for headbanging with me through all the concerts. I will always cherish the magical Nightwish concert in Antwerp with you, Kristhell, Ivan and Kristina. Jessica, thank you for sharing so many tipsy Tuesdays with me (at Café de Rat with the wonderful bartender Lucinda and/or Thomas). Having someone who speaks a similar but apparently not the same language helps a lot to feel at home in a foreign country. I am very sorry that I don't speak German properly. Our passion for science, music and beer made so many happy and special moments in the Netherlands (besides the headaches). Thank you for taking care of me, being there for me, believing in me and for all the motivational speeches you gave.

I also want to thank the Café Jan Primus for hosting us each Wednesday and for introducing me to more friends. Laura, thank you for being the best bartender in the world and for introducing me to your parents Siggie and Rob. The three of you adopted me very quickly. You always gave me good advice and also stability if I needed it. Thank you also for helping me with my thesis and assuring my parents that I am doing a good

job in surviving in the Netherlands, despite obvious food problems. I also want to thank Justus for not being grumpy with me. Marcel, I enjoyed all the conversations we had, may you rest in peace. Marc, thank you for always having the right answer, who needs Wikipedia if you have a Marc around. Thank you also for having Torun. Torun, you were my most favorite Dutch dog, thank you for all the cuddles you offered and for understanding my moods, may you rest in peace.

Damit meine Mutter nicht immer sagen kann, dass sie wieder nichts versteht, schreibe ich die letzten Zeilen auf Deutsch. Mama und Papa, ohne euer Vertrauen und eurer Hilfe wäre ich jetzt nicht hier. Man muss auch mal meinem Hund Kiara recht herzlich danken, dass sie soviel auf meine Eltern aufgepasst hat und sie, trotz ihres hohen Alters, immer auf Trab hält. Mama und Papa, es bedeutet mir unendlich viel, dass ihr immer auf mich gehört habt, wenn ich meinen eigenen Weg gehen wollte, auch wenn dieser nicht immer leicht war. Ich weiß, wie schwer es Euch gefallen ist, dass ich die Reise in die Niederlande angetreten habe. Dies kam alles ziemlich plötzlich. Danke, dass Ihr versucht habt mit der Technik Schritt zu halten, damit wir uns oft sehen können (Skype, a so a bledsinn). Ohne Eure Unterstützung hätte ich es nie geschafft. Und ja, ich weiß, auch wenn ich jetzt ein Doktor bin, würdet Ihr euch nicht einmal ein Taschentuch von mir verschreiben lassen. Ich kann Euch beide beruhigen, so ein „richtiger“ Doktor bin ich immer noch nicht. Also die Welt wird nicht untergehen. Danke für alles, ich habe Euch (und natürlich auch Kiara) sehr lieb.

Curriculum Vitae

Lisa Bauer was born on the 28th December in Vienna, Austria. In 2006 she completed her secondary education at the Realgymnasium De la Salle Schule Strebersdorf, Vienna. She then obtained her Bachelor's degree in Microbiology and Genetics from the University of Vienna after a two month internship in the lab of Tim Skern under the supervision of Flávia G. G. Leite. The main goal during her bachelor thesis was to purify and characterize two proteases from Vaccinia Virus. After obtaining her Bachelor's degree she enrolled in the Master's program Microbiology and molecular Immunobiology at the University of Vienna. In 2015 she completed her Master's thesis in the lab of Andreas Bergthaler under the supervision of Christopher Schliehe at the Center for Molecular Medicine of the Austrian Academy of Sciences in Vienna (CeMM). She was involved in the characterization of the methyltransferase Setdb2 which mediated virus-induced susceptibility to bacterial superinfections.

She then joined the lab of Armin Djamei at the Gregor Mendel Institute for molecular Plant Biology of the Austrian Academy of Sciences (GMI) in Vienna as a research assistant. She was involved in setting up a new pathosystem to study the fungus *Ustilago bromivora* and the host grass *Brachypodium* as well as characterizing a phytohormone sensing transcription factor of the maize pathogen *Ustilago maydis*.

In October 2015, Lisa moved to the Netherlands to join the Frank van Kuppeveld's group at the Utrecht University as an Early Stage Researcher in the European Marie Curie Initial Training Network Antivirals. The topic of her thesis was the characterization of FDA-approved drugs inhibiting enterovirus replication and the development of novel broad-spectrum anti-enterovirus compounds. During her PhD she performed two academic secondments in the lab of Andrea Brancale (Cardiff University) and Thierry Langer (University of Vienna) to learn the basics of structure-based and ligand-based drug design, respectively.

In March 2020, Lisa joined the team of Debby van Riel as a post-doc at the Erasmus Medical Center in Rotterdam where she will study how respiratory viruses can invade extra-respiratory tissues.

List of Publications

Bauer, L.; Manganaro, R.; Zonsics, B.; Hurdiss, D. L.; Zwaagstra, M.; Donselaar, T.; Welter, N. G. E.; van Kleef, R.; Lopez, M. L.; Bevilacqua, F.; Raman, T.; Ferla, S.; Bassetto, M.; Neyts, J.; Strating, J.; Westerink, R. H. S.; Brancale, A.; van Kuppeveld, F. J. M., Rational design of highly potent broad-spectrum enterovirus inhibitors targeting the nonstructural protein 2C. *PLoS Biol* 2020, *18* (11), e3000904.

Sooksawasdi Na Ayudhya, S.; Meijer, A.; **Bauer, L.**; Oude Munnink, B.; Embregts, C.; Leijten, L.; Siegers, J. Y.; Laksono, B. M.; van Kuppeveld, F.; Kuiken, T.; Geurts-van Kessel, C.; van Riel, D.; Lakdawala, S., Enhanced Enterovirus D68 Replication in Neuroblastoma Cells Is Associated with a Cell Culture-Adaptive Amino Acid Substitution in VP1. *mSphere* 2020, *5* (6).

Manganaro, R.*; Zonsics, B.*; **Bauer, L.***; Lorenzo Lopez, M.; Donselaar, T.; Zwaagstra, M.; Saporito, F.; Ferla, S.; Strating, J.; Coutard, B.; Hurdiss, D. L.; van Kuppeveld, F. J. M.; Brancale, A., Synthesis and antiviral effect of novel fluoxetine analogues as enterovirus 2C inhibitors. *Antiviral Res* 2020, *178*, 104781.

Schuster, S.; Overheul, G. J.; **Bauer, L.**; van Kuppeveld, F. J. M.; van Rij, R. P., No evidence for viral small RNA production and antiviral function of Argonaute 2 in human cells. *Sci Rep* 2019, *9* (1), 13752.

Bauer, L.*; Manganaro, R.*; Zonsics, B.*; Strating, J.; El Kazzi, P.; Lorenzo Lopez, M.; Ulferts, R.; van Hoey, C.; Mate, M. J.; Langer, T.; Coutard, B.; Brancale, A.; van Kuppeveld, F. J. M., Fluoxetine Inhibits Enterovirus Replication by Targeting the Viral 2C Protein in a Stereospecific Manner. *ACS Infect Dis* 2019, *5* (9), 1609-1623.

Bauer, L.; Ferla, S.; Head, S. A.; Bhat, S.; Pasunooti, K. K.; Shi, W. Q.; Albulescu, L.; Liu, J. O.; Brancale, A.; van Kuppeveld, F. J. M.; Strating, J., Structure-activity relationship study of itraconazole, a broad-range inhibitor of picornavirus replication that targets oxysterol-binding protein (OSBP). *Antiviral Res* 2018, *156*, 55-63.

Bauer, L.*; Lyoo, H.*; van der Schaar, H. M.; Strating, J. R.; van Kuppeveld, F. J., Direct-acting antivirals and host-targeting strategies to combat enterovirus infections. *Curr Opin Virol* 2017, *24*, 1-8.

Ulferts, R.; de Boer, S. M.; van der Linden, L.; **Bauer, L.**; Lyoo, H. R.; Mate, M. J.; Lichiere, J.; Canard, B.; Lelieveld, D.; Omta, W.; Egan, D.; Coutard, B.; van Kuppeveld, F. J., Screening of a Library of FDA-Approved Drugs Identifies Several Enterovirus Replication Inhibitors That Target Viral Protein 2C. *Antimicrobial agents and chemotherapy* 2016, *60* (5), 2627-38.

Rabe, F.; Seitner, D.; **Bauer, L.**; Navarrete, F.; Czedik-Eysenberg, A.; Rabanal, F. A.; Djamei, A., Phytohormone sensing in the biotrophic fungus *Ustilago maydis* - the dual role of the transcription factor Rss1. *Molecular microbiology* 2016, *102* (2), 290-305.

List of Publications

Rabe, F.; Bosch, J.; Stirnberg, A.; Guse, T.; **Bauer, L.**; Seitner, D.; Rabanal, F. A.; Czedik-Eysenberg, A.; Uhse, S.; Bindics, J.; Genenbacher, B.; Navarrete, F.; Kellner, R.; Ekker, H.; Kumlehn, J.; Vogel, J. P.; Gordon, S. P.; Marcel, T. C.; Munsterkotter, M.; Walter, M. C.; Sieber, C. M.; Mannhaupt, G.; Guldener, U.; Kahmann, R.; Djamei, A., A complete toolset for the study of *Ustilago bromivora* and *Brachypodium* sp. as a fungal-temperate grass pathosystem. *Elife* 2016, 5.

Schliehe, C.; Flynn, E. K.; Vilagos, B.; Richson, U.; Swaminathan, S.; Bosnjak, B.; **Bauer, L.**; Kandasamy, R. K.; Griesshammer, I. M.; Kosack, L.; Schmitz, F.; Litvak, V.; Sissons, J.; Lercher, A.; Bhattacharya, A.; Khamina, K.; Trivett, A. L.; Tessarollo, L.; Mesteri, I.; Hladik, A.; Merkle, D.; Kubicek, S.; Knapp, S.; Epstein, M. M.; Symer, D. E.; Aderem, A.; Bergthaler, A., The methyltransferase Setdb2 mediates virus-induced susceptibility to bacterial superinfection. *Nature immunology* 2015, 16 (1), 67-74.